Technical University of Denmark

Design and Optimization of an Integrated Biomass Gasification and Solid Oxide Fuel Cell System

Bang-Møller, Christian; Rokni, Masoud; Henriksen, Ulrik Birk; Elmegaard, Brian

Publication date:
2010

Document Version
Publisher's PDF, also known as Version of record

Design and Optimization of an Integrated Biomass Gasification and Solid Oxide Fuel Cell System

PhD Thesis

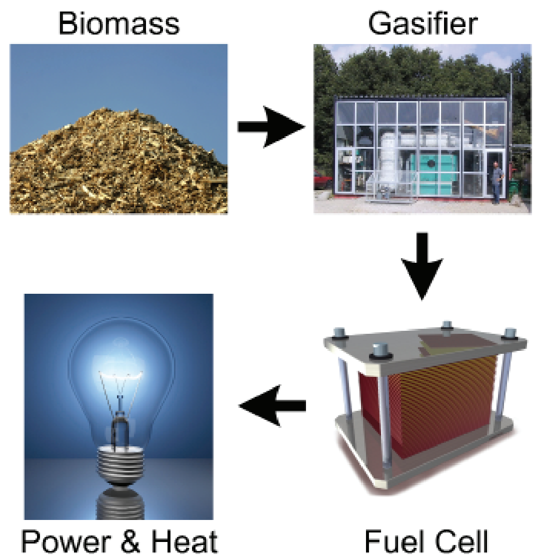

Christian Bang-Møller
DCAMM Special Report no. S112
April 2010

DTU Mechanical Engineering
Department of Mechanical Engineering

DESIGN AND OPTIMIZATION OF AN INTEGRATED BIOMASS GASIFICATION AND SOLID OXIDE FUEL CELL SYSTEM

By

Christian Bang-Møller

A thesis submitted in partial fulfilment of the requirements for the degree of

DOCTOR OF PHILOSOPHY

at the

TECHNICAL UNIVERSITY OF DENMARK

2010

Christian Bang-Møller

DESIGN AND OPTIMIZATION OF AN INTEGRATED BIOMASS GASIFICATION AND SOLID OXIDE FUEL CELL SYSTEM

Technical University of Denmark
Department of Mechanical Engineering
Section of Thermal Energy Systems
Ph.D. Thesis
ISBN: 978-87-89502-98-4
DCAMM Special report no.: S112

Cover illustrations from iStockphoto, Biomass Gasification Group, and Troels Marstrand/Ingeniøren.

PREFACE

This thesis is submitted as a partial fulfilment of the requirements for the Ph.D. degree at the Technical University of Denmark.

The three year study was carried out at the Department of Mechanical Engineering, Section of Thermal Energy Systems from February 2007 to April 2010 under the supervision of Associate Professor Masoud Rokni and co-supervision of Associate Professor and Head of Section Brian Elmegaard and Associate Professor Ulrik Birk Henriksen.

An external research stay was conducted from August 2008 to November 2008 in Golden, Colorado, USA, at Colorado School of Mines (CSM) and the National Renewable Energy Laboratory (NREL), a research facility under the U.S. Department of Energy. Supervisors at CSM were Assistant Professor Robert Braun, Division of Engineering, and Professor Anthony M. Dean, Chemical Engineering Department.

The Ph.D. study was funded by the Technical University of Denmark and included membership of two research schools: DCAMM (Danish Center for Applied Mathematics and Mechanics) and HyFC (Hydrogen and Fuel Cell Academy).

The thesis is written as a monograph, but a number of papers have been published based on the work in this research study (see List of Publications on page IX).

Christian Bang-Møller
Kgs. Lyngby, April 2010

ABSTRACT

Development of sustainable power plants has gained focus in the recent years and utilization of biomass resources are seen as a pathway towards a sustainable combined heat and power (CHP) production. Biomass resources are distributed, thus decentralized biomass conversion would avoid extensive cost for biomass transportation. Traditional decentralized CHP plants suffer from low net electrical efficiencies compared to central power stations, though. Especially small-scale and dedicated biomass CHP plants have poor electrical power yield. Improving the electrical power yield from small-scale CHP plants based on biomass will improve the competitiveness of decentralized CHP production from biomass as well as move the development towards a more sustainable CHP production.

The aim of this research is to contribute to enhanced electrical efficiencies and sustainability in future decentralized CHP plants. The work deals with the coupling of thermal biomass gasification and solid oxide fuel cells (SOFCs), and specific focus is kept on exploring the potential performance of hybrid CHP systems based on the novel two-stage gasification concept and SOFCs. The two-stage gasification concept is developed and demonstrated at the Technical University of Denmark and performs with a high cold gas efficiency, 93% (LHV), and a clean product gas suitable for electrochemical conversion in SOFCs.

A zero-dimensional component model of an SOFC, including an electrochemical model, is developed and calibrated against published data from Topsoe Fuel Cells A/S. The SOFC component model predicts the SOFC performance at various operating conditions and is suited for implementation in system-level models using the simulation software DNA. Furthermore, it is used for issuing guidelines for optimal SOFC operation.

A system-level modelling study of three conceptual plant designs based on two-stage gasification of wood chips with a thermal biomass input of ~0.5

MW_{th} (LHV) is presented. Product gas is converted in a micro gas turbine (MGT) in the first plant design, in SOFCs in the second, and in a combined SOFC-MGT arrangement in the third. The plant scenarios are investigated by system-level modelling combining zero-dimensional component models including the developed SOFC component model. The SOFCs convert the product gas more efficiently than the MGT, which is reflected by the net electrical efficiency of the gasifier and MGT system in opposition to the gasifier and SOFC configuration – η_{el}=27% versus η_{el}=43% (LHV). By combining SOFCs and a MGT, the SOFC off gases are utilized in the MGT to generate additional power and the SOFCs are pressurized, which improves the efficiency to as much as η_{el}=55% (LHV). Variation of the different operating conditions reveals an optimum for the chosen pressure ratio with respect to the resulting electrical efficiency. Furthermore, the SOFC operating temperature and fuel utilization should be maintained at a high level and the cathode temperature gradient maximized.

Based on 1^{st} and 2^{nd} law analyses, the plant layout of the SOFC-MGT scenario is optimized obtaining a net electrical efficiency of η_{el}=58% (LHV). The performance gain is mainly ensured by an improved heat exchanger network. The optimization effort only required the installation of one additional component, an extra product gas preheater, ensuring reduced exergy destructions in several components and an increased TIT, thus boosting the MGT power output.

RESUMÉ (DANISH SUMMARY)

Opmærksomhed på udvikling af bæredygtige kraftværker er forøget de senere år, og udnyttelse af biomasseressourcer ses som en vej mod bæredygtig kraftvarmeproduktion. Biomasseressourcer dyrkes spredt, hvorved omsætning af disse biomasseressourcer i decentrale anlæg vil kunne reducere omkostninger forbundet med transport af biomassen. Dog lider traditionelle decentrale kraftvarmeværker under lav el-virkningsgrad sammenlignet med centrale værker. Specielt små og dedikerede biomassekraftvarmeværker har lavt el-udbytte. Forøget el-udbytte i decentrale biomassekraftvarmeværker vil forbedre konkurrenceevnen for små biomassekraftvarmeværker og skubbe udviklingen mod en mere bæredygtig kraftvarmeproduktion.

Formålet med denne forskning er at bidrage til forhøjede el-virkningsgrader og bæredygtighed i fremtidige decentrale kraftvarmeværker. Studiet omhandler sammenkoblingen af termisk biomasseforgasning og fastoxidbrændselsceller (Solid Oxide Fuel Cells, SOFCs) med fokus på vurdering af potentialet i kraftvarmeanlæg baseret på den udviklede totrinsforgasningsproces og SOFC-brændselsceller. Totrinsforgasningsprocessen er udviklet og demonstreret på Danmarks Tekniske Universitet, og processen opnår en høj koldgasvirkningsgrad, 93 % baseret på nedre brændværdi (LHV), og producerer en ren forgasningsgas, som er anvendelig til elektrokemisk omsætning i SOFC-brændselsceller.

En nuldimensionel komponentmodel af en SOFC, inklusiv en elektrokemisk model, er udviklet og kalibreret mod publicerede data fra Topsoe Fuel Cells A/S. SOFC-komponentmodellen beregner el-virkningsgraden af brændselscellerne afhængig af operationsbetingelser, og modellen er velegnet til brug i systemmodellering ved brug af simuleringsværktøjet DNA. Ydermere anvendes SOFC-komponentmodellen til at stikke retningslinjer for optimal drift af brændselscellerne.

Et systemmodelleringsstudie udføres for tre konceptuelle anlægsdesign baseret på totrinsforgasning af træflis med et termisk biomasse input på ~0.5 MW_{th} (LHV). Forgasningsgassen omsættes i en mikrogasturbine (MGT) i det første anlægsdesign, i SOFC-brændselsceller i det andet og i et kombineret SOFC-MGT system i det tredje. De tre anlægsdesign er analyseret ved hjælp af systemmodellering ved at sammensætte nuldimensionelle komponentmodeller, inklusiv den udviklede SOFC-komponentmodel. Brændselscellerne omsætter forgasningsgassen mere effektivt end mikrogasturbinen, hvilket ses i el-virkningsgraderne for forgasser og MGT-systemet samt forgasser og SOFC-systemet – η_{el}=27 % mod η_{el}=43 % (LHV). Ved at kombinere brændselsceller og mikrogasturbine udnyttes udstødningsgasserne fra brændselscellerne til yderligere el-produktion, og brændselscellerne tryksættes, hvilket resulterer i en væsentligt højere el-virkningsgrad på η_{el}=55 % (LHV). Parametervariation af de forskellige operationsbetingelser viser, at trykforholdet har et optimum i forhold til den resulterende el-virkningsgrad. Ydermere bør brændselscellernes operationstemperatur og brændselsomsætningsgrad fastholdes på et højt leje, og katodetemperaturgradienten bør maksimeres.

Baseret på energi- og exergianalyser optimeres systemdesignet af SOFC-MGT scenariet så det opnår en el-virkningsgrad på η_{el}=58 % (LHV). Den højere el-virkningsgrad skyldes hovedsageligt et forbedret varmevekslernetværk. Optimeringen kræver kun installering af én komponent yderligere, en ekstra forgasningsgasforvarmer, som reducerer exergidestruktionen i flere komponenter samt forhøjer turbineindløbstemperaturen, hvorved mikrogasturbinens el-udbytte forøges.

ACKNOWLEDGEMENTS

I would like to express my deepest gratitude to all the people who supported and assisted me during the last three years of tenure at the Section of Thermal Energy Systems, Department of Mechanical Engineering, Technical University of Denmark (DTU).

I am most thankful to my supervisor, Associate Professor Masoud Rokni, who as a relatively new faculty member at DTU took in his first Ph.D. student without knowing me or the procedures of Ph.D. supervision in Denmark. Still, Masoud perfectly managed to assist with guidance and fruitful discussions whenever needed. Masoud, thank you for investing so much time and energy.

I also thank Associate Professor and Head of Section Brian Elmegaard, Senior Scientist Jesper Ahrenfeldt, and Ph.D. student Lasse R. Clausen for useful discussions from time to time.

Special thanks are also extended to all my colleagues at the Section, who all contributed to a nice and warm workplace filled with humour. Furthermore, my fellow Ph.D. students; Lasse R. Clausen, Wiebke Brix, Martin R. Kærn, Elham Hosseinzadeh, Caspar A. Christiansen, and Michael V. Jensen, as well as Research Assistant Fabio Scappin are wished the best of luck with their research projects.

My stay at Colorado School of Mines (CSM) and National Renewable Energy Laboratory (NREL) in Golden, Colorado, USA, would not have been possible without the assistance of several people. First and foremost, Assistant Professor Robert Braun is acknowledged for his guidance and expertise in SOFC modelling during my stay. Furthermore, Professor Anthony M. Dean and Senior Scientist Bob Evans deserve special thanks for making the stay in Golden possible, and Professor Søren Linderoth for establishing the contact to NREL in the first place. Additionally, I deeply thank my new friends; Berkeley, Jay, Matt, Nate, and all the others for making my stay in Colorado an incredible experience including fantastic weekend trips in the astonishing nature of the Rockies. Finally, the Denmark-America Foundation and Thanks To Scandinavia are acknowledged for their funding of my external research stay.

Last and most importantly, I deeply thank my dear Maria for her love and patience. I know this Ph.D. has kept me busy for quite a long time, and for that reason, I am glad it is now finalized.

List of Publications

The work in this PhD study has led to several publications in different formats. Below is listed the publications of significance. The papers can be found in the Appendix G, Appendix H, and Appendix I.

I. **ISI Journal Paper**
Bang-Møller C., Rokni M. Thermodynamic Performance Study of Biomass Gasification, Solid Oxide Fuel Cell and Micro Gas Turbine Hybrid Systems. *Energy Conversion and Management*. 2010, vol. 51, issue 11, pp. 2330-2339. doi:10.1016/j.enconman.2010.04.006.

II. **Proceedings Paper - Peer Reviewed Manuscript**
Bang-Møller C., Rokni M. Modelling a Combined Heat and Power Plant based on Gasification, Micro Gas Turbine and Solid Oxide Fuel Cells. In: Elmegaard B., Veje C., Nielsen M.P., Mølbak T. (eds.), *Proceedings of SIMS 50: Modelling of Energy Technology*. ISBN 978-87-89502-88-5. The Technical University of Denmark. Fredericia, Denmark. 2009, pp. 189-196.

III. **Proceedings Paper - Peer Reviewed Abstract**
Bang-Møller C., Rokni M. Modelling of a Biomass Gasification Plant Feeding a Hybrid Solid Oxide Fuel Cell and Micro Gas Turbine System. In: Sønderberg P.L., Larsen H.H. (eds.), *Proceedings of Risø International Energy Conference 2009: Energy solutions for CO_2 emission peak and subsequent decline*. ISBN 978-87-550-3783-0. Risø National Laboratory for Sustainable Energy. Roskilde, Denmark. 2009, pp. 289-299.

TABLE OF CONTENTS

LIST OF FIGURES

LIST OF TABLES

NOMENCLATURE

Roman Symbols

A_{ij}	number of atoms of element *j* in each molecule of compound *i* [-]
ASR	area specific resistance [Ω cm^2]
CC	carbon conversion factor [-]
E	reversible open circuit voltage [V]
E_{act}	activation energy [J mol^{-1}]
F	Faradays constant [C mol^{-1}]
$\dot{G}$	Gibbs free energy [J s^{-1}]
g_f	Gibbs free energy [J mol^{-1}]
h	enthalpy [kJ kg^{-1}]
h_f	enthalpy of formation [J mol^{-1}]
i	current density [mA cm^{-2}]
i_{as}	anode limiting current density [mA cm^{-2}]
i_n	internal current density [mA cm^{-2}]
i_0	exchange current density [mA cm^{-2}]
k	total number of chemical compounds leaving the system [-]
LHV	lower heating value [kJ kg^{-1}]
$\dot{m}$	mass flow [kg s^{-1}]
METH	fraction of non-equilibrium methane [vol-%]
N	total number of chemical elements in the system [-]
$\dot{n}$	molar flow [mol s^{-1}]
n_e	number of transferred electrons for each molecule of fuel [-]
n_e^{BV}	number of transferred electrons in Butler-Volmer equation [-]
p	pressure [bar]
P	electric power [W or kW]
PR	pressure ratio [-]
Q_{DH}	district heating production [kJ s^{-1}]
r	ohmic resistance [kΩ cm^2]
R	universal gas constant [J K^{-1} mol^{-1}]
T	temperature [K]

U_F	fuel utilization factor for fuel cell [%]
V	potential/overpotential [V]
w	total number of chemical compounds entering the system [-]
$\dot{W}$	mechanical work [kW]
x	mass fraction [-]
y	molar fraction [-]

Greek Symbols

α	charge transfer coefficient [-]
γ	pre-factor of exchange current density [mA cm^{-2}]
δ	thickness [cm]
Δ	change/difference
ε	heat exchanger effectiveness [%]
η_{CHP}	energy based combined heat and power efficiency [%]
$\eta_{cold\ gas}$	gasifier cold gas efficiency [%]
η_{conv}	SOFC conversion efficiency (neglecting fuel utilization) [%]
η_{el}	energy based electrical efficiency [%]
η_{rev}	reversible fuel cell efficiency [%]
η_{SOFC}	overall SOFC efficiency [%]
η_{v}	voltage efficiency of fuel cell [%]
η_{ψ}	exergy efficiency [%]
$\eta_{\psi,CHP}$	exergy based combined heat and power efficiency [%]
$\eta_{\psi,el}$	exergy based electrical efficiency [%]
$\eta_{\psi,gasifier}$	exergy based gasifier efficiency [%]
λ	Lagrange multiplier [-]
σ_e	oxygen ion conductivity [S cm^{-1}]
$\sigma_{e,0}$	pre-factor of ion conductivity [S cm^{-1}]
$\dot{\Psi}$	exergy flow rate [kW]

Superscripts

0	standard conditions
BV	Butler-Volmer

Subscripts

a	anode
act	activation
c	cathode
C	carbon
cell	single fuel cell
con	consumption
conc	concentration
DH	district heating
e	electrolyte or electrical

elec	electrode
FO	full oxidation
i	interconnect
in	inlet stream
net	netto
ohm	ohmic
out	outlet stream
p	product
PG	product gas
pinch	pinch point
r	reactant
th	thermal
tot	total

Abbreviations

AC	Alternating current
AFC	Alkaline fuel cell
BIGCC	Biomass-based integrated gasification combined cycle
BoP	Balance of plant
CGO	Cerium gadolinium oxide
CHP	Combined heat and power
COS	Carbonyl sulphide
COT	Compressor outlet temperature
DC	Direct current
DH	District heating
DMFC	Direct methanol fuel cell
DNA	Dynamic Network Analysis
DOE	U.S. Department of Energy
DTU	The Technical University of Denmark
GDC	Gadolinium-doped ceria
HHV	Higher heating value
LHV	Lower heating value
LSM	Lanthanum strontium manganite
MCFC	Molten carbonate fuel cell
MGT	Micro gas turbine
NETL	National Energy Technology Laboratory
NREL	National Renewable Energy Laboratory
ORC	Organic Rankine cycle
PAFC	Phosphoric acid fuel cell
PEMFC	Proton exchange membrane fuel cell
ppmv	Parts per million (volume-based)
PR	Pressure ratio
SH	Superheated
SOFC	Solid oxide fuel cell

S/C	Steam-to-carbon ratio
TIT	Turbine inlet temperature
TOFC	Topsoe Fuel Cell A/S
TOT	Turbine outlet temperature
WGS	Water-gas-shift
YSZ	Yttria-stabilized zirconia

Chapter 1 INTRODUCTION

1.1 MOTIVATION

Development of sustainable and efficient combined heat and power (CHP) plants have gained more attention as climate change, security of the supply, and depletion of fossil fuels have become increasingly well-known issues. Biomass represents a sustainable alternative to fossil fuels because conversion of biomass is carbon-neutral as long as re-planting takes place. Biomass releases the same amount of CO_2 during combustion as previously captured during growth.

Distributed production of biomass feedstocks results in increased cost for fuel transportation, thus local conversion of biomass to electricity and heat can minimize this cost. Still, the most cost-effective biomass use for power generation at present is co-firing in large modern coal power plants [1]. This is due to the high electrical efficiency in modern central power stations compared to decentralized and smaller plants. Modern central coal power plants can obtain net electrical efficiencies of around 50%, while the performances of decentralized and smaller power plants (<30 MW_e) typically suffer from significantly lower electrical efficiencies. Especially decentralized and dedicated biomass CHP plants suffer from low electrical efficiencies, reaching only 30-34% on dry biomass in the typical size of 5-25MW_e [1]. Thus, the main barriers for widespread use of biomass in CHP productions are low conversion efficiency and distributed biomass feedstocks. Therefore, focus should be kept on developing more efficient decentralized CHP plants for use of local biomass feedstocks. Furthermore, decentralized power generation is located closer to the end-user, thus reducing grid losses and expanding the potential for district heating.

Efficient power producing technologies for small-scale production typically include gas engines, gas turbines, and fuel cells – all of which require gaseous fuel. An efficient way of reforming biomass into a usable gaseous fuel is by thermochemical processing in a gasifier. Therefore, combining thermal biomass gasification and efficient product gas conversion may enable the design of a sustainable and efficient small-scale CHP plant. The Biomass Gasification Group at The Technical University of Denmark (DTU) has developed a novel and efficient two-stage gasification process (Viking [2]), which produces a very clean product gas from wood chips. The cleanliness of the product gas is very important for many downstream conversion processes, e.g., fuel cells.

Fuel cells present an opportunity to achieve significant efficiency improvements of electricity producing plants. Especially the fuel cell type SOFC (Solid Oxide Fuel Cell) has the advantage of efficient power production. Furthermore, SOFCs operate with high exhaust gas temperature, which can be utilized for additional power generation in heat engines or used for other heating purposes, whether internal in or external to the system. The Danish SOFC developer Topsoe Fuel Cell A/S claims that the electrical efficiency of distributed power generation can be increased from average 40% in traditional power plants to 55% when using SOFC technology [3]. SOFCs can electrochemically convert H_2 and CO to electricity and heat as well as internally reform CH_4 into more H_2 and CO due to their high operating temperature and the presence of a nickel catalyst. Compared to other fuel cell types, these conversion pathways make SOFCs very fuel flexible and ideal for conversion of product gas from thermal gasification.

The usability of a fuel cell is limited without auxiliary components to supply reactants, perform heat management, and do power conditioning. To exploit the great potential of fuel cells, the system of auxiliary components surrounding the fuel cell (BoP – Balance of Plant) needs to be properly designed and optimized. Traditionally, the area of fuel cell research mainly focus on materials, electrochemistry, and stack development, but research within the function and design of the complete system is just as important and will in time gain more focus as the commercial usage of fuel cells approaches.

The combination of thermal gasification and SOFCs is very interesting in the context of utilizing local biomass for decentralized CHP production, as long as the SOFCs can tolerate the alternative gas composition fed to the fuel cells. EU projects (e.g., BioCellus [4] and Green-Fuel-Cell [5]) have investigated the impact on SOFCs when using product gas from thermal biomass gasification. In the BioCellus project, single SOFCs fuelled with product gas from the DTU two-stage gasifier (Viking) were tested, and initial tests showed no significant degradation from impurities even at low steam-to-carbon (S/C) ratios.

A research project dealing with plant layout and optimization of the combination of gasification and SOFC technology can investigate different possibilities of process integration aiming at high net electrical efficiency.

1.2 Objectives

The overall aim of this research is to contribute to enhanced electrical efficiencies and sustainability in future decentralized CHP plants. For reasons described in the motivation above, the work is focused on studying the potential of combining thermal biomass gasification and SOFCs.

More specifically, the research aims to:

I. Investigate potential performances of small-scale CHP plant designs based on the two-stage gasification concept (Viking) and downstream power and heat generation from SOFCs.

II. Develop an SOFC component model with the sufficient level of details to perform plant simulations at various operating conditions.

III. Locate any optimum of crucial operating parameters with regard to the system performances, and determine the systems' sensitivity to these operating conditions, especially operating conditions related to the SOFCs.

IV. Identify the best-performing plant concept and complete an optimization of the system layout and operating parameters to reveal the potential performance of two-stage gasification and SOFC hybrid systems.

1.3 Methodology

The applied methodology for the present research study can be divided into seven steps as listed below. In practice, several steps were conducted in parallel rather than sequentially.

1. Development of three conceptual plant designs based on literature review.

2. Development of a zero-dimensional SOFC model able to handle product gas from thermal biomass gasification as fuel and prepared for integration in a network of component models to enable plant simula-

tions. Calibration of the predicted SOFC performance and completion and assessment of a model test by a parametric study.

3. Development and calibration of a steady-state system-level model of the two-stage gasification plant.

4. Development of complete steady-state system-level models of the three conceptual plant designs.

5. Parametric study of the plant performances by plant simulations.

6. Conduction and assessment of 1^{st} and 2^{nd} law analyses to identify inefficiencies within the best-performing plant of the three studied plant concepts and suggest suitable system optimization efforts.

7. Simulations and assessment of an optimized version of the best-performing plant of the three studied plant concepts.

As mentioned, the aim is to address an enhanced performance of decentralized CHP plants, but the scale of the modelled plant configurations in this study is limited to the largest demonstrated size of the two-stage gasification concept, ~0.5 MW_{th} (LHV). The optimized plant design from this work can then directly be used for a future demonstration plant or form the basis for the design of full-scale decentralized CHP plants in the MW_e class based on thermal biomass gasification and SOFCs.

1.4 THESIS OUTLINE

The thesis is divided into eight chapters. Following this first chapter and based on literature review, Chapter 2 includes a description of thermal biomass gasification (including the two-stage gasification concept), SOFCs, and relevant issues concerning coupling of thermal biomass gasification and SOFCs. Furthermore, Chapter 2 describes the history and current development status of gasifier and SOFC hybrid systems. In Chapter 3, three plant concepts are chosen for further investigation and the system layouts are described. Chapter 4 provides a detailed description of the developed SOFC component model, including an electrochemical model predicting the SOFC performance depending on operating conditions. Additionally, a calibration and parametric study of the SOFC model is described in Chapter 4. The developed system-level models of the three plant scenarios are presented in Chapter 5 including modelling and calibration of the two-stage gasification process. In Chapter 6, the simulation results of a parametric system study are presented and an assessment of the key plant performance data is performed. Chapter 7 includes an optimization of the best-performing plant of the three studied based on 1^{st} and 2^{nd} law analyses. Furthermore, the performances of the original and optimized plants are compared. Finally, Chapter 8 summarizes the findings of this research and gives recommendations for further work.

Chapter 2 BASIS FOR THE STUDY OF COUPLING GASIFICATION AND SOFCS

To be able to understand the issues of combining thermal gasification of biomass with SOFCs, it is necessary to understand the processes inside a biomass gasifier as well as inside an SOFC. The fundamentals of these technologies are briefly described in this Chapter along with an overview of gas cleaning technologies and a description of the history and state-of-the-art of integrated biomass gasification and SOFC systems.

2.1 THERMAL BIOMASS GASIFICATION

Main processes to convert biomass into power or fuels are biochemical conversion and thermochemical conversion. Biochemical conversion uses the path of fermentation or anaerobic digestion, while thermochemical conversion paths consist of pyrolysis, gasification, and combustion [6]. Combustion produces heat whereas pyrolysis and gasification produce combustible gaseous compounds for easier use in subsequent fuel and/or power production. In the following, the processes inside a gasifier will be described briefly followed by a short overview of gasifier designs and a description of the two-stage gasification concept.

2.1.1 THE PROCESSES INSIDE A GASIFIER

Pyrolysis (devolatilization) decomposes carbonaceous materials by heat in the absence of oxygen. Gases, small quantities of vaporized liquid (tars[1]), and a solid residue (char), containing fixed carbon and ash, are produced as

[1] Defined by Milne [7] as: "The organics, produced under thermal or partial-oxidation regimes (gasification) of any organic material, are called "tars" and are generally assumed to be largely aromatic."

seen in eq. (2.1). The temperature region in which the pyrolysis process takes place is 230-700°C, and the produced gases are H_2, CO, CO_2, CH_4, and H_2O [8].

$$\text{Cabonaceous material} + \text{Heat} \rightarrow \text{Gases} + \text{Tars} + \text{Char} \tag{2.1}$$

Gasification further decomposes the fixed carbon into gas compounds in the presence of a gasifying agent and at a higher temperature than the pyrolysis process (typically 800-1100°C) [8]. The gasifying agent can be air, oxygen, steam, and/or carbon dioxide. The main gasification reactions are as follows: [8] [9]

$$C + H_2O = H_2 + CO \text{ (water gas reaction)} \tag{2.2}$$

$$C + CO_2 = 2CO \text{ (Boudouard reaction)} \tag{2.3}$$

$$C + 2H_2 = CH_4 \text{ (hydrogasification reaction)} \tag{2.4}$$

$$CO + H_2O = H_2 + CO_2 \text{ (water-gas-shift reaction)} \tag{2.5}$$

The heat for the endothermic pyrolysis and gasification reactions can be supplied by combustion of char according to eqs. (2.6) and (2.7), and the combustion products can also act as reactants in the gasification reactions:

$$C + \tfrac{1}{2}O_2 = CO \text{ (partial oxidation reaction)} \tag{2.6}$$

$$C + O_2 = CO_2 \text{ (complete oxidation reaction)} \tag{2.7}$$

In a gasifier both pyrolysis, combustion, and gasification occur, and the composition of the produced gas depend on parameters such as gasifier design, fuel composition, moisture content in fuel, gasifying agent, operating temperature, and operating pressure of the gasifier [8]. The gasifier can also be heated by external heat sources. External heating is called allothermal gasification, whereas internal heating, by eqs. (2.6) and (2.7), is called autothermal gasification.

Generally, thermal gasification of biomass leads to five primary contaminants in the product gas; particulates, tars, sulphur, alkali compounds, and nitrogen-containing compounds. Particulates are solid-phase materials entrained in the produced gas flow and typically consist of ash or unconverted carbon. Tars cover a range of complex higher hydrocarbons or oxidized organics formed in the pyrolysis process, and they typically leave the gasifier as vaporized liquids. At lower temperatures many tar compounds condense, entailing risk of plugging or fouling equipment. Sulphur compounds in the produced gas originate from the sulphur content in gasifier feedstock. Biomass feedstocks have low sulphur content compared to coal. Minerals in the ash of the feedstock vaporize at temperatures about 700°C, and alkali compounds can be formed. These alkali compounds condensate into/on solids in the gas flow at around 650°C and can deposit and/or be corrosive to metal surfaces. Proper removal of particulates at lower temperatures will significantly reduce alkali loading. Ammonia is the primary nitrogen-containing compound formed, and it originates from the nitrogen content in the feedstock. Usually, ammonia in the product gas is undesired because it leads to NO_x formation when burned. [10]

Both particulate and tar loading are very depended on the gasifier design, whereas sulphur, alkali, and nitrogen-containing compounds depend on the feedstock. The heating value of tars is not negligible, so it is desired that they are converted in the gasifier or utilized in some way. More details on contaminants from biomass gasification can be found in the DOE/NREL report by Stevens [10], and comments on gas cleaning techniques are given later in this Chapter.

2.1.2 Gasifier Designs

Generally gasifiers can be divided into two design types; fixed bed and moving bed. Fixed bed gasifiers are characterized by a reactor design where a solid fuel feed is added in the top and stationary placed in a bed as shown in Figure 2.1. Fixed bed gasifiers can be updraft or downdraft gasifiers, and the difference is the direction of the gasifying agent flow compared to the solid fuel (co-current vs. counter-current), also shown in Figure 2.1. In the updraft gasifier, the partial oxidation takes place in the bottom heating the gasification of char, the pyrolysis process, and the drying zone on top. The produced gas is cooled through the drying zone, and tars and different hydrocarbons from the pyrolysis process escape easier because they do not pass through the hot char bed or the oxidation zone. In the downdraft gasifier, the partial oxidation takes place between the pyrolysis and char gasification zones. Here, the pyrolysis products pass through the oxidation zone and the hot char bed reducing the tars and hydrocarbons. Therefore, the temperature of the product gas leaving the downdraft gasifier is higher than that of the updraft design. [10]

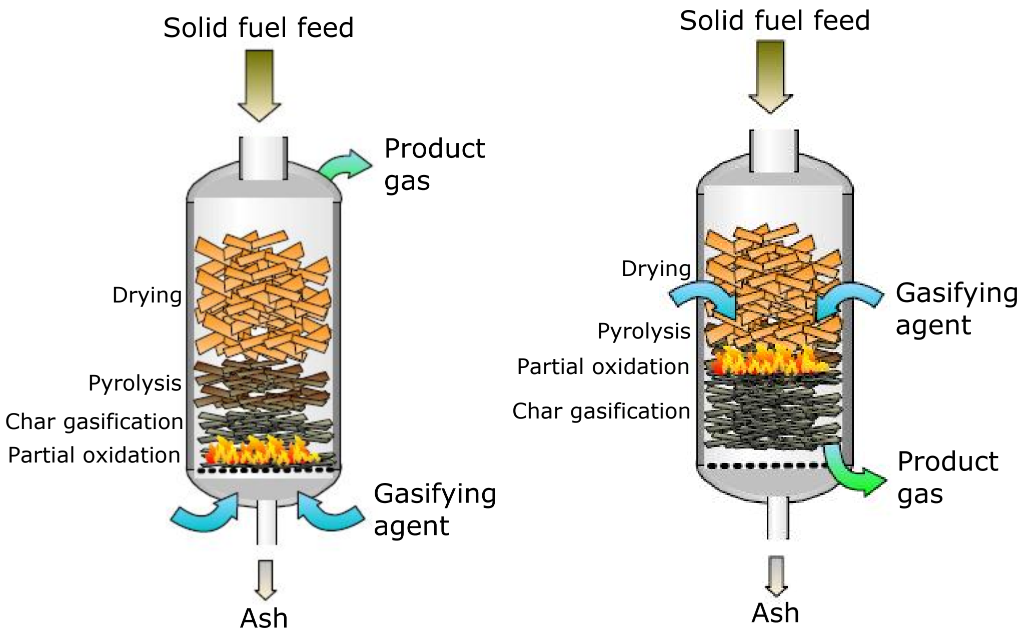

Figure 2.1: Sketches of an updraft (left) and a downdraft (right) autothermal fixed bed gasifier [figures of unknown origin].

The lower temperature of the exiting product gas in the updraft gasifier ensures a more efficient gasification than in the downdraft gasifier because the heat losses are lower. On the other hand, the downdraft gasifier produces a cleaner gas than the updraft gasifier (see Table 2.1). Fixed bed gasifiers can be built in small to medium scale (up to a few MW_{th}) [10].

Table 2.1: Particulate and tar levels from different biomass gasifier designs [10].

Gasifier type	Particulate loading [g Nm^{-3}]	Tar loading [g Nm^{-3}]
Fixed bed		
Downdraft	0.1-0.2	0.1-1.2
Updraft	0.1-1.0	20-100
Moving bed		
Bubbling fluidized bed	2-20	1-15
Circulating fluidized bed	10-35	1-15

Moving bed gasifiers are defined as gasifiers where the bed material is either fluidized by the gasifying agent or entrained in a gas flow and co-fed with an oxidant to a reactor working as a burner operating at fuel rich conditions. Fluidized bed gasifiers can be bubbling fluidized bed gasifiers or circulating fluidized bed gasifiers. In the bubbling fluidized bed gasifier, the bed material is agitated by the gasifying agent flowing through it. In the circulating fluidized bed gasifier, the bed material is circulated between the gasifier and typically a cyclone separating gas from bed material. The bed material is recirculated to the gasifier, and heating of the gasifier can either be by partial oxidation in the gasifier or by indirect heating through heating of the circulating bed material. Turbulence in the moving bed gasifiers ensures effective mixing and heat transfer, but also higher levels of particulates in the product gas (see Table 2.1). The tar loading is higher than the downdraft fixed bed gasifier but lower than the updraft gasifier, and the product gas leaves the moving bed gasifiers at relatively high temperatures. Moving bed gasifiers can be sized for medium-scale to large-scale facilities (MW_{th} scale). [10]

2.1.3 Two-Stage Gasification

In the so-called Viking gasifier (75 kW_{th} [2]) demonstrated by the Biomass Gasification Group at the Technical University of Denmark, the pyrolysis and gasification processes are divided into two separate reactors as depicted in Figure 2.2. Wet biomass (wood chips) is fuelled to the first reactor where drying and pyrolysis takes place, before the pyrolysis products (600°C) are fed to the second reactor, which is a downdraft fixed bed char gasifier. The drying and pyrolysis reactor is externally heated, in this case by the exhaust gas from a gas engine fuelled with the producer gas. In between pyrolysis and char gasification, partial oxidation of the pyrolysis products provides the heat for the endothermic char gasification reactions by addition of preheated air, and a temperature of 1100-1300°C is reached in this zone. Char is gasified in the fixed bed, where H_2O and CO_2 act as gasifying agents in the char gasification reactions at temperatures of 1100-800°C [11]. The Viking gasifier operates near atmospheric pressure.

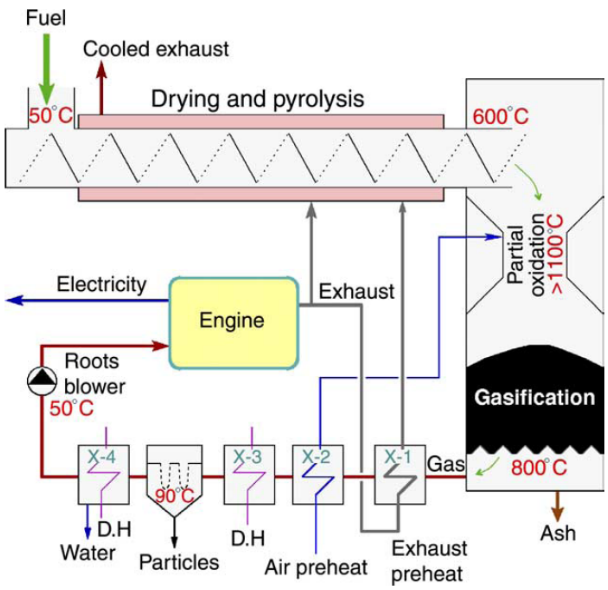

Figure 2.2: Flow sheet of the Viking gasifier [2].

Tars formed in the pyrolysis process are cracked in the high-temperature partial oxidation zone reducing the tar content by a factor of 100, and as the partially oxidized pyrolysis products pass through the char bed, the tar loading is further reduced by a factor of 100 [2]. Thus, the tar content in the product gas leaving the gasifier is extremely low. In one paper [2] from the developers of the Viking gasifier it was stated that the tar content in the produced gas was below 15 mg Nm^{-3}, and in another paper [11], the Viking developers presented results from three different tar measurement techniques, where only one of the three techniques could detect 0.02-0.1 mg Nm^{-3} naphthalene in the raw gas before gas cleaning. The key to this low tar content is the high-temperature cracking in the partial oxidation zone and the reduction when passing through the char bed. Introducing the correct amount of air, ensuring good mixing with the pyrolysis gas in the partial oxidation zone, and avoiding any of the partially oxidized pyrolysis gas to bypass the char bed are crucial issues for the level of success in producing a low tar gas [12].

The raw product gas leaves the char gasification reactor at 800°C and is cooled in two preheating steps and a district heating production, before it is cleaned from particulates in a bag filter at approximately 90°C (slightly above the water dew point) [2]. Hereafter, the cleaned gas is further cooled and water is condensed. More district heating is produced in this step. The flow of product gas is ensured by a blower, and the resulting dry gas composition and lower heating value of the clean product gas are as stated in Table 2.2. Also the cold gas efficiency of the gasifier and the net electrical efficiency of the system including the gas engine are shown in Table 2.2, and their definitions can be found in eqs. (2.8) and (2.9). As previously mentioned, the downdraft gasifier design usually obtains lower cold gas efficiency than the updraft design because of the higher outlet temperature and thereby heat losses. Since the drying and pyrolysis processes are externally heated by waste heat, the resulting cold gas efficiency is high compared to traditional downdraft gasifiers.

Table 2.2: Dry gas composition, LHV as well as efficiencies for the Viking gasifier [11].

H_2 (vol-%)	30.5
CO (vol-%)	19.6
CO_2 (vol-%)	15.4
CH_4 (vol-%)	1.16
N_2 (vol-%)	33.3
LHV (MJ kg^{-1})	6.2
Cold gas efficiency	93%
Net electrical efficiency	25%

$$\eta_{\text{cold gas}} = \frac{\dot{m}_{\text{cold product gas}} LHV_{\text{cold product gas}}}{\dot{m}_{\text{biomass}} LHV_{\text{biomass}}} \tag{2.8}$$

$$\eta_{\text{el}} = \frac{P_{\text{net}}}{\dot{m}_{\text{biomass}} LHV_{\text{biomass}}} \tag{2.9}$$

Some contaminants are present in the cleaned gas and measurements on these are listed in Table 2.3. As expected, the level of impurities from a downdraft fixed bed gasifier is low (cf., Table 2.1). However, the very low tar content is ensured by the tar destruction technique used in the two-stage gasification approach. The amount of sulphur in the product gas is directly depended on the sulphur content in the biomass feedstock. By means of the two-stage gasification process, extensive gas cleaning can be avoided. Thus, the plant complexity can potentially be kept low (and thereby also reduce the plant cost).

Table 2.3: Measured contaminants in producer gas after bag filter and condenser.

Tars (mg Nm^{-3})	<1
Naphtalene [11]+[13]	0.02-0.25
Anthracene [13]	0.05-0.08
Sulphur (ppmv)	<2
H_2S [13]	<1
COS [13]	0.930
Ammonia (mg Nm^{-3}) [11]	60-140[a]
Dust (mg Nm^{-3}) [14]	<5

[a] 520-540 mg Nm^{-3} in the raw gas.

The Viking gasifier is a demonstration plant with a thermal biomass input of only 75 kW_{th}, but the concept is scalable up to the range of 3-10 MW_{th} [15]. A sketch of the medium size two-stage gasification concept is depicted in Figure 2.3. Here, the biomass drying and pyrolysis are divided into separate reactors, where the drying is done by superheated steam produced from the gas engine exhaust, and the pyrolysis reactor is heated by the hot product gas. The reactor size of the dryer and the residence time in the dryer are substantially reduced, when the drying medium is in direct contact with the biomass [16].

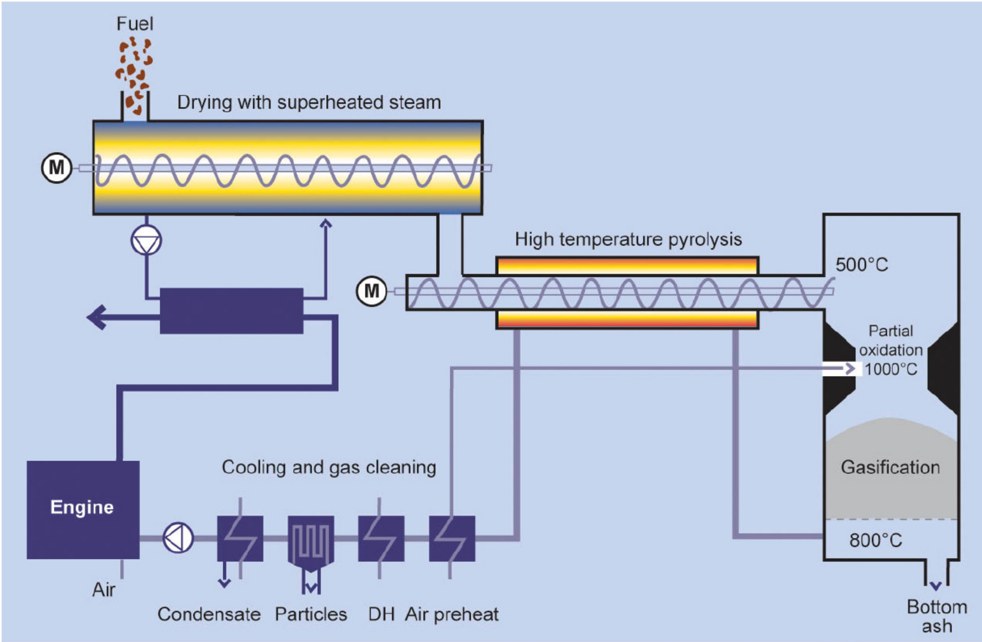

Figure 2.3: The two-stage gasification concept upscaled to 3-10 MW_{th} [15].

A 600 kW_{th}/200 kW_e pilot plant of the two-stage gasification concept has been built in 2007 by DTU, COWI, and Weiss [16], proving the scalability of this gasification concept.

2.2 Solid Oxide Fuel Cells

A fuel cell is an energy converting technology producing electricity directly from oxidizing a fuel through electrochemical reactions. Various types of fuel cells exist with different advantages and disadvantages, but generally they are known for their high efficiency, simplicity, low emissions, and silent operation [17]. Besides that, fuel cells are also efficient when operating at part load.

A typical way to characterize a fuel cell type is by its electrolyte material. An overview of the most common fuel cell types and their characteristics is presented in Table 2.4.

The high-temperature fuel cells (MCFC and SOFC) have the greatest potential to be integrated in larger CHP systems, as shown in Figure 2.4, because the high-quality heat from the fuel cells can be utilized for additional power production in a bottoming cycle or for other heating purposes. Therefore only these high-temperature fuel cell types are relevant to this study.

Table 2.4: Fuel cell types and their characteristics.

Fuel cell type	Mobile ion [17]	Operating temperature [17]	Direct fuels[a]
Alkaline (AFC)	OH^-	50-200°C	H_2
Proton exchange membrane (PEMFC)	H^+	30-100°C	H_2
Direct methanol (DMFC)	H^+	20-90°C	CH_3OH
Phosphoric acid (PAFC)	H^+	~220°C	H_2
Molten carbonate (MCFC)	CO_3^{2-}	~650°C	H_2, CO
Solid oxide (SOFC)	O^{2-}	650[b]-1000°C	H_2, CO

[a] Here defined as the fuels that can be electrochemically converted in the fuel cell.
[b] Research efforts are trying to lower the operating temperature of SOFCs to reduce material costs.

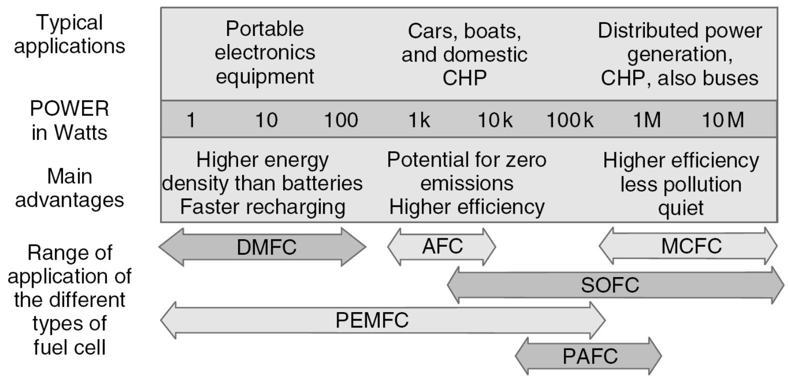

Figure 2.4: Scale of applications for different fuel cell types [17].

This study is confined to looking at the SOFC type only and not the MCFC, even though MCFCs also have the potential to be a part of future CHP plants.

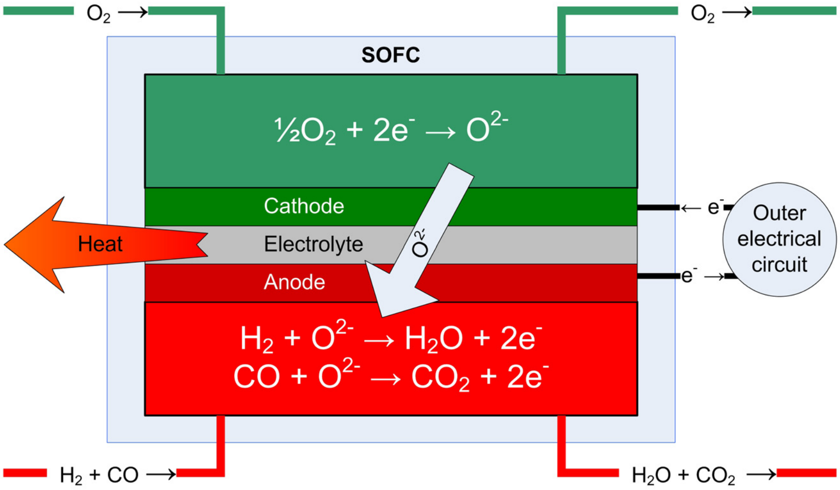

Figure 2.5: A sketch of a solid oxide fuel cell and the electrode reactions.

As seen in Figure 2.5, the SOFC can both electrochemically convert H_2 and CO on the nickel containing anode by reaction with oxygen ions coming from the cathode side through the ion conducting electrolyte. Oxygen ions are the mobile ions in SOFCs, whereas other fuel cell types have other mobile ions (see Table 2.4). Besides H_2O and CO_2, the anode reactions produce electrons, which are led through an outer electrical circuit to meet with oxygen on the cathode and produce oxygen ions. The transport of electrons is characterized as an electrical current.

Furthermore, SOFCs can internally reform CH_4 and NH_3 into H_2 and CO due to their high operating temperature and the presence of a nickel catalyst. This makes SOFCs very fuel flexible and ideal for converting gas from gasifiers, or other reforming processes, compared to other fuel cell types. The reforming reactions are shown in eq. (2.10) [18] and eq. (2.11) [19]. Additionally, the water-gas-shift reaction, as shown in eq. (2.5), will balance the ratio between H_2 and CO depending on the operating conditions.

$$CH_4 + H_2O \rightarrow CO + 3H_2 \ \text{(steam reforming)} \tag{2.10}$$

$$3NH_3 \rightarrow N_2 + 3H_2 \tag{2.11}$$

A single fuel cell generates a potential of the level of 1 V, so to reach a higher potential they are connected in series in stacks. Several cell designs exist, but the most common two are the planar and tubular design. More general information on fuel cells and stack designs can be found in Larminie and Dicks [17] and more specific on SOFCs in Singhal and Kendall [18].

In Denmark, the players within SOFC R&D and production are Risø DTU (National Laboratory for Sustainable Energy) and Topsoe Fuel Cell A/S (TOFC). The SOFC type developed at Risø and TOFC is of the planar design. It is anode-supported and the anode consists of nickel and yttria-stabilized zirconia (YSZ), the electrolyte of YSZ and the cathode of lanthanum strontium manganite (LSM) and YSZ [20].

2.2.1 Tolerance to Impurities

SOFCs have certain tolerances to different contaminants in the fuel fed to the anode. Among these are sulphur compounds, which are poisonous to the nickel anode when present. At the anode conditions, all sulphur compounds will be converted into hydrogen sulphide (H_2S), which is chemisorbed on the nickel surface [21], thus passivating the active sites. Rostrup-Nielsen et al. [21] indicated that the electrochemical reactions are less sensitive to sulphur poisoning than the internal reforming reactions, which are highly affected. They also reported that at 800°C, addition of 10 ppmv of H_2S in the fuel feed (reformer gas) to a 10-cell TOFC stack had no impact on the SOFC performance, while 50 ppmv of H_2S resulted in a reduced cell potential. Rasmussen and Hagen [22] demonstrated an initial cell voltage drop of 10% from adding 2 ppmv H_2S at 850°C using hydrogen as fuel at 1000 mA cm^{-2}. The poisoning effect increase with decreasing temperature and also factors such as fuel, current density, time, and sulphur concentration affects the impact [22] [23], so it seems to be difficult to find consensus on a specific tolerance level to H_2S for nickel based SOFC anodes. At least the poisonous impact from H_2S is reversible at moderate levels (<40 ppmv), meaning that the SOFC performance will recover when the sulphur contaminant is removed [21] [22]. Development of sulphur tolerant anodes is a research field of increasing interest [24], and some have shown promising results [25] [26]. This development could further improve the fuel flexibility of SOFCs and remove the need for a sulphur clean-up step before feeding the fuel to the anode. Generally, the impact of sulphur poisoning seems to be a potential reduction, so to certain extend, the problem could be dealt with by cell or stack dimensioning.

Chlorine compounds such as the hydrogen halide HCl (hydrogen chloride) and alkali halides are usually represented by HCl only [26]. HCl is poisonous to nickel anodes and is expected to affect the anode by similar mechanisms as H_2S, but the extent of degradation from HCl is less [27]. The degradation is also reversible as H_2S. Based on literature and own research, Trembly et al. [27] state that HCl will not reduce the SOFC performance when below a concentration of 1 ppm. Stable performance could be achieved with 20 ppm HCl in the fuel [27], so to certain extend HCl poisoning could also be dealt with by dimensioning as for H_2S poisoning. Aravind et al. [26] showed promising test results with a Ni/GDC anode tolerating up to 9 ppm of H_2S and HCl.

Tolerance to particulates is not well-described in the open literature. Particulates of ash and/or unconverted carbon can deposit on the anode, thus blocking the gas diffusion paths, blocking catalytic sites, or provoke anode layer delamination due to mechanically induced tensions [28]. Hofmann et al. [28] made tests on SOFCs (Ni/GDC anode) with real product gas from biomass gasification and accidently exposed the Ni/GDC anode to ash and char particulates smaller than 5-10 μm in diameter during operation. Normally particulates were removed by first a cyclone and then a metal candle filter, but the metal candle filter failed in one of the tests. Particulates were later identified on the surface of the anode. No contaminants were observed on the anode when the metal candle filter was functioning.

Tars are not necessarily poisonous to SOFCs. Presence of tars can induce carbon deposition on nickel containing anodes at certain conditions, which results in degradation of the SOFC performance. This has been reported by Singh et al. [29] in a theoretical study. Solid carbon is formed through the Boudouard reaction and methane cracking (going from right to left in eqs. (2.3) and (2.4)). The extend of carbon deposition depends on various parameters such as temperature, S/C ratio, current density, and anode material. The carbon deposition decreases with the increase of S/C ratio or with the increase of current density [29]. Mermelstein et al. [30] showed by experiments, that carbon deposition was reduced significantly in both Ni/YSZ and Ni/CGO anodes fed with 15 mg Nm^{-3} tars in a H_2/N_2 fuel mix at 765°C, when the S/C ratio was greater than 1. Higher fuel utilization (>50%) should make SOFCs able to operate at lower S/C ratios with reduced carbon formation because H_2O and CO_2 produced from the electrochemical reactions will suppress carbon deposition and/or remove deposited carbon [30]. Hofmann et al. [14] used C-H-O ternary diagrams to predict and experiments to show, that solid carbon formation was not formed when fuelling an SOFC with product gas from the Viking gasifier at a temperature of 850°C, a current density of 260 mA cm^{-2}, a fuel utilization of 30%, and a S/C ratio of 0.5. This was also due to the very low tar content in the product gas from the Viking gasifier and an activated carbon filter removing some of the tars. 0.17 mg Nm^{-3} of naphthalene was present in the gas at the anode inlet. According to the statement by [30] above, it should be possible to operate at an even lower S/C ratio than 0.5 without carbon deposition, if the fuel utilization of 30% was increased significantly.

2.3 OVERVIEW OF GAS CLEANING

Cleaning of the produced gas is often essential for downstream end-use technologies. To be able to meet the requirements of these technologies different clean-up steps should be considered.

To remove particulates, cyclones, barrier filters, electrostatic filter, or wet scrubbers can be used. Cyclones can remove up to 90% of particulates larger than 5 µm in diameter at high temperatures (only limited by material constraints). Barrier filters can remove particulates of 0.5 to 100 µm in size. Barrier filters can be constructed of metals or ceramics for hot gas cleaning, or woven materials (bag filters) for cleaning up to 350°C. Electrostatic filters can operate up to 500°C or more and can remove 99% of particulates smaller than 0.1 µm, while wet scrubbers are very efficient for particulates larger than 1 µm, but at temperatures below 100°C. [10]

Tar loading is very much depended on gasifier design, so first of all, tars should be limited by design considerations. Otherwise, tars can be dealt with by physical, catalytic, and thermal removal. Through the physical tar removal route, the tars are condensed and filtered. Catalytic destruction decomposes tars to additional product gas either in situ or in a downstream reactor. The non-metallic catalyst dolomite has proven to remove 95-99% of tars at 750-900°C under laboratory conditions. Thermal destruction decomposes tars to additional product gas at temperatures above 1200°C and without a catalyst. [10]
Thermal destruction is the technique used in the two-stage Viking gasifier between the pyrolysis process and char gasification.

Concerning sulphur, the relatively small amounts of H_2S from biomass gasification can be removed by absorption onto metal oxide pellets in a bed at about 480°C [10]. Dayton et al. [31] report that the upper temperature limit for the most common H_2S sorbent ZnO is 600°C. COS is on the other hand more effectively adsorbed in an active carbon bed. Sakanishi et al. [32] suggest a metal-supported active carbon bed for simultaneous removal of H_2S and COS.
Commercial H_2S absorption by ZnO is presently available. Removal is recommended at 300-400°C, but can also be done from ambient conditions up to 450°C. Even combined removal of H_2S and COS is available. [33]

Alkali compounds condense into solids or on particulates below 650°C. Hereby alkali compounds can be removed in the same manner as particulates. Particulate size can be below 5 µm, so cyclones will not be effective. Research is being conducted on alkali traps for removing alkali compounds at high temperature. [10]

From the SOFC point of view, it is not needed to remove ammonia, since it can be converted in the fuel cell as described earlier. Therefore, gas conditioning techniques for ammonia removal are not investigated here.

Hot gas cleaning technologies have gained increasing interest because cooling of the hot producer gas from the gasifier can be avoided. This can be beneficial when coupling gasification with other high-temperature technologies because of better heat management.

2.4 HISTORY AND DEVELOPMENT STATUS

Gasification and fuel cells were first combined with the intention to improve coal to electricity efficiencies. In the early 1980s, advanced coal gasification and MCFC (Molten Carbonate Fuel Cell) systems were explored under DOE [34], but in 1988 Reed and Das [35] mentioned in their book on biomass gasifier systems that fuel cells are a potentially interesting technology to generate electricity from biomass derived producer gas.

The first to report on a thermodynamic analysis of the combination of a biomass gasifier and SOFCs were Alderucci et al. in 1994 [36]. In this early publication a fluidized bed gasifier, using either steam or CO_2 as gasifying agent, was studied, and equilibrium calculations were used to predict the conversion levels in the gasifier. The SOFC electrical efficiency was calculated at different gasifier operating conditions such as the gasifier operating temperature. In the case of a gasifier operating temperature of 700°C, the SOFC performed with electrical efficiencies of 47% using steam as gasifying agent and 51% using CO_2. Efficiencies of the entire system were not calculated.

The coupling of biomass gasification and high temperature fuel cells was also mentioned by Craig and Mann [37] in 1996 in a reported study on BIGCC (Biomass-based Integrated Gasification Combined Cycle) as a future potentially high-efficient CHP production from biomass.

A thorough design study of an SOFC and gas turbine system combined with biomass gasification was published in 2000 by Barchewitz and Palsson [38]. This work calculated total system efficiencies of a plant producing 4-5 MW_e. The gasifier was a pressurized autothermal air-blown circulating fluidized bed gasifier and the SOFCs were of planar design. It was assumed that all tars were cracked inside the gasifier, which is most unlikely in this type of gasifier. Barchewitz and Palsson referred to Ståhl and Neergaard [39], while Ståhl and Neergaard reported on problems associated with tars in the product gas. A recuperator recovering heat from the gas turbine outlet was included and the resulting electrical system efficiency was found to be 58.5% at an optimal pressure of 2.65 bar. The low operating pressure was caused by the recuperative loop (see, e.g., Saravanamuttoo et al. [40] or a brief explanation in the end of Chapter 3). By reducing the SOFC stack size and increasing the gas turbine output, the efficiency was reduced to 55.1% at 5.25 bar, but the capital costs were also reduced.

Hutton et al. [41] reported in 2003 on a feasibility study of a thermally integrated downdraft biomass gasifier and SOFC system, where a net electrical efficiency of 38% (based on HHV) was predicted. The thermal integration featured heating of the gasifier by the burned off gases from the SOFCs, reducing or neglecting the need for air supply to the gasifier (depended on the moisture content in the woody biomass).

In 2004, Omosun et al. [42] modelled two biomass-fuelled SOFC systems where the effect of hot versus cold gas cleaning on system efficiencies and costs were studied. The electrical system efficiencies were similar at around 22%, but the hot gas cleaning showed better heat management and thereby overall cogeneration efficiency. The low electrical efficiency was due to low fuel utilization in the SOFC (set to 50%) and the fact that the SOFC off gases were burned and used for district heating production and drying of biomass. Compared to the work of Barchewitz and Palsson, the efficiencies are substantially lower pointing out the importance of utilizing the SOFC off gases in a proper manner. In the case of Barchewitz and Palsson, this is done in a recuperated gas turbine. Additionally, removal of sulphur compounds was not included in the study by Omosun et al. in opposition to tars, particulates and alkali compounds, even though sulphur is very poisonous to SOFCs.

Sucipta et al. [43] published in 2007 a performance analysis of a tubular SOFC and recuperated MGT hybrid system fuelled with gasified biomass using air, oxygen, or steam as gasifying agent. A scenario using pure methane was used as reference. Electrical efficiencies of the hybrid system without the gasification process were found to be 46.4%, 48.9%, and 50.8% for air, oxygen, and steam, respectively. The reference scenario using pure methane performed 59%. The main reasons for the lower performance in the biomass scenarios were the lower heating value of and inactive species in the biomass producer gas.

In 2008, Fryda et al. [44] modelled an autothermal (air) biomass gasifier integrated with SOFCs and/or a micro gas turbine with a biomass throughput of 200 kg/h (almost 900 kW_{th} (LHV)). The combination of a gasifier, SOFCs, and a micro gas turbine achieved the highest electrical efficiency of

40.6%. Surprisingly, the gasifier and micro gas turbine system outperformed the gasifier and SOFC combination with an electrical efficiency of 26.1% versus 20.0%. An electrical efficiency below 20% of the SOFC in the gasifier and SOFC combination seems unrealistically low if dimensioned and operated properly.

As seen from the above descriptions of studies on biomass gasification and SOFC hybrid systems, this specific field is heavily based on modelling studies. Experimental investigations are usually limited to lab scale tests of single SOFCs operated on biomass derived producer gas, typically to test SOFC tolerance to trace species [14] [26] [28] [45] [46]. Oudhuis et al. [47] reported on proof-of-principle lab-scale tests with an oxygen-blown biomass gasifier and a 5-cell SOFC stack (Sulzer HEXIS) for up to 48 hours of operation. The SOFC stack achieved an electrical efficiency of 41% at a fuel utilization of 80%.

Recently, two EU projects, BioCellus [4] and Green-Fuel-Cell [5], have been completed. Both projects dealt with issues of combining biomass gasification and SOFCs, and special focus was on obtaining a clean producer gas from appropriate gasifier design and/or hot gas cleaning. Thermal integration between an allothermal biomass gasifier and tubular SOFCs by means of liquid metal heat pipes transferring the excess heat from the SOFCs to the gasifier comprise a novel coupling for small-scale CHP, which were also presented in the BioCellus project [48] [49] [50] [51]. Based on a modelling study, Panopoulos et al. [50] report that a total electrical efficiency of 36% (32% by exergy [51]) at 70% fuel utilization and a current density of 250 mA cm^{-2} can be achieved to produce 140 kW_e. Successful testing of single cell SOFCs operated on producer gas from the Viking gasifier for 150 hours were also conducted in the BioCellus framework [14].

2.5 KEY ISSUES RELEVANT TO THIS STUDY

From the literature some important points have shown when it comes to combining thermal biomass gasification and SOFCs in a sustainable and efficient decentralized CHP production.

Providing a clean producer gas which meets the requirements of the SOFC is essential. This can be obtained partly by proper gasifier design and also by downstream gas conditioning. Especially the tar and particulate loadings can be reduced from appropriate gasifier design, whereas compounds originating from inorganics in the biomass feedstock are less sensitive to gasifier design.

Utilization of SOFC off gases is also important to obtain high system efficiency, since not all producer gas is converted in the SOFC. Therefore, the SOFC off gases contain unconverted fuel and also high-quality heat, which can be exploited for additional power generation or heating purposes. Several studies have shown that gas turbine technology can exploit the SOFC off gases to produce additional power.

Heat management is also of great importance to the resulting system efficiency, whether it is within in the gasification process, the SOFC system, or any additional parts of the system, or it is between the different system parts. In this context, methods for cooling the SOFC should get attention, and if a gas turbine is included in the system, use of a recuperator have shown to be beneficial. Alternatively, the hot gas turbine exhaust can be used to generate steam for a Rankine cycle if the plant size is big enough.

The cold gas efficiency of the gasifier should be as high as possible, since it is hard to compensate for losses from the gasification process in the latter parts of the system. This was also shown in [52].

Furthermore it must be expected, that keeping the system design simple and choosing state-of-the-art components will contribute to the design of an efficient CHP plant with reasonable investment and maintenance costs.

Chapter 3 INVESTIGATED PLANT CONFIGURATIONS

Based on the literature review forming a basis for this study in the previous chapter, three conceptual system layouts have been chosen for further investigation. These are all based on thermal gasification of biomass, as in the Viking two-stage gasification concept, supplying producer gas for downstream electricity generation. The reason for choosing the Viking gasifier concept is the production of a very clean gas from this plant reducing the need for extensive gas conditioning. Furthermore, the cold gas efficiency is very high, forming the basis for an efficient plant. In spite of the use of a downdraft gasifier reactor in the Viking concept, the cold gas efficiency is very high, and this is due to external heating of the reactor where drying and pyrolysis takes place (only where drying takes place in the upscaled concept, cf., Figure 2.3). Hereby, the need for adding air to heat the gasifier is reduced, and less of the feed to the gasifier is burned. The product gas is also less diluted with N_2.

Downstream the biomass gasification, product gas is converted to electricity and heat for district heating purposes. This is done in three different scenarios; using only a micro gas turbine (MGT), using only SOFCs, or using both combined. Studying these three scenarios is expected to give an overview of the benefit from choosing an efficient SOFC over a conventional technology and also the advantage of combining these to gain even higher electric power yield. The potential performance of combining biomass gasification, by the two-stage concept, and SOFCs should also be revealed.

Since the hybrid system should work as a decentralized CHP plant, the size should be in the range of 5-30MW_e (some decentralized plants can be smaller or larger) [53]. The size chosen in this study, though, is determined by the currently available two-stage gasifier size of around 0.5 MW_{th} (as previously mentioned a 600 kW_{th}/200 kW_e pilot plant has been demonstrated [16]). Thus, the chosen size in this study aims at very small decentralized CHP plants and future demonstration plants. Nevertheless, it must be expected that larger plants will perform at least as good as the chosen plant size. It is assumed that the cold gas efficiency and product gas composition are the same as for the Viking gasifier (75 kW_{th}). It is expected that the two-stage gasification concept is scalable up to 10 MW_{th} as depicted in Figure 2.3, but also even further up to 50 MW_{th} using a fluid bed design [15], so the potential for designing decentralized CHP plants based on gasification by the two-stage concept is present. The chosen plant size is also sufficient for the ability to include a MGT in the system, but not big enough to include a steam based Rankine cycle downstream the gas turbine. Instead, the excess heat in the gas turbine exhaust is recuperated to the compressed air intake. Since the thermal plant input is fixed, the electric power production is depended on the electrical efficiency of the hybrid system.

Flow sheets of the three conceptual scenarios are sketched in Figure 3.1, and the alternative flow directions in the scenarios using only a MGT or only SOFCs are indicated by two kinds of dashed lines.

Wet wood is fed to the dryer, producing dry wood and steam, which both are led to the gasifier. For reasons of simplification, the pyrolysis takes place inside the gasification reactor in this modelling study. In the demonstrated 75 kW_{th} Viking gasifier, the drying and pyrolysis reactor is heated by the gas engine exhaust gases, but around 80% of the heat supplied to this reactor is used for drying [16]. Furthermore, some of the gas engine exhaust is superheated by the hot product gas from the gasifier before it is sent to the drying and pyrolysis reactor as seen in Figure 2.2. It is therefore assumed that the pyrolysis process is not heated by external heat from the gas engine, but by heat from the gasifier, which is also the case in the upscaled version of the two-stage concept depicted in Figure 2.3. Thus, only the drying process is externally heated in this investigation. Since change of the outlet temperature from the modelled gasification reactor will affect the raw gas composition, the air input to the gasification reactor is preheated more in this study than in the demonstrated Viking gasifier to compensate for the heat consumption from the endothermic pyrolysis process inside the gasifier. The temperature of the slightly cooled product gas after the air preheater should be the same in this study and in the demonstrated two-stage gasification concept, but measurements on this temperature is unknown to the author. From a system point of view, it is just important to obtain the correct cold gas efficiency and gas composition, unless additional thermal integration between the gasification and power generating part of the system is necessary.

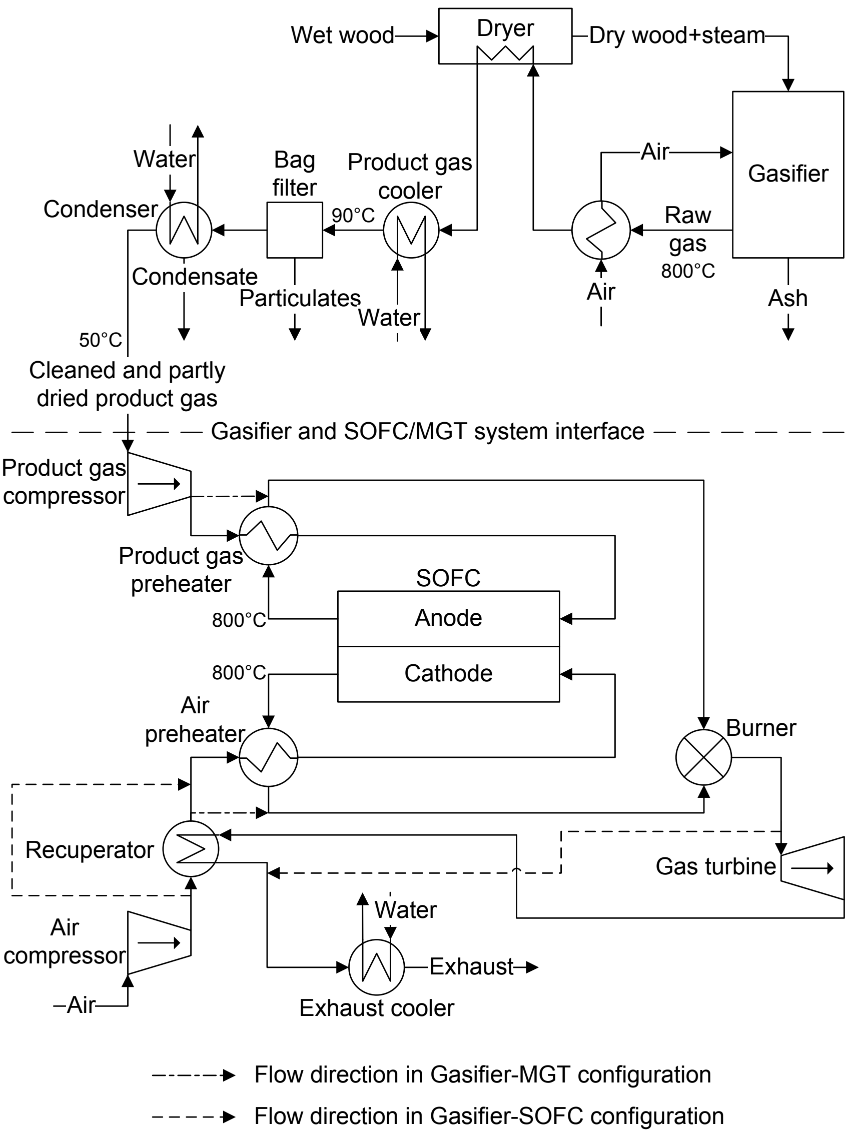

Figure 3.1: Flow sheet of the three scenarios studied.

External heating of the biomass drying process is in this case done by hot product gas instead of the hot exhaust gas from the power generating subsystem. Hence, some district heating production is moved from the product gas cooler to the exhaust cooler, but the cold gas efficiency and electrical efficiency are not affected. By means of this, the gasifying part and the power producing part of the hybrid plant are separated, ensuring that independent operation of the two subsystems is possible. This can be an advantage from a regulation viewpoint or during start-up and shut-down procedures. Furthermore, in this way an existing gasification plant could easily be modified to include SOFCs and/or a MGT downstream the gasification process.

As for the Viking gasifier, a bag filter removing particulates is the only gas cleaning device in the considered system. The product gas is cooled to 90°C before it is led through the filter. It is assumed that no alkali compounds leave the gasifier plant entrained in the producer gas flow, since all alkalis should be condensed at such low temperatures, thus removed along with particulates in the bag filter. The sulphur content is expected to be very low (see Table 2.3), so no sulphur clean-up step is included. If it was found necessary, a ZnO bed could be located somewhere after the gasifier air preheater depending on the preferred operating temperature of such a sulphur removal unit. Introducing a ZnO bed would not affect the rest of the system by other means than a small pressure drop and heat loss. If a ZnO bed was used, a S/C ratio above 1.66 at 400°C should be kept to avoid carbon deposition [54], thus, depending on the chosen operation temperature of the ZnO bed, addition of water might be necessary. As a last step in the biomass gasification process, the product gas is cooled to condense some of the water reaching a product gas temperature of around 50°C.

As mentioned, the power generating part of the system has three scenarios; one where all components in Figure 3.1 are in use (which from now on will be referred to as the SOFC-MGT configuration), and two where some components are bypassed. In one of the latter scenarios the SOFCs including preheaters are bypassed, by which all electric power generation is provided by the MGT, and this scenario is named the MGT configuration. The last scenario bypasses the MGT expander and recuperator and only uses the SOFCs for power generation, and this scenario is from now on referred to as the SOFC configuration.

In all three scenarios, the product gas is supplied by a product gas compressor and the air by an air compressor. Suction from the product gas compressor ensures gas flow in the gasification process. In the SOFC configuration, the two compressors are working as blowers, since the power generating system is not pressurized, contrary to the MGT and SOFC-MGT configurations. The SOFC feeds are preheated by the SOFC off gases (800°C) to be able to keep the temperature difference through the SOFCs at an acceptable level, and subsequently the off gases are combusted in a burner to convert remaining combustibles. The hot flue gas from the burner is either utilized for additional power generation in the MGT (MGT and SOFC-MGT configurations) or for district heating production (SOFC configuration).

When the MGT is used, a recuperator is included for additional preheating of the air supplied to the SOFC cathode. If the cathode inlet and outlet temperatures are unchanged, the impact of including a recuperator will be an increased temperature of the cathode off gas introduced in the burner and hence a higher turbine inlet temperature (TIT). Accordingly, the power production from the MGT and the electrical efficiency will rise. Furthermore, the pressure ratio (PR) will have an optimum at a relatively low level when introducing a recuperator compared to operation without a recuperator [40]. At high PRs, the temperature of the MGT expander outlet will be lower than the air compressor outlet, neglecting the option of recuperating. The optimum is a result of a trade off between gain in efficiency from exploiting heat in the exhaust gas and loss in efficiency from lowering the PR.

Chapter 4 A ZERO-DIMENSIONAL SOLID OXIDE FUEL CELL MODEL

To investigate SOFC processes or hybrid systems including SOFCs, as two of the plant configurations presented in the previous chapter, a component model predicting the performance of the SOFCs has been developed. To be able to optimize system parameters, such as operating temperature and pressure, it is necessary to develop an SOFC component model that can predict the SOFC performance depended on its operating conditions. The zero-dimensionel component model is added to the existing component library of the simulation tool DNA (Dynamic Network Analysis), which is used in this modelling study. DNA is a simulator made for simulation of mathematical models representing thermodynamic processes. By use of the methodology of network theory in electrical engineering, a procedure for modelling thermodynamic processes is applied. DNA can handle both steady-state and transient process models and has build-in thermodynamic state models of common fluids and solid fuels as well as a component model library. Common equipment, such as heat exchangers, turbomachineries, and burners, is available from the component model library. Furthermore, balancing of energy and mass is done automatically. The FORTRAN-based DNA is free and open source, and more information on DNA can be found in [55], [56], and [57]. The SOFC component model listing can be found in Appendix B.

The developed SOFC submodel calculates the air and fuel outlet compositions and the electrical power production. The calculations are based on the inlet air and fuel compositions and flow rates as well as operating conditions of the SOFC. The operating conditions are partly described by input parameters given directly to the SOFC submodel. These parameters are presented in Table 4.1. The rest comes from system interaction (e.g., operating pressure and inlet temperatures). The SOFC submodel includes an electrochemical model for predicting the electrochemical performance of the SOFC.

Table 4.1: Direct inputs to the SOFC submodel.

Fuel utilization factor	U_F	0.85
Operating temperature	T_{SOFC}[a]	800°C
Anode pressure loss	Δp_a	5 mbar
Cathode pressure loss	Δp_c	10 mbar
Current density	i	300 mA cm^{-2}

[a] Equals the SOFC anode and cathode outlet.

In the submodel only H_2 is electrochemically converted in the anode, but the model takes into account that CO produces an extra H_2 molecule through the water-gas-shift (WGS) reaction, while four additional H_2 molecules are produced from CH_4 through internal steam reforming (cf., eq. (2.10)) and WGS of produced CO (cf., eq. (2.5)). Thus, full conversion of CH_4 and CO is assumed. This assumption is fair because the high-temperature and active catalyst containing anode environment ensures (1) fast steam reforming and WGS to reach equilibrium and (2) continuous removal of reforming products via electrochemical reactions [17]. Conversion of NH_3 (cf., eq. (2.11)) is not included in this submodel, thus the total molar flow of H_2 in the anode, after internal steam reforming and WGS, will be as expressed in eq. (4.1).

$$\dot{n}_{H_2,tot} = \dot{n}_{H_2,in} + \dot{n}_{CO,in} + 4\dot{n}_{CH_4,in} \quad (4.1)$$

$$H_2 + O^{2-} \rightarrow H_2O + 2e^- \text{ (anode reaction)} \quad (4.2)$$

$$\tfrac{1}{2}O_2 + 2e^- \rightarrow O^{2-} \text{ (cathode reaction)} \quad (4.3)$$

$$H_2 + \tfrac{1}{2}O_2 \rightarrow H_2O \text{ (overall reaction)} \quad (4.4)$$

The electrode reactions and the overall fuel cell reaction are as shown in eqs. (4.2) to (4.4). Direct electrochemical conversion of CO (see reaction in Figure 2.5) is neglected because it is most likely that the competing and faster WGS reaction will be the dominant reaction pathway for CO [59]. The amount of hydrogen that is electrochemically converted depends on the fuel utilization factor (U_F), which is defined in eq. (4.5).

$$U_F = \frac{\dot{n}_{H_2,tot} - \dot{n}_{H_2,out}}{\dot{n}_{H_2,tot}} \quad (4.5)$$

The overall fuel cell reaction reveals that the amount of consumed oxygen is half the amount of consumed hydrogen. The cathode outlet composition is calculated by the following equations; the only species taken into account being O_2, N_2, CO_2, H_2O, and Ar.

$$\dot{n}_{O_2,\text{con}} = \frac{U_F \dot{n}_{H_2,\text{tot}}}{2} \tag{4.6}$$

$$\dot{n}_{\text{c,out}} = \dot{n}_{\text{c,in}} - \dot{n}_{O_2,\text{con}} \tag{4.7}$$

$$y_{O_2,\text{out}} = \frac{\dot{n}_{\text{c,in}} y_{O_2,\text{in}} - \dot{n}_{O_2,\text{con}}}{\dot{n}_{\text{c,out}}} \tag{4.8}$$

$$y_{j,\text{out}} = \frac{\dot{n}_{\text{c,in}} y_{j,\text{in}}}{\dot{n}_{\text{c,out}}}, \quad j = \{N_2, CO_2, H_2O\} \tag{4.9}$$

$$y_{\text{Ar,out}} = 1 - y_{O_2,\text{out}} - y_{N_2,\text{out}} - y_{CO_2,\text{out}} - y_{H_2O,\text{out}} \tag{4.10}$$

For the anode flow channel it is assumed that chemical equilibrium is reached at the outlet at the operating temperature and pressure. Chemical equilibrium is characterized by the total Gibbs free energy having its minimum value. With this assumption, the fuel composition leaving the anode can be found by the Gibbs free energy minimization method. This methodology is described in Appendix A and is based on Smith et al. [58] and Elmegaard [56]. In to the Gibbs free energy minimization calculations enters the gas fed to the anode along with the consumed oxygen coming from the cathode (cf., eq. (4.6)). Chemical equilibrium at the anode outlet temperature and pressure is assumed for the following chemical compounds: H_2, CO, CO_2, H_2O, CH_4, and N_2 (Ar is not taken into account).

It is also assumed that the temperature of the solid structure of the SOFC is lumped and equal to the SOFC operating temperature. Furthermore, all gases are considered ideal gases. Finally, it is assumed that the performance of a single SOFC applies for the entire SOFC stack.

Power production from the SOFC depends on the amount of chemical energy fed to the anode and the electrical efficiency of the SOFC (η_{SOFC}) as stated in eq. (4.11). The SOFC efficiency is defined in eq. (4.12) as the product of the reversible efficiency (η_{rev}), the voltage efficiency (η_{V}), and the fuel utilization factor (U_F) [60].

$$P_{\text{SOFC}} = [(\Delta h_f)_{H_2} \dot{n}_{H_2,\text{in}} + (\Delta h_f)_{CO} \dot{n}_{\text{CO,in}} + (\Delta h_f)_{CH_4} \dot{n}_{CH_4,\text{in}}]\eta_{\text{SOFC}} \tag{4.11}$$

$$\eta_{\mathrm{SOFC}} = \eta_{\mathrm{rev}} \eta_{\mathrm{v}} U_{\mathrm{F}} \tag{4.12}$$

The reversible efficiency is the maximum possible efficiency defined as the relationship between the maximum available electrical energy (change in Gibbs free energy) and the change in enthalpy of formation, both of which are associated with *full* oxidation of the fuel [60]. This relationship is shown in eq. (4.13).

$$\eta_{\mathrm{rev}} = \frac{(\Delta g_{\mathrm{f}})_{\mathrm{FO}}}{(\Delta h_{\mathrm{f}})_{\mathrm{FO}}} \tag{4.13}$$

The expression for the change in Gibbs free energy of formation at full oxidation is shown in eq. (4.14) when considering H_2, CO, CO_2, H_2O, CH_4, and N_2 in the fuel feed. The Gibbs free energies in eq. (4.14) should be determined at the SOFC operating temperature and the partial pressure of the specific reactant or product species. Stoichiometric combustion of the fuel results in a content of CO_2 and H_2O in the product stream as stated in eqs. (4.15) and (4.16). The necessary content of O_2 in the reactant stream for full oxidation to occur can be found in eq. (4.17).

$$\begin{aligned}(\Delta g_{\mathrm{f}})_{\mathrm{FO}} = \; & y_{\mathrm{CO_2,out,FO}} (g_{\mathrm{f}})_{\mathrm{CO_2,p}} + y_{\mathrm{H_2O,out,FO}} (g_{\mathrm{f}})_{\mathrm{H_2O,p}} \\ & - y_{\mathrm{H_2,in}} (g_{\mathrm{f}})_{\mathrm{H_2,r}} - y_{\mathrm{CO,in}} (g_{\mathrm{f}})_{\mathrm{CO,r}} - y_{\mathrm{CH_4,in}} (g_{\mathrm{f}})_{\mathrm{CH_4,r}} \\ & - y_{\mathrm{CO_2,in}} (g_{\mathrm{f}})_{\mathrm{CO_2,r}} - y_{\mathrm{H_2O,in}} (g_{\mathrm{f}})_{\mathrm{H_2O,r}} - y_{\mathrm{O_2,in,FO}} (g_{\mathrm{f}})_{\mathrm{O_2,r}}\end{aligned} \tag{4.14}$$

$$y_{\mathrm{CO_2,out,FO}} = y_{\mathrm{CO,in}} + y_{\mathrm{CH_4,in}} + y_{\mathrm{CO_2,in}} \tag{4.15}$$

$$y_{\mathrm{H_2O,out,FO}} = y_{\mathrm{H_2,in}} + 2 y_{\mathrm{CH_4,in}} + y_{\mathrm{H_2O,in}} \tag{4.16}$$

$$y_{\mathrm{O_2,in,FO}} = \tfrac{1}{2} y_{\mathrm{H_2,in}} + \tfrac{1}{2} y_{\mathrm{CO,in}} + 2 y_{\mathrm{CH_4,in}} \tag{4.17}$$

The change in enthalpy of formation is expressed in eq. (4.18), and in this model it is based on LHVs.

$$(\Delta h_{\mathrm{f}})_{\mathrm{FO}} = (\Delta h_{\mathrm{f}})_{\mathrm{H_2}} y_{\mathrm{H_2,in}} + (\Delta h_{\mathrm{f}})_{\mathrm{CO}} y_{\mathrm{CO,in}} + (\Delta h_{\mathrm{f}})_{\mathrm{CH_4}} y_{\mathrm{CH_4,in}} \tag{4.18}$$

The voltage efficiency (η_{v}) expresses the electrochemical performance of the SOFC. The calculation of voltage efficiency is described in the following Section.

4.1 ELECTROCHEMICAL MODEL

The electrochemical model is used to calculate the cell potential and voltage efficiency of the SOFC. Both of these values depend on the operating conditions, including temperature, pressure, gas compositions, fuel and oxidant utilization, and load (current density). The operating temperature in Table 4.1 is assumed to be valid for representing the solid temperature of the SOFC in the electrochemical model, and the temperature of the solid structure is denoted T in this description of the electrochemical model. The cell potential and voltage efficiency are defined in eqs. (4.19) and (4.20), respectively.

$$V_{\mathrm{cell}} = E - V_{\mathrm{act}} - V_{\mathrm{ohm}} - V_{\mathrm{conc}} \tag{4.19}$$

$$\eta_{\mathrm{v}} = \frac{V_{\mathrm{cell}}}{E} \tag{4.20}$$

In the following part of the Section, the Nernst potential, or reversible open circuit voltage, (E) and overpotentials are calculated. The total overpotential has contributions from the activation (V_{act}), ohmic (V_{ohm}), and concentration (V_{conc}) overpotentials, which all are described later in this Section.

As a result of the current being drawn from the cell, the partial pressure of both reactants and products change through the cell. Thus, in this study the partial pressure of the jth species is an average across the respective electrode and is here defined as an arithmetic mean between inlet and outlet in eqs. (4.21) and (4.22). The outlet molar fractions are determined by the Gibbs free energy minimization method as described earlier. $\overline{p}_{\mathrm{a}}$ and $\overline{p}_{\mathrm{c}}$ are average partial pressures of the anode and cathode compartment, respectively, taking any pressure losses into account. The average partial pressure of the available hydrogen after internal steam reforming and WGS of CH_4 and CO can be determined from eq. (4.23), equivalent to eq. (4.1), when assuming full conversion of CH_4 and CO to H_2. The WGS and steam reforming reactions can be found in eqs. (2.5) and (2.10).[2]

$$\overline{p}_j = \left(\frac{y_{j,\mathrm{out}} + y_{j,\mathrm{in}}}{2} \right) \overline{p}_{\mathrm{a}}, \quad j = \{\mathrm{H_2}, \mathrm{CO}, \mathrm{CH_4}, \mathrm{CO_2}, \mathrm{H_2O}, \mathrm{N_2}\} \tag{4.21}$$

$$\overline{p}_{\mathrm{O_2}} = \left(\frac{y_{\mathrm{O_2},\mathrm{out}} + y_{\mathrm{O_2},\mathrm{in}}}{2} \right) \overline{p}_{\mathrm{c}} \tag{4.22}$$

[2] Note, that eq. (4.23) is only valid in water-rich environments. A more generally applicable model is described in Appendix J together with estimates on the error of using eq. (4.23).

$$\overline{p}_{H_2,\mathrm{tot}} = \overline{p}_{H_2} + \overline{p}_{CO} + 4\overline{p}_{CH_4} \tag{4.23}$$

E can be calculated from the Nernst equation:

$$E = \frac{-\Delta g_f^{\ 0}}{n_e F} + \frac{RT}{n_e F}\ln\left(\frac{\overline{p}_{H_2,\mathrm{tot}}\sqrt{\overline{p}_{O_2}}}{\overline{p}_{H_2O}}\right) \tag{4.24}$$

Because it is assumed that all CO and CH_4 are converted to H_2 before the electrochemical reactions take place, both the change in standard Gibbs free energy ($\Delta g_f^{\ 0}$) and the number of electrons transferred for each molecule of fuel (n_e) are determined for the reaction of H_2 only. Thus, $n_e = 2$ [61] and $\Delta g_f^{\ 0} = (g_f^{\ 0})_{H_2O} - (g_f^{\ 0})_{H_2} - \frac{1}{2}(g_f^{\ 0})_{O_2}$. Note that the standard Gibbs free energy is evaluated at standard pressure, but is still a function of temperature [18].

The activation overpotential is due to an energy barrier (activation energy) that the reacting species must overcome in order to drive the electrochemical reactions. The activation overpotential of each electrode is a non-linear function of the current density and is usually expressed by the Butler-Volmer equation [18] [61] [62] [63] shown in eq. (4.25).

$$i = i_0\left\{\exp\left(\alpha\frac{n_e^{BV} F V_{act}}{RT}\right) - \exp\left(-(1-\alpha)\frac{n_e^{BV} F V_{act}}{RT}\right)\right\} \tag{4.25}$$

i_0 is the exchange current density, α the charge transfer coefficient, and n_e^{BV} the number of electrons transferred in the single elementary rate-limiting step that the Butler-Volmer equation represents. A value of 0.5 for the charge transfer coefficient is commonly used for fuel cell applications [62], and hereby, the activation overpotential for one electrode can be expressed as in eq. (4.26) as shown by Chan et al. [62]. The value of n_e^{BV} is commonly assumed to be equal to 1 [61].

$$V_{act} = \frac{2RT}{n_e^{BV} F}\sinh^{-1}\left(\frac{i}{2i_0}\right) \tag{4.26}$$

The total activation overpotential in this model is hereby defined as the sum of the activation overpotential of each electrode and is based on Chan et al. [62] and Zhu and Kee [61]:

$$V_{act} = V_{act,a} + V_{act,c} = \frac{2RT}{F}\left[\sinh^{-1}\left(\frac{i+i_n}{2i_{0,a}}\right) + \sinh^{-1}\left(\frac{i+i_n}{2i_{0,c}}\right)\right] \tag{4.27}$$

In this case, an internal current density (i_n) is added to the actual current density in order to account for the mixed potential caused by fuel crossover and electrons passing through the electrolyte. The importance of the internal current density in the case of SOFCs is much less than that for low temperature fuel cells. Thus, the value of i_n is usually very small for SOFCs [17]. In this study, the value of i_n is adjusted when calibrating the electrochemical model. The exchange current density (i_0) is a measure of the level of activity on the electrode at i=0 mA cm^{-2} and is different for the anode and cathode. Chan et al. [62] use constants to represent both anodic and cathodic exchange current densities, while Zhu and Kee [61] use an expression making the exchange current densities depend on reactant concentrations. Neither of these methods take into account the dependence of temperature that the exchange current densities have. If constant exchange current densities are used, it can be seen from eq. (4.27) that increasing temperature means increasing activation overpotential at the same current density. Thus, increasing temperature will have a negative influence on the SOFC performance, which contradicts with experimental experience. Therefore, to be able to model SOFC performance at various temperatures, the exchange current densities need to depend on temperature. Costamagna et al. [64] studied ways of modelling the exchange current densities from literature, and explicitly tested two empirical models of the anodic exchange current density for Ni/YSZ electrodes with dependence on species concentration and temperature. One is based on results found by Mogensen et al. [65] [66], and this expression is also the one chosen in a later paper by Costamagna et al. [67]. The expression can be found in eq. (4.28) and is also used in this study. The cathodic exchange current density is based on Achenbach [68] and is also used by Costamagna et al. in [64] and [67]. The expression is shown in eq. (4.29). The values of γ and E_{act} can be found in Table 4.2.

$$i_{0,a} = \gamma_a \left(\frac{\overline{p}_{H_2,tot}}{\overline{p}_a}\right)\left(\frac{\overline{p}_{H_2O}}{\overline{p}_a}\right)\exp\left(\frac{-E_{act,a}}{RT}\right) \tag{4.28}$$

$$i_{0,c} = \gamma_c \left(\frac{\overline{p}_{O_2}}{\overline{p}_c}\right)^{0.25}\exp\left(\frac{-E_{act,c}}{RT}\right) \tag{4.29}$$

The ohmic overpotential is caused by the ohmic resistance towards the oxygen ions passing through the electrolyte and the electrons passing through the electrodes and interconnects. The ohmic overpotential is dominated by the resistance in the ion conducting electrolyte [61] [62]. According to Braun [69], the ion resistance accounts for 80% of the total ohmic losses. Thus, only the ion resistance through the electrolyte is considered in this model, so the ohmic overpotential is defined as below in eqs. (4.30) to (4.32). The temperature-dependent correlation for the ionic conductivity of the electrolyte (σ_e) is taken from Zhu and Kee [61]. The thickness of the electrolyte (δ_e), the pre-factor ($\sigma_{e,0}$), and activation energy of transport of oxygen ions ($E_{act,e}$) for the calculation of the ionic conductivity of the electrolyte are listed in Table 4.2. $\sigma_{e,0}$ and $E_{act,e}$ are valid for YSZ electrolytes.

$$V_{ohm} = (i + i_n)\, r_e \tag{4.30}$$

$$r_e = \frac{\delta_e}{\sigma_e} \tag{4.31}$$

$$\sigma_e = \frac{\sigma_{e,0}}{T} \exp\left(-\frac{E_{act,e}}{RT} \right) \tag{4.32}$$

The concentration overpotential is a result of the limitations of diffusive transport of reactants and products between the flow channel and the electrode-electrolyte interface. The effect is increasing with current density, and at a certain current density limit this transport of species is not fast enough to feed the electrochemical reactions taking place, and the partial pressure of reactants at the electrode-electrolyte interface approaches zero. The anode and cathode current density limits are different, and they are dependent on microstructural characteristics of the respective electrode and operating conditions of the SOFC. Detailed models describing this concentration overpotential due to limitation of the diffusive transport are available in the literature (e.g., Zhu and Kee [61], Chan et al. [62], and Kim et al. [70]). For anode supported SOFCs, where the anode layer is much thicker than the cathode layer, the anode limiting current density is much lower than the cathode limiting current density. Thus, the concentration overpotential is dominated by the anode contribution [69] [61]. For reasons of simplification, and since operation at very high current densities are not intended in this study, the anode limiting current density (i_{as}) is assumed to be constant, while the contribution to the concentration overpotential from the cathode is neglected. Also, the cathode concentration overpotential in the model by Chan et al. [62] is infinitesimal. The following expression of the total concentration overpotential is used in this model, and it is based on Kim et al. [70] and Braun [69]:

$$V_{\text{conc}} = -\frac{RT}{n_{\text{e}}F}\left[\ln\left(1-\frac{i+i_{\text{n}}}{i_{\text{as}}}\right)-\ln\left(1-\frac{\bar{p}_{\text{H}_2,\text{tot}}(i+i_{\text{n}})}{\bar{p}_{\text{H}_2\text{O}}i_{\text{as}}}\right)\right] \tag{4.33}$$

The assumed constant anode limiting current density (i_{as}) can be found in Table 4.2. The value of i_{as} is intended to represent SOFC stacks and not single cells because single cells can have much higher limiting current densities.

Table 4.2: Constants in the electrochemical model.

R	8.314 J K^{-1} mol^{-1}	
F	96 485 C mol^{-1}	
n_{e}	2	
i_{n}	6 mA cm^{-2} [a]	
γ_{a}	5.5×10^{9} mA cm^{-2}	[64]
γ_{c}	7.0×10^{8} mA cm^{-2}	[64]
$E_{\text{act,a}}$	1.2×10^{5} J mol^{-1}	[64]
$E_{\text{act,c}}$	1.2×10^{5} J mol^{-1}	[64]
δ_{e}	10×10^{-4} cm	[71]
$E_{\text{act,e}}$	0.8×10^{5} J mol^{-1}	[61]
$\sigma_{\text{e,0}}$	3.6×10^{5} S cm^{-1}	[61]
i_{as}	1000 mA cm^{-2}	(assumed)

[a] Determined by calibration (cf., Section 4.1.1).

So to summarize, the following main equations represent the electrochemical model that predicts the voltage efficiency of the SOFC as a function of species concentration and operating temperature and pressure:

$$\eta_{\text{v}} = \frac{V_{\text{cell}}}{E}, \quad V_{\text{cell}} = E - V_{\text{act}} - V_{\text{ohm}} - V_{\text{conc}}$$

$$E = \frac{-\Delta g_{\text{f}}^{\,0}}{n_{\text{e}}F} + \frac{RT}{n_{\text{e}}F}\ln\left(\frac{\bar{p}_{\text{H}_2,\text{tot}}\sqrt{\bar{p}_{\text{O}_2}}}{\bar{p}_{\text{H}_2\text{O}}}\right)$$

$$V_{\text{act}} = \frac{2RT}{F}\left[\sinh^{-1}\left(\frac{i+i_{\text{n}}}{2i_{0,\text{a}}}\right)+\sinh^{-1}\left(\frac{i+i_{\text{n}}}{2i_{0,\text{c}}}\right)\right],$$

$$i_{0,\text{a}} = \gamma_{\text{a}}\left(\frac{\bar{p}_{\text{H}_2,\text{tot}}}{\bar{p}_{\text{a}}}\right)\left(\frac{\bar{p}_{\text{H}_2\text{O}}}{\bar{p}_{\text{a}}}\right)\exp\left(\frac{-E_{\text{act,a}}}{RT}\right)$$

$$i_{0,\text{c}} = \gamma_{\text{c}}\left(\frac{\bar{p}_{\text{O}_2}}{\bar{p}_{\text{c}}}\right)^{0.25}\exp\left(\frac{-E_{\text{act,c}}}{RT}\right)$$

$$V_{\mathrm{ohm}} = (i + i_{\mathrm{n}})\, r_{\mathrm{e}}\,, \quad r_{\mathrm{e}} = \frac{\delta_{\mathrm{e}}}{\sigma_{\mathrm{e}}}\,, \quad \sigma_{\mathrm{e}} = \frac{\sigma_{\mathrm{e,0}}}{T} \exp\left(-\frac{E_{\mathrm{act,e}}}{RT} \right)$$

$$V_{\mathrm{conc}} = -\frac{RT}{n_{\mathrm{e}} F} \left[\ln\left(1 - \frac{i + i_{\mathrm{n}}}{i_{\mathrm{as}}} \right) - \ln\left(1 - \frac{\bar{p}_{\mathrm{H_2,tot}} (i + i_{\mathrm{n}})}{\bar{p}_{\mathrm{H_2O}} i_{\mathrm{as}}} \right) \right]$$

4.1.1 Calibration of the Electrochemical Model

In the following Section, the electrochemical model of the SOFC is calibrated. Because the model aims to represent the performance of 2nd generation SOFCs from Topsoe Fuel Cell A/S and Risø DTU (National Laboratory for Sustainable Energy), published experimental stack performance data for this SOFC type have been used for calibrating the electrochemical model. These cells are anode supported and the anode consists of Ni/YSZ, the electrolyte of YSZ, and the cathode of LSM/YSZ [20].

The value of the limiting current density, used in the correlation describing the concentration overpotential in eq. (4.33), is assumed because stack performance data at high current densities are not available to the author. A value of 1000 mA cm^{-2} is assumed. Of course, this brings some uncertainty into the model at high current densities, but operation in the high current density region is not performed in the conceptual analysis of the studied system scenarios. If this is needed, calibration in the high current density region is recommended.

Concerning the ohmic overpotential, the specific conductivity of the electrolyte, calculated using eq. (4.32), is based on values representing YSZ as published by Zhu and Kee [61]. At 800°C, this results in a specific conductivity of 0.043 S cm^{-1}. An electrolyte thickness of 10 µm – similar to the 2nd generation TOFC/Risø cells, as described by Linderoth et al. [71] – is used to calculate the ohmic resistance.

The open circuit voltage, $V_{\mathrm{cell}}(i=0$ mA $cm^{-2})$, is adjusted by adding an internal current density of 6 mA cm^{-2} to the actual current density. Hereby, the overpotentials are not zero at $i=0$ mA cm^{-2}, and the open circuit voltage decreases.

The activation overpotential is adjusted to fit the resulting cell potential to the polarization curve published by Linderoth et al. [71]. This is done by applying calibration factors to the exchange current densities. Adjusting the anodic exchange current density by a factor of 2 and the cathodic exchange current density by a factor of 0.5 makes a satisfying fit.

For the data from [71], an active cell area of 81 cm^2 per cell has been assumed. The conditions as stated in [71] are: 75-cell stack (12x12 cm^2 footprint), 800°C, fuelled with 2000 Nlitre h^{-1} H_2 and 1200 Nlitre h^{-1} N_2 (which corresponds to U_F=28% at 18 A or approximately 220 mA cm^{-2} with the assumed active cell area) and 5075 Nlitre h^{-1} of air. The same conditions are applied in the SOFC component model during calibration. A mix of H_2 and N_2 represents a fuel with both active and inert substances, similar to product gas from gasification. Since the air flow is an input in the SOFC model during calibration, a heat loss/supply is allowed to be able to keep the operating temperature. Both modelled and experimental data as well as the error relative to the experimental data are presented in Figure 4.1. The relative error refers to the right-hand side y-axis. The calibration was done at atmospheric pressure.

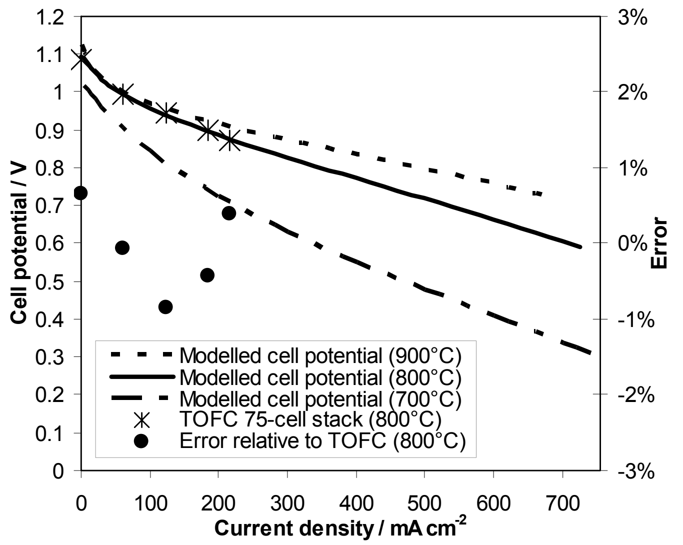

Figure 4.1: Single cell polarization curves based on a 75-cell stack at 800°C and the SOFC model, respectively. The modelled performance is shown for 700, 800, and 900°C, and the relative error between the modelled and experimental performance is shown at 800°C.

The model shows excellent agreement with the experimental data in the region where experimental data are available. The relative error does not exceed ±1%. Above i=220 mA cm^{-2}, the actual TOFC SOFC performance is unknown to the author. As seen in Table 4.1, a current density of 300 mA cm^{-2} was chosen to represent the SOFC load in the following results. Even though 300 mA cm^{-2} is just outside the experimental dataset from [71], it is assumed that the SOFC model represents the TOFC performance to a satisfactory level at this load.

4.2 PARAMETRIC STUDY OF SOFC PERFORMANCE

By varying different operating conditions, the influence of these operating conditions on the performance of the SOFCs is studied. Along with that, the behaviour of the SOFC component model is tested, to see if it acts as expected. The reference conditions in this parametric study are shown in Table 4.3. Some of these conditions are varied one at a time in the following test. Unless otherwise stated, the reference conditions are used. Furthermore it should be noted, that the electric power output is given and kept constant, and that heat losses are neglected. The value of the electric power output is not mentioned because it is not relevant in this parametric study, and since it is kept constant, the fuel flow varies with the SOFC performance. The air flow is controlled by the cooling need of the SOFCs.

Table 4.3: Reference conditions in parametric study.

Fuel	Product gas[a] or 97 vol-% H_2 + 3 vol-% H_2O	
Fuel utilization factor	U_F	0.85
Operating temperature	T_{SOFC}[b]	800°C
Operating pressure	p_{SOFC}	1 bar
Anode temperature difference	ΔT_a	150°C
Cathode temperature difference	ΔT_c	200°C
Anode pressure loss	Δp_a	0 mbar
Cathode pressure loss	Δp_c	0 mbar
Current density	i	300 mA cm^{-2}

[a] 26% H_2, 30% N_2, 18% CO, 12% CO_2, 13% H_2O, and 1% CH_4 by volume.
[b] Equals the SOFC anode and cathode outlet.

First, the influence of current density on the different overpotentials are examined and depicted using product gas similar to that from the Viking gasifier, Figure 4.2, and using hydrogen with 3 vol-% of water, Figure 4.3, as fuels. Also the resulting cell potential and power density is plotted. The dominant polarization loss is the activation overpotential for both fuels, but the concentration overpotential also has great influence when approaching the limiting current density of 1000 mA cm^{-2}. On the contrary, the ohmic overpotential is relatively low, though increasing with current density as for all three overpotentials. The modelled polarization curve and corresponding overpotentials cannot be directly compared to general results from literature because it is calibrated specifically to one TOFC stack. Though, the sizes of the three overpotentials – relative to each other – seem reasonable when compared to the model by Chan et al. for anode supported SOFCs operated at 800°C, at atmospheric pressure, and with hydrogen (fig. 6 in [62]); activation overpotential being the highest, ohmic polarization the lowest, and the losses from gas diffusion limitations in between. Better performance is obtained when using almost pure hydrogen compared to the more dilute product gas. This is due to lower activation overpotential, while the Nernst potential, ohmic losses, and concentration losses seem unaffected by the fuel choice. The average partial pressure of hydrogen after internal steam reforming and WGS ($\bar{p}_{H_2,tot}$), eq. (4.23), is approximately 0.56 bar and 0.28 bar when fuelled with hydrogen and product gas, respectively. The reason is

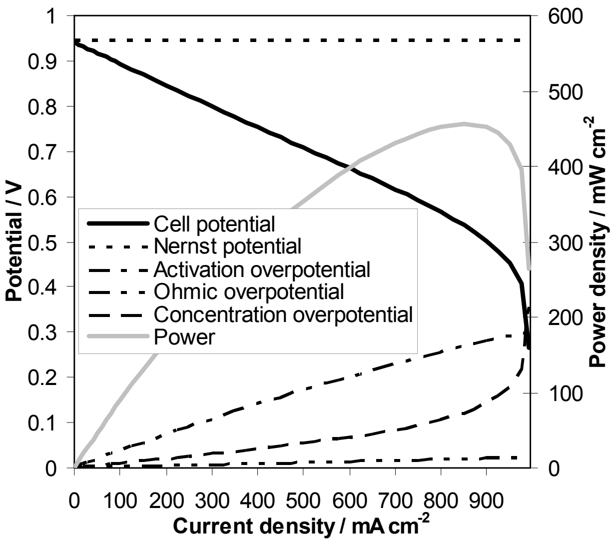

Figure 4.2: Nernst potential, polarization losses and resulting single cell potential and power density as a function of current density, when operating on product gas.

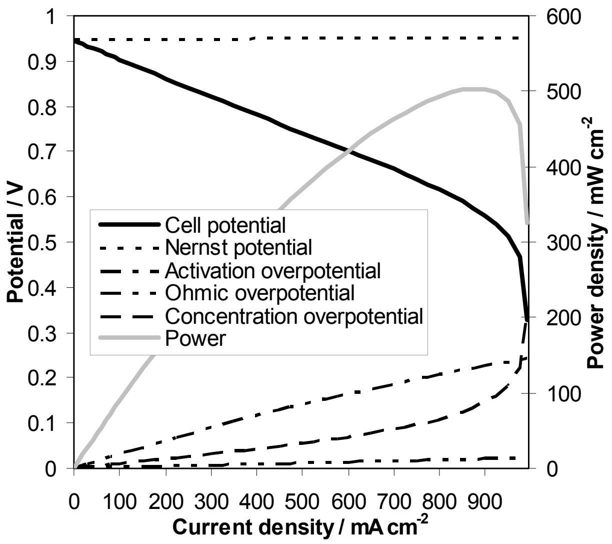

Figure 4.3: Nernst potential, polarization losses and resulting single cell potential and power density as a function of current density, when operating on hydrogen with 3 vol-% of water.

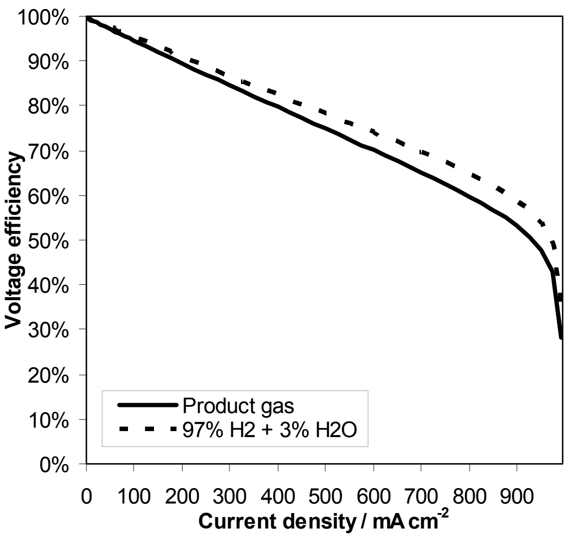

Figure 4.4: Voltage efficiency as a function of current density for two different fuels.

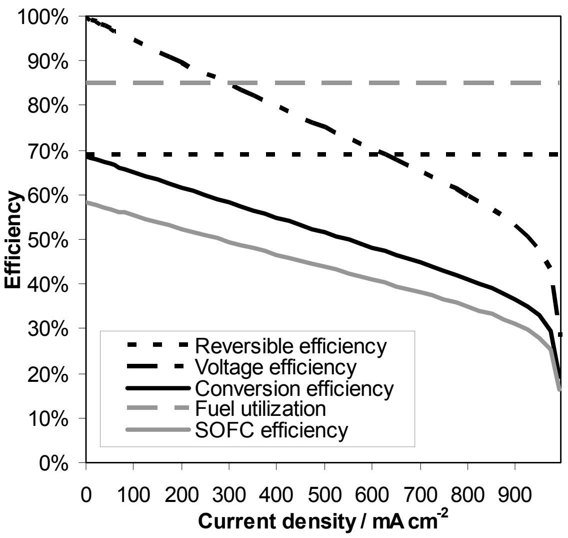

Figure 4.5: Fuel cell efficiencies as a function of current density using product gas.

the inert parts (mainly N_2) in the product gas. Offhand, this should explain the better performance using almost pure hydrogen as fuel. Examining the expressions used in the electrochemical model, it is found that the Nernst potential, eq. (4.24), and the concentration overpotential, eq. (4.33), more exactly are depended on the ratio between $\overline{p}_{\mathrm{H_2,tot}}$ and $\overline{p}_{\mathrm{H_2O}}$, when only varying the fuel composition - $\overline{p}_{\mathrm{O_2}}$ is constantly close to $p_{\mathrm{O_2,in}}$ because a high excess flow of air is used to cool the SOFCs. Since $\overline{p}_{\mathrm{H_2O}}$ is approximately 0.44 bar and 0.24 bar with hydrogen and product gas, respectively, the ratios between $\overline{p}_{\mathrm{H_2,tot}}$ and $\overline{p}_{\mathrm{H_2O}}$ are almost the same with the two fuels (1.26 and 1.14, respectively). Thus, the Nernst potential and concentration overpotential are similar with the two fuels, along with the ohmic overpotential, which is not affected by fuel choice. This leaves only the activation overpotential to be significantly depended on fuel choice, which also can be seen by examining the anodic exchange current density expression, eq. (4.28). In this expression, the anodic exchange current density is depended on the product of, rather than the ratio between, $\overline{p}_{\mathrm{H_2,tot}}$ and $\overline{p}_{\mathrm{H_2O}}$. This product is higher when using hydrogen (0.25 versus 0.07), resulting in a higher anodic exchange current density and, thereby, a lower activation overpotential. In reality, the Nernst potential and concentration overpotential can be affected by fuel choice because using eq. (4.23) ($\overline{p}_{\mathrm{H_2,tot}}$) is not always valid (cf., Appendix J).

In Figure 4.4, the voltage efficiencies, defined in eq. (4.20), resulting from the ratio between the cell potential and the Nernst potential from Figure 4.2 and Figure 4.3, are shown for easy comparison between the two fuel types. Voltage efficiencies are measures of the electrochemical performance of the SOFC. The different fuel cell efficiencies using product gas are depicted in Figure 4.5 as a function of current density. The reversible efficiency, defined in eq. (4.13), is not affected by the load, whereas the voltage efficiency is sensible to the chosen current density because it is proportional to the cell potential. A conversion efficiency is here defined as the product of the reversible efficiency and the voltage efficiency (cf., eq. (4.34)). This conversion efficiency describes how well the *reacting* fuel is converted to electricity, without taking the loss of excess fuel into account. From a system point of view, the conversion efficiency, as it is defined here, can give a better view on the performance of the SOFC when combined with other thermal cycles, e.g., a Brayton cycle. In hybrid systems, excess fuel from the SOFC can be utilized elsewhere and is not necessarily a loss. The fuel utilization might even be kept low to satisfy other parts of the hybrid system than the SOFC.

$$\eta_{\mathrm{conv}} = \eta_{\mathrm{rev}}\eta_{\mathrm{v}} \tag{4.34}$$

By including the fuel utilization factor, the overall SOFC efficiency is obtained. At i=300 mA cm^{-2}, the overall SOFC efficiency from added fuel to electricity is 49%, while the voltage efficiency and conversion efficiency is 85% and 58%, respectively.

As for the study on influence of current density on overpotentials, resulting cell potential and power density as well as the associated efficiencies, the

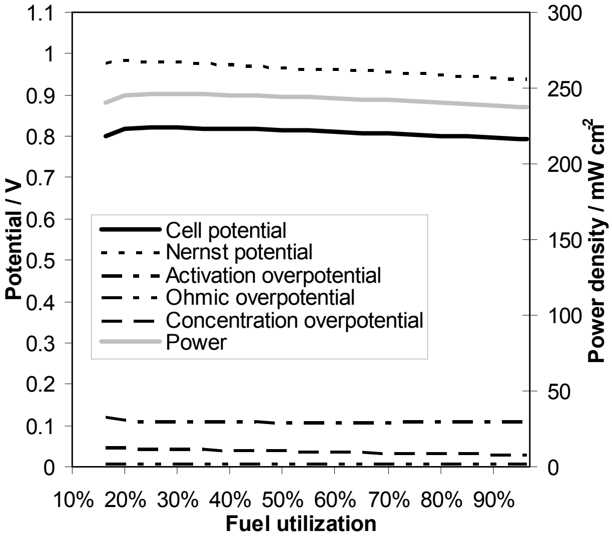

Figure 4.6: Nernst potential, polarization losses, and resulting single cell potential and power density as a function of fuel utilization, when operating on product gas.

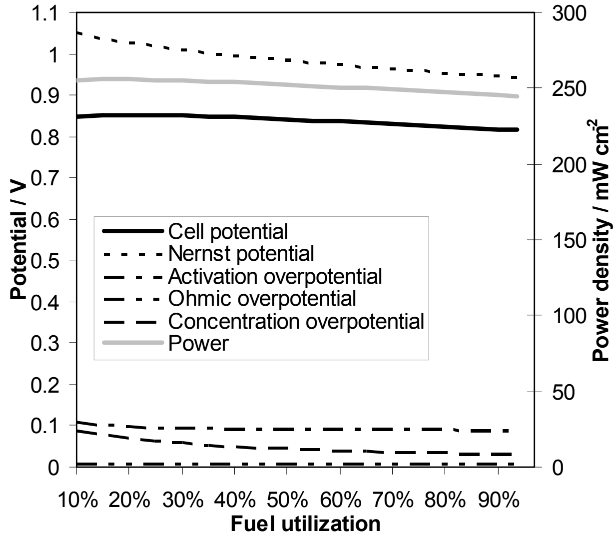

Figure 4.7: Nernst potential, polarization losses, and resulting single cell potential and power density as a function of fuel utilization, when operating on hydrogen with 3 vol-% of water.

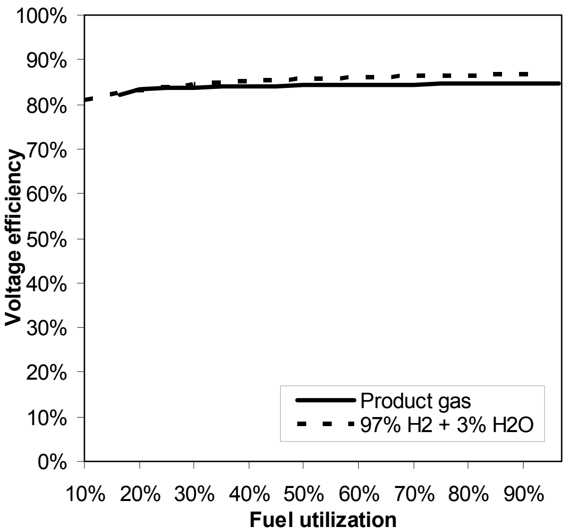

Figure 4.8: Voltage efficiency as a function of fuel utilization for two different fuels.

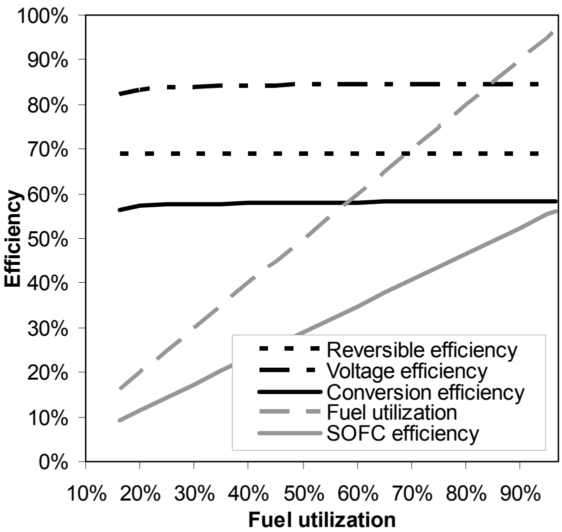

Figure 4.9: Fuel cell efficiencies as a function of fuel utilization using product gas.

following description looks at varying fuel utilization. The reference value of U_F is 85%. When the fuel utilization factor is increased, less unreacted fuel leaves the anode compartment. Thus, the average partial pressure of available hydrogen is reduced and the average partial pressure of water is increased. This explains the decreasing tendency of the Nernst potential with increasing fuel utilization in Figure 4.6 and Figure 4.7. Still, the average partial pressure of oxygen in the cathode flow channel is not changing significantly in most of the fuel utilization range because the excess air flow is very high. Though, at very low fuel utilization, the air flow reduces notably, because the higher fuel flow delivers significant cooling of the SOFC (the air flow is calculated based on the cooling need to maintain the operating temperature). Hereby, the average oxygen partial pressure decreases along with the Nernst potential. Considering the case when fuelling with product gas, the mass flow of air fed to the cathode at U_F=16% is reduced to 17% of the corresponding flow when operating at U_F=85%. This phenomenon ensures the presence of an optimum in the resulting cell potential, which can be seen in Figure 4.6 at approximately 25% fuel utilization. In Figure 4.7, the influence from reducing air flow cannot be seen, since the air mass flow at U_F=16% is only reduced to 85% of the corresponding flow at U_F=85%. Thus, the average partial pressure of oxygen is not notably affected, thereby not decreasing the Nernst potential. Still, the resulting cell potential has an optimum around U_F=20%, but this appears to be due to increased anodic concentration overpotential at low fuel utilization when fuelled by hydrogen with 3 vol-% of water. From eq. (4.33), describing the concentration overpotential, it is evident that the concentration overpotential is only governed by the ratio between $\overline{p}_{H_2,tot}$ and $\overline{p}_{H_2O}$ when changing the fuel utilization. In the case of using hydrogen with 3 vol-% of water, this ratio increases more when lowering the fuel utilization factor than in the case using product gas (at U_F=85%, the ratios between $\overline{p}_{H_2,tot}$ and $\overline{p}_{H_2O}$ are 1.3 and 1.1 for hydrogen and product gas, respectively, while at U_F=16%, the ratios are 8.1 and 3.0, respectively). This explains the more pronounced increase in the concentration overpotential when decreasing the fuel utilization in the case of using almost pure hydrogen versus using product gas.

The voltage efficiencies at varying fuel utilization, when using either hydrogen or product gas, are compared in Figure 4.8. The electrochemical performance when fuelled by humidified hydrogen is slightly higher when the fuel utilization is above 30%. In Figure 4.9, the reversible efficiency, when fuelled by product gas, is constantly 69% no matter the chosen fuel utilization. The reversible efficiency is only depended on the fuel composition at inlet as well as the operating temperature and pressure. The voltage efficiency is not very sensitive to the fuel utilization, and similar for the conversion efficiency. From this, it can be concluded that the *reacting* product gas in the SOFC is converted almost equally efficient above U_F=25%. The picture changes radically, if the loss of excess fuel is taken into account. If so, the fuel utilization should be maintained at a high level. The importance of utilizing all the fuel is evident, but can also be done downstream the SOFC.

The performance of SOFCs depends significantly on the chosen operating temperature as illustrated in Figure 4.10 to Figure 4.13. Decreasing the tem-

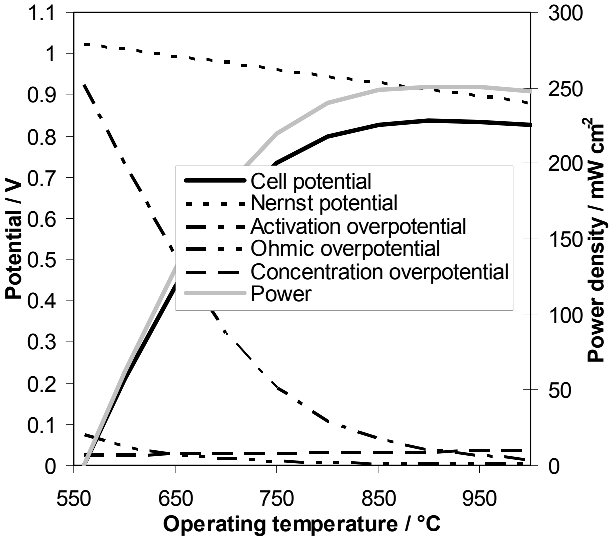

Figure 4.10: Nernst potential, polarization losses, and resulting single cell potential and power density as a function of operating temperature, when operating on product gas.

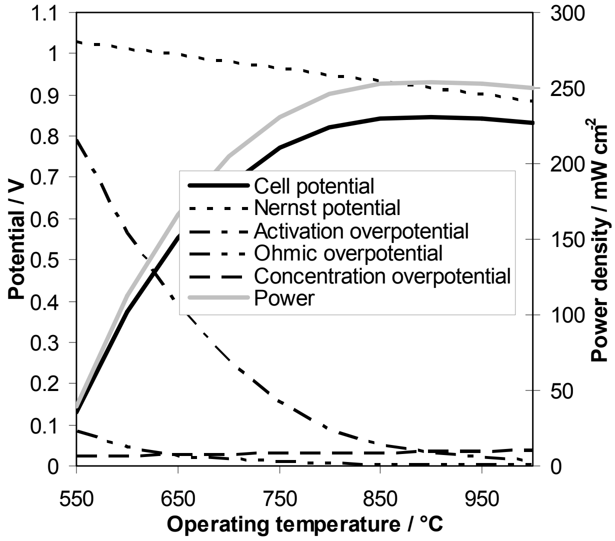

Figure 4.11: Nernst potential, polarization losses, and resulting single cell potential and power density as a function of operating temperature, when operating on hydrogen with 3 vol-% of water.

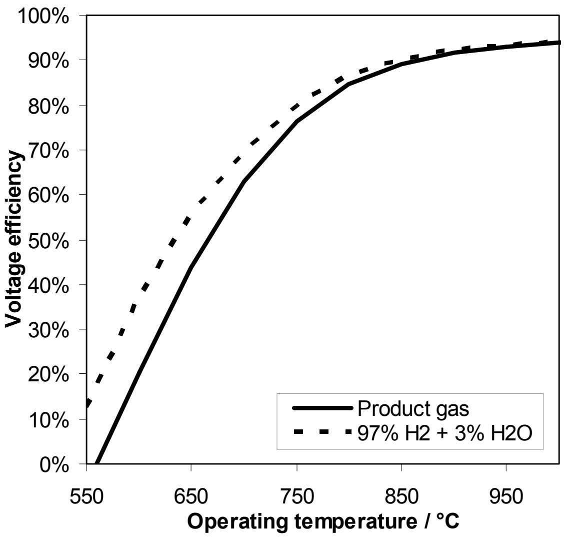

Figure 4.12: Voltage efficiency as a function of operating temperature for two different fuels.

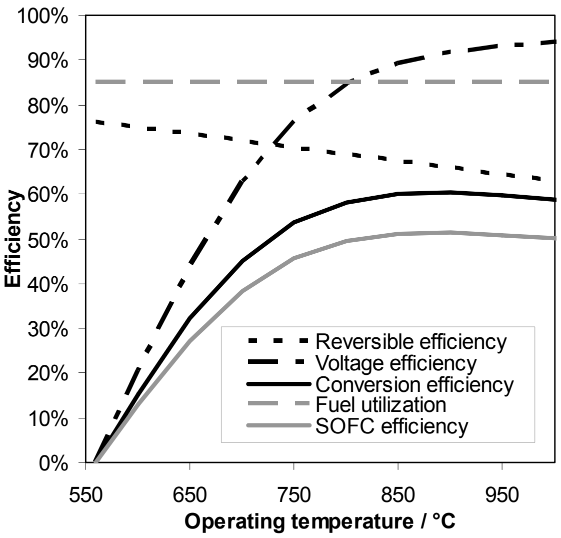

Figure 4.13: Fuel cell efficiencies as a function of operating temperature using product gas.

perature from the reference value of 800°C severely degrades the performance no matter the chosen fuel. From Figure 4.10 and Figure 4.11, it is obvious that the major contributor to the performance trend is the activation overpotential. Lowering the temperature increases the activation overpotential dramatically. From eq. (4.27), it seems that the activation overpotential should increase with increasing temperature, but the exchange current densities, eqs. (4.28) and (4.29), ensure the opposite trend. This underlines the importance of using temperature depended exchange current densities in the model, and not constants, if the model should be able to predict the performance at various temperature levels. At lower temperature, the ionic conductivity of the electrolyte (σ_e), eq. (4.32), decreases causing the ohmic overpotential to increase. The concentration overpotential, on the other hand, is directly proportional to the temperature, as seen in eq. (4.33), so the losses from limited gas diffusion increases with rising temperature, though very moderately. The Nernst potential, eq. (4.24), shows a decreasing trend at rising temperature, which dominates and causes the resulting cell potential to drop, when the temperature is above 900°C.

Considering both fuels in Figure 4.12, it can be concluded, that the electrochemical performance increase with rising temperature in all of the shown temperature range. Contrary for product gas in Figure 4.13, the reversible efficiency, eq. (4.13), decrease with increasing temperature causing the conversion efficiency, eq. (4.34), and the overall SOFC efficiency, eq. (4.12), to peak around 900°C at approximately 60% and 51%, respectively. The decreasing tendency of the reversible efficiency at rising temperature is due to the lower change in the Gibbs free energy of formation (cf., eq. (4.14)) at higher temperature.

The influence of operating pressure is depicted in Figure 4.14 to Figure 4.17. None of the overpotentials are depended on the operating pressure. The only parameters, included in the expressions describing the overpotentials, which are depended on pressure, are either ratios between partial pressures or ratios between partial pressure and absolute pressure, the latter being equal to the molar fraction. On the other hand, the Nernst potential, eq. (4.24), increases with growing pressure, improving the resulting cell potential. The increasing tendency with growing pressure in eq. (4.24) only originates from the increasing oxygen partial pressure because the increasing partial pressure of hydrogen and water counterbalance each other.

The voltage efficiencies for the two studied fuel types are rather constant with varying pressure as depicted in Figure 4.16. Increasing the operating pressure from 1 to 20 bar improves the voltage efficiency from 84.5% to 85.6% in the case of running on product gas and from 86.5% to 87.4% running on hydrogen. The reversible efficiency, eq. (4.13), in Figure 4.17

shows an increasing trend with growing pressure. This is a result of an increase in the change in Gibbs free energy of formation (cf., eq. (4.14)), which is evaluated at the partial pressure of the specific reactant or product species. Hereby, the resulting SOFC efficiency shows a moderate sensitivity to the chosen operating pressure. The performance gain from increasing the pressure is greatest in the low pressure region near, atmospheric conditions, expressed by the higher slope.

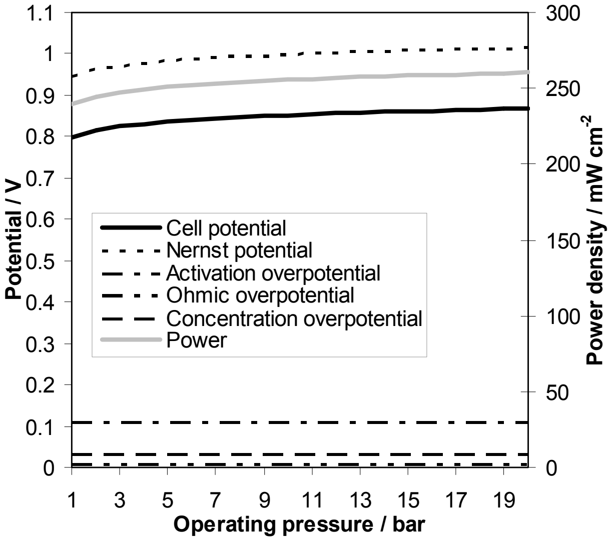

Figure 4.14: Nernst potential, polarization losses, and resulting single cell potential and power density as a function of operating pressure, when operating on product gas.

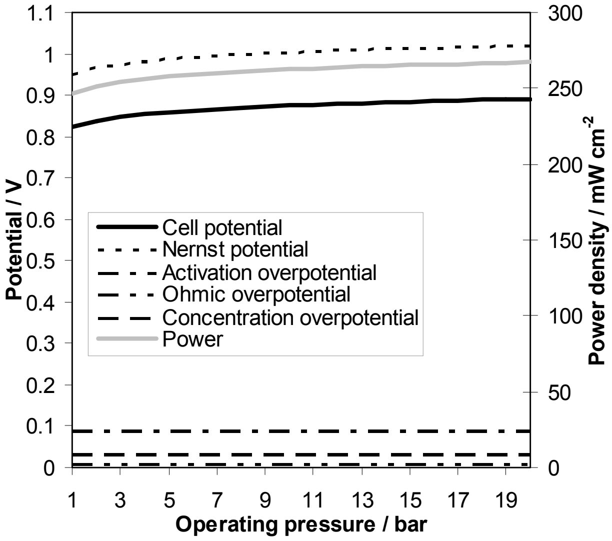

Figure 4.15: Nernst potential, polarization losses, and resulting single cell potential and power density as a function of operating pressure, when operating on hydrogen with 3 vol-% of water.

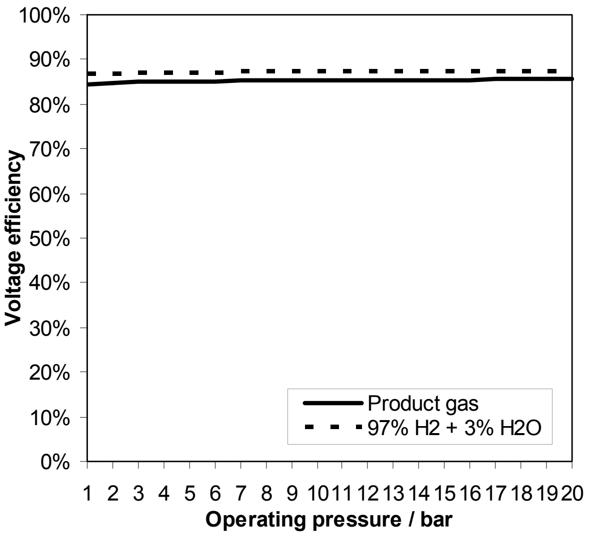

Figure 4.16: Voltage efficiency as a function of operating temperature for two different fuels.

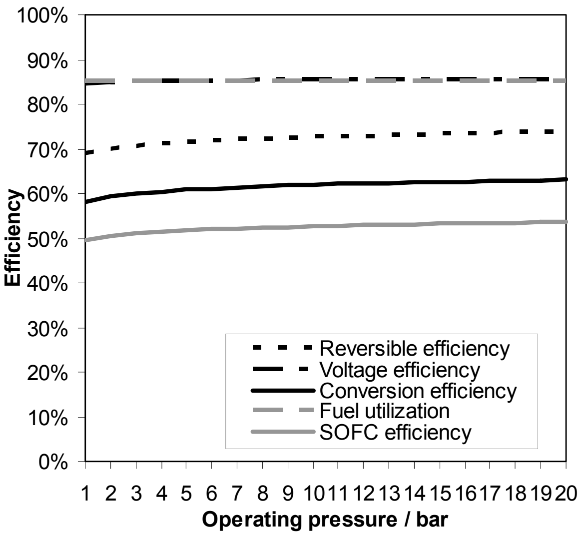

Figure 4.17: Fuel cell efficiencies as a function of operating temperature using product gas.

4.3 SUMMARY

An SOFC component model has been developed for use in process simulations. The component model is zero-dimensional, but still predicts the electrical power production of SOFCs at various operating conditions and fuel types. This is convenient when optimizing important system parameters.

Calibration of the SOFC component model was performed against literature, with the aim of representing the SOFC performance of 2nd generation SOFCs from Topsoe Fuel Cell A/S and Risø DTU (National Laboratory for Sustainable Energy).

The SOFC component model can also be used to evaluate the influence of operating conditions on the SOFC performance. This was examined in the parametric study. The SOFC performance showed to be highly sensitive to the selected current density (cf., Figure 4.5 when fuelled by product gas). Higher current density reduces the SOFC efficiency. The electrical power production increases with increasing current density, though, until closing in on the limiting current density. From an energy efficiency viewpoint, the current density should be as low as possible, but to produce a specified amount of electrical power, lowering the current density will increase the investment costs. Thus, from an economical viewpoint, an optimal current density exists at a higher level compared to that of an energy efficiency viewpoint. Varying the fuel utilization factor greatly impacts the resulting SOFC efficiency, and Figure 4.9 implies that the fuel utilization should be maintained at a high level. Still, the electrochemical performance is rather insensitive to the chosen fuel utilization in most of the studied range of fuel utilization. At very low fuel utilization, the fuel flow becomes high enough to cool the SOFC significantly. Thus, a limited air flow can reduce the SOFC performance because the air flow is calculated based on the cooling need. Also, the efficiency from producing electricity from the *reacting* fuel in the SOFC is almost constant. Hereby, the fuel utilization can be changed, for reasons originating in the rest of the system, without decreasing or increasing how efficiently the reacting fuel in the SOFC is converted to electricity. The influence of temperature on the SOFC performance is severe. The electrochemical performance increases with temperature (cf., Figure 4.13 for the case of product gas), but the overall SOFC efficiency reaches a peak at high temperature due to the decreasing reversible efficiency. It should be noted, that the model is not validated in all of the temperature range shown in Figure 4.13, but only at 800°C. The whole range is included to ease the understanding of the reasons to the temperature dependency of the SOFC performance. The sensitivity of the SOFC performance to the chosen operating pressure is only moderate. The SOFC efficiency shows an increasing trend with increasing pressure, but highest impact of increasing pressure is obtained just above atmospheric pressure, while less impact shows at higher pressures. Thus, the operating pressure does not necessarily need to be maximized.

The parametric study shows that the SOFC performance predicted by the SOFC component model is depended on the different operating conditions. The described dependencies can also be used as guidelines for optimal SOFC operation. The component model is accepted for further use in the coming system-level models.

Chapter 5 DEVELOPMENT OF THE PROCESS MODELS

Mathematical models describing the thermodynamic processes of the three studied scenarios have been developed to be able to investigate their steady-state performances. The models rely on connecting zero-dimensional component models to generate complete system-level models. As mentioned in the introduction to Chapter 4, the simulation tool used in this modelling study is DNA (Dynamic Network Analysis), which is made for simulations of mathematical models representing thermodynamic processes. Plant model listings can be found in Appendix C, Appendix D, and Appendix E.

Minor adjustments in the system layouts are made for the mathematical models compared to the chosen systems presented in Chapter 3, Figure 3.1. These can be seen in Figure 5.1 and are; mixing of dryer steam and preheated air before introduction to the gasification reactor, and removal of all impurities in a gas cleaning unit instead of only particulates in a bag filter. The reason for mixing preheated air and dryer steam is that the gasifier component model is defined in such a way that the solid feedstock enters separately from gases. Since it is assumed that the product gas after particulate removal is clean enough in this study, and that the impact of remaining impurities are neglected, a simple gas cleaning component model removing all impurities is used. Not illustrated is an inverter, converting the SOFC electric power production from DC to AC, as well as a generator situated on the shaft of the gas turbine producing the net electric MGT power. In the SOFC configuration (without a MGT), the product gas and air blowers are driven by an electric motor. Furthermore, it is assumed that heat losses from components (except the inverter and generator) and pipework are neglected, and that carbon deposition will not occur in any components.

The stated temperatures in Figure 5.1 are the chosen temperature conditions for the studied scenarios. Some of the values are given in the component models, and the rest can be found in Table 5.1 that contains the system-level inputs. 15°C and atmospheric pressure are the ambient conditions, and regarding pressures in the system, these are defined in some components and calculated from stated pressure drops elsewhere.

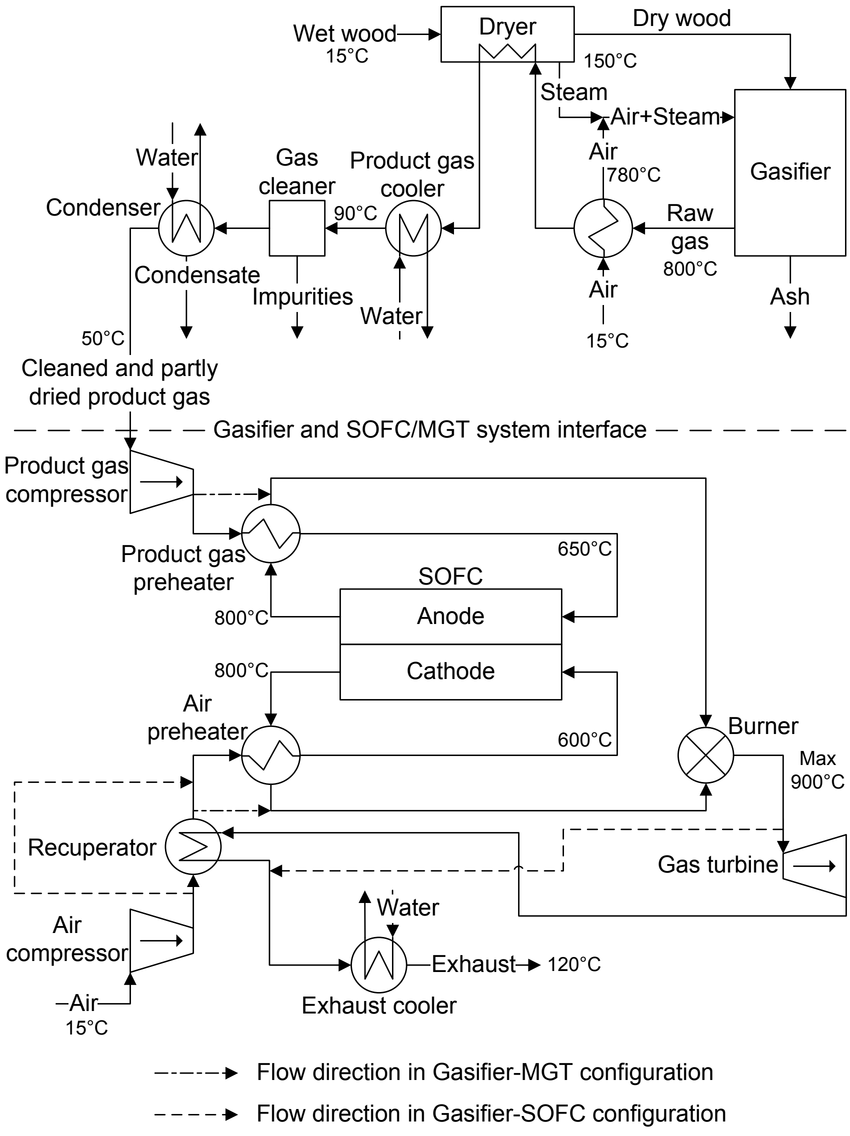

Figure 5.1: Flow sheet of modelled scenarios with specified temperature conditions.

The raw gas temperature of 800°C coming out of the gasification reactor is defined in the gasifier component model, and likewise for the SOFC electrode outlets, the off gas temperatures of 800°C are defined in the SOFC component model. The preheated air for the gasifier (780°C), the preheated product gas (650°C), the preheated air for the SOFC (600°C), and the exhaust gas temperature (120°C) are all defined indirectly by introducing a pinch point temperature difference in the heat exchanger component models (cf., Table 5.7). The gas cleaning temperature (90°C) and temperature of the cleaned and partly dried product gas leaving the gasification plant (50°C) are equal to those of the Viking demonstration plant.

The mass flow of air fed to the SOFC cathode is calculated based on the cooling need of the SOFC to be able to keep its operating temperature. The pressure on the cathode side is derived from the anode side through the burner submodel, which sets the pressure of fuel and oxidant feed to be equal.

Table 5.1: System-level inputs.

Media	T / °C	p / bar	$\dot{m}$ / kg h^{-1}
Wet wood	15	1.013	154.8[a]
Dry wood	150		
Ambient air (gasifier)	15		
Ash		1.013	
Cooled product gas	90		
Cleaned and partly dried product gas	50		
Burner fuel inlet / preheated product gas (anode inlet)		Varied[b]	
Ambient air (SOFC/MGT)	15	1.013	
Exhaust		1.013	

[a] Corresponds to a thermal input of 499.2 kW_{th} (LHV).

[b] Defined in the burner inlet in the MGT scenario, the anode inlet in the SOFC-MGT scenario, and is not an input in the SOFC configuration.

Table 5.2: Solid biomass data.

Ultimate analysis / wt-% (dry)		
C	48.8	[11]
H	6.2	[11]
O	43.9	[11]
S	0.02	[11]
N	0.17	[11]
Ash	0.91	[11]
Properties		
LHV	18.28 MJ kg^{-1} (dry)	[11]
c_p	1.35 kJ kg^{-1} K^{-1}	
x_{H2O}	32.2 wt-%	[11]

Table 5.3: Air composition, predefined in DNA.

Compound	Molar fraction / vol-%
N_2	77.29
O_2	20.75
H_2O	1.01
Ar	0.92
CO_2	0.03

The input media to the process is solid biomass and air, and these are specified in Table 5.2 and Table 5.3, respectively. The solid biomass used in this work is the same as used in the Viking gasifier as published by Ahrenfeldt et al. [11]. The biomass feedstock is added as woodchips of primarily beech with small amounts of oak [11]. The small amount of chlorine documented in [11] is not included in the solid biomass in this study. Anyway, the main part of the chlorine in the biomass published by Ahrenfeldt et al. [11] originates from spraying the wood with seawater to avoid it from drying up when stored and not from the biomass source itself.

All the inputs to the system-level models can be found by collecting data from Table 4.1, Table 4.2, Table 5.1, Table 5.2, Table 5.3, Table 5.4, Table 5.6, and Table 5.7.

5.1 SUBMODELS

Connecting submodels of the different components constitute the total process model. In the following, documentations of the employed component models are presented. Main components in the total process are the gasifier and the SOFC, while components like heat exchangers are considered peripheral. The MGT consists of several components, but these are described together in one Section below because the MGT components are considered as connected in one main technology of the total process. The SOFC component model is described in detail in Chapter 4, therefore not described here. Direct input parameters stated in the component model descriptions below are user defined inputs. In addition to these, the submodels get inputs from their connections to the rest of the system. These can be user defined from a system level (Table 5.1) or outputs from other component models.

5.1.1 GASIFIER

The gasifier component model calculates the product gas composition and the produced ashes based on the inlet media compositions and the operating conditions. The input parameters defining the operating conditions in the gasifier submodel are given in Table 5.4. The gasifier pressure loss is defined as the difference between the inlet air and steam mixture and the outlet product gas.

Table 5.4: Direct inputs to the gasifier submodel.

Operating pressure	$p_{\text{gasifier}}{}^{a}$	0.998 bar
Operating temperature	$T_{\text{gasifier}}{}^{a}$	800°C
Pressure loss	$\Delta p_{\text{gasifier}}$	5 mbar
Carbon conversion factor	CC	1
Additional non-equilibrium methane in product gas	$METH$	0.01 vol-%[b]

[a] Equals the gasifier outlet.

[b] Determined by calibration (cf., Section 5.1.1.1).

In the gasifier, the incoming flows are converted into product gas and ashes. The ashes are represented by SiO_2 and unconverted carbon. SiO_2 originates from a defined content in the inlet biomass, while the unconverted carbon is controlled by a defined carbon conversion factor (*CC*). The amount and composition of ashes are calculated by eqs. (5.1), (5.2), and (5.3).

$$\dot{m}_{\text{ash,out}} = \dot{m}_{\text{wood,in}}[x_{\text{SiO}_2\text{,in}} + x_{\text{C,in}}(1 - CC)] \tag{5.1}$$

$$x_{\text{SiO}_2\text{,out}} = \frac{\dot{m}_{\text{wood,in}} x_{\text{SiO}_2\text{,in}}}{\dot{m}_{\text{ash,out}}} \tag{5.2}$$

$$x_{\text{C,out}} = 1 - x_{\text{SiO}_2\text{,out}} \tag{5.3}$$

As for the SOFC submodel, it is assumed that chemical equilibrium is reached at outlet at the operating temperature and pressure, so the Gibbs free energy minimization method is applied (cf., Appendix A). The product gas from the gasifier model can consist of the following chemical compounds at equilibrium: H_2, N_2, CO, CO_2, H_2O, CH_4, H_2S, and Ar.

An option for adjusting the methane content in the product gas is included in order to reach product gas compositions, which contain more methane than in the corresponding composition at equilibrium. Thus, the product gas composition can be adjusted to match realistic gas compositions, e.g., from the Viking gasifier. The input parameter *METH* is used for this adjustment and is defined as the amount of additional methane in the product gas that does not originate from the equilibrium calculations.

5.1.1.1 Gasification Process Calibration

In the following Section, the gasification process is calibrated. To calibrate the gasification process modelled here, all of the modelled gasification plant, from the biomass feedstock to the cleaned and dried product gas, is compared to the complete Viking gasifier plant. Both the test data from the Viking gasifier and calculated data from the gasifier model are based on a biomass feedstock as reported by Ahrenfeldt et al. [11] and described in Table 5.2. In the gasifier model, the parameter *METH* is adjusted to achieve an acceptable CH_4 content in the product gas. By setting *METH* equal to 0.01 vol-% (as shown in Table 5.4), the calculated dry gas composition becomes similar to that of the Viking gasifier. As seen in Figure 5.2 and Table 5.5, the produced gas composition and the LHV from the gasifier model are close to the Viking data. The CO_2 content shows the greatest deviation, whereas the resulting LHVs are similar. The overall performance of the modelled gasifier is also similar to that of the Viking gasifier, as indicated by the cold gas efficiencies (defined in eq. (2.8)).

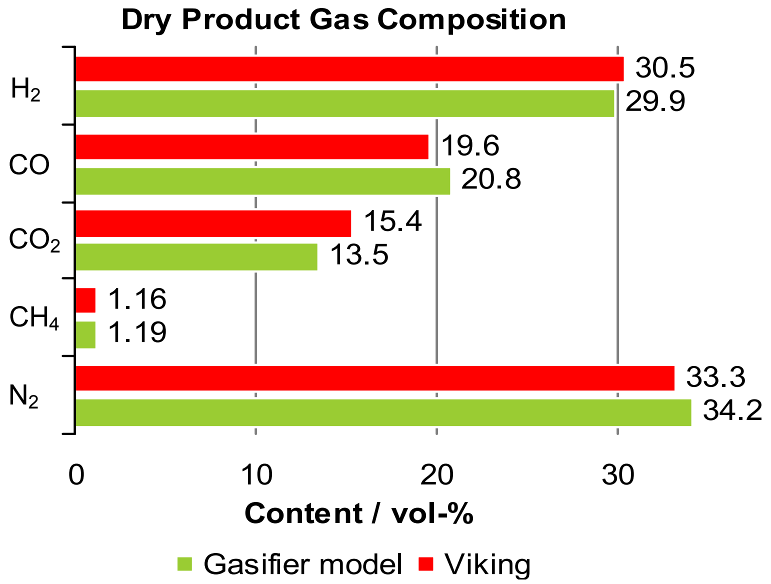

Figure 5.2: Comparison of dry product gas composition from the gasifier model with experimental data [11] from the Viking gasifier.

Table 5.5: LHV and cold gas efficiency of the gasifier model and the Viking gasifier.

	Gasifier model	Viking gasifier [11]
LHV (MJ kg^{-1})	6.3	6.2
Cold gas efficiency	94%	93%

5.1.2 Micro Gas Turbine

Modelling of gas turbines is well described in the open literature. The reader is referred to Saravanamuttoo et al. [40] for details. Characteristics of the turbomachinery and other components connected to the MGT are listed in Table 5.6. The MGT components are only used in the MGT and SOFC-MGT configurations. In the SOFC case, fuel and air blowers are used instead of compressors, and these are driven by electric motors. Inputs related to the components in the SOFC configuration can be found in the next Section describing peripheral equipment.

Table 5.6: Inputs related to the MGT components.

	Isentropic eff. / %	Mechanical eff. / %	
Fuel and air compressor[a]	75	98	
	Isentropic eff. / %	TIT / °C	
Gas turbine expander[a]	84	900[b]	
	Δp		
Burner	0.6‰[c]		
	$\Delta p_{\text{hot side}}$ / mbar	$\Delta p_{\text{cold side}}$ / mbar	ε / %
Recuperator[a]	10	10	85
	Efficiency / %		
Generator[a]	95		

[a] Only used in the MGT and SOFC-MGT configurations.
[b] Only an input in the MGT configuration.
[c] 0.6‰ equals 1.5 mbar if 2.5 bar is present at the inlet.

The air and product gas compressor submodels calculate the mechanical power required to increase the pressure of the working fluid. This is done based on specified isentropic and mechanical efficiencies. The gas turbine submodel works in the same manner as the compressor submodels, except that no mechanical losses are taken into account. The turbine inlet temperature is limited to 900°C in the Gasifier-MGT case, while it varies in the SOFC-MGT arrangement. The performances of the compressors and MGT expander correspond to common performance data for a MGT of this scale, e.g., see [44], but it should be noted that the operating conditions are non-conventional due to a low turbine inlet temperature in the SOFC-MGT case and a low heating value of the fuel gas in all cases. The outlet pressure from the MGT expander depends on the total pressure loss downstream the MGT, because of the plant exhaust pressure, which is fixed at 1.013 bar. Because of the pressure drop in the recuperator and exhaust cooler, the outlet pressure from the MGT expander is slightly higher (1.033 bar). Constant heat exchanger effectiveness is applied to the recuperator to ensure realistic performance.

5.1.3 Peripheral Equipment

Besides the gasifier and SOFC component models, modelling the rest of the components are mostly standard. These are therefore not described in detail, but are briefly discussed below. Furthermore, the peripheral equipment component models are not considered for validation or calibration.

The biomass dryer reduces the water content in the biomass from 32.2 wt-% to 5 wt-% by heating it to 150°C. During the drying process in the Viking gasifier, the hot product gas directly heats the biomass in a stream separated dryer. Contrary, the upscaled two-stage gasification process (cf., Figure 2.3) uses steam drying by heating a steam loop. In the latter case, the steam is in direct contact with the biomass. The modelling of the drying process is done by introducing a steam loop to transfer the heat from the product gas to the biomass as illustrated in Figure 5.3. The superheated steam dries the biomass, and the moisture from the biomass leaves the dryer together with the hot steam. The excess steam is separated from the steam loop and is exactly equal to the amount that evaporates from the biomass. To model a stream separated dryer as in the Viking gasifier, pressure and heat losses in the steam loop are set equal to zero and the steam blower is assumed to be ideal. By means of this, the drying process model will correspond to heating the biomass directly with hot product gas in a stream separated dryer component. Introducing pressure losses in the steam loop, along with realistic isentropic and mechanical efficiencies of the steam blower, will correspond to modelling of the steam drying process of the upscaled two-stage gasification concept. In this study, the steam drying process of the upscaled two-stage gasification concept is used.

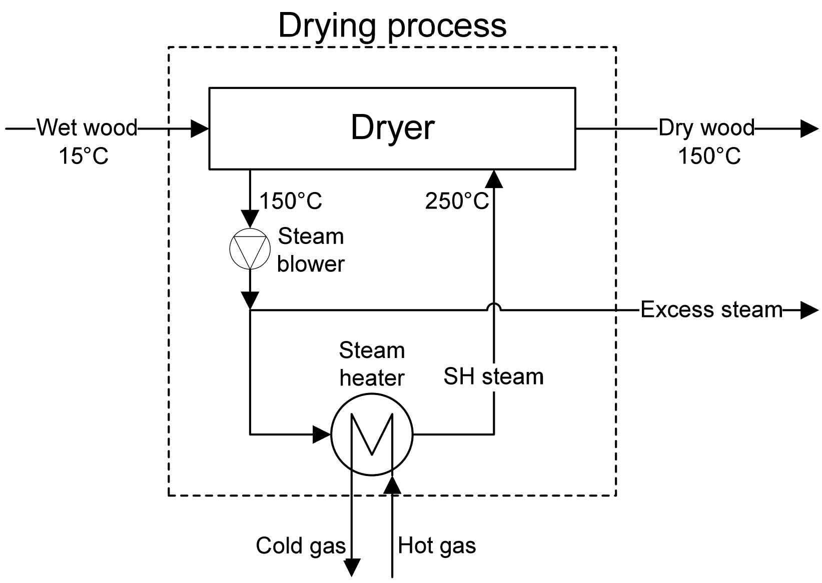

Figure 5.3: Layout of modelled drying process.

The pressure loss in every component in the SOFC air supply stream and burner exhaust stream is assumed to be 10 mbar, whereas the pressure loss in each of the remaining components is assumed to be 5 mbar; the exception being the burner, which has a pressure loss of 0.6‰ of the inlet presure. In [2], a pressure loss of 4.9 mbar is reported for the gas cleaner in the Viking gasifier, which fits well with the 5 mbar assumption used here. The pressure losses defined in the peripheral components are shown in Table 5.7 along with other inputs.

Table 5.7: Direct inputs to the peripheral equipment

Heat exchangers			
	$\Delta p_{\text{hot side}}$ / mbar	$\Delta p_{\text{cold side}}$ / mbar	ΔT_{pinch} / °C
Air preheater (gasifier)	5	5	20
Steam heater (dryer)	5	5	
Product gas cooler	5	5	
Condenser	5	5	
Product gas preheater [a]	5	5	150
Air preheater (SOFC)[a]	10	10	200
Exhaust cooler	10	5	90
Turbomachineries			
	Isentropic eff. / %	Mechanical eff. / %	
Fuel and air blower[b]	60	98	
Steam blower (dryer)	60	98	
Others			
	$\Delta p_{\text{biomass}}$ and Δp_{steam} / mbar	$x_{\text{H2O,dry wood}}$ / %	$T_{\text{SH steam}}$ / °C
Drying process	5	5	250
	Δp		
Gas cleaner	4.9 mbar [2]		
Burner	0.6‰		
	Efficiency / %		
Inverter (DC to AC)	95		
Electric motor[b]	95		

[a] Only used in the SOFC and SOFC-MGT configurations.
[b] Only used in the SOFC configuration.

As previously mentioned, the pinch point temperature differences in the SOFC air and product gas preheaters and the exhaust cooler are used as indirect inputs to define outlet temperatures. For the case of the SOFC preheaters, and within the studied SOFC operating temperature range, this means that when changing the SOFC operating temperature, the temperature difference between inlet and outlet is kept constant. The condenser removes some of the water content in the product gas, resulting in a water content of 12.7 vol-%. The resulting S/C ratio is 0.41, which is somewhat low, but it is justified by the very low tar content in the clean product gas and the high fuel utilization in the SOFC. Hoffman et al. [14] used a S/C ratio of 0.5 and a fuel utilization of 30% when successfully operating SOFCs fed with cleaned product gas from the Viking gasifier. As mentioned in Section 2.2.1, increasing the fuel utilization should make SOFCs able to operate at lower S/C ratios. If necessary, water/steam could be added to the product gas stream before the SOFC, but that is not considered in this work.

Because the air and product gas compressors work as blowers in the SOFC scenario, a lower isentropic efficiency of 60% is used in that scenario. The steam blower used for steam drying is acting as a blower in all scenarios.

The gas cleaner component model simply separates all trace species from the product gas stream and adds a pressure loss to the system. The burner component model assumes perfect combustion and calculates the exhaust gas composition and temperature. The only components having a heat loss are the electrical generator/motor and the DC/AC inverter, where conversion losses are applied for either conversion between electrical and mechanical power or conversion from DC to AC electric power.

Chapter 6 SIMULATIONS OF THE CONCEPTUAL PLANT DESIGNS

By use of the developed models, the simulation tool DNA is used to generate system performance results for the plant configurations investigated. The behaviour of the different plant concepts are studied and discussed by varying critical operating conditions, providing an overview of the optimal conditions and performance of each plant configuration.

Detailed descriptions of the simulated system configurations can be found in Chapter 3. The inputs presented in the previous Chapter 4 and Chapter 5 are also used in these simulations unless otherwise stated.

6.1 PARAMETRIC STUDY OF SYSTEM PERFORMANCES

6.1.1 PRESSURE RATIO

The performance of the different system configurations vary greatly with the operating conditions, and the chosen pressure ratio is of great importance to the resulting system performance. As traditionally, the pressure ratio is defined over the air compressor, and, as seen in Figure 6.1, the different system configurations have different optima with regard to this operating pressure ratio. In Figure 6.2, the corresponding turbine inlet temperatures (TIT), turbine outlet temperatures (TOT), and air compressor outlet temperatures (COT) are shown for the two pressurized systems.

When operating at a constant TIT of 900°C, the MGT configuration shows an optimum at a pressure ratio of 3.7, performing with an electric efficiency of 26.8% (LHV). The recuperator ensures an optimum at a relatively low pressure ratio (see explanation in the end of Chapter 3). Obviously, the pressure in the SOFC case is constantly near atmospheric pressure, because the gain in SOFC performance at elevated pressure is less than the losses associated with generating the higher pressure. This system performs at an electrical efficiency of 43.1% at a pressure ratio close to 1. The SOFC configuration has a higher efficiency because conversion in the SOFCs is more efficient than in the MGT, but the SOFCs cannot utilize all of the fuel. With a fuel utilization of 85%, a substantial portion of the fuel passes through the anode and is converted to heat in the burner. By combining the SOFC and MGT in the SOFC-MGT configuration, this heat can be used for additional electricity production. At the optimum operating pressure ratio of 2.5, the combined system configuration reaches an electrical efficiency of 55.0%, thereby outperforming the two simpler configurations. The substantial increase in efficiency is mainly the result of better utilization of unconverted fuel and excess heat from the SOFCs, but it is also due to the pressurized operation of the SOFCs.

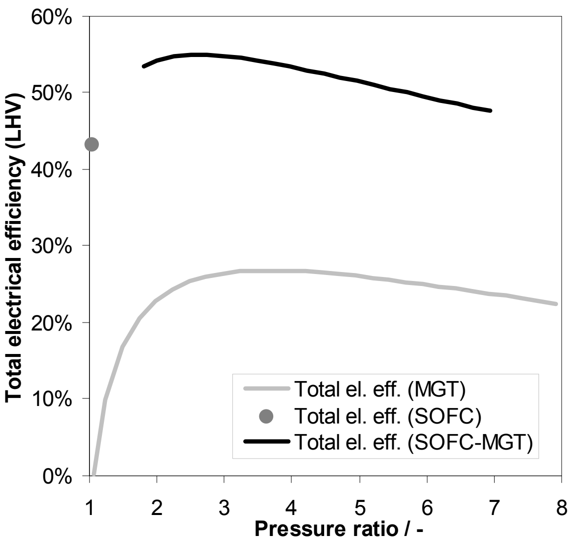

Figure 6.1: Energetic electric efficiency at different operating pressure ratios. The operating pressure ratio is defined over the air compressor.

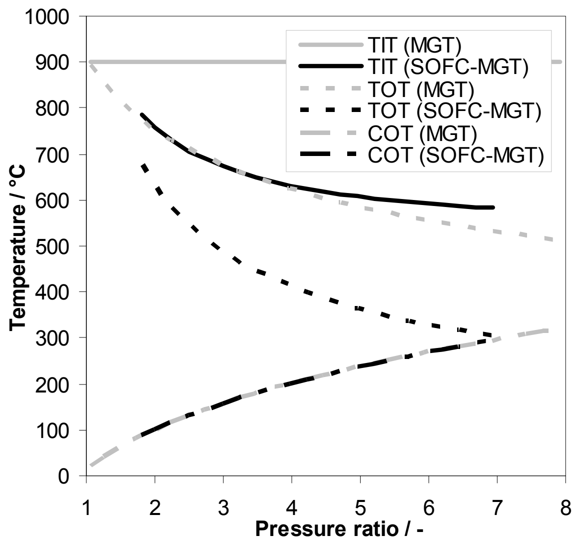

Figure 6.2: Turbine inlet temperatures (TIT), turbine outlet temperatures (TOT), and air compressor outlet temperatures (COT) at different operating pressure ratios. Only the two pressurized system scenarios are illustrated.

In the MGT configuration, the TIT is an input and constant because the air flow fed to the burner is not known from the cooling need of the SOFC stack, contrary to the SOFC-MGT configuration. In the SOFC-MGT arrangement, the TIT decreases with an increasing pressure ratio. This relationship is due to the fact that an increasing *PR* increases the COT and reduces the TOT, which means that less heat is transferred in the recuperator. Therefore, more heat must be transferred in the SOFC air preheater to reach the same cathode inlet temperature. More heat transfer in the SOFC air preheater results in a lower temperature of the cathode off gas fed to the burner, thus decreasing the TIT. Furthermore, the TIT is lower in the SOFC-MGT case compared to the MGT scenario because less fuel is used to produce heat in the burner. A TIT of 706°C is reached at a *PR*=2.5. The optimal *PR* is lower in the SOFC-MGT scenario relative to the MGT arrangement due to the lower TIT. Characteristically, lowering the TIT of a recuperated gas turbine will lower the optimal *PR*. The slight increase in the SOFC efficiency observed with increasing pressure is not sufficient to change the resulting electrical efficiency trend of the hybrid system. Note that above a *PR* of approximately 6.7 in the SOFC-MGT case, the TOT becomes lower than the COT, making it impossible to use a recuperator. Below a *PR*=1.8, the heat transfer in the recuperator is sufficiently high to heat the air above the desired cathode inlet temperature.

6.1.2 Operating MGT/SOFC Temperature

The performance of the MGT configuration is also dependent on the allowed TIT as depicted in Figure 6.3. Decreasing the TIT by 100°C to 800°C lowers the electrical efficiency to 24.3% - a drop of 2.5 percentage points. Considering the SOFC configuration, the sensitivity to the SOFC operating temperature is even greater than the sensitivity to the TIT in the MGT case. Lowering the SOFC operating temperature by 100°C to 700°C decreases the electrical efficiency to 32.8% - a drop of 10.3 percentage points. This differential effect indicates that the SOFC operating temperature has a greater influence on SOFC performance than the TIT has on MGT performance in the mentioned temperature range. In the SOFC-MGT configuration, a drop in the SOFC operating temperature of 100°C to 700°C decreases the electrical efficiency to 47.2% - a drop of 7.8 percentage points. Furthermore, the two scenarios incorporating SOFC technology reveals an optimum operating SOFC temperature of approximately 900°C. This is a result of a reducing reversible efficiency of the SOFC with increasing temperature, which also was illustrated in the parametric study of the SOFC model, see Figure 4.13. In the SOFC-MGT scenario, the SOFC operating temperature cannot get below approximately 650°C, because at such a low operating temperature, the recuperator heats the air intake above the desired cathode inlet temperature.

The progress in research and development aimed at lowering the SOFC operating temperature may facilitate the use of cheaper materials, but will also influence the system performance. Figure 6.3 does not give a truthful picture of how much the SOFC performance is affected when lowering the operating temperature through serious research efforts, because it must be expected that a goal of these research efforts is to keep a reasonable SOFC performance even at lower operating temperatures. Therefore, the SOFC component model used in these studies cannot predict the correct SOFC efficiency of newly or future developed intermediate temperature SOFCs. Undoubtedly though, lowering the operating temperature of the SOFCs in the SOFC-MGT configuration will affect the rest of the electricity producing process causing the system performance to decrease. As mentioned and shown in Figure 6.3, the MGT performance decreases when lowering the TIT, and in the SOFC-MGT configuration, the TIT is also sensitive to the chosen SOFC operating temperature. This is clear from the slope of the TIT as a function of the SOFC operating temperature in the SOFC-MGT configuration illustrated in Figure 6.3. The slope is less steep in the SOFC-MGT configuration than in the MGT case, though, because a lower SOFC operating temperature will cause less preheating of the SOFC inlets to ensure maintenance of the same temperature difference across the electrodes. From this, it is evident that a change in the SOFC operating temperature has reduced impact on the temperature of the anode and cathode off gases fed to the burner, hence also the resulting TIT.

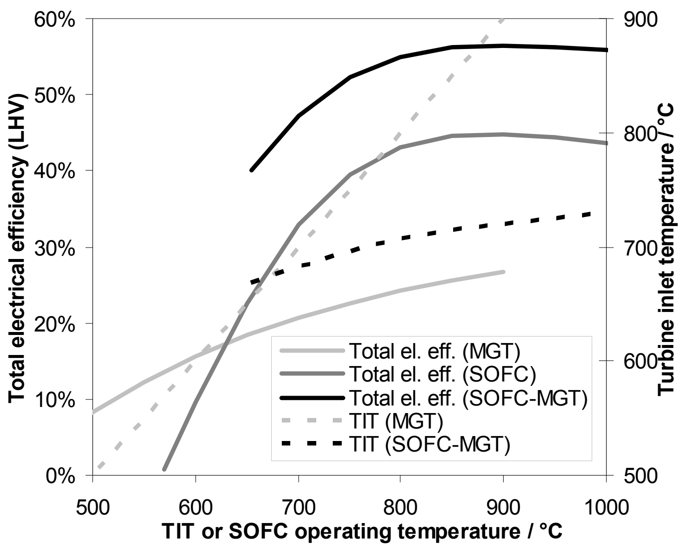

Figure 6.3: Energetic electric efficiency and TIT at different TIT or SOFC operating temperatures. The TIT in the MGT configuration is defined at the gas turbine inlet and the SOFC operating temperature in the two other configurations is defined at the anode/cathode outlets. The maximum allowed TIT is 900°C.

Potentially other bottoming cycles could be beneficial, e.g., a Rankine cycle, if the SOFC operating temperature is lowered. For the scale considered here, a traditional Rankine cycle based on steam would not be feasible, but Rankine cycles based on alternative working fluids could be relevant – i.e., organic Rankine cycles (ORCs). ORC system outputs can range from the kW_e to the MW_e scale, the working fluid can be tailored to let the ORC meet the required conditions from the topping system, and the process allows the use of low temperature heat sources [73] [74]. It is outside the scope of this work to study possible plant configurations incorporating an ORC, but it should also be mentioned that it seems possible to include both a MGT and an ORC according to Invernizzi et al. [75], hence increasing the performance of the bottoming process producing electricity from the product gas.

Due to the technology development trends, a MGT development that allows for a higher TIT and an SOFC development that enables lowering of the SOFC temperature could lessen the gap between the electrical efficiencies of the MGT and the SOFC configurations. No matter what, the scenario using both SOFCs and a MGT will still be the most efficient plant configuration of the studied.

6.1.3 Fuel Utilization in SOFCs

The amount of product gas that is utilized in the SOFCs affects the system performances in the SOFC and SOFC-MGT scenarios. The reference value of U_F is 85%. As illustrated in Figure 6.4, the system electrical efficiency decreases with decreasing fuel utilization in the SOFCs. This seems obvious in the SOFC configuration because the excess fuel is only producing heat in the burner. In the SOFC-MGT arrangement, the excess fuel is utilized in the MGT, but the electrical efficiency of the MGT is lower than that of the SOFCs ensuring a decreasing system performance trend with decreasing fuel utilization. The sensitivity to the fuel utilization is slightly greater in the SOFC scenario.

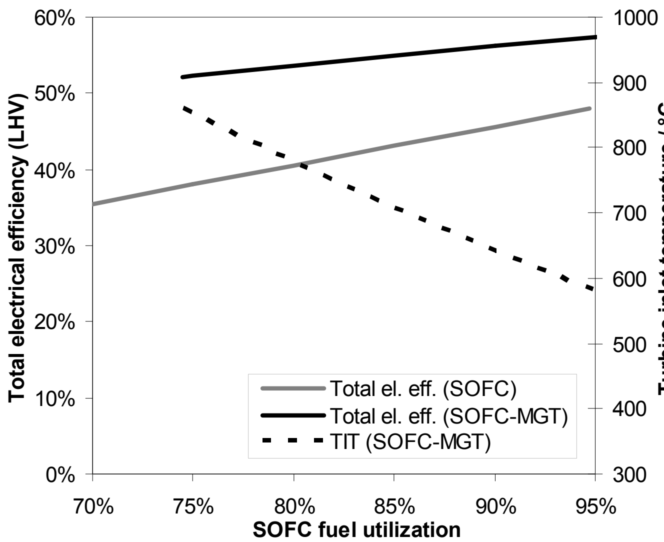

Figure 6.4: Energetic electrical efficiency and TIT as a function of SOFC fuel utilization.

The TIT in the SOFC-MGT configuration turns out to be significantly sensitive to the chosen U_F. The TIT increases from 706°C to 852°C when decreasing the fuel utilization from 85% to 75%. Thereby, the TIT approaches the maximum value of 900°C. Below approximately 75% fuel utilization in the SOFC-MGT scenario, the recuperator heats the air to a temperature above the desired cathode inlet temperature due to the higher TIT, and thereby TOT. This narrows the operational window of possible fuel utilization factors in the SOFC-MGT configuration when using a recuperator, whereas the SOFC scenario can operate at much lower fuel utilization (down to approximately 25% has been successfully simulated). As described in the parametric study of the SOFC performance in Section 4.2, the fuel flow contributes significantly to the SOFC cooling at very low fuel utilization causing a lower air flow (the air flow is controlled by the cooling need to maintain the operating temperature). Thus, the SOFC system configuration also meets a lower fuel utilization limit, when the reduced air flow lowers the SOFC performance significantly. The exact lower fuel utilization limit in the SOFC scenario has not been determined in this study because it is not of interest to operate at very low fuel utilization.

With respect to the system electrical efficiency, it can be concluded that the fuel utilization in the SOFCs should be maintained at a high level. In the SOFC-MGT arrangement, it should also be noted that the fuel utilization factor can be regulated to adjust the TIT to a desired level.

6.1.4 Temperature Gradient of SOFC Cathode

An important aspect of SOFC systems is SOFC cooling. Given the SOFC inlet and outlet temperatures are fixed, air flow through the cathode is determined by the cooling requirement of the SOFCs in order to maintain a certain operating temperature. In Figure 6.5, the cathode inlet temperature is varied. It is equivalent to changing the temperature gradient across the cathode (ΔT_c). A higher inlet temperature (a lower ΔT_c) decreases the electrical efficiency of the system. This effect is more pronounced in the SOFC-MGT configuration than in the SOFC case. An increase in the cathode inlet temperature from 600 to 680°C results in a decrease in the electrical efficiency of the SOFC-MGT arrangement from 50.3% to 44.1%, while it only drops from 36.4% to 35.9% in the SOFC configuration. In the SOFC scenario, the air compressor (working as a blower) consumes more power when the ΔT_c is decreased because a higher mass flow of air must be fed to the cathode to ensure a constant SOFC temperature. Thus, the parasitic losses increase, which in turn, slightly lower the electrical efficiency of the system. In the SOFC-MGT arrangement, the higher mass flow of air also passes through the MGT expander, thereby compensating for the greater air compressor work. The higher sensitivity to the chosen cathode inlet temperature in the

SOFC-MGT scenario is explained by the following two facts: One, a lower ΔT_c results in a lower temperature of the cathode off gas fed to the burner (more heat transfer in the SOFC air preheater), and consequently, a lower TIT; and two, a lower ΔT_c necessitates a higher mass flow of air to maintain the same SOFC operating temperature, which ensures a more lean mixture in the burner and thereby decreases the TIT. Therefore, lowering the ΔT_c lowers the TIT, which decreases the MGT output and hence the electrical efficiency of the SOFC-MGT system.

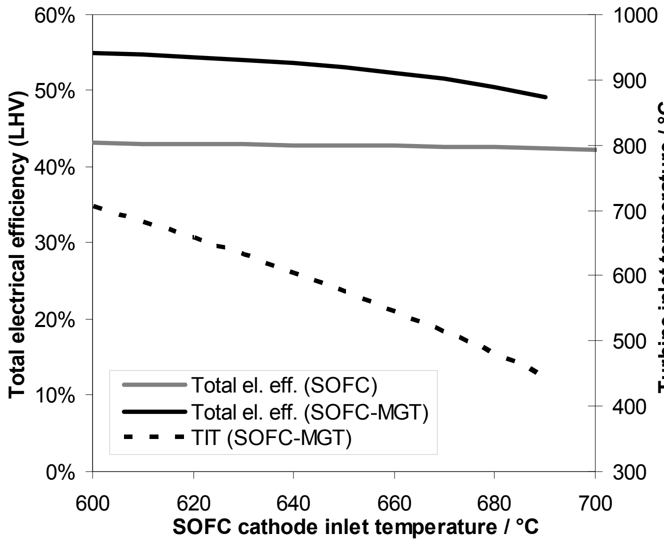

Figure 6.5: Energetic electrical efficiency and TIT as a function of SOFC cathode inlet temperature.

6.1.5 SOFC CURRENT DENSITY

The sensitivity of the model results to the chosen SOFC current density is shown in Figure 6.6. At the reference current density value of 300 mA cm^{-2}, the SOFC efficiency (defined in eq. (4.12)) is 49.5% in the SOFC configuration and 50.7% in the SOFC-MGT arrangement. The difference in SOFC efficiencies is due to the higher SOFC operating pressure in the SOFC-MGT case. Raising the SOFC load to 500 mA cm^{-2} reduces the SOFC efficiencies to 43.9% and 45.1% in the SOFC and SOFC-MGT scenarios, respectively. These decreases result in reductions in the total electrical efficiency to 37.9% and 51.1% - equivalent to respective losses of 5.2 and 3.9 percentage points. These losses cause relative changes in electrical efficiency of 12.1% and 7.1%, respectively, for a 66.7% increase in current density. Therefore, the model is only moderately sensitive to the chosen current density. Furthermore, it is evident that a downstream MGT can raise the electrical efficiency of the total system above the performance of the SOFC alone. As mentioned earlier, this benefit is due to the utilization of excess fuel from the SOFCs. The sensitivity of the system electrical efficiency to the current density is also slightly reduced when including a MGT.

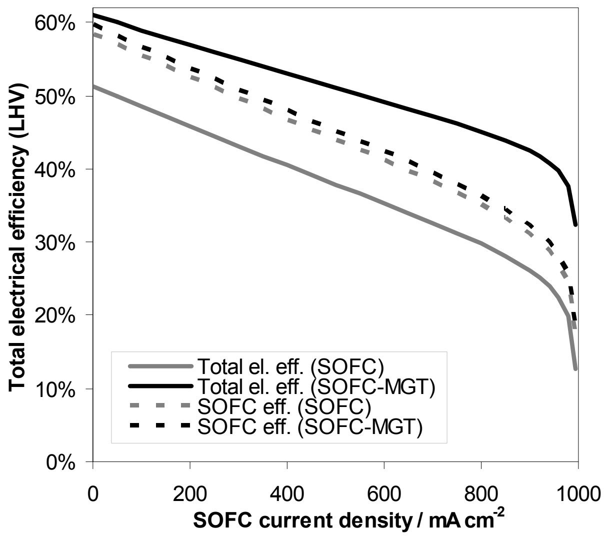

Figure 6.6: System electrical efficiency and SOFC efficiency as a function of SOFC current density.

6.1.6 Cold and Partly Dried Product Gas Temperature (and S/C)

In the demonstrated Viking gasification plant, the product gas is cooled to 50°C to condense some of the water in the gas before feeding it to a gas engine. This temperature of 50°C after the condenser is also used in this study, but the influence of varying this parameter is examined below.

First of all, the resulting system electrical efficiencies of the three studied scenarios are not affected significantly, as shown in Figure 6.7, when changing the product gas temperature after the condenser from 40°C to 90°C. This temperature cannot reach levels below 40°C because the coolant (DH water) in the inlet to the condenser is 30°C (assuming a pinch temperature difference of 10°C). Since the gas cleaner, situated upstream relative to the condenser, operates at 90°C, the product gas temperature after the condenser can only reach 90°C (without any cooling in the condenser). Surprisingly, the trends in Figure 6.7 seem to change around 55°C. This can be explained by Figure 6.8, where the S/C ratio is illustrated. The S/C ratio is similar in all three concepts. Above approximately 55°C, the condenser only cools the product gas without condensing any water, while below approximately 55°C, water is condensed thereby changing the gas composition. This change in gas composition explains the change in trends around 55°C. It should be noted, that lowering the S/C ratio increases the risk of carbon deposition. Without any condensing, a S/C ratio of 0.51 is obtained, while at the reference temperature of 50°C, the S/C ratio is 0.41. As mentioned in the end of Section 2.2.1, it seems plausible to operate SOFCs on product gas from the Viking gasifier with a S/C ratio of around or just below 0.5 and still avoid carbon deposition.

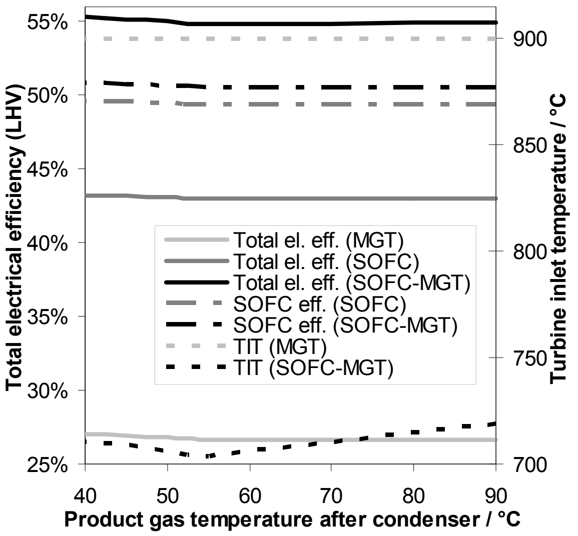

Figure 6.7: Energetic electric efficiency at different product gas temperatures leaving the gasification part of the hybrid system. Note, the scale of the electrical efficiency on the y-axis is narrower than the rest of the figures in this Chapter.

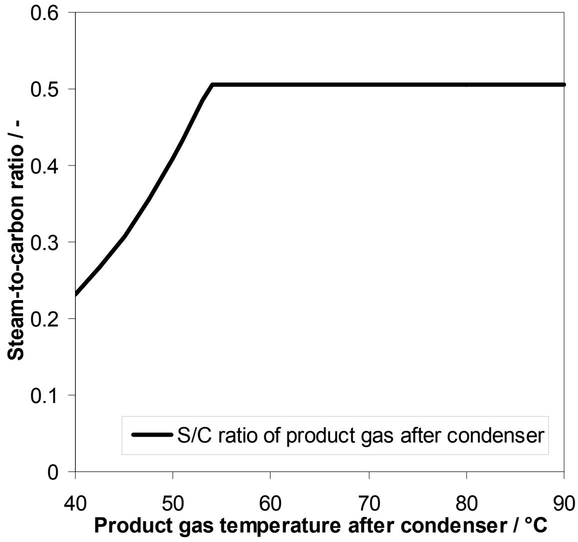

Figure 6.8: Steam-to-carbon ratios at different product gas temperatures leaving the gasification part of the hybrid system.

Decreasing the product gas temperature after the condenser from 55°C improves the efficiency of the MGT system. This is due to two facts: One, the fuel compressor work decreases; and two, a lower S/C ratio ensures a less dilute fuel. The lower fuel compressor work is caused by a lower mass flow and a cooler compressor inlet. The SOFC efficiency is constant at constant S/C ratio, while at decreasing S/C ratio, the SOFC performance increases due to a less dilute fuel. The same trend is seen for the system performance in the SOFC scenario. A lower product gas temperature before the fuel compressor will, as in the MGT case, decrease the power consumption of the compressor, but since it only works as a blower in this scenario, the impact is even less than in the MGT configuration. As for the two other scenarios, the SOFC-MGT case also benefits from a less dilute fuel, when the product gas temperature after the condenser is below 55°C. Besides the increase in SOFC performance, also the MGT performance in the SOFC-MGT arrangement increases when lowering the S/C ratio illustrated by the increasing TIT. Above 55°C the trend is different; an increasing product gas temperature at the fuel compressor inlet increases the TIT. The performance gain from an increased TIT exceeds the performance drop from higher power consumption by the fuel compressor.

All in all, the choice of product gas temperature after the condenser is unimportant to the system performance, but can be relevant because of the varying S/C ratio. The condenser could be removed to reduce plant complexity.

6.1.7 Isentropic Efficiency of Air Compressor/Blower

To investigate the influence of the turbomachinery performance, the isentropic efficiency of the air compressor has been varied. A similar study could also be done using the MGT expander or product gas compressor, but that is not performed here. Instead, the air compressor is chosen to represent the turbomachinery. The majority of the required compressor work is consumed by the air compressor because the mass flow of air is significantly larger than the mass flow of product gas.

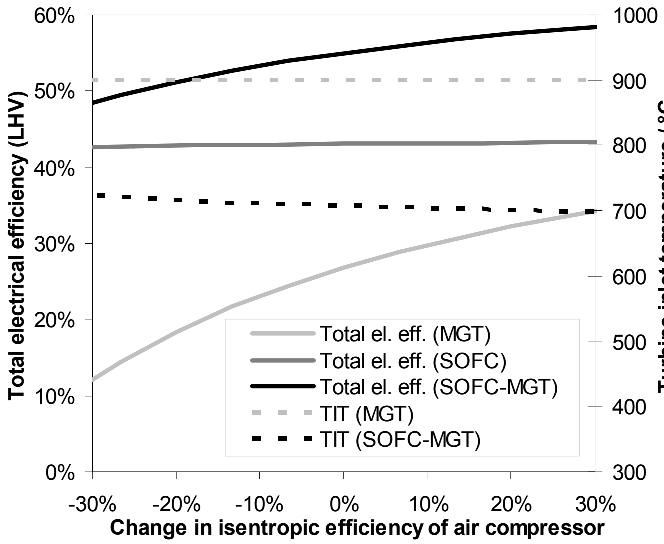

Figure 6.9: System electrical efficiency and TIT as a function of a relative change in the isentropic efficiency of the air compressor.

In Figure 6.9, the system performance is illustrated by the total electrical efficiency and TIT as a function of a relative change in the isentropic efficiency of the air compressor. A relative change is used because the isentropic efficiency of the air compressor in the SOFC configuration is lower than in the two other scenarios (the air compressor works as a blower in the non-pressurized SOFC configuration). The reference values of the isentropic efficiencies used can be found in Table 5.6 and Table 5.7. The sensitivity of the system performance to the air compressor performance in the SOFC arrangement is insignificant – at least within a range of the relative change in isentropic efficiency of ±30%. This is due to the fact that the power consumption from turbomachineries in the SOFC configuration is not significant compared to the net power production of the system. In the two pressurized system arrangements, the sensitivity is greater. It is greatest in the MGT case, where a 20% decrease in the isentropic efficiency results in a system electrical efficiency of 18.4% – a drop of 8.4 percentage points or 31%. In the SOFC-MGT case, a 20% decrease in the isentropic efficiency results in a system electrical efficiency of 51.2% – a drop of 3.8 percentage points or 7%. This clearly shows that the SOFC-MGT arrangement is only moderately sensitive to the air compressor performance, whereas the MGT scenario is highly sensitive. The TIT is constant in the MGT configuration (input), while a slightly decreasing trend of the TIT can be seen at increasing air compressor performance in the SOFC-MGT arrangement. The slight decrease is caused by a reduced amount of heat generation in the air compressor at increasing compressor performance. The TIT is not affected significantly, though.

6.1.8 SUMMARY

The parametric study of the system performances has revealed different trends and optima as well as windows of possible operation. Here follows a summary of the findings.

The MGT scenario showed a high sensitivity to the chosen pressure ratio and revealed an optimum of 3.7. The choice of turbine inlet temperature also turned out to greatly influence the MGT performance, and it can be concluded that the TIT should be maximized (limited by material constraints). Infinitesimal influence on the MGT system performance was shown from the chosen product gas temperature after the condenser in the gasifier plant part, and the resulting S/C ratio does not seem important to the MGT configuration. The condenser could be removed to reduce cost and plant complexity. Finally, the chosen isentropic efficiency of the air compressor affected the MGT system significantly.

The SOFC system configuration was not pressurized, so the operating pressure ratio was constantly around 1. The choice of operating temperature of the SOFC had great influence on the SOFC system performance and actually revealed an optimum at approximately 900°C, which is higher than the reference value of 800°C. From a system electrical efficiency point of view, the SOFC operating temperature should be maintained at a high level. The fuel utilization factor should also be maintained at a high level because the excess fuel is not used to produce additional power in this scenario. Within the studied range of temperature differences across the cathode, significant impact on the system performance was not shown. From an efficiency point of view, the SOFC current density should be minimized, but a lower current density will also result in a lower power production. Since the investment cost of SOFCs is significant in this kind of system, it will not be feasible to minimize the current density, but rather to determine the optimal current density from an economical viewpoint. As for the MGT scenario, the chosen product gas temperature after the condenser has infinitesimal influence on the SOFC system performance. Contrary to the MGT case, the resulting S/C ratio can be important to avoid carbon deposition in the SOFCs. If a higher S/C ratio is needed, the product gas temperature after the condenser could be increased or the condenser removed. Since the SOFC arrangement is not pressurized, the sensitivity of the system performance is not affected significantly by the performance of the turbomachineries.

In the SOFC-MGT scenario, similar to the MGT case, the pressure ratio affected the system performance significantly and an optimum was found at a pressure ratio of 2.5. The influence on the system electrical efficiency of varying the SOFC operating temperature revealed an optimum around 900°C. Like in the SOFC configuration, it is recommended to maintain a high SOFC operating temperature in the SOFC-MGT scenario. When combining SOFCs and a MGT, the SOFC fuel utilization factor should still be maintained at a high level from a system electrical efficiency viewpoint, but the parametric study also revealed that the fuel utilization in the SOFCs can be varied to regulate the turbine inlet temperature. Contrary to the SOFC configuration, the temperature difference across the cathode showed a moderate influence on the system performance. In this case, the temperature difference should be maximized (limited by thermal stresses in the SOFCs) to keep a high turbine inlet temperature. As mentioned in the SOFC case above, the current density should be minimized from an efficiency viewpoint, but optimized from an economical viewpoint. In any case, the current density has significant impact on the system performance. The choice of product gas temperature after the condenser was unimportant to the system electrical efficiency, but, as for the SOFC case, the resulting water content or S/C ratio can influence the risk of carbon deposition in the SOFC. Finally, the system performance showed significant sensitivity to the isentropic efficiency of the air compressor.

Generally, it can be concluded, that inclusion of a MGT in an SOFC system, besides increasing the system electrical efficiency, ensures a lower sensitivity of the electrical efficiency to operating conditions of the SOFCs. If the SOFC performance for some reason decreases it will produce less electricity but additional heat. The additional heat can be utilized by the MGT, though at a lower conversion efficiency. Even more generally, it can be stated that combining SOFCs with downstream heat engines ensures a system performance with a higher robustness to conditions causing varying SOFC performance. On the other hand, the operational window of the SOFC-MGT configuration is limited compared to the MGT scenario and SOFC scenario.

6.2 KEY DATA

Key data from the three studied plant configurations are presented in Table 6.1. The gasifier plant part is similar in all configurations, performing with a cold gas efficiency of 94.0% and an exergy efficiency of 80.8%. The subsystems converting the product gas to power and heat are where the studied systems differ. The respective optimal pressure ratio in each configuration is used besides the reference input values presented in Chapter 4 and Chapter 5. The SOFC-MGT subsystem clearly has the best energetic and exergetic electrical efficiencies. Notably, the exergy electrical efficiencies of the subsystems are slightly higher than the corresponding energy-based ones. This is because the exergy content in the input product gas fed to the subsystem is lower than the energy content. In the demonstrated Viking gasifier, the product gas is converted to electric power by an internal combustion gas engine and a generator at an efficiency of 29.1% [11]. Thus, the MGT does not seem better than a gas engine – especially when considering that the gas engine would be expected to achieve a higher efficiency at the scale of the studied plant configurations. As expected, the SOFC stack appears to be the most efficient power producing single technology of the considered. In the SOFC-MGT case, power production is mainly derived from the SOFCs, which produce 82-83% of the net AC power, when accounting for the power consumption of the compressors in the MGT net power production. In the SOFC configuration, the power consumption from the compressors is accounted for in the SOFC net power production, but the power consumption is much lower because of no pressurization.

Considering the total systems, the electrical efficiencies are slightly lower because the losses of the gasifier plant are included. The CHP efficiencies, or cogeneration efficiencies, do not differ significantly in the two scenarios including SOFCs, but in the MGT case, the CHP efficiency is lower. This is governed by the heat loss through the flue gas exiting the plant, which is greatest in the MGT configuration because of a higher air and exhaust flow. The higher air flow also explains the higher exergetic input through the air fed to the subsystem in the MGT arrangement.

Table 6.1: Key data for the studied plant configurations.

	Gasifier-MGT	Gasifier-SOFC	Gasifier-SOFC-MGT
Gasifier plant key data			
Biomass throughput / kg h^{-1}	154.8	154.8	154.8
Energetic biomass input ($\dot{m}_{biomass} LHV_{biomass}$) / kW_{th}	499.2	499.2	499.2
Exergetic biomass input ($\dot{\Psi}_{biomass}$) / kW	572.4	572.4	572.4
Exergetic air input to gasifier ($\dot{\Psi}_{air,gasifier}$) / kW	0.2	0.2	0.2
Steam blower power ($P_{steam\ blower}$) / kW	0.7	0.7	0.7
Energetic product gas output ($\dot{m}_{PG} LHV_{PG}$) / kW_{th}	469.1	469.1	469.1
Exergetic product gas output ($\dot{\Psi}_{PG}$) / kW	463.1	463.1	463.1
$\eta_{cold\ gas}$ / % [a]	94.0	94.0	94.0
$\eta_{\psi,gasifier\ plant}$ / % [b]	80.8	80.8	80.8
Subsystem key data			
PR / -	3.7	1.04	2.5
Exergetic air input to subsystem ($\dot{\Psi}_{air,subsystem}$) / kW	4.9	3.6	3.5
MGT net power production ($P_{net,MGT}$) / kW_e	134.5 [c]	-	48.5 [c]
SOFC net power production ($P_{net,SOFC}$) / kW_e	-	215.7 [c]	226.7
SOFC cell potential (V_{cell}) / V	-	0.800	0.820
$\eta_{el,subsystem}$ / % [d]	28.7	46.0	58.7
$\eta_{\psi,el,subsystem}$ / % [e]	28.7	46.2	59.0
Total system key data			
Total net power production ($P_{net,tot}$) / kW_e [f]	133.8	215.0	274.5
Total district heating production (Q_{DH}) / kJ s^{-1}	240.3	199.0	137.8
Exergy of heat production ($\dot{\Psi}_{DH}$) / kW	29.0	24.0	16.6
$\eta_{el,total\ system}$ / % (LHV) [g]	26.8	43.1	55.0
$\eta_{CHP,total\ system}$ / % (LHV) [h]	74.9	82.9	82.6
$\eta_{\psi,el,total\ system}$ / % [i]	23.2	37.3	47.6
$\eta_{\psi,CHP,total\ system}$ / % [j]	28.2	41.5	50.5

[a] Defined in eq. (2.8).

[b] Defined as $\eta_{\Psi,gasifier\ plant} = \dot{\Psi}_{PG} / (\dot{\Psi}_{biomass} + \dot{\Psi}_{air,gasifier} + P_{steam\ blower})$.

[c] Power consumption of the fuel and air compressors/blowers are included here.

[d] Defined as $\eta_{el,subsystem} = (P_{net,MGT} + P_{net,SOFC}) / (\dot{m}_{PG} LHV_{PG})$.

[e] Defined as $\eta_{\Psi,el,subsystem} = (P_{net,MGT} + P_{net,SOFC}) / (\dot{\Psi}_{PG} + \dot{\Psi}_{air,subsystem})$.

[f] Including steam blower power consumption.

[g] Defined as $\eta_{el,total\ system} = P_{net,tot} / (\dot{m}_{biomass} LHV_{biomass})$.

[h] Defined as $\eta_{CHP,total\ system} = (P_{net,tot} + Q_{DH}) / (\dot{m}_{biomass} LHV_{biomass})$.

[i] Defined as $\eta_{\Psi,el,total\ system} = P_{net,tot} / (\dot{\Psi}_{biomass} + \dot{\Psi}_{air,gasifier} + \dot{\Psi}_{air,subsystem})$.

[j] Defined as $\eta_{\Psi,CHP,total\ system} = (P_{net,tot} + \dot{\Psi}_{DH}) / (\dot{\Psi}_{biomass} + \dot{\Psi}_{air,gasifier} + \dot{\Psi}_{air,subsystem})$.

Below, temperature and pressure levels and mass flow rates are applied to a flow sheet of the SOFC-MGT scenario. The operational data in Figure 6.10 correspond to the same conditions as the key data of the SOFC-MGT scenario presented in Table 6.1. The applied dryer steam temperatures in the steam drying process can be found in Figure 5.3.

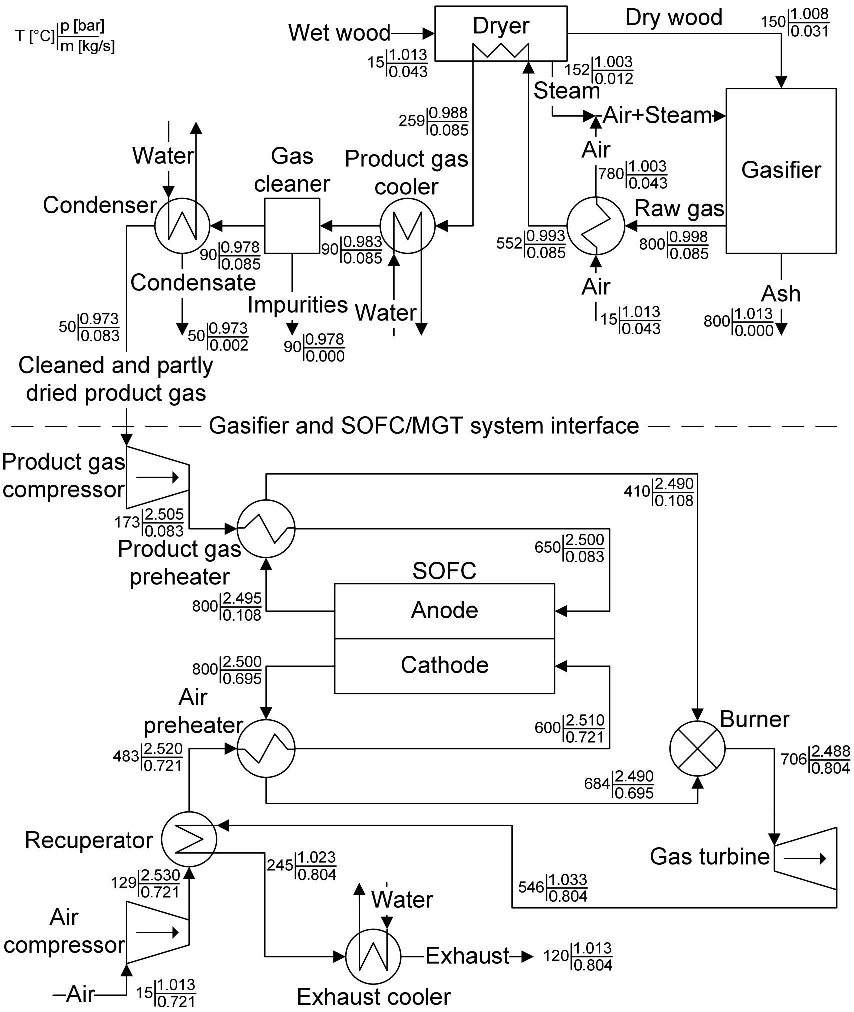

Figure 6.10: Flow sheet of the SOFC-MGT configuration with applied temperatures, pressures, and mass flow rates.

6.2.1 COMPARISON WITH LITERATURE

The performance of the subsystem in the SOFC-MGT scenario can be compared to the results of Sucipta et al. [43]. As described in Section 2.4, Sucipta et al. reported on a combined SOFC and recuperated MGT system fed with product gas from biomass gasification using either air, oxygen, or steam as gasifying agent. Net electrical efficiencies of the SOFC-MGT system part were 46.4%, 48.9%, and 50.8% for air, oxygen, and steam, respectively (LHV). In this study, the efficiency reaches 58.7% (LHV). The gasifying agent in the two-stage gasification concept is a mixture because air is used for partial oxidation but steam and CO_2 are used for gasifying the char. The lower efficiency in the study by Sucipta et al. is due to a lower electrical efficiency of the SOFCs, between 35% and 38% (LHV), whereas the SOFCs in this study reach approximately 50%. A fuel utilization of 85% is used in both studies, while the current density, temperature, and pressure ratio are 300 mA cm^{-2}, 800°C, and 2.5 in this study and were 320 mA cm^{-2}, 900-950°C, and 2.9 in the study by Sucipta et al. Sucipta et al. used a S/C ratio of 2.5 (0.41 in this study), which could be part of the reason. The SOFCs modelled by Sucipta et al. are tubular, but it is not clear whether the model is calibrated against experimental data or not.

The total plant performance of the SOFC-MGT scenario can be compared to the results of Fryda et al. [44] and Barchewitz and Palsson [38]. As described in Section 2.4, an autothermal (air) biomass gasifier feeding an SOFC and recuperated MGT system performed with a net electrical efficiency of the complete plant of 40.6% (LHV) in the study by Fryda et al. The reason for the lower efficiency in the study by Fryda et al. compared to this study is partly a lower cold gas efficiency of the gasifier, substantial heat losses in the gas cleaning system, a higher S/C ratio of 2, and a lower SOFC performance. The modelled SOFC in the work by Fryda et al. was operated at 85% fuel utilization, a current density of 428 mA cm^{-2}, a temperature of 900°C, and a pressure of 4 bar. The operating pressure was not optimized with respect to the net electrical efficiency of the hybrid system, though. In the study by Barchewitz and Palsson, a pressurized autothermal air-blown circulating fluidized bed gasifier fed planar SOFCs with a bottoming recuperated gas turbine. This plant reached a net electrical efficiency of 58.5% (LHV) at an optimal pressure of 2.65 bar, which is higher than the performance of 55.0% (LHV) found in this study. The size of the plant in the study by Barchewitz and Palsson was 4-5 MW_e, so better turbomachinery and a higher TIT were used compared to this study, which explains the better performance.

From two of the three comparisons above, it seems that the modelled SOFC performance in this study is relatively high. This impression could be caused by too low SOFC performance estimations in the works by Sucipta et al. and Fryda et al., but could also originate from the calibration of the SOFC model in this study. More detailed analysis on the reliability of the SOFC model calibration is left for future work. On the other hand, both the SOFC-MGT plant performance and optimal pressure ratio fit well with the results from the work by Barchewitz and Palsson.

Chapter 7 OPTIMIZATION OF THE SOFC-MGT SCENARIO

Based on the findings in the previous Chapter, the SOFC-MGT scenario has been chosen for optimization. The optimization is based on 1st and 2nd law analyses. The plant model listing for the optimized SOFC-MGT scenario can be found in Appendix F.

7.1 1ST AND 2ND LAW ANALYSES

1st law efficiency is defined as the ratio of useful energy products to total energy inputs, and by use of 1st law analysis the plant performance can be evaluated as seen in the presented results (cf., Table 6.1). 2nd law efficiency is defined congruently as the ratio of exergy in useful products (e.g., electrical power) to total exergy inputs, and by use of 2nd law analysis (often called exergy analysis) inefficiencies due to irreversibilities within the plant can be located.

A Sankey diagram of the energy flows in the SOFC-MGT configuration is presented in Figure 7.1. The Sankey diagram clearly shows the flow of energy, e.g., it clearly shows that a substantial heat amount is transferred from the anode to the cathode. The energy transferred through the membrane is calculated by 1st law balancing of one of the electrodes, but the O^{2-} flow from the cathode to the anode is not differentiated from the heat flow from the anode to the cathode. Therefore, the illustrated energy flow is a net energy flow between the electrodes. Besides that, it is apparent how important the recuperator is as it recovers significant heat amounts for additional power production that else would have been only contributing to a higher district heating production. In addition, it is evident that 55% of the biomass feedstock is converted into net electric power, while about 28% of it is used for producing hot water for district heating purposes. Of the 17% of wasted energy, nearly all of it is expelled with the flue gas. If only electric power is considered a valued product, 45% of the energy input is wasted. Of the 45%, 85% is expelled in the flue gas leaving the recuperator. From a 1st law viewpoint, the apparent energy inefficiency is the flue gas loss, indicating that the improvement of the plant performance seems to lie solely in making use of the flue gas. However, the 1st law analysis does not properly indicate other significant areas of improvements. Hence, a 2nd law analysis has been employed to reveal and quantify the inefficiencies in the system.

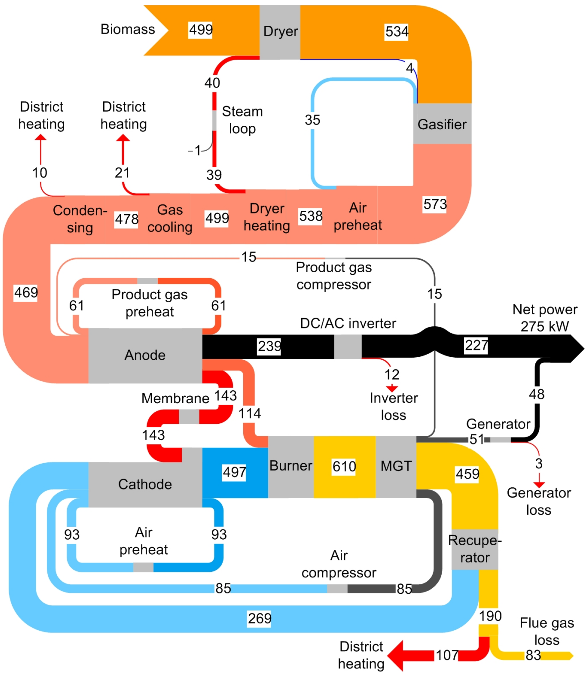

Figure 7.1: Sankey diagram of the energy flows (rounded values in [kJ s^{-1}]) in the SOFC-MGT arrangement.

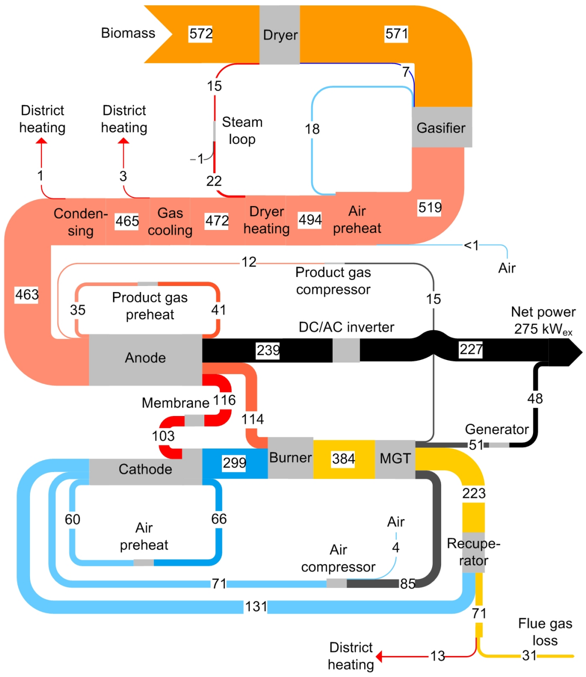

Figure 7.2: Sankey diagram of the exergy flows (rounded values in [kJ s^{-1}]) in the SOFC-MGT arrangement. Also called Grassmann diagram when based on exergy.

The overall 2nd law efficiencies, or exergy efficiencies, of the studied plant configurations have been presented in Table 6.1, but by studying the exergy flows within the plant, the performances of single components and their importance to the overall system can be evaluated. This is done for the SOFC-MGT scenario by studying the provided exergy flow diagram depicted in Figure 7.2. The exergy contents in the different flows are calculated by DNA using the method described by Bejan et al. [76]. The reference conditions are 15°C and 1 bar. In opposition to energy, exergy can be destroyed, illustrated by the differences between input and output of the components in Figure 7.2. Furthermore, the exergy in the biomass feedstock is larger than the energy content because the exergy content of solid and liquid fuels is calculated on a HHV basis [76], while the energy content is based on the LHV. Comparing Figure 7.1 and Figure 7.2 underlines the low exergetic value of heat, especially low-temperature heat, and the high exergetic value of chemical, mechanical, and electrical energy. In Figure 7.2, all the exergy destruction in the SOFCs is applied to the membranes.

The exergy destructions in the different components in Figure 7.2 are illustrated in Figure 7.3. Figure 7.3 clearly shows that the largest exergy destruction lies in the gasification reactor, 77.6 kW_{ex}, 13% of the plant exergy input and almost 27% of the total exergy loss in the plant. This covers pyrolysis, partial oxidation, and char gasification, though, because these are not separated in the modelling of the gasification process. Furthermore, mixing of steam and air fed to the gasifier accounts for approximately 4.9 kW_{ex} of the total 77.6 kW_{ex} of exergy destruction in the gasifier. Additionally, 31.2 kW_{ex} is leaving the plant in the flue gas and 28.7 kW_{ex} is destroyed in the burner. Thus, a bit more than 5% of the plant exergy input and 11% of the total plant exergy loss leaves the plant in the flue gas, while 5% of the exergy input and 10% of the total exergy loss is destroyed in the burner. The exergy destruction in the SOFCs is moderate compared to the other components, 12.9 kW_{ex}, slightly more than 2% of the plant exergy input and almost 5% of the total exergy loss in the plant.

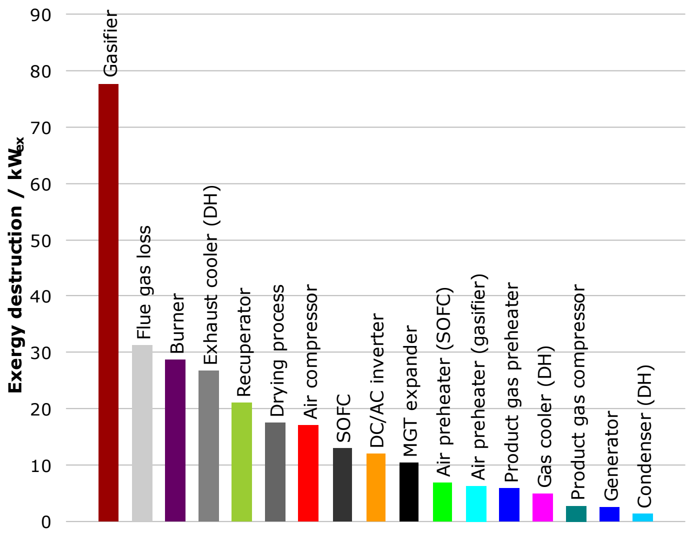

Figure 7.3: Exergy losses and destructions in the different components of the SOFC-MGT plant configuration. Total exergy destruction and loss in the plant is approximately 286 kW_{ex}.

The exergy destruction in the burner can be divided into contributions from mixing and the irreversible combustion process. Similar issues have been discussed by Dunbar and Lior [77]. Evaluating the exergy destruction in the burner reveals that mixing of the reactants accounts for 15.7 kW_{ex}, while the irreversible combustion process accounts for 13.0 kW_{ex}. Of the 15.7 kW_{ex} loss due to mixing, approximately 1.9 kW_{ex} is caused by thermal equilibration, i.e., reaching an even temperature of the mixture. The rest of the mixing loss, 13.8 kW_{ex}, is caused by diffusion. If the anode and cathode off gases fed to the burner had the same temperature, the losses due to thermal equilibration would disappear. In the studied SOFC-MGT scenario, the depleted product gas and air flow fed to the burner have temperatures of 410°C and 684°C, respectively (cf., Figure 6.10).[3]

Of the total exergy loss of approximately 286 kW_{ex}, almost 28% is lost in heat exchangers and 11% in turbomachineries, underlining the importance of heat exchanger performance. Assuming the gasifier, the SOFCs, the inverter, and the generator are state-of-the-art, minimization of exergy destructions or losses to increase plant performance should be found within the flue gas loss, the burner, the heat exchanger network, and the turbomachinery.

In Table 7.1, the exergy efficiencies of the plant components are listed along with defined inputs and products. The lowest exergy efficiencies are found in the exhaust cooler and product gas cooler, both producing district heating. The reason for the low exergy efficiencies are the great temperature difference between the hot and cold side of the heat exchangers. This indicates a potential for improving the heat exchanger network. Especially the exhaust cooler performance is important because the exergy flow through this component is high and thereby the exergy destruction is significant.

The exergy efficiency of the burner is high, 93.1%, but the exergy destruction is still significant according to Figure 7.3. As for the exhaust cooler, the exergy flow through the burner is high, causing significant exergy destruction despite the high exergy efficiency. As discussed below Figure 7.3, the exergy destruction in the burner could be reduced by having more equal temperatures of the anode and cathode off gases fed to the burner, e.g., by preheating.

The exergy efficiency of the SOFC component is very high, 98.3%, because the high-temperature off gases are considered valued products along with the produced electricity. Obviously, the exergy content of the product gas flow decreases through the SOFCs due to the conversion to electricity, but the exergy content of the air flow increases. The physical exergy content of the SOFC off gases is high due to the high temperature ensuring very high

[3] The exergy destruction caused by mixing is determined by evaluating the exergy destruction in a modelled mixer with the same inlet conditions as the burner. The part due to thermal equilibration can be determined by evaluating the reduction in exergy loss when the inlet temperatures are evened out. The rest of the mixing loss is attributable to diffusion.

exergy efficiency. On the other hand, if only the electricity is considered a valued product, the exergy efficiency drops dramatically to only 30.9%. Considering only the chemical exergy of the product gas input and the electricity output, the resulting exergy efficiency of the SOFCs is 51.5%.

Table 7.1: Exergy efficiencies of components from defined inputs and products[a]*. The components are listed in order according to the exergy destructions seen in Figure 7.3.*

Component	*Input(s)*	*Product(s)*	η_Ψ / %
Gasifier	Dry wood, steam, air	Product gas	87.0
Burner	Anode off gas, cathode off gas	Combustion products	93.1
Exhaust cooler (DH)	Exergy decrease of exhaust gas	Exergy increase of DH water	32.6
Recuperator	Exergy decrease of MGT expander exhaust	Exergy increase of air	86.2
Drying process[b]	Wet biomass, heat from product gas, steam blower power	Dry biomass, steam	97.1
Air compressor	Mechanical work	Exergy increase of air	79.8
SOFC	Product gas input, air input	DC electric power, product gas output, air output	98.3
DC/AC inverter	DC electric power	AC electric power	95.0
MGT expander	Exergy decrease of combustion products	Mechanical work	93.6
Air preheater (SOFC)	Exergy decrease of cathode off gas	Exergy increase of SOFC air	89.6
Air preheater (gasifier)	Exergy decrease of product gas	Exergy increase of gasifier air	74.5
Product gas preheater	Exergy decrease of anode off gas	Exergy increase of product gas	84.4
Gas cooler (DH)	Exergy decrease of product gas	Exergy increase of DH water	34.4
Product gas compressor	Mechanical work	Exergy increase of product gas	81.7
Generator	Mechanical work	AC electric power	95.0
Condenser (DH)	Exergy decrease of product gas	Exergy increase of DH water	90.1

[a] Defined as $\eta_\Psi = \dot{\Psi}_{\text{product}} / \dot{\Psi}_{\text{input}}$.

[b] Includes dryer, steam blower, and steam heater (see Figure 5.3).

7.1.1 RECOMMENDATIONS FOR OPTIMIZATION

From the 1st and 2nd law analyses, potential modifications for optimizing the plant performance can be derived. The goals of the optimization are to reduce the exergy losses or destructions of; (1) heat exchanging, (2) the burner, (3) the turbomachinery, and (4) the flue gas leaving the plant. The plant components are assumed to be state-of-the-art, so focus is kept on improving the system layout and operating conditions, e.g., by improving the heat exchanger performances by matching temperature levels, improving the burner performance by increasing the temperatures of the burner inlets, and improving the MGT expander by increasing the TIT. Below, suggested modifications to the SOFC-MGT system are listed.

I. Better Use of Hot Product Gas for Additional Anode Feed Preheating

The product gas leaving the gasifier air preheater has a high temperature of 552°C. In the SOFC-MGT scenario presented above, the hot product gas is used to heat dryer steam from 152°C to 250°C in the steam heater of the drying process. The large temperature difference of the product gas and dryer steam is not favourable, so it is suggested to use the high quality heat of the product gas for something else. Specifically, it is suggested to preheat the pressurized product gas in two steps instead of one, the first being heated by the product gas leaving the gasifier air preheater and the second by the anode off gas. The first preheater should preheat the pressurized product gas as much as possible. Thus, less heat exchange will be necessary in the second step preheater to reach the desired product gas temperature of 650°C at the anode inlet, thereby increasing the temperature of the anode off gas leaving the second preheater and entering the burner. Therefore, introducing a first step product gas preheater will address three of the four established goals. The hot product gas leaving the gasifier air preheater is better utilized, the exergy destruction in the burner is reduced because of the increased temperature of the depleted product gas fed to the burner, and the performance of the MGT expander is improved because of an increased TIT.

II. Use of Exhaust Gas Heat for the Biomass Drying Process

It is suggested to heat the drying process by the flue gas leaving the recuperator. The temperature of the flue gas downstream the recuperator is 245°C in the SOFC-MGT scenario presented above, so, at first, it seems that the superheated steam temperature can only reach up to around 235°C and not the 250°C that is intended. If suggestion I above is implemented, a higher TIT is obtained, thus the TOT and flue gas outlet temperature of the recuperator will also be higher. Therefore, reaching a superheated steam temperature of 250°C is expected to be feasible.

III. Reduce the Stack Temperature
The loss through the flue gas is substantial seen from the 1st law analysis and, surprisingly, also from the 2nd. It is suggested to reduce the stack temperature from 120°C to 90°C to make better use of the excess heat in the exhaust cooler. A stack temperature of 90°C is found to be realistic.

7.2 OPTIMIZED SOFC-MGT SCENARIO

Applying the modifications suggested by the 1st and 2nd law analyses in the previous Section, an optimized SOFC-MGT configuration is simulated. The system layout is presented in Figure 7.4.

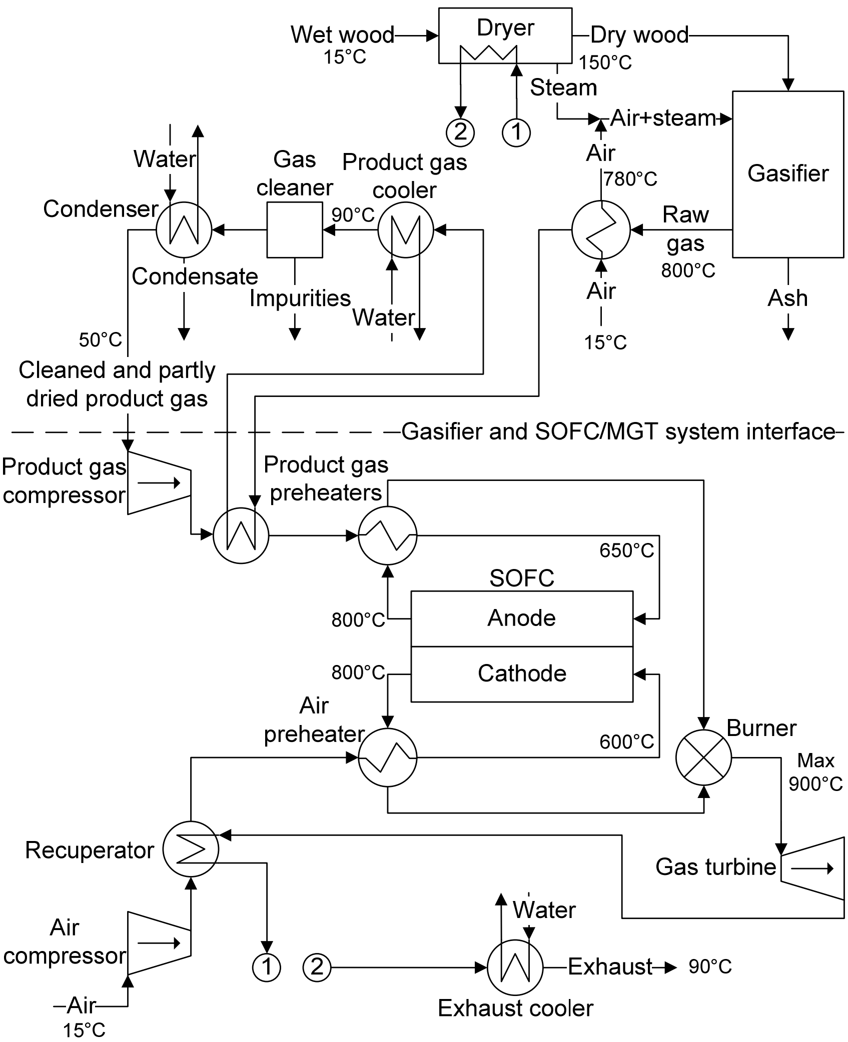

Figure 7.4: System layout of optimized SOFC-MGT scenario.

The exhaust gas downstream the recuperator is delivering heat to the biomass drying process by heating dryer steam in the steam heater (see Figure 5.3). The conditions for the steam heater are the same as in the original SOFC-MGT arrangement (see Table 5.7). The hot product gas leaving the gasifier air preheater, that previously heated the drying process, preheats the pressurized product gas in a first step preheater, while the anode off gas preheats the pressurized product gas in a second step preheater. The added first step preheater ensures a higher temperature of the anode off gas leaving the second step preheater and entering the burner. Since the first step product gas preheater works as a recuperator, a heat exchanger effectiveness of 85% is applied. Pressure drops of 5 mbar are applied to both sides of the first step preheater. Finally, the temperature of the exhaust gas leaving the hybrid system is lowered from 120°C to 90°C.

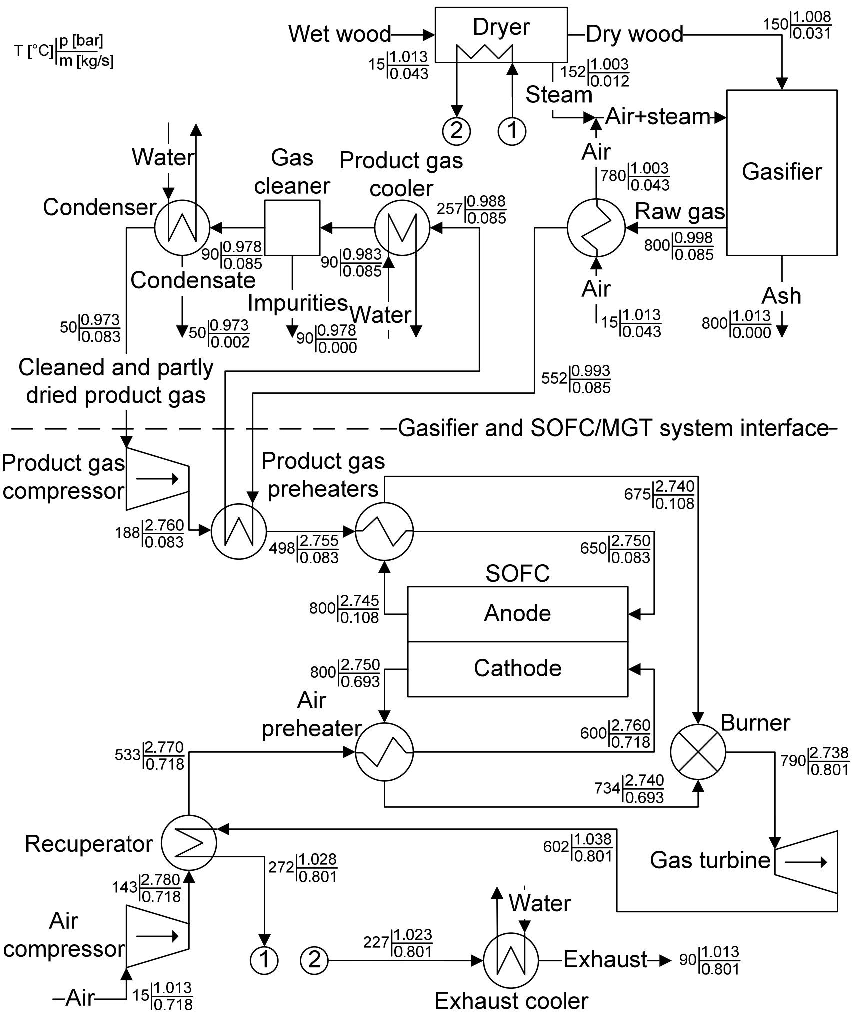

Figure 7.5: Flow sheet of optimized SOFC-MGT configuration with applied temperatures, pressures, and mass flow rates.

Table 7.2: Key data for the original and optimized SOFC-MGT configurations.

	Gasifier-SOFC-MGT	Optimized gasifier-SOFC-MGT
Gasifier plant key data		
Biomass throughput / kg h^{-1}	154.8	154.8
Energetic biomass input ($\dot{m}_{biomass} LHV_{biomass}$) / kW_{th}	499.2	499.2
Exergetic biomass input ($\dot{\Psi}_{biomass}$) / kW	572.4	572.4
Exergetic air input to gasifier ($\dot{\Psi}_{air,gasifier}$) / kW	0.2	0.2
Steam blower power ($P_{steam\ blower}$) / kW	0.7	0.7
Energetic product gas output ($\dot{m}_{PG} LHV_{PG}$) / kW_{th}	469.1	469.1
Exergetic product gas output ($\dot{\Psi}_{PG}$) / kW	463.1	463.1
$\eta_{cold\ gas}$ / % [a]	94.0	94.0
$\eta_{\psi,gasifier\ plant}$ / % [b]	80.8	80.8
Subsystem key data		
PR / -	2.5	2.7
Exergetic air input to subsystem ($\dot{\Psi}_{air,subsystem}$) / kW	3.5	3.5
MGT net power production ($P_{net,MGT}$) / kW_e [c]	48.5	63.8
SOFC net power production ($P_{net,SOFC}$) / kW_e	226.7	227.3
SOFC cell potential (V_{cell}) / V	0.820	0.822
$\eta_{el,subsystem}$ / % [d]	58.7	62.1
$\eta_{\psi,el,subsystem}$ / % [e]	59.0	62.4
Total system key data		
Total net power production ($P_{net,tot}$) / kW_e [f]	274.5	290.4
Total district heating production (Q_{DH}) / kJ s^{-1}	137.8	146.2
Exergy of heat production ($\dot{\Psi}_{DH}$) / kW	16.6	17.6
$\eta_{el,total\ system}$ / % (LHV) [g]	55.0	58.2
$\eta_{CHP,total\ system}$ / % (LHV) [h]	82.6	87.5
$\eta_{\psi,el,total\ system}$ / % [i]	47.6	50.4
$\eta_{\psi,CHP,total\ system}$ / % [j]	50.5	53.4

[a] Defined in eq. (2.8).

[b] Defined as $\eta_{\Psi,gasifier\ plant} = \dot{\Psi}_{PG} / (\dot{\Psi}_{biomass} + \dot{\Psi}_{air,gasifier} + P_{steam\ blower})$.

[c] Power consumption of the fuel and air compressors are included here.

[d] Defined as $\eta_{el,subsystem} = (P_{net,MGT} + P_{net,SOFC}) / (\dot{m}_{PG} LHV_{PG})$.

[e] Defined as $\eta_{\Psi,el,subsystem} = (P_{net,MGT} + P_{net,SOFC}) / (\dot{\Psi}_{PG} + \dot{\Psi}_{air,subsystem})$.

[f] Including steam blower power consumption.

[g] Defined as $\eta_{el,total\ system} = P_{net,tot} / (\dot{m}_{biomass} LHV_{biomass})$.

[h] Defined as $\eta_{CHP,total\ system} = (P_{net,tot} + Q_{DH}) / (\dot{m}_{biomass} LHV_{biomass})$.

[i] Defined as $\eta_{\Psi,el,total\ system} = P_{net,tot} / (\dot{\Psi}_{biomass} + \dot{\Psi}_{air,gasifier} + \dot{\Psi}_{air,subsystem})$.

[j] Defined as $\eta_{\Psi,CHP,total\ system} = (P_{net,tot} + \dot{\Psi}_{DH}) / (\dot{\Psi}_{biomass} + \dot{\Psi}_{air,gasifier} + \dot{\Psi}_{air,subsystem})$.

The conditions throughout the system change in the optimized scenario. The resulting temperatures, pressures, and mass flow rates in the different flows can be found in Figure 7.5. Key data for the optimized SOFC-MGT scenario are presented in Table 7.2 along with key data for the original SOFC-MGT scenario.

The system performance clearly improves in the optimized SOFC-MGT arrangement. The net electrical efficiency increases from 55.0% to 58.2% and the exergetic electrical efficiency from 47.6% to 50.4%. It is seen from Table 7.2 that it is mainly an increased net MGT power production that ensures the performance gain. This is due to the increased burner inlet temperatures and TIT. The higher temperature of the air inlet to the burner is caused by a higher TOT and hence a greater air temperature rise in the recuperator. The share of AC power generation from the SOFCs is reduced from 82-83% to approximately 78%. Furthermore, the optimal *PR* increases from 2.5 to 2.7. As described in Section 6.1.1, a higher TIT moves the optimal *PR* to a higher level. The slightly increased *PR* also explains the small increase in SOFC net power output. Additionally, it is evident from Figure 7.5 that the flue gas temperature after the recuperator reaches 272°C, which is sufficient for the drying process.

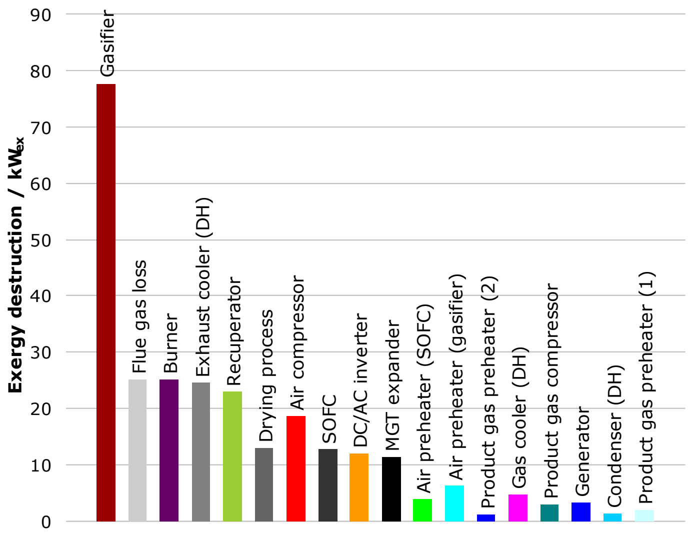

Figure 7.6: Exergy losses and destructions in the different components of the optimized SOFC-MGT plant configuration. Total exergy destruction and loss in the plant is approximately 269 kW$_{ex}$. The components are listed in the same order as in Figure 7.3.

It should be noted that some uncertainty is connected to the temperature of the product gas leaving the gasifier air preheater. This is due to the simplified model of the gasification process (combining pyrolysis, partial oxidation, and char gasification in one component) and the temperature of the preheated gasifier air in the Viking gasifier, which is unknown to the author.

Figure 7.6 shows the exergy losses in the optimized SOFC-MGT system, and in Table 7.3, the changes in exergy destructions between the original and optimized scenarios are listed along with the exergy efficiencies of the components. The only new component is the first step product gas preheater. The total exergy loss in the optimized plant is approximately 269 kW_{ex}, around 17 kW_{ex} or 6% less than in the original case. Only components are listed in Table 7.3, so the change in exergy loss through the emitted flue gas is not included. Exergy lost in the flue gas loss is reduced by 6.0 kW_{ex} due to a reduced stack temperature.

The additional product gas preheater (first step) improves the performance of the original product gas preheater (second step) significantly (from η_ψ=84.4% to η_ψ=92.0%). The total exergy destruction due to product gas preheating is reduced by 2.9 kW_{ex}, even though it is done in two components instead of one. The first step product gas preheater also improves the performance of the burner and MGT expander because of increased temperatures downstream the SOFCs. The exergy destruction in the burner is reduced to 25.2 kW_{ex} of which 13.9 kW_{ex} is due to mixing and 11.4 kW_{ex} is due to the irreversible combustion process. Of the exergy destruction caused by mixing, only 0.1 kW_{ex} is caused by thermal equilibration (13.8 kW_{ex} by diffusion). If compared to the contributions to the exergy destruction in the burner in the original SOFC-MGT system (described below Figure 7.3), the exergy destruction due to thermal equilibration is reduced by 1.8 kW_{ex} and due to the irreversible combustion process by 1.6 kW_{ex}. Thus, more equal temperatures of the burner inlets reduce the losses caused by the thermal equilibration, and the higher temperatures of the burner inlets reduce the losses caused by the combustion. The loss due to diffusion is the same as in the original scenario. The drying process is improved because the temperature differences in the steam heater are smaller. The reduced exergy destruction in the drying process of approximately 4.5 kW_{ex} is all due to improved steam heater performance.

Some components experience a greater exergy destruction in the optimized SOFC-MGT scenario than in the original one (e.g., the recuperator, compressors, MGT expander, and generator), but generally, all exergy efficiencies of the components either increase or are constant. The increased exergy destructions in some components originate from higher exergy inputs to the respective components and not reduced performance.

Table 7.3: Comparison of exergy destructions and exergy efficiencies[a] of components from the original and optimized SOFC-MGT scenarios. The components are listed in order according to the exergy destructions in Figure 7.6.

Component	*Change in exergy destruction / kW_{ex}*	*Original η_ψ / %*	*Optimized η_ψ / %*
Gasifier	0.00	87.0	87.0
Burner	-3.45	93.1	94.7
Exhaust cooler (DH)	-2.17	32.6	36.3
Recuperator	2.06	86.2	86.9
Drying process[b]	-4.47	97.1	97.8
Air compressor	1.46	79.8	80.3
SOFC	-0.08	98.3	98.4
DC/AC inverter	0.03	95.0	95.0
MGT expander	1.12	93.6	94.0
Air preheater (SOFC)	-3.03	89.6	89.8
Air preheater (gasifier)	0.00	74.5	74.5
Product gas preheater (2)	-4.77	84.4	92.0
Gas cooler (DH)	-0.11	34.4	34.4
Product gas compressor	0.25	81.7	82.1
Generator	0.81	95.0	95.0
Condenser (DH)	0.00	90.1	90.1
Product gas preheater (1)	1.87[c]	-	91.7[d]

[a] Inputs and products are defined in Table 7.1.
[b] Includes dryer, steam blower, and steam heater (see Figure 5.3).
[c] Equal to the absolute exergy destruction of this component in the optimized scenario because this component was not included in the original configuration.
[d] Input: Exergy decrease of cooled product gas. Product: Exergy increase of heated product gas.

An additional optimization effort can be performed by introducing a first step preheater of the gasifier air, situated before the existing gasifier air preheater. This first step gasifier air preheater can be heated by the flue gas after the flue gas has heated the drying process and before the exhaust cooler. The temperature of the flue gas between the drying process and the exhaust cooler is 227°C. The cooling of the raw product gas in the second step air preheater will then be reduced and additional heat can be added to the pressurized product gas in the first step product gas preheater, thus increasing the product gas inlet to the burner, TIT, burner performance, and MGT expander performance. If this additional optimization suggestion is applied, the optimal *PR* increases slightly from 2.7 to 2.8, the TIT from 790°C to 802°C, and the net electrical efficiency from 58.2% to 58.6%. This is a relatively small performance gain when installing a first step gasifier air preheater compared to the introduction of a first step product gas preheater. Hence, this optimization effort is not documented in detail in this study. To find out if the latter suggested optimization is worth the effort, the increased revenue due to the small performance gain should be compared to the investment and maintenance costs of the additional heat exchanger and piping.

If costs were analyzed or a higher S/C ratio of the product gas was found necessary, removal of the condenser could be considered.

7.3 SUMMARY

1^{st} and 2^{nd} law analyses have been performed on the SOFC-MGT scenario revealing inefficiencies within the system. The gasifier reactor (including pyrolysis, partial oxidation, and char gasification) caused the greatest exergy destruction but still reached an exergy efficiency of 87%. Almost 28% of the total exergy loss in the plant took place in heat exchangers, 11% in turbomachineries, 10% in the burner, and 11% was lost via the flue gas leaving the plant. Exergy destruction attributable to the SOFCs only contributed to nearly 5% of the total exergy destruction in the plant, performing with an exergy efficiency of approximately 98%.

Assuming the plant components to be state-of-the-art, potential improvements of the system layout have been proposed and tested by additional process simulations. Improving the heat exchanger network by matching temperature levels showed to be beneficial, and the inclusion of a first step product gas preheater had a positive impact on several other components, e.g., the burner and MGT expander. All in all, the optimization effort only required the installation of one additional heat exchanger and still increased the performance of the SOFC-MGT plant substantially. The energetic net electrical efficiency increased from 55.0% to 58.2% and the exergetic net electrical efficiency from 47.6% to 50.4%. Mainly, additional net power production from the MGT ensured the performance gain of the plant. In the optimized scenario, heat for drying the biomass was supplied by the exhaust from the SOFC-MGT subsystem instead of hot product gas from the gasifier reactor. Furthermore, the temperature of flue gas leaving the plant was reduced from 120°C to 90°C increasing the cogeneration efficiency from 82.6% to 87.5% based on energy and from 50.5% to 53.4% based on exergy.

Chapter 8 CONCLUDING REMARKS

The aim of this research was to contribute to enhanced electrical efficiencies and sustainability in future decentralized CHP plants. The work dealt with the coupling of thermal biomass gasification and SOFCs, and specific focus was kept on exploring the potential performance of hybrid CHP systems based on the novel two-stage gasification concept and SOFCs.

8.1 SUMMARY OF FINDINGS

Based on a review of existing literature, it was found essential to produce a clean product gas when aiming at electrochemical conversion in SOFCs. This showed to be partly obtainable by appropriate gasifier design and else by gas conditioning. The cleanliness of the product gas from the two-stage gasifier design ensured the need for only simple gas conditioning downstream the gasifier. For this reason, and high cold gas efficiency, the two-stage gasification concept was chosen for the studied plant scenarios.

Three conceptual plant designs were investigated in this study, all based on two-stage gasification of wood chips with a thermal biomass input of ~0.5 MW_{th} (LHV). The difference between the conceptual plant designs were the way of producing power and heat from the product gas from the gasification process. One scenario used a micro gas turbine (MGT), another SOFCs, and a third a combined SOFC and MGT system. The plant scenarios were investigated by system-level modelling combining zero-dimensional component models using the simulation software DNA. The modelled two-stage gasification process was calibrated against performance data from the demonstrated two-stage gasifier (Viking).

It was necessary to develop a new SOFC component model to predict the SOFC performance at various operating conditions. The SOFC component model included an electrochemical model, which was calibrated against published data from Topsoe Fuel Cell A/S representing their 2nd generation SOFCs. A parametric study revealed the sensitivity of the SOFC performance to different operating conditions, and the results can be used as guidelines for optimal SOFC operation. At the reference conditions (300 mA cm^{-2}, 800°C, 1 bar, and 85% fuel utilization), the electric efficiency of the SOFCs reached 49% using product gas from two-stage biomass gasification. The SOFC performance showed to be slightly reduced compared to using hydrogen due to a lower hydrogen partial pressure. The parametric study also revealed a severe sensitivity of the SOFC performance to the SOFC operating temperature. Decreasing the temperature from the reference value of 800°C reduced the electrical SOFC efficiency significantly. Also, the fuel utilization greatly influenced the electrical SOFC efficiency and should be maintained at a high level, but the SOFC converted the *reacting* fuel to electricity equally efficient in the studied range of fuel utilizations, though. Hence, the fuel utilization could be changed, for reasons originating elsewhere in the system, without changing how efficiently the reacting fuel in the SOFC was converted to electricity. The SOFC performance only showed a moderate gain from increasing operating pressure, predominantly at low pressure.

From plant simulations, the performances and parametric tendencies of the studied plant configurations were investigated. Similar for all plant scenarios were the gasifier plant part performing with a cold gas efficiency of 94% and an exergy efficiency of 81%. The pressure ratio showed to be an important parameter in the two pressurized systems, revealing optimum values of 3.7 in the MGT scenario and 2.5 in the SOFC-MGT scenario with respect to the net electrical efficiencies of the plants. The turbine inlet temperature (TIT) should be maximized to enhance MGT performance, but was limited by a cold and lean burner feed in the SOFC-MGT scenario caused by the SOFC operation. The influence of turbomachinery performance was only significant in the two pressurized systems. Furthermore, it was found that for all three plant scenarios, the condenser, situated as the last step in the gasification plant part, could be removed without affecting the plant performances. Hereby, the plant complexities could be reduced, thus also the plant investment costs. Additionally, removal of the condenser would increase the steam-to-carbon (S/C) ratio of the product gas from 0.41 to 0.51, thus reducing the risk of carbon deposition in the SOFCs. Of the SOFC operating parameters important to the system performance, the SOFC operating temperature and fuel utilization was crucial. The SOFC operating temperature should be maintained at a high level to avoid both decreased SOFC performance and MGT performance. The latter caused by a lower TIT. The fuel utilization should also be maintained at a high level to ensure use of the most of the fuel in the SOFCs because of their superior electrical efficiency.

In the SOFC-MGT scenario, the SOFC fuel utilization could also be used to regulate the TIT, but still the optimal plant performance was at high fuel conversion in the SOFCs. Also the current density had great impact on the SOFC and system performances, but the choice of current density is an issue of SOFC dimensioning and should be evaluated from an economical viewpoint. A greater temperature difference across the cathode reduced the necessary mass flow of air to cool the SOFC, but in the SOFC scenario, this temperature difference did not have significant impact on the system performance because of the low influence of air compressor work when operating the SOFC at atmospheric pressure. Contrary in the SOFC-MGT scenario, the chosen temperature difference across the cathode should be maximized to keep a high TIT and system performance (limited by thermal stresses in the SOFCs).

At the optimal pressure ratio, the MGT scenario performed with a net electrical efficiency of 27% (LHV) and a cogeneration efficiency of 75% (LHV), producing 134 kW_e AC power and 240 kJ s^{-1} of district heating. The corresponding exergy efficiencies were 23% and 28%, respectively. The SOFC plant scenario performed better than the MGT scenario reaching a net electrical efficiency of 43% (LHV) and a cogeneration efficiency of 83% (LHV), producing 215 kW_e AC power and 199 kJ s^{-1} of district heating. The corresponding exergy efficiencies were 37% and 42%, respectively. The SOFC-MGT plant scenario showed the greatest potential performing with a net electrical efficiency of 55% (LHV) and a cogeneration efficiency of 83% (LHV) at the optimal pressure ratio. The AC power production reached 275 kW_e and the district heating production 138 kJ s^{-1}. The corresponding exergy efficiencies were 48% and 51%, respectively. The inclusion of a MGT in an SOFC system not only ensured a higher electrical efficiency, but also ensured less sensitivity of the electrical efficiency to the operating conditions of the SOFCs. At lower SOFC performance, the SOFCs produced less electricity but additional heat. The additional heat could be utilized by the MGT, though at a lower conversion efficiency. Generally, it can be stated that combining SOFCs with downstream heat engines ensures a higher system performance and a greater robustness to conditions causing varying SOFC performance. On the other hand, the SOFC-MGT scenario showed that higher system complexity limits the operational window of several parameters.

From 1st and 2nd law analyses, the SOFC-MGT scenario was optimized reaching a net electrical efficiency of 58% (LHV) and a cogeneration efficiency of 88% (LHV). The performance gain was ensured by an improved heat exchanger network and a decreased plant exhaust temperature. The additional power generation was produced by the MGT because the inclusion of a first step product gas preheater reduced exergy destructions in several components and increased the TIT. All in all, the optimization effort only required the installation of one additional heat exchanger and still increased the performance of the SOFC-MGT plant substantially.

8.2 RECOMMENDATIONS FOR FURTHER WORK

8.2.1 SOFC COMPONENT MODEL

A zero-dimensional SOFC component model was developed for the DNA simulation tool in a FORTRAN environment. The SOFC model included an electrochemical model contributing to the prediction of the overall SOFC performance depending on operating conditions like temperature, pressure, fuel utilization, and gas compositions.

The data used for calibration could be improved. The active cell area in the dataset is not published in the open literature (confidential) forcing it to be assumed in this study. Hence, it was assumed to be 81 cm^2 per cell. A different active cell area would change the calibration and the SOFC performance. Therefore, a dataset with sufficient information would enable better calibration. With the assumed active cell area, the published dataset only covered a current density range from 0 to ~220 mA cm^{-2}, and the reference operation point used in this study was 300 mA cm^{-2}. Hence, an extended dataset including high current density operation would improve the reliability of the calibrated SOFC component model, even though the polarization curve is almost linear from 220 to 300 mA cm^{-2}.

As discussed in Appendix J, CO should not be considered equal to H_2 nor inert when calculating the anodic exchange current density. It is suggested to find a more generic expression for the anodic exchange current density, and one approach is suggested in the end of Appendix J.

The concentration overpotential is caused by limitations of diffusive transport of reactants and products between the flow channel and the electrode-electrolyte interface. The effect is increasing with current density, and at a certain current density limit, this transport of species is not fast enough to feed the electrochemical reactions taking place. In the electrochemical model of the SOFCs, this limiting current density is assumed constant. In reality, the SOFC operating conditions and the microstructural characteristics of the electrodes will affect the limiting current density. Detailed models describing the limiting current density are available and could be implemented in the SOFC component model for better performance predictions at higher current densities.

Incorporating dependency of inlet temperatures to the predicted SOFC performance could be relevant. In the current SOFC component model, the temperature of the solid SOFC structure is assumed to be equal to the outlet temperature of the SOFCs. Thus, no negative effects of lower inlet temperatures, i.e., lower solid temperature and performance close to the inlets, are taken into account. The obvious approach would be to upgrade the model to be at least one-dimensional, but it could be interesting to investigate if use of an average temperature or the like is satisfactory, hence keeping the simplicity of zero-dimensional component models.

8.2.2 MODELLED GASIFICATION PROCESS

In the two-stage gasification concept, pyrolysis takes place in a separate reactor prior to the reactor where partial oxidation and char gasification occurs. Furthermore, the pyrolysis reactor is heated by the product gas leaving the gasification reactor. In the modelled gasification process, both pyrolysis, partial oxidation, and char gasification takes place in one gasifier component eliminating the potential for alternative thermal integration with that part of the gasification process. Still, the resulting product gas composition and cold gas efficiency are similar to those of the demonstrated two-stage gasifier. Development of a pyrolysis component model would improve the level of detail in the gasification process and enable investigation of additional process integration. Furthermore, access to temperature data of all inlets and outlets of the components in the demonstrated two-stage gasifier would enable better calibration of the modelled gasification process.

8.2.3 OPTIMIZATION EFFORTS

Besides the optimization efforts implemented in Chapter 7, additional ideas evolved during the progress of this study, unfortunately, without finding the time to test their potential. The ideas are listed below:

- *Methanation*
  By including a methanation reactor (opposite of steam reforming, eq. (2.10)) prior to the SOFC anodes, the methane content in the product gas could be increased and internal reforming of the methane would contribute to the SOFC cooling. Hereby, the excess air flow on the cathode side could be decreased. Furthermore, the exothermic methanation process could eliminate the need for a product gas preheater (anode in/out heat exchanger), thereby ensuring a higher temperature of the product gas fed to the burner and a higher TIT. Water produced in the methanation process would also increase the S/C ratio, thus lowering the risk of carbon formation in the SOFCs.

- *Enriched air for gasifier*
  The composition of the product gas from the gasifier contains a lot of N_2 (approximately one third on a dry volume basis). By reducing the N_2 content in the air fed to the gasifier, the N_2 content in the product gas would also be reduced. This could be done by membrane technology utilizing materials with O_2 permeability. Membranes can enrich air to the cost of pressurization (approximately 38% O_2 at 2 bar and 55% O_2 at 5 bar [78]). Thus, the system performance gain from a less N_2-dilute product gas should cover the additional compressor work.

- *Cathode off gas recycling*
  By cooling and recycling cathode off gas to the cathode inlet, the mass flow of air supplied by the air compressor could be reduced, and still, a high mass flow through the cathode could be maintained to ensure sufficient SOFC cooling. Proper utilization of the heat in the cathode off gas would be needed. By this method, the TIT could be increased and, at the same time, the size of the turbomachinery and recuperator could be reduced, thus lowering the investment costs. Nagel et al. [52] underlined that the air-to-fuel ratio is highly cost effective in such systems as it determines equipment size. Furthermore, the lower exhaust mass flow would reduce the exergy lost in the flue gas.

8.3 OUTLOOK

The thermodynamic potential of combining biomass gasification and efficient conversion of product gas in SOFCs to generate sustainable power and heat has been shown in this study. This was based on a developed SOFC component model, which the author hopes can contribute to many later studies of SOFC plants in general using DNA. A couple of projects concerning SOFC-based plants already use the developed SOFC component model.

The modelled scenarios in this study have aimed at the scale of the largest two-stage gasifier demonstrated today, ~0.5 MW_{th} (LHV). Thus, in the best and optimized scenario, the power output is only ~0.3 MW_e. That is sufficient for very small decentralized CHP plants, but larger decentralized CHP plants in the size of 5-30 MW_e should also be investigated. A potential for even higher electrical efficiencies exists in these larger plants because of better turbomachinery at that scale. Steam-based Rankine cycles might also be relevant, e.g., heated by the gas turbine exhaust. The progress of upscal-

ing is also limited by the development of larger two-stage gasifiers. The two-stage gasification concept is claimed to be scalable up to 3-10 MW_{th} reaching even higher cold gas efficiency [15]. Alternatively, other gasifier types could be investigated, but high cold gas efficiency and clean product gas are vital.
The feasibility of a CHP plant is not only governed by its thermodynamic performance, but also investment and maintenance costs drive the competitiveness of a plant. Thus, economic issues should also be investigated before final conclusions can be made on the prospect of future CHP plants based on biomass gasification and SOFCs. Yet, it is difficult to predict the investment costs of novel gasifiers and SOFCs because they are not yet fully commercial. If reasonable estimates on future gasifier and SOFC prices are made, preliminary investigations of the economic feasibility can be performed. The method of thermoeconomics, applying the concept of cost to exergy, can be used to evaluate cost formations in the plant [76] [79].

Furthermore, issues like start-up strategy and dynamic behaviour, which were not considered in this study, can be very important issues when comparing plant performances.

A research project, aiming at long-term testing of SOFC operation on product gas from the demonstrated 75 kW_{th} two-stage gasifier, is under way. Based on the research in this study, evaluation of the long-term SOFC tests, and additional system analyses, the research project will make an assessment of the potential of combining two-stage biomass gasification and SOFCs. If the conclusion of the research project indicates a promising future for two-stage gasifier and SOFC couplings, later pilot scale demonstration is expected.

8.4 FINAL STATEMENT

An investigation of the potential performance of biomass gasification and SOFC hybrid systems for decentralized CHP production has been conducted. The investigation incorporated detailed component-level modelling of the SOFCs, system-level modelling of the complete process, and optimization of the plant layout. The two-stage gasification concept was found ideal for a high-efficient SOFC-based CHP plant due to its high cold gas efficiency and clean product gas. Besides ensuring the predicted SOFC performance to be dependent on the operating conditions, the SOFC component model was used to issue guidelines for optimal SOFC operation. A great potential for combined two-stage gasification and SOFC power generation was revealed. Net electrical plant efficiencies of 50-60% (LHV) was found achievable when integrating gas turbine technology to utilize the SOFC off gases, thus establishing greater electric power yield compared to traditional decentralized CHP plants, which only achieve net electrical plant efficiencies of 30-34% (LHV) on biomass. Future experimental tests and demonstrations should verify the predicted potential presented in this study.

REFERENCES

[1]
International Energy Agency. IEA Energy Technology Essentials: Biomass for power generation and CHP (No. 3). 2007.
https://www.iea.org/techno/Essentials.htm (accessed April 2010).

[2]
Henriksen U., Ahrenfeldt J., Jensen T.K., Gøbel B., Bentzen J.D., Hindsgaul C., Sørensen L.H. The design, construction and operation of a 75 kW two-stage gasifier. *Energy*. 2006, vol. 31, issue 10-11, pp. 1542–1553.

[3]
Topsoe Fuel Cell A/S. Business Areas, Distributed Generation. 2010.
http://www.topsoefuelcell.com/business_areas/dg.aspx (accessed April 2010).

[4]
BioCellus (Biomass Fuel Cell Utility System). Project supported by the European Commission through the 6th Framework Program. Contract No.: 502759. Period: September 2004 to August 2007.
http://www.biocellus.com/ (accessed November 2009).
http://cordis.europa.eu/fetch?CALLER=FP6_PROJ&ACTION=D&DOC=3346&CAT=PROJ&QUERY=1170700802932&RCN=73981&DOC=1&QUERY=0125351e01e6:bb14:7d1a2b4f (accessed November 2009).

[5]
Green-Fuel-Cell (SOFC Fuel cell fueled by biomass gasification gas). Project supported by the European Commission through the 6th Framework Program. Contract No.: 503122. Period: September 2004 to August 2007.
http://cordis.europa.eu/fetch?CALLER=FP6_PROJ&ACTION=D&DOC=3265&CAT=PROJ&QUERY=1170700800992&RCN=73958&DOC=1&QUERY=0125352ebbdf:2201:41d2bba5 (accessed November 2009).

[6]
Kumar A., Jones D.D., Hanna M.A. Thermochemical Biomass Gasification: A Review of the Current Status of the Technology. *Energies*. 2009, vol. 2, issue 3, pp. 556-581.

[7]
Milne T.A., Evans R.J., Abatzoglou N. Biomass Gasifier "Tars": Their Nature, Formation, and Conversion. U.S. Department of Energy Report. NREL/TP-570-25357. 1998. p. v.

[8]
Basu P. Combustion and gasification in fluidized beds. CRC Press. 2006. ISBN 0849333962. pp. 63-67.

[9]
Reed T. Biomass gasification – principles and technology. Energy technology review no. 67. Noyes Data Corporation. 1981. ISBN 0815508522. p. 120.

[10]
Stevens D.J. Hot Gas Conditioning: Recent Progress with Larger-Scale Biomass Gasification Systems; Update and Summary of Recent Progress. U.S. Department of Energy Report. NREL/SR-510-29952. 2001. pp. 5-34.

[11]
Ahrenfeldt J., Henriksen U., Jensen T.K., Gøbel B., Wiese L., Kather A., Egsgaard H. Validation of a Continuous Combined Heat and Power (CHP) Operation of a Two-Stage Biomass Gasifier. *Energy & Fuels*. 2006, vol. 20, issue 6, pp. 2672-2680.

[12]
Brandt P., Larsen E., Henriksen U. High Tar Reduction in a Two-Stage Gasifier. *Energy & Fuels*. 2000, vol. 14, issue 4, pp. 816-819.

[13]
Iversen H.L., Henriksen U., Ahrenfeldt J., Bentzen J.D. D25 Performance characteristics of SOFC membranes at two stage gasifier (confidential). Technical report from the EU project BioCellus (Biomass Fuel Cell Utility System), 6th Framework Programme, Contract No: 502759. 2006.

[14]
Hofmann Ph., Schweiger A., Fryda L., Panopoulos K.D., Hohenwarter U., Bentzen J.D., Ouweltjes J.P., Ahrenfeldt J., Henriksen U., Kakaras E. High temperature electrolyte supported Ni-GDC/YSZ/LSM SOFC operation on two-stage Viking gasifier product gas. *J Power Sources*. 2007, vol. 173, issue 1, pp. 357–366.

[15]
Bentzen J.D., Hummelshøj R.M., Henriksen U., Gøbel B., Ahrenfelt J., Elmegaard B. Upscale of the two-stage gasification process. In: van Swaaij W.P.M., Fjällström T., Helm P., Grassi A. (eds.), *Proceedings of 2. World Conference and Technology Exhibition on Biomass for Energy and Industry*. Rome, Italy. 2004.

[16]
Energinet.dk. Opskalering og demonstration af totrinsprocessen – slutrapport (in Danish). ForskEL 6529 (FU4202). December 2007. p. 4.
http://www.energinet.dk/da/menu/Forskning/ForskEL-programmet/Projekter/Afsluttede/Projekt+6529+%28FU4202%29.htm (accessed November 2009)

[17]
Larminie J., Dicks A. Fuel Cell Systems Explained. 2nd ed. West Sussex: John Wiley & Sons Ltd. ISBN 0-470-84857-X. 2003. p. 15, 23, 241, and 247.

[18]
Singhal S.C., Kendall K. High temperature solid oxide fuel cells: fundamentals, design and applications. Oxford: Elservier Ltd. ISBN 1856173879. 2003. p. 60, 300, and 339.

[19]
Wojcik A., Middleton H., Damopoulos L., Van herle J. Ammonia as a fuel in solid oxide fuel cells. *J Power Sources*. 2003, vol. 118, issue 1-2, pp. 342-348.

[20]
Christiansen N., Hansen J.B., Holm-Larsen H., Linderoth S., Larsen P.H., Hendriksen P.V., Mogensen M. Solid oxide fuel cell development at Topsoe Fuel Cell and Risø. *Fuel Cells Bulletin*. 2006, vol. 2006, issue 8, pp. 12-15.

[21]
Rostrup-Nielsen J.R., Hansen J.B., Helveg S., Christiansen N., Jannasch A.-K. Sites for catalysis and electrochemistry in solid oxide fuel cell (SOFC) anode. *Appl Physics A*. 2006, vol. 85, issue 4, pp. 427-430.

[22]
Rasmussen J.F.B., Hagen A. The effect of H2S on the performance of Ni-YSZ anodes in solid oxide fuel cells. *J Power Sources*. 2009, vol. 191, issue 2, pp. 534-541.

[23]
Matsuzaki Y., Yasuda I. The poisoning effect of sulfur-containing impurity gas on a SOFC anode: Part I. Dependence on temperature, time, and impurity concentration. *Solid State Ionics*. 2000, vol. 132, issue 3-4, pp. 261-269.

[24]
Gong M., Liu X., Trembly J., Johnson C. Sulfur-tolerant anode materials for solid oxide fuel cell application. *J Power Sources*. 2007, vol. 168, issue 2, pp. 289-298.

[25]
Sasaki K., Susuki K., Iyoshi A., Uchimura M., Imamura N., Kusaba H., Teraoka Y., Fuchino H., Tsujimoto K., Uchida Y., Jingo N. H2S poisoning of solid oxide fuel cells. *J Electrochem Society*. 2006, vol. 153, issue 11, pp. A2023-9.

[26]
Aravind P.V., Ouweltjes J.P., Woudstra N., Rietveld G. Impact of biomass-derived contaminants on SOFCs with Ni/gadolinia-doped ceria anodes. *Electrochemical and Solid-State Letters*. 2008, vol. 11, issue 2, p. B24-8.

[27]
Trembly J.P., Gemmen R.S., Bayless D.J. The effect of coal syngas containing HCl on the performance of solid oxide fuel cells: Investigations into the effect of operational temperature and HCl concentration. *J Power Sources*. 2007, vol. 169, issue 2, pp. 347-354.

[28]
Hofmann Ph., Panopoulos K.D., Fryda L.E., Schweiger A., Ouweltjes J.P., Karl, J. Integrating biomass gasification with solid oxide fuel cells: Effect of real product gas tars, fluctuations and particulates on Ni-GDC anode. *Int J Hydrogen Energy*. 2008, vol. 33, issue 11, pp. 2834-2844.

[29]
Singh D., Hernández-Pacheco E., Hutton P.N., Patel N., Mann M.D. Carbon deposition in an SOFC fueled by tar-laden biomass gas: a thermodynamic analysis. *J Power Sources*. 2005, vol. 142, issue 1-2, pp. 194-199.

[30]
Mermelstein J., Brandon N., Millan M. Impact of Steam on the Interaction between Biomass Gasification Tars and Nickel-Based Solid Oxide Fuel Cell Anode Materials. *Energy & Fuels*. 2009, vol. 23, issue 10, pp. 5042-5048.

[31]
Dayton D.C., Ratcliff M., Bain R. Fuel Cell Integration - A Study of the Impacts of Gas Quality and Impurities. U.S. Department of Energy Report. NREL/MP-510-30298. 2001. p. 16.

[32]
Sakanishi K., Wu Z., Matsumura A., Saito I., Hanaoka T., Minowa T., Tada M., Iwasaki T. Simultaneous removal of H2S and COS using activated carbons and their supported catalysts. *Catalysis Today*. 2005, vol. 104, issue 1, pp. 94-100.

[33]
Haldor Topsøe A/S. Feed Purification Catalyst – HTZ. Catalyst for sulphur absorption. 2009.
http://www.topsoe.com/business_areas/ammonia/processes/~/media/PDF%20files/Feed_purification/Topsoe_feed_purification_cat_htz.ashx (accessed December 2009).

[34]
Gmeindl F.D., Geisbrecht R.A., Craig K.R., Kasper S., Shah V.B. New Directions in MCFC Systems. In: *Proceedings of the Ninth Annual Gasification and Gas Stream Cleanup Contractors Meeting*. DOE/METC-89/6107. Morgantown, WV. June 1989.

[35]
Reed T., Das A. Handbook of biomass downdraft gasifier engine systems. U.S. Department of Energy Report. SERI/SP-271-3022. 1988. p. 117.

[36]
Alderucci V., Antonucci P.L., Maggio G., Giordano N., Antonucci V. Thermodynamic analysis of SOFC fuelled by biomass-derived gas. *Int J Hydrogen Energy*. 1994, vol. 19, issue 4, pp. 369-376.

[37]
Craig K.R., Mann M.K. Cost and Performance Analysis of Biomass-Based Integrated Gasification Combined-Cycle (BIGCC) Power Systems. U.S. Department of Energy Report. NREL/TP-430-21657. 1996.

[38]
Barchewitz L., Palsson J. Design of an SOFC system combined to the gasification of biomass. In: McEvoy A.J. (ed.), *Proceedings of the 4th European SOFC Forum*. Lucerne, Switzerland. 2000, vol. 1, pp. 59-68.

[39]
Ståhl K., Neergaard M. Experiences from the biomass fuelled IGCC plant at Värnamo. In: Kopetz H. et al. (eds.), *Proceedings of the 10th European Conference and Technology Exhibition, Biomass for Energy and Industry*. Wurzburg, Germany. June 1998, pp. 291-294.

[40]
Saravanamuttoo H.I.H., Rogers G.F.C., Cohen H., Straznicky P.V. Gas Turbine Theory. Sixth edition. Essex: Pearson Education Ltd. ISBN 978-0-12-222437-6. 2009. pp. 49-50 and pp. 85-88.

[41]
Hutton P.N., Musich M.A., Patel N., Schmidt D.D., Timpe R.C. Feasibility study of a thermally integrated SOFC-gasification system for biomass power generation. US Department of Energy, National Energy Technology Laboratory Cooperative Agreement. Phase 1. Interim report, No. DE-FC26-98FT40321, Energy and Environmental Research Center, University of North Dakota, 2003.

[42]
Omosun A.O., Bauen A., Brandon N.P., Adjiman C.S., Hart D. Modelling system efficiencies and costs of two biomass-fuelled SOFC systems. *J Power Sources*. 2004, vol. 131, issue 1-2, pp. 96-106.

[43]
Sucipta M., Kimijima S., Suzuki K. Performance analysis of the SOFC-MGT hybrid system with gasified biomass fuel. *J Power Sources*. 2007, vol. 174, issue 1, pp. 124-135.

[44]
Fryda L., Panopoulos K.D., Kakaras E. Integrated CHP with autothermal biomass gasification and SOFC–MGT. *Energy Conver and Manag*. 2008, vol. 49, issue 2, pp. 281-290.

[45]
Hofmann Ph., Panopoulos K.D., Aravind P.V., Siedlecki M., Schweiger A., Karl J., Ouweltjes J.P., Kakaras E. Operation of solid oxide fuel cell on biomass product gas with tar levels >10 g Nm^{-3}. *Int J Hydrogen Energy*. 2009, vol. 34, issue 22, pp. 9203-9212.

[46]
Ouweltjes J.P., Aravind P.V., Woudstra N., Rietveld G. Biosyngas utilization in solid oxide fuel cells with Ni/GDC anodes. *J Fuel Cell Science and Technology*. 2006, vol. 3, issue 4, pp. 495-498.

[47]
Oudhuis A.B.J., Bos A., Ouweltjes J.P., Rietveld G., van der Giesen A.B. High efficiency and products from biomass and waste; experimental results of proof of principle of staged gasification and fuel cells. In: van Swaaij W.P.M., Fjällström T., Helm P., Grassi A. (eds.), *Proceedings of the Second World Conference and Technology Exhibition on Biomass for Energy, Industry and Climate Protection*. Rome, Italy. 2004.

[48]
Karl J., Frank N., Karellas S., Saule M., Hohenwarter U. Conversion of syngas from biomass in solid oxide fuel cells. *J Fuel Cell Science and Technology*. 2009, vol. 6, issue 2, 021005 (6 pp.).

[49]
Karellas S., Karl J., Kakaras E. An innovative biomass gasification process and its coupling with microturbine and fuel cell systems. *Energy*. 2009, vol. 33, issue 2, pp. 284-291.

[50]
Panopoulos K.D., Fryda L.E., Karl J., Poulou S., Kakaras E. High temperature solid oxide fuel cell integrated with novel allothermal biomass gasification – Part I: Modelling and feasibility study. *J Power Sources*. 2006, vol. 159, issue 1, pp. 570-585.

[51]
Panopoulos K.D., Fryda L., Karl J., Poulou S., Kakaras E. High temperature solid oxide fuel cell integrated with novel allothermal biomass gasification – Part II: Exergy analysis. *J Power Sources*. 2006, vol. 159, issue 1, pp. 586-594.

[52]
Nagel F.P., Schildhauer T.J., McCaughey N., Biollaz S.M.A. Biomass-integrated gasification fuel cell systems - Part 2: Economic analysis. *Int J Hydrogen Energy*. 2009, vol. 34, issue 16, pp. 6826-6844.

[53]
DONG Energy (2009) - Small-scale CHP plants.
http://www.dongenergy.com/en/business%20activities/generation/electricity%20generation/small_scale_chp_plants/pages/small-scale%20chp%20plants.aspx (accessed December 2009)

[54]
Nagel F.P., Schildhauer T.J., Biollaz S.M.A. Biomass-integrated gasification fuel cell systems - Part 1: Definition of systems and technical analysis. *Int J Hydrogen Energy*. 2009, vol. 34, issue 16, pp. 6809-6825.

[55]
DNA (Dynamic Network Analysis). General thermal energy system simulation tool developed at the Section of Thermal Energy Systems (former Energy Engineering Section), Department of Mechanical Engineering, Technical University of Denmark.
http://orbit.dtu.dk/RecordLinkPage.external?sp=recid&sp=231251
(accessed April 2010)

[56]
Elmegaard B. Simulation of boiler dynamics – Development, Evaluation and Application of a General Energy System Simulation Tool (PhD thesis). Report Number ET–PhD 99–02. ISBN 87–7475–222–7. The Technical University of Denmark. 1999.

[57]
Elmegaard B., Houbak N. DNA – A General Energy System Simulation Tool. In: Amundsen J. et al. (eds.), *SIMS 2005 46th Conference on Simulation and Modeling*. Tapir Academic Press. Trondheim, Norway. 2005, pp. 43-52.

[58]
Smith J.M., Van Ness H.C., Abbott M.M. Introduction to Chemical Engineering Thermodynamics. Fifth edition. New York: McGraw-Hill. ISBN 007059239X. 1996. pp. 525-527.

[59]
Holtappels P., Haart L.G.J. De, Stimming U., Vinke I.C., Mogensen M. Reaction of CO/CO2 gas mixtures on Ni-YSZ cermet electrodes. *J Appl Electrochemistry*. 1999, vol. 29 issue 5, pp. 561-568.

[60]
Zhu H., Kee R.J. Thermodynamics of SOFC efficiency and fuel utilization as functions of fuel mixtures and operating conditions. *J Power Sources*. 2006, vol. 161, issue 2, pp. 957-964.

[61]
Zhu H., Kee R.J. A general mathematical model for analyzing the performance of fuel-cell membrane-electrode assemblies. *J Power Sources*. 2003, vol. 117, issue 1-2, pp. 61-74.

[62]
Chan S.H., Khor K.A., Xia Z.T. A complete polarization model of a solid oxide fuel cell and its sensitivity to the change of cell component thickness. *J Power Sources*. 2001, vol. 93, issue 1-2, pp. 130-140.

[63]
Aloui T., Halouani K. Analytical modeling of polarizations in a solid oxide fuel cell using biomass syngas product as fuel. *Appl Therm Eng*. 2007, vol. 27, issue 4, pp. 731-737.

[64]
Costamagna P., Honegger K. Modeling of solid oxide heat exchanger integrated stacks and simulation at high fuel utilization. *J Electrochem Society*. 1998, vol. 145, issue 1, pp. 3995-4007.

[65]
Mogensen M., Lindegaard T. The kinetics of hydrogen oxidation on a Ni-YSZ SOFC electrode at 1000degC. In: Singal S.C., Iwahara T. (eds.), *Solid oxide fuel cells, 3. International symposium on solid oxide fuel cells*. Honolulu, USA. The Electrochemical Society Proceedings Series. Pennington, NJ. 1993, proceedings vol. 93-4, pp. 484-493.

[66]
Mogensen M. Electrode kinetics of SOFC anodes and cathodes. In: Poulsen F.W., Bentzen J.J., Jacobsen T., Skou E., Østergård M.J.L. (eds.), *Proceedings of the 14th Risø International Symposium on Material Science, High temperature electrochemical behaviour of fast ion and mixed conductors*. Risø National Laboratory. Roskilde, Denmark. 1993, pp. 117-135.

[67]
Costamagna P., Selimovic A., Del Borghi M., Agnew G. Electrochemical model of the integrated planar solid oxide fuel cell (IP-SOFC). *Chem Eng J*. 2004, vol. 102, issue 1, pp. 61-69.

[68]
Achenbach E. Three-dimensional and time-dependent simulation of a planar solid oxide fuel cell stack. *J Power Sources*. 1994, vol. 49, issue 1-3, pp. 333-348.

[69]
Braun R. *Optimal Design and Operation of Solid Oxide Fuel cell Systems for Small-scale Stationary Applications* (PhD Thesis). University of Wisconsin-Madison. 2002. p. 80 and 82.

[70]
Kim J.W., Virkar A.V., Fung K.Z., Mehta K., Singhal S.C. Polarization effects in intermediate temperature, anode-supported solid oxide fuel cells. *J Electrochem Society*. 1999, vol. 146, issue 1, pp. 69-78.

[71]
Linderoth S., Larsen P.H., Mogensen M., Hendriksen P.V., Christiansen N., Holm-Larsen H. Solid Oxide Fuel Cell (SOFC) Development in Denmark. *Materials Science Forum*. 2007, vol. 539-543, pp. 1309-1314.

[72]
Christiansen N., Hansen J.B., Holm-Larsen H., Linderoth S., Larsen P.H., Hendriksen P.V., Mogensen M. Solid Oxide Fuel Cell Development at Topsoe Fuel Cell A/S and Risø. In: Bossel U. (ed.), *7th European Solid Oxide Fuel Cell Forum*. European Fuel Cell Forum. Lucerne. 2006, File No. B034.

[73]
Angelino G., di Paliano P.C. Organic Rankine cycles (ORCs) for energy recovery from molten carbonate fuel cells. In: *Proceedings of 35th Intersociety Energy Conversion Engineering Conference*. American Institute of Aeronautics and Astronautics. Las Vegas. 2000, vol. 2, pp. 1400-1409.

[74]
Schuster A., Karellas S., Kakaras E., Spliethoff H. Energetic and economic investigation of Organic Rankine Cycle applications. *Appl Therm Eng*. 2009, vol. 29, issue 8-9, pp. 1809-1817.

[75]
Invernizzi C., Iora P., Silva P. Bottoming micro-Rankine cycles for micro-gas turbines. *Appl Therm Eng*. 2007, vol. 27, issue 1, pp. 100-110.

[76]
Bejan A., Tsatsaronis G., Moran M. Thermal Design & Optimization. John Wiley and Sons Inc. ISBN 0471584673. 1996. pp. 113-166.

[77]
Dunbar W. R., Lior N., Sources of Combustion Irreversibility, *Comb Sci Technol*. 1994, vol. 103, issue 1, pp. 41-63.

[78]
Baker R.W. Membrane Technology and Applications. Second edition. West Sussex: John Wiley and Sons Ltd. ISBM 0470854456. 2004. p. 336.

[79]
Valero A., Serra L., Uche J. Fundamentals of Exergy Cost Accounting and Thermoeconomics. Part I: Theory. *J Energy Resour Technol*. 2006, vol. 128, issue 1, pp. 1-8.

[80]
White W.B., Johnson S.M., Dantzig C.B. Chemical Equilibrium in Complex Mixtures. *J Chem Phys*. 1958, vol. 28, issue 5, pp. 751-755.

Appendix A THE GIBBS FREE ENERGY MINIMIZATION METHOD

A chemical equilibrium is characterized by the fact, that the total Gibbs free energy of a system has its minimum value. This characteristic can be used to calculate the gas composition at chemical equilibrium, at specified temperature and pressure, without considering the reaction pathway of the chemical compounds involved. This Gibbs free energy minimization methodology is described in this appendix and is based on Smith et al. [58] and Elmegaard [56]. The Gibbs free energy minimization methodology was first described by White et al. [80].

Considering a gas mixture of k ideal gas compounds, the total Gibbs free energy of the system can be expressed as:

$$\dot{G}_{\text{tot}} = \sum_{i=1}^{k} \dot{n}_i \left[g_i^0 + RT \ln(y_i p) \right] \tag{A.1}$$

$\dot{n}$ being the molar flow, g^0 the molar specific standard Gibbs free energy, and y the molar fraction – all three for each gas compound. g^0 is only a function of temperature.

The minimum value of the expression for the total Gibbs free energy of the system should be found within the material balance constraints. The reacting compounds are not conserved in the system, but the total number of atoms of each chemical element[4] should be preserved.

[4] A chemical element is a chemical substance made up of one type of atom (e.g., H). A chemical compound (e.g., H_2 or CO_2) consists of more than one chemical element.

Considering a system with w chemical compounds entering into the system and k chemical compounds leaving the system at chemical equilibrium, the material balance can be expressed,

$$\begin{aligned} &\sum_{v=1}^{w} \dot{n}_{v,\text{in}} A_{vj} = \sum_{i=1}^{k} \dot{n}_{i,\text{out}} A_{ij} \ , \quad j = \{1, 2, ..., N\} \ \Leftrightarrow \\ &\sum_{i=1}^{k} \dot{n}_{i,\text{out}} A_{ij} - \sum_{v=1}^{w} \dot{n}_{v,\text{in}} A_{vj} = 0 \, , \quad j = \{1, 2, ..., N\} \end{aligned} \tag{A.2}$$

where A_{vj} is the number of atoms of element j in each molecule of entering compound v, A_{ij} is the number of atoms of element j in each molecule of leaving compound i. N is the total number of different chemical elements in the system. Eq. (A.2) describes the material constraints and consists of N equations, the unknown parameter being $\dot{n}_{i,\text{out}}$, one for each leaving chemical compound. Thus, k unknowns.

A Lagrange multiplier (λ) is introduced to each of the N material constraints, and the material constraints are summarized:

$$\begin{aligned} &\lambda_j \left(\sum_{i=1}^{k} \dot{n}_{i,\text{out}} A_{ij} - \sum_{v=1}^{w} \dot{n}_{v,\text{in}} A_{vj} \right) = 0 \, , \quad j = \{1, 2, ..., N\} \ \Leftrightarrow \\ &\sum_{j=1}^{N} \lambda_j \left(\sum_{i=1}^{k} \dot{n}_{i,\text{out}} A_{ij} - \sum_{v=1}^{w} \dot{n}_{v,\text{in}} A_{vj} \right) = 0 \end{aligned} \tag{A.3}$$

Since eq. (A.3) is equal to zero, a new function, F, identical to $\dot{G}_{\text{tot}}$ at the system outlet, can be defined as:

$$F = \dot{G}_{\text{tot,out}} + \sum_{j=1}^{N} \lambda_j \left(\sum_{i=1}^{k} \dot{n}_{i,\text{out}} A_{ij} - \sum_{v=1}^{w} \dot{n}_{v,\text{in}} A_{vj} \right) \tag{A.4}$$

The function F is equal to $\dot{G}_{\text{tot,out}}$, but also incorporates the material constraints, and, as for $\dot{G}_{\text{tot,out}}$, the minimum value of F represents chemical equilibrium. To find the outlet gas composition at chemical equilibrium, the set of outlet molar flows, $\dot{n}_{i,\text{out}}$, should be chosen so the function F is at a minimum. F can be minimized by setting the partial derivatives of F, with respect to the molar flow of each outlet compound $\dot{n}_{i,\text{out}}$, equal to zero. Thus,

$$\frac{\partial F}{\partial \dot{n}_{i,\text{out}}} = \frac{\partial \dot{G}_{\text{tot,out}}}{\partial \dot{n}_{i,\text{out}}} + \sum_{j=1}^{N} \lambda_j A_{ij} = 0\,,\;\; i = \{1,2,...,k\} \;\Leftrightarrow$$
$$g^0_{i,\text{out}} + RT\ln(y_{i,\text{out}}\,p) + \sum_{j=1}^{N} \lambda_j A_{ij} = 0\,,\;\; i = \{1,2,...,k\} \qquad \text{(A.5)}$$

From eq. (A.5) a set of k equations are defined, one for each chemical compound leaving the system, the unknown parameters being $y_{i,\text{out}}$ and λ_j.

Since,

$$y_{i,\text{out}} = \frac{\dot{n}_{i,\text{out}}}{\sum_{i=1}^{k} \dot{n}_{i,\text{out}}}\,,\;\; i = \{1,2,...,k\} \qquad \text{(A.6)}$$

eq. (A.5) can be expressed by use of molar flows instead of molar fractions:

$$g^0_{i,\text{out}} + RT\ln\left(\frac{\dot{n}_{i,\text{out}}}{\sum_{i=1}^{k} \dot{n}_{i,\text{out}}}\,p\right) + \sum_{j=1}^{N} \lambda_j A_{ij} = 0\,,\;\; i = \{1,2,...,k\} \qquad \text{(A.7)}$$

Then, eqs. (A.2) and (A.7) constitute N material balance equations and k equilibrium equations having N unknown Lagrange multipliers (λ_j) and k unknown outlet molar flows ($\dot{n}_{i,\text{out}}$). This system of N+k equations with N+k unknowns can readily be solved determining the outlet molar flows (and Lagrange multipliers), and the outlet gas composition can then be determined from eq. (A.6).

In the case of using the Gibbs free energy minimization method for calculating the outlet composition of the SOFC anode, as described in Chapter 4, the following chemical compounds and elements are included:

Inlet: $v = \{H_2, CO, CH_4, CO_2, H_2O, N_2, O_2\}$
Outlet: $i = \{H_2, CO, CH_4, CO_2, H_2O, N_2\}$
Elements: $j = \{H, C, O, N\}$

Then, k=6 and N=4, resulting in a set of 10 equations with 10 unknowns. The O_2 is coming from the cathode side, and $\dot{n}_{O_2,\text{in}}$ can be found from eq. (4.6). Operating temperature and pressure of the SOFC are used in eq. (A.7).

In the case of using the Gibbs free energy minimization method for calculating the outlet composition of the gasifier, as described in Section 5.1.1, the following chemical compounds and elements are included:

Inlet: $v = \{C_? H_? O_?, H_2O, N_2, O_2, Ar, CO_2\}$

Outlet: $i = \{H_2, CO, CH_4, CO_2, H_2O, N_2, Ar, H_2S\}$

Elements: $j = \{H, C, O, N, Ar, S\}$

Then, k=8 and N=6, resulting in a set of 14 equations with 14 unknowns. The solid biomass composition is not defined here, but the composition used in the two-stage Viking gasifier can be found in Table 5.2. The ashes and additional methane (*METH*) are not included in the equilibrium calculations. Operating temperature and pressure of the gasifier are used in eq. (A.7).

Appendix B SOFC COMPONENT MODEL LISTING

Included in this Appendix are:

- SOFC component model code (11 pages)
- Flow sheet of SOFC component test with node numbers (1 page)
- DNA Input for SOFC component test (2 pages)
- DNA Output for SOFC component test (2 pages)

The input and output data only represent one simulation using the reference conditions.

```
C**********************************************************************
      SUBROUTINE SOFCEQ0D_CBM (KOMTY,ANTLK,ANTEX,ANTKN,ANTPK,ANTM1,
     $     MEDIE,ANTME,VARME,ANTEL, VAREL,parnam,zanam
     $     ,MDOT,P,H,E,Q,ZA,PAR,RES,X_J,KOMDSC,KMEDDS,K_PAR,K_LIG
     $     ,K_BET,k_inp)
C**********************************************************************
C
C  SOFCEQ0D_CBM is a model of a Solid Oxide Fuel Cell with outlet gas
C  composition based on chemical equilibrium. It is based on the simple
C  SOFCEQ_2 (BE 2004), so N2 can be used on the anode side.
C  The calculation of the reversible efficiency (ETAMAX) have been
C  corected and the voltage efficiency is calculated by an
C  electrochemical model based on the operating conditions instead of
C  being an input parameter.
C***********************************************************************
C
CA FKOMP - INPUT  - Flag with the value:
CA                    1: Initialize the component.
CA                    2: Initialize with actual system.
CA                    3: Fluid composition calculation (constant).
CA                    4: Find residuals.
CA                    5: Find residuals and check variables.
CA                    6: Output information about component.
CA MDOT  - INPUT  - Massflows from nodes.
CA P     - INPUT  - Pressure in nodes.
CA X_J   - INPUT  - Fluid composition.
CA KOMTY - OUTPUT - Component name.
CA ANTPK - OUTPUT - Number of parameters for the component.
CA ANTLK - OUTPUT - Number of equations in the component.
CA ANTEX - OUTPUT - Number of independent equations in the component.
CA ANTED - OUTPUT - Number of differential independent equations.
CA ANTKN - OUTPUT - Number of nodes connected to the component.
CA ANTM1 - OUTPUT - Number of massflows in the first conservation of
CA                  mass equation.
CA ANTM2 - OUTPUT - Number of massflows in the second.
CA DYCOM - OUTPUT - Type of conservation equations (static or dynamic
CA                  mass and internal energy on side 1 and 2 respectively;
CA                  and dynamic solid internal energy).
CA MEDIE - IN/OUT - Media (fluid) of the connected nodes.
CA                  The values mean :
CA                    -4    : Any gas
CA ANTME - OUTPUT - Number of fluids with variable composition.
CA VARME - OUTPUT - Pointer to fluid numbers (with variable composition).
CA ANTEL - OUTPUT - Number of computed compounds in these variable fluids.
CA VAREL - OUTPUT - Compound numbers in variable fluids.
CA RES   - OUTPUT - Residuals for the component.
C
C  ANTST - Number of fluid compounds in DNA.
C
CL XMIX  Composition of the mixture.
CL K_PAR Parameter description.
CL K_LIG Equation description.
CL K_BET Condition description.
CL K_MED Media description.
C
C  Subroutines : COMINF
C
C
CP Programmer: Christian Bang-Møller (CBM), TES, MEK, DTU, 2010
C***********************************************************************

C  Including the common "environment"
      INCLUDE 'ENVIRO.INI'
      INCLUDE 'THERPROP.DEC'
      INCLUDE 'GASI.DEC'

C  Parameter variables
      INTEGER             ANTLK, ANTEX, ANTKN, MEDIE(6), ANTPK,
     :                    ANTM1, ANTME, VARME(4), ANTEL(4),
     :                    VAREL(ANTST,4)
      DOUBLE PRECISION    X_J(MAXME,ANTST),RES(39),MDOT(4),P(4),H(4),
     :                    E,Q,PAR(7),ZA(22)
      CHARACTER*3         DYCOM(5)
      CHARACTER*80        KOMTY,PARNAM(7),ZANAM(22)

C  Local variables
```

```
      INTEGER I,J
      DOUBLE PRECISION  NIN(ANTST+1),NOUT(ANTST+1),ETASYS,G(6),HG(6),R,
     $     M_BR_OUT,M_AIR_OUT,T3,T4,TGAS,ETAPRO,U,V,S,X,DUM,
     $     M_BL(4),NO2IN,NH2IN,DP1,DP2,PGAS,UF,ETAMAX,T0,GMAX,
     $     DT,i_load,eta_DCAC,F,n_e,i_n,STCR,
     $     p_anode,p_cathode,p_H2,p_H2eq,p_CO,p_CH4,p_CO2,p_H2O,p_O2,
     $     p_N2,p_H2Opr,
     $     V_cell,
     $     E_nernst,p_standard,G_s(3),G_standard,G2(5),G_real,
     $     V_act,V_act_a,V_act_c,c_a,c_c,i_0_a_0,i_0_c_0,i_0_a,i_0_c,
     $     gamma_a,gamma_c,E_act_a,E_act_c,i_0_a2,i_0_c2,i_0_a3,
     $     V_ohm,sigma_e_0,E_act_e,sigma_e,delta_e,R_e,
     $     V_conc,i_as,
     $     n_ptot_FO,p_pCO2_FO,p_pH2O_FO,p_O2_FO,G_O2_FO,G_pCO2_FO,
     $     G_pH2O_FO,GO2

      CHARACTER*100       K_PAR(7)
      CHARACTER*500       K_LIG(23), K_BET, KOMDSC
      character*1000      K_INP
      CHARACTER*100       KMEDDS(6)
      EXTERNAL           COMINF
      INCLUDE 'THERPROP.INI'
      INCLUDE 'GASI.INI'

C=======================================================================
      GOTO (200,200,1,400,400,200) FKOMP
 1    RETURN
C-----------------------------------------------------------------------
C   Component name
C-----------------------------------------------------------------------
c   100 CONTINUE
c       KOMTY     = 'SOFCEQ0D_CBM'
c       GOTO 9999
C-----------------------------------------------------------------------
C   Component characteristics
C----------------------------------------------------------------------
  200 CONTINUE
      KOMTY     = 'SOFCEQ0D_CBM'
      ANTKN     =  6
      ANTPK     =  7
      ANTLK     =  17
      ANTEX     =  23
      ANTM1     =  4
      MEDIE(1)  =  anygas$
      MEDIE(2)  =  anygas$
      MEDIE(3)  =  anygas$
      MEDIE(4)  =  anygas$
      MEDIE(5)  = power$
      MEDIE(6)  =  heat$
      ANTME     =  4
      VARME(1)  =  NODE1$
      ANTEL(1)  =  0
      VARME(2)  =  NODE2$
      ANTEL(2)  =  0
      VARME(3)  =  NODE3$
      ANTEL(3)  =  6
      VARME(4)  =  NODE4$
      ANTEL(4)  =  5
      VAREL(1,3)=H2$
      VAREL(2,3)=CO$
      VAREL(3,3)=CO2$
      VAREL(4,3)=H2O_G$
      VAREL(5,3)=CH4$
      VAREL(6,3)=N2$
      VAREL(1,4)=O2$
      VAREL(2,4)=N2$
      VAREL(3,4)=CO2$
      VAREL(4,4)=H2O_g$
      VAREL(5,4)=AR$
      ZANAM(1)  = 'MULTIPLIER H'
      ZANAM(2)  = 'MULTIPLIER C'
      ZANAM(3)  = 'MULTIPLIER N'
      ZANAM(4)  = 'MULTIPLIER O'
      ZANAM(5)  = 'GIBBS ENERGY'
      ZANAM(6)  = 'ETAMAX'
      ZANAM(7)  = 'ETASYS'
```

```
      ZANAM(8)  = 'UF'
      ZANAM(9)  = 'ETATOT'
      ZANAM(10)  = 'STCR'
      ZANAM(11)  = 'E_nernst'
      ZANAM(12)  = 'V_act'
      ZANAM(13)  = 'V_ohm'
      ZANAM(14)  = 'V_conc'
      ZANAM(15)  = 'V_cell'
      ZANAM(16)  = 'GMAX'
      ZANAM(17)  = 'G(T)'
      ZANAM(18)  = 'G(p,T)'
      ZANAM(19)  = 'p_H2eq'
      ZANAM(20)  = 'R_e'
      ZANAM(21)  = 'i_load'
      ZANAM(22)  = 'eta_DCAC'

      PARNAM(1)  = 'FUEL UTILIZATION'
      PARNAM(2)  = 'TGAS'
      PARNAM(3)  = 'DP FUEL'
      PARNAM(4)  = 'DP AIR'
      PARNAM(5)  = 'DT OUTLETS'
      PARNAM(6)  = 'Current density'
      PARNAM(7)  = 'DC/AC conversion efficiency'

      IF (FKOMP.EQ.6) GOTO 600
***   FKOMP = 3
      GOTO 9999
C-----------------------------------------------------------------------
C  Component equations. All in residual form.
C  Do not include the conservation laws, since these are treated
C  automatically by DNA.
C-----------------------------------------------------------------------
  400 CONTINUE
      VAREL(1,3)=H2$
      VAREL(2,3)=CO$
      VAREL(3,3)=CO2$
      VAREL(4,3)=H2O_G$
      VAREL(5,3)=CH4$
      VAREL(6,3)=N2$

      UF=PAR(1)
      TGAS=PAR(2)
      DP1=PAR(3)
      DP2=PAR(4)
      DT=PAR(5)
C     (DT: Optional temperature difference between anode and cathode outlets)
      i_load=PAR(6)
      eta_DCAC=PAR(7)

      R    = 8.314D0
      T0   = 298.15D0
      PGAS = P(3)

C Pressure losses
      RES(1)  = P(1)-DP1-P(3)
      RES(2)  = P(2)-DP2-P(4)
      p_anode=(P(1)+P(3))/2
      p_cathode=(P(2)+P(4))/2

C Temperature of outlet gases
C (Anode outlet temperature equals TGAS)
      CALL STATES(P(3),H(3),T3,V,S,X,DUM,1,2,MEDIE(3))
      CALL STATES(P(4),H(4),T4,V,S,X,DUM,1,2,MEDIE(4))
      RES(3)  = T3-T4-DT
      RES(4)  = T3-TGAS

C Molar mass of the gases [kg/kmol]
      M_BL(1)=0.D0
      M_BL(2)=0.D0
      M_BL(3)=0.D0
      M_BL(4)=0.D0
      DO I=1,ANTST
        M_BL(1)=X_J(MEDIE(1),I)*M_MOL(I)+M_BL(1)
        M_BL(2)=X_J(MEDIE(2),I)*M_MOL(I)+M_BL(2)
        M_BL(3)=X_J(MEDIE(3),I)*M_MOL(I)+M_BL(3)
        M_BL(4)=X_J(MEDIE(4),I)*M_MOL(I)+M_BL(4)
```

```
      ENDDO

C Calculate mole flow of each species in to the reaction (used for Gibbs mini)
C (species in the anode inlet)
      NIN(ANTST+1)=0.D0
      DO I=1,ANTST
        NIN(I)=MDOT(1)*X_J(MEDIE(1),I)/M_BL(1)
        NIN(ANTST+1)=NIN(ANTST+1)+NIN(I)
      ENDDO

C The available hydrogen (after steam reforming and water gas shift)
      NH2IN=NIN(H2$)+NIN(CO$)+4*NIN(CH4$)
C Consumed oxygen
C (UF is defined so the actual hydrogen consumption is UF*NH2IN)
C (UF affects the Gibbs free energy minimization through the amount of consumed oxygen)
      NO2IN=UF*NH2IN/2
      NIN(O2$)=NIN(O2$)+NO2IN

C Flow of used air
      RES(5)  = MDOT(2)+MDOT(4)-NO2IN*M_MOL(O2$)
C Composition of used air
      RES(6)  = MDOT(2)/M_BL(2)*X_J(MEDIE(2),O2$)-NO2IN+
     $      MDOT(4)/M_BL(4)*X_J(MEDIE(4),O2$)
      RES(7)  = MDOT(2)/M_BL(2)*X_J(MEDIE(2),N2$)+
     $      MDOT(4)/M_BL(4)*X_J(MEDIE(4),N2$)
      RES(8)  = MDOT(2)/M_BL(2)*X_J(MEDIE(2),CO2$)+
     $      MDOT(4)/M_BL(4)*X_J(MEDIE(4),CO2$)
      RES(9)  = MDOT(2)/M_BL(2)*X_J(MEDIE(2),H2O_G$)+
     $      MDOT(4)/M_BL(4)*X_J(MEDIE(4),H2O_G$)
      RES(10)  = 1.D0-X_J(MEDIE(4),O2$)-X_J(MEDIE(4),N2$)-
     $      X_J(MEDIE(4),CO2$)-X_J(MEDIE(4),H2O_G$)-
     $      X_J(MEDIE(4),AR$)

C Calculate mole flow of each species out from the reaction (used for Gibbs mini)
C (species in the anode outlet)
      NOUT(ANTST+1)=0.D0
      DO I=1,ANTST
        NOUT(I)=(-MDOT(3))*X_J(MEDIE(3),I)/M_BL(3)
        NOUT(ANTST+1)=NOUT(ANTST+1)+NOUT(I)
      ENDDO



C ------------------------------------------------------------------------------------
C Start----Calculation of anode outlet composition from Gibbs free energy minimization-----
C ------------------------------------------------------------------------------------
C  Gibbs free energy of each compound
C  (at outlet and without oxygen)
      CALL STATES(P(3),H(3),TGAS,V,S,X,U,1,2,MEDIE(3))
      TGAS = TGAS+273.15D0

      DO I=1,6
         CALL GIBBS(VAREL(I,3),TGAS,P(3)*X_J(MEDIE(3),VAREL(I,3)),G(I))
      ENDDO

      CALL GIBBS(O2$,TGAS,P(3)*X_J(MEDIE(3),O2$),GO2)

C  Partial derivatives of the function to be minimized with respect to
C  each species molar fraction
      DO I=1,6
         RES(I+10)=G(I)
         DO J=1,4
            RES(I+10)  = RES(I+10)  + ZA(J)*EL(VAREL(I,3),J)
         ENDDO
      ENDDO

C  Molar balance for each atom (H,C,N)
C  O balance is substituted by summation of molar fractions
      DO J=1,3
        RES(16+J)  = 0.D0
        DO I=1,ANTST
          RES(16+J)=RES(16+J)-(NIN(I)-NOUT(I))*EL(I,J)
        ENDDO
      ENDDO
      RES(20)=1.D0
      DO I=1,ANTST
```

```
          RES(20)= RES(20)-X_J(MEDIE(3),I)
        ENDDO

C  Summation of total Gibbs free energy of the considered species
C  (H2,CO,CO2,H2O,CH4,N2 at anode outlet)
        RES(21) = ZA(5)
        DO I=1,6
           RES(21) = RES(21) - G(I) * X_J(MEDIE(3),VAREL(I,3))
        ENDDO
C -----------------------------------------------------------------------------------------
C End-----Calculation of anode outlet composition from Gibbs free energy minimization------
C -----------------------------------------------------------------------------------------



C -----------------------------------------------------------------------------------------
C Start-----Calculating VOLTAGE EFFICIENCY (ETASYS) based on polarization losses-----------
C -----------------------------------------------------------------------------------------
C    CONSTANTS
C     The universal gas constant (R) is already given above
C     Faradays constant [C/mol]:
        F=96485
C     Number of moles of transferred electrons, n_e [mol e-/mol fuel (H2eq)]:
C     (equal to 2 since H2 (equivalent) is the only fuel in this electrochemical model,
C     [H. Zhu & R.J. Kee, J Power Sources 117 (2003) 61-74])
        n_e=2
C     Internal current density [mA/cm^2]:
C     (mixed potential and fuel crossover) (used for calibrating OCV)
        i_n=6


C    PARTIAL PRESSURES (AVERAGE)
C     Partial pressures before internal reforming [bar]:
C     (average between inlet and outlet)
        p_H2=(X_J(MEDIE(1),H2$)+X_J(MEDIE(3),H2$))/2*p_anode
        p_CO=(X_J(MEDIE(1),CO$)+X_J(MEDIE(3),CO$))/2*p_anode
        p_CO2=(X_J(MEDIE(1),CO2$)+X_J(MEDIE(3),CO2$))/2*p_anode
        p_H2O=(X_J(MEDIE(1),H2O_G$)+X_J(MEDIE(3),H2O_G$))/2*p_anode
        p_CH4=(X_J(MEDIE(1),CH4$)+X_J(MEDIE(3),CH4$))/2*p_anode
        p_N2=(X_J(MEDIE(1),N2$)+X_J(MEDIE(3),N2$))/2*p_anode
C        p_Ar=(X_J(MEDIE(1),Ar$)+X_J(MEDIE(3),Ar$))/2*p_anode
        p_O2=(X_J(MEDIE(2),O2$)+X_J(MEDIE(4),O2$))/2*p_cathode

C     Equivalent hydrogen partial pressure after internal reforming and
C     before anode reaction [bar]:
C     (derived from steam reforming and shift reactions)
        p_H2eq=p_H2+p_CO+4*p_CH4

C     Partial pressure of water product [bar]:
        p_H2Opr=p_H2O


C    NERNST POTENTIAL
C     (based on [H. Zhu & R.J. Kee, J Power Sources 117 (2003) 61-74])

C     Change in Gibbs free energy of formation [J/mol]:
C     (G_standard is for hydrogen conversion at standard pressure and operating temp,
C     [S.C. Singhal & K. Kendall, High-Temperature Solid Oxide Fuel Cells: Fundamentals,
C     Design and Application (2003), p. 60])
        p_standard=1
        CALL GIBBS(H2$,TGAS,p_standard,G_s(1))
        CALL GIBBS(O2$,TGAS,p_standard,G_s(2))
        CALL GIBBS(H2O_G$,TGAS,p_standard,G_s(3))
        G_standard=G_s(3)-G_s(1)-0.5*G_s(2)
C     (G_real is for hydrogen conversion at average partial pressures and
C     operating temperature)
        G_real=G_standard-R*TGAS*log(p_H2eq*sqrt(p_O2)/p_H2Opr)

C     Nernst potential - ideal voltage [V]:
        E_nernst=(-G_real)/(n_e*F)


C    ACTIVATION OVERPOTENTIAL
C     (based on [S.H. Chan et al., J Power Sources 93 (2001) 130-140, eq. 9],
C     [H. Zhu & R.J. Kee, J Power Sources 117 (2003) 61-74],
C     and [T. Aloui & K. Halouani, Appl Thermal Eng 27 (2007) 731-737, eq. 8])
```

```
C     Exchange current densities [mA/cm^2] based on [Costamagna & Honegger,
C     J. Electrochom. Soc., Vol. 145, No. 11 (1998) 3995-4007, table 3 and eq. 7+8]:
C     (eq. 7 is based on [Mogensen and Lindegaard, Solid Oxide Fuel Cells III (1993) 484])
C     (eq. 8 is based on [Achenbach, J Power Sources 49 333 (1994)])
C     (Ni/YSZ anode and LSM cathode)
      gamma_a=2*5.5D9
      gamma_c=0.5*7.0D8
      E_act_a=1.2D5
      E_act_c=1.2D5
      i_0_c=gamma_c*(p_O2/p_cathode)**0.25*exp(-E_act_c/(R*TGAS))
      i_0_a=gamma_a*(p_H2eq/p_anode)*(p_H2Opr/p_anode)*
     $     exp(-E_act_a/(R*TGAS))
C     Eq. 6 from [Costamagna & Honegger] based on Yamamura:
C      i_0_a3=3.5*2.9D7*(p_H2eq/p_anode)*(p_H2Opr/p_anode)**(-0.5)*
C     $     exp(-E_act_a/(R*TGAS))

C     Exchange current densities [mA/cm^2] based on [Zhu & Kee]:
C     Anode exchange current density constant:
C     (used to calibrate activation overpotential)
C      i_0_a_0=5000
C     Cathode exchange current density constant (table 2 in [Zhu & Kee]):
C     (LSM-YSZ cathode)
C      i_0_c_0=750
C     Correlations based on eq. 29 in [Zhu & Kee]:
C      i_0_a2=i_0_a_0*(p_H2eq/p_anode)
C      i_0_c2=i_0_c_0*(p_O2/p_cathode)**0.5

C     Activation overpotential (eq. 33d+33e in [Chan]):
C     [arcsinh(x)=ln(x+sqrt(x^2+1))]
      c_a=(i_load+i_n)/(2*i_0_a)
      V_act_a=2*R*TGAS/(F)*log(c_a+sqrt(c_a**2+1))
      c_c=(i_load+i_n)/(2*i_0_c)
      V_act_c=2*R*TGAS/(F)*log(c_c+sqrt(c_c**2+1))
      V_act=V_act_a+V_act_c

C     Alternative activation overpotential method:
C     (based on [J. Larminie & A. Dicks, Fuel cell systems explained (2003), p. 52]
C     and [F. Calise et al. Energy 31 (2006) 3278-3299])
C     From table 2 in [Calise]:
C      gamma_a=2.13D7
C      gamma_c=1.49D7
C      E_act_a=1.1D5
C      E_act_c=1.1D5
C      alpha_a=0.5
C      alpha_c=0.5
C     Internal current density [mA/cm^2] (mixed potential) (table 2 in [Calise]):
C      i_n=2
C     Exchange current densities (eq. 10+11 in [Calise]) [mA/cm^2]:
C      i_0_a=gamma_a*(p_H2eq/p_anode)*(p_H2Opr/p_anode)*
C     $     exp(-E_act_a/(R*TGAS))
C      i_0_c=gamma_c*(p_O2/p_cathode)**0.25*exp(-E_act_c/(R*TGAS))
C     Summation of anode and cathode overpotential (p. 52 in [Larminie] and
C     eq. 12+13 in [Calise]):
C      A_act_a=R*TGAS/(n_e*alpha_a*F)
C      A_act_c=R*TGAS/(n_e*alpha_c*F)
C      V_act=0.5*(A_act_a+A_act_c)*log((i_load+i_n)/(i_0_a**(A_act_a/
C     $      (A_act_a+A_act_c))+i_0_c**(A_act_c/(A_act_a+A_act_c))))
C     (0.5 is a calibration factor)


C    OHMIC OVERPOTENTIAL
C     Method by [H. Zhu & R.J. Kee, J Power Sources 117 (2003) 61-74]:
C     (ohmic resistance in an SOFC is typically dominated by ion resistance through the
C     electrolyte, thus the contributions from the electrodes and interconnects are neglected)
C     (based on a YSZ electrolyte)
C     Pre-factor of ionic conductivity [S*K/cm, S=ohm^(-1)], table 2 in [Zhu & Kee]:
      sigma_e_0=3.6D5
C     Activation energy of transport of oxygen ions [J/mol], table 2 in [Zhu & Kee]:
      E_act_e=8.0D4
C     Ionic conductivity of the electrolyte [S/cm or Ohm^(-1)*cm^(-1)], eq. 33 in [Zhu & Kee]:
      sigma_e=sigma_e_0/TGAS*exp(-E_act_e/(R*TGAS))

C     Electrolyte thickness [cm]:
C     [S. Linderoth et al., Materials Science Forum Vols. 539-543 (2007) 1309-1314, p. 1310]
      delta_e=10D-4
```

```
C     Area specific ohmic resistance of the electrolyte [Ohm*cm^2], eq. 34 in [Zhu & Kee]:
      R_e=delta_e/sigma_e

C     Ohmic polarization losses [(mA/cm^2)*(Ohm*cm^2)/1000=V]
      V_ohm=(i_load+i_n)*R_e/1000

C     Method by [S.H. Chan et al., Journal of Power Sources 103 (2002) 188-200, eq. 13-15 +
C     table 3] and [Bessette et al., Journal of Electrochemical Society, Vol. 142,
C     No. 11 (1995), table 1]:
C     Coefficients:
C      a_ohm_a=0.00298
C      b_ohm_a=-1392
C      a_ohm_c=0.00811
C      b_ohm_c=600
C      a_ohm_e=0.00294
C      b_ohm_e=10350
C      a_ohm_i=0.1256
C      b_ohm_i=4690
C     Layer thicknesses [cm]:
C     [S.H. Chan et al., Journal of Power Sources 93 (2001) 130-140, table 1]
C     (anode supported cell)
C      delta_a=750D-4
C      delta_c=50D-4
C      delta_e=40D-4
C     [S.H. Chan et al., Journal of Power Sources 103 (2002) 188-200, table 3]
C      delta_i=100D-4
C     Area specific resistance - ASR=[Ohm*cm^2]:
C      rho_a=a_ohm_a*exp(b_ohm_a/TGAS)
C      r_a=delta_a*rho_a
C      rho_c=a_ohm_c*exp(b_ohm_c/TGAS)
C      r_c=delta_c*rho_c
C      rho_e=a_ohm_e*exp(b_ohm_e/TGAS)
C      r_e=delta_e*rho_e
C      rho_i=a_ohm_i*exp(b_ohm_i/TGAS)
C      r_i=delta_i*rho_i
C      ASR=0.75*(r_a+r_c+r_e+r_i)
C     (0.75 is a calibration factor)


C    CONCENTRATION OVERPOTENTIAL
C     Method by [Kim, J.W. et al., J Electrochem Soc, 146 (1) (1999) 69-78]
C     and [Braun, R., Optimal Design and Operation of SOFC Systems for Small-scale Stationary
C     Applications (PhD thesis) (2002), eq. 4.8]:
C     (for anode-supported SOFCs i_cs>>i_as and the cathode concentration overpotential is
C     neglected)
C      Limiting current density of anode [mA/cm^2]:
C      (here assumed to be constant)
       i_as=1000
C      Concentration overpotential [V]:
       V_conc=-R*TGAS/(n_e*F)*(log(1-(i_load+i_n)/i_as)-
     $     log(1+(p_H2eq*(i_load+i_n))/(p_H2Opr*i_as)))

C     Method by [F. Calise et al., Energy 31 (2006) 3278-3299, eq. 20]:
C     Limiting current density [mA/cm^2]:
C      i_l=900
C      V_conc2=-R*TGAS/(n_e*F)*log(1-(i_load+i_n)/i_l)


C    SINGLE CELL POTENTIAL
      V_cell=E_nernst-V_act-V_ohm-V_conc


C    VOLTAGE EFFICIENCY
      ETASYS=V_cell/E_nernst
C ------------------------------------------------------------------------------------------
C End------Calculating VOLTAGE EFFICIENCY (ETASYS) based on polarization losses------------
C ------------------------------------------------------------------------------------------


C ------------------------------------------------------------------------------------------
C Start-----------------Calculating REVERSIBLE EFFICIENCY (ETAMAX)-------------------------
C ------------------------------------------------------------------------------------------
C The reversible effciency is the ratio between the change in Gibbs free energy of formation
C and the change in enthalpy of formation (here LHV) at full oxidation of the inlet fuel.
C [Zhu, H. and Kee, R.J., J Power Sources 161 (2006), p. 958]
```

```
C    Gibbs free energy of the reactants
C    (based on partial pressures at inlet and SOFC operating temperature)
      CALL GIBBS(H2$,TGAS,P(1)*X_J(MEDIE(1),H2$),G2(1))
      CALL GIBBS(CO$,TGAS,P(1)*X_J(MEDIE(1),CO$),G2(2))
      CALL GIBBS(CO2$,TGAS,P(1)*X_J(MEDIE(1),CO2$),G2(3))
      CALL GIBBS(H2O_G$,TGAS,P(1)*X_J(MEDIE(1),H2O_G$),G2(4))
      CALL GIBBS(CH4$,TGAS,P(1)*X_J(MEDIE(1),CH4$),G2(5))

C    Gibbs free energy of the stoichiometric amount of oxygen at Full Oxidation (FO)
C    (considering the following 6 species: H2, CO, CH4, CO2, H2O, and N2)
      p_O2_FO=(0.5*X_J(MEDIE(1),H2$)+0.5*X_J(MEDIE(1),CO$)+
     $     2*X_J(MEDIE(1),CH4$))*P(1)
      CALL GIBBS(O2$,TGAS,p_O2_FO,G_O2_FO)

C    Partial pressure and Gibbs free energy of the products CO2 and H2O at Full Oxidation (FO)
C    (considering the following 6 species: H2, CO, CH4, CO2, H2O, and N2)
      n_ptot_FO=NIN(CO$)+3*NIN(CH4$)+NIN(CO2$)+NIN(H2$)+NIN(H2O_G$)+
     $     NIN(N2$)
      p_pCO2_FO=(NIN(CO$)+NIN(CH4$)+NIN(CO2$))/n_ptot_FO*P(3)
      p_pH2O_FO=(NIN(H2$)+2*NIN(CH4$)+NIN(H2O_G$))/n_ptot_FO*P(3)
      CALL GIBBS(CO2$,TGAS,p_pCO2_FO,G_pCO2_FO)
      CALL GIBBS(H2O_G$,TGAS,p_pH2O_FO,G_pH2O_FO)

C    Maximum change in Gibbs free energy at Full Oxidation (FO) [J/mol]
C    (based on partial pressures at inlet for reactants and outlet for products)
C    (considering the following 6 species: H2, CO, CH4, CO2, H2O and N2. Here N2 balances out)
      GMAX = ((NIN(CO$)+NIN(CH4$)+NIN(CO2$))*G_pCO2_FO+
     $      (NIN(H2$)+2*NIN(CH4$)+NIN(H2O_G$))*G_pH2O_FO-
     $     NIN(H2$)*G2(1)-NIN(CO$)*G2(2)-NIN(CH4$)*G2(5)-
     $     NIN(CO2$)*G2(3)-NIN(H2O_G$)*G2(4)-
     $      (0.5*NIN(H2$)+0.5*NIN(CO$)+2*NIN(CH4$))*G_O2_FO)
     $     /NIN(ANTST+1)

C    Reversible efficiency (deltaG/deltaH)
      ETAMAX = (-GMAX)/
     $      (NED_H(H2$)*X_J(MEDIE(1),H2$)+
     $     NED_H(CO$)*X_J(MEDIE(1),CO$)+
     $     NED_H(CH4$)*X_J(MEDIE(1),CH4$))
C -----------------------------------------------------------------------------------------
C End------------------Calculating REVERSIBLE EFFICIENCY (ETAMAX)--------------------------
C -----------------------------------------------------------------------------------------


C    Relation between power and heat loss
C    (eta_DCAC is added to account for DC to AC conversion losses)
      RES(22)     = E+(NED_H(H2$)*NIN(H2$)+NED_H(CO$)*NIN(CO$)+
     $     NED_H(CH4$)*NIN(CH4$))*ETAMAX*ETASYS*UF*eta_DCAC

C    Steam to carbon ratio at anode inlet
      STCR=X_J(MEDIE(1),H2O_G$)/
     $      (X_J(MEDIE(1),CH4$)+X_J(MEDIE(1),CO$)+X_J(MEDIE(1),CO2$))

C    Printing of relevant variables
      RES(23)=ZA(6)-ETAMAX
      RES(24)=ZA(7)-ETASYS
      RES(25)=ZA(8)-UF
      RES(26)=ZA(9)-ETAMAX*ETASYS*UF
      RES(27)=ZA(10)-STCR
      RES(28)=ZA(11)-E_nernst
      RES(29)=ZA(12)-V_act
      RES(30)=ZA(13)-V_ohm
      RES(31)=ZA(14)-V_conc
      RES(32)=ZA(15)-V_cell
      RES(33)=ZA(16)-GMAX
      RES(34)=ZA(17)-G_standard
      RES(35)=ZA(18)-G_real
      RES(36)=ZA(19)-p_H2eq
      RES(37)=ZA(20)-R_e
      RES(38)=ZA(21)-i_load
      RES(39)=ZA(22)-eta_DCAC


      IF (FKOMP.EQ.5) GOTO 500
      GOTO 9999
C-----------------------------------------------------------------------
```

```
C  Solution check
C-----------------------------------------------------------------------
  500 CONTINUE
      IF (MDOT(1).LT.-1D-10) GOTO 550
      IF (MDOT(2).LT.-1D-10) GOTO 550
      IF (MDOT(3).GT.1D-10) GOTO 550
      IF (MDOT(4).GT.1D-10) GOTO 550
C       DO I=1,ANTST
C         PRINT*,X_J(MEDIE(3),I),X_J(MEDIE(4),I)
C       ENDDO
      GOTO 9999
  550 FBETI = .FALSE.
      GOTO 9999
C-----------------------------------------------------------------------
C  Write component information
C-----------------------------------------------------------------------
  600 CONTINUE
      KOMDSC = 'Solid oxide fuel cell with given hydrogen utilization'//
     $      ' and current density. Composition of the depleted fuel'//
     $      ' is calculated by chemical equilibrium.'//
     $      ' The voltage efficiency ($\\eta_{v}$) is predicted by an'//
     $      ' electrochemical model based on the operating conditions.'//
     $      ' A DC to AC conversion efficiency is also applied.¤'
      K_PAR(1) = 'Hydrogen utilization: $\\alpha$  [--]¤'
      K_PAR(2) = 'Operating temperature: $T_{cell}$ [\\degC]¤'
      K_PAR(3) = 'Pressure loss fuel: $\\Delta p_{13}$ [--]¤'
      K_PAR(4) = 'Pressure loss air: $\\Delta p_{24}$ [--]¤'
      K_PAR(5) = 'Temperature difference between anode and '//
     $     'cathode outlet: $\\Delta T_{out}$ [\\degC]¤'
      K_PAR(6) = 'Current density: $i_{load}$ [mA cm^{-2}]¤'
      K_PAR(7) = 'DC to AC conversion efficiency: $\\eta_{DCAC}$ [--]¤'
      K_LIG(1) = 'Pressure loss fuel: $p_3=p_1(1-\\beta_{13})$¤'
      K_LIG(2) = 'Pressure loss air: $p_4=p_2(1-\\beta_{24})$¤'
      K_LIG(3) = 'Temperature of outlet fuel: $T_3=T_{cell}$¤'
      K_LIG(4) = 'Temperature of outlet air: $T_4=T_3-\\Delta T_{out}$¤'
      K_LIG(5) = 'Mass flow of used air: '//
     $     '$\\dot{m}_4=\\dot{m_2}-'//
     $     '\\dot{n}_{\\mathrm{O_2,actual}}M_{\\mathrm{O_2}}$¤'
      K_LIG(6) = 'Oxygen balance on air side: '//
     $     '$\\frac{\\dot{m}_4}{M_4}y_{\\mathrm{O_2},4}='//
     $     '\\frac{\\dot{m_2}}{M_2}y_{\\mathrm{O_2},2}-'//
     $     '\\dot{n}_{\\mathrm{O_2,actual}}$¤'
      K_LIG(7) = 'Nitrogen balance on air side: '//
     $     '$\\frac{\\dot{m}_4}{M_4}y_{\\mathrm{N_2},4}='//
     $     '\\frac{\\dot{m_2}}{M_2}y_{\\mathrm{N_2},2}$¤'
      K_LIG(8) = 'Carbon dioxide balance on air side: '//
     $     '$\\frac{\\dot{m}_4}{M_4}y_{\\mathrm{CO_2},4}='//
     $     '\\frac{\\dot{m_2}}{M_2}y_{\\mathrm{CO_2},2}$¤'
      K_LIG(9) = 'Water balance on air side: '//
     $     '$\\frac{\\dot{m}_4}{M_4}y_{\\mathrm{H_2O},4}='//
     $     '\\frac{\\dot{m_2}}{M_2}y_{\\mathrm{H_2O},2}$¤'
      K_LIG(10) = 'Summation of molar fractions of used air: '//
     $     '$y_{\\mathrm{O_2},4}+y_{\\mathrm{N_2},4}+'//
     $     'y_{\\mathrm{CO_2},4}+y_{\\mathrm{H_2O},4}+'//
     $     'y_{\\mathrm{Ar},4}=1$¤'
      K_LIG(11) = 'Partial derivative of Gibbs energy of outlet '//
     $     'gas with respect to Hydrogen content of gas:'//
     $     '$$\\frac{\\partial F}'//
     $     '{\\partial \\dot{n}_{\\mathrm{H_2,out}}}='//
     $     '\\frac{g_{\\mathrm{H_2,out}}^0}{RT}+'//
     $     '\\ln(y_{\\mathrm{H_2,out}}p_3)+'//
     $     '\\sum_{j\\mathrm{ in H,C,O}}'//
     $     '\\mu_j \\mathbf{A}_{\\mathrm{H_2},j}$$, '//
     $     'where $\\mathbf{A}$ is a matrix with information on the'//
     $     ' moles of $j$ in each mole $\\mathrm{H_2}$. ¤'
      K_LIG(12) = 'Partial derivative of Gibbs energy of outlet '//
     $     'gas with respect to Carbon Monoxide content of gas:'//
     $     '$$\\frac{\\partial F}'//
     $     '{\\partial \\dot{n}_{\\mathrm{CO,out}}}='//
     $     '\\frac{g_{\\mathrm{CO,out}}^0}{RT}+'//
     $     '\\ln(y_{\\mathrm{CO,out}}p_3)+'//
     $     '\\sum_{j\\mathrm{ in H,C,O}}'//
     $     '\\mu_j \\mathbf{A}_{\\mathrm{CO},j}$$, '//
     $     'where $\\mathbf{A}$ is a matrix with information on the'//
     $     ' moles of $j$ in each mole $\\mathrm{CO}$. ¤'
      K_LIG(13) = 'Partial derivative of Gibbs energy of outlet '//
```

```
     $     'gas with respect to Carbon Dioxide content of gas:'//
     $     '$$\\frac{\\partial F}'//
     $     '{\\partial \\dot{n}_{\\mathrm{CO_2,out}}}='//
     $     '\\frac{g_{\\mathrm{CO_2,out}}^0}{RT}+'//
     $     '\\ln(y_{\\mathrm{CO_2,out}}p_3)+'//
     $     '\\sum_{j\\mathrm{ in H,C,O}}'//
     $     '\\mu_j \\mathbf{A}_{\\mathrm{CO_2},j}$$, '//
     $     'where $\\mathbf{A}$ is a matrix with information on the'//
     $     ' moles of $j$ in each mole $\\mathrm{CO_2}$. ¤'
      K_LIG(14) = 'Partial derivative of Gibbs energy of outlet '//
     $     'gas with respect to water content of gas:'//
     $     '$$\\frac{\\partial F}'//
     $     '{\\partial \\dot{n}_{\\mathrm{H_2O,out}}}='//
     $     '\\frac{g_{\\mathrm{H_2O,out}}^0}{RT}+'//
     $     '\\ln(y_{\\mathrm{H_2O,out}}p_3)+'//
     $     '\\sum_{j\\mathrm{ in H,C,O}}'//
     $     '\\mu_j \\mathbf{A}_{\\mathrm{H_2O},j}$$, '//
     $     'where $\\mathbf{A}$ is a matrix with information on the'//
     $     ' moles of $j$ in each mole $\\mathrm{H_2O}$. ¤'
      K_LIG(15) = 'Partial derivative of Gibbs energy of outlet '//
     $     'gas with respect to methane content of gas:'//
     $     '$$\\frac{\\partial F}'//
     $     '{\\partial \\dot{n}_{\\mathrm{CH_4,out}}}='//
     $     '\\frac{g_{\\mathrm{CH_4,out}}^0}{RT}+'//
     $     '\\ln(y_{\\mathrm{CH_4,out}}p_3)+'//
     $     '\\sum_{j\\mathrm{ in H,C,O}}'//
     $     '\\mu_j \\mathbf{A}_{\\mathrm{CH_4},j}$$, '//
     $     'where $\\mathbf{A}$ is a matrix with information on the'//
     $     ' moles of $j$ in each mole $\\mathrm{CH_4}$. ¤'
      K_LIG(16) = 'Partial derivative of Gibbs energy of outlet '//
     $     'gas with respect to nitrogen content of gas:'//
     $     '$$\\frac{\\partial F}'//
     $     '{\\partial \\dot{n}_{\\mathrm{N_2,out}}}='//
     $     '\\frac{g_{\\mathrm{N_2,out}}^0}{RT}+'//
     $     '\\ln(y_{\\mathrm{N_2,out}}p_3)+'//
     $     '\\sum_{j\\mathrm{ in H,C,O}}'//
     $     '\\mu_j \\mathbf{A}_{\\mathrm{N_2},j}$$, '//
     $     'where $\\mathbf{A}$ is a matrix with information on the'//
     $     ' moles of $j$ in each mole $\\mathrm{N_2}$. ¤'
      K_LIG(17) = 'Molar balance for Hydrogen: '//
     $     '$\\sum_{i \\mathrm{ in inlet gas}}'//
     $     '\\dot{n}_{i,\\mathrm{in}}\\mathbf{A}_{i,\\mathrm{H}}-'//
     $     '\\sum_{i \\mathrm{ in outlet gas}}'//
     $     '\\dot{n}_{i,\\mathrm{out}}\\mathbf{A}_{i,\\mathrm{H}}$¤'
      K_LIG(18) = 'Molar balance for Carbon: '//
     $     '$\\sum_{i \\mathrm{ in inlet gas}}'//
     $     '\\dot{n}_{i,\\mathrm{in}}\\mathbf{A}_{i,\\mathrm{C}}-'//
     $     '\\sum_{i \\mathrm{ in outlet gas}}'//
     $     '\\dot{n}_{i,\\mathrm{out}}\\mathbf{A}_{i,\\mathrm{C}}$¤'
      K_LIG(19) = 'Molar balance for Nitrogen: '//
     $     '$\\sum_{i \\mathrm{ in inlet gas}}'//
     $     '\\dot{n}_{i,\\mathrm{in}}\\mathbf{A}_{i,\\mathrm{N}}-'//
     $     '\\sum_{i \\mathrm{ in outlet gas}}'//
     $     '\\dot{n}_{i,\\mathrm{out}}\\mathbf{A}_{i,\\mathrm{n}}$¤'
      K_LIG(20) = 'Sum of molar fractions in used fuel: '//
     $     '$\\sum_{i \\mathrm{ in outlet gas}}=1$¤'
      K_LIG(21) = 'Gibbs energy of depleted fuel:'//
     $     '$G = \\sum_{i \\mathrm{in outlet gas}} '//
     $     '\\dot{n}_i \\left( g_i^0 + R T \\ln{y_ip} \\right)$¤'
      K_LIG(22) = 'Voltage efficiency from an electrochemical model: '//
     $     '$\\eta_{v}(T_{cell},p,y_{i},\\alpha,i_{load})$¤'
      K_LIG(23) = 'Power production: '//
     $     '$\\dot{E}=\\eta_{max}\\eta_{v}\\alpha\\eta_{DCAC}'//
     $     '\\sum_{i \\mathrm{in fuel}} H_u,i$, where '//
     $     '$\\alpha=\\frac{\\dot{n}_{\\mathrm{H_2,cons}}}'//
     $     '{\\dot{n}_{\\mathrm{H_2}}+\\dot{n}_{\\mathrm{CO}}'//
     $     '+4\\dot{n}_{\\mathrm{CH_4}}}$¤'
      K_BET = '$\\dot{m}_1 \\gt 0 $\\\\$\\dot{m}_2 \\gt 0 $\\\\'//
     $     '$\\dot{m}_3 \\gt 0 $\\\\$\\dot{m}_4 \\gt 0 $¤'
      KMEDDS(1) = 'Fuel inlet¤'
      KMEDDS(2) = 'Air inlet¤'
      KMEDDS(3) = 'Depleted fuel out¤'
      KMEDDS(4) = 'Used air out¤'
      KMEDDS(5) = 'Power¤'
      KMEDDS(6) = 'Heat loss¤'
      K_INP='STRUC sofc sofceq0d_CBM 1 2 3 4 201 301 0.85 800 0 0 0 '//
```

```
      $      '300 0.95\\\\'//
      $      'FLUID fuel H2 0.8 CO2 0.1 N2 0.1\\\\'//
      $      'MEDIA 1 fuel 2 SIMPLE_AIR 3 USEDFUEL 4 FLUEGAS\\\\'//
      $      'START Y_J USEDFUEL H2 0.2 Y_J USEDFUEL CH4 1e-6\\\\'//
      $      'START Y_J USEDFUEL H2O-G 0.3\\\\'//
      $      'START Y_J USEDFUEL CO 0.2 Y_J USEDFUEL CO2 0.2 '//
      $      'Y_J USEDFUEL N2 0.1\\\\'//
      $      'START Y_J FLUEGAS N2 0.8 Y_J FLUEGAS O2 0.2\\\\'//
      $      'ADDCO m sofc 1 1 t sofc 1 700 p 1 3 '//
      $      't sofc 2 700 p 2 3\\\\'//
      $      'START t sofc 3 800 t sofc 4 800 m sofc 2 100 '//
      $      'm sofc 3 -10\\\\'//
      $      'START p 2 3 p 3 3 p 4 3 \\\\'//
      $      'ADDCO q sofc 301 0¤'
       GOTO 9999
C
 9999  CONTINUE
       RETURN
       END

C========================================================================
```

Flow sheet of SOFC component test with node numbers

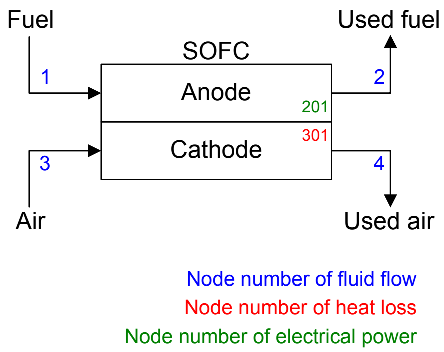

```
title SOFC component test

fluid FUEL H2 0.2614 N2 0.30198 CO 0.1814 CO2 0.1179 H2O-G 0.1269 CH4 0.01042

media 3 STANDARD_AIR 1 FUEL 2 USEDFUEL 4 USEDAIR

C ---------------------------------SOFC---------------------------------------
struc sofc sofceq0d_CBM /
    {fuel and air inlets} 1 3 /
    {fuel and air outlets} 2 4  /
    {nodes for power and heat loss} 201 301 /
    {parameters: utilization, temperature} 0.85 800 /
    {pressure loss ratios} 0 0 /
    {temperature difference between anode and cathode outlet} 0 /
    {current density [mA/cm2]} 300 /
    {DC to AC conversion efficiency [-]} 1

addco p 3 1 t sofc 3 600
addco p 1 1 t sofc 1 650
addco e sofc 201 -10000
addco q sofc 301 0




C ~~~~~~~~~~~~~~~~~~~~~~~~~~~~~~~~~~~~~~~~~~~~~~~~~~~~~~~~~~~~~~~~~~~~~~~~~~~~~~~~~~~~~~~~~~~
~~~~~
C ~~ Start of list of generated initial guesses.
C ~~ The values are the results of the latest simulation.
C ~~~~~~~~~~~~~~~~~~~~~~~~~~~~~~~~~~~~~~~~~~~~~~~~~~~~~~~~~~~~~~~~~~~~~~~~~~~~~~~~~~~~~~~~~~~
~~~~~
START M     sofc                     1  0.3570149203519879E+01 {~~}
START P                         1  0.1000000000000002E+01 {~~}
START H     sofc                     1 -0.3556798254615437E+04 {~~}
START M     sofc                      3  0.2821245195002270E+02 {~~}
START P                          3  0.1000000000000002E+01 {~~}
START H     sofc                      3  0.5194065598541852E+03 {~~}
START M     sofc                     2 -0.4653675564564562E+01 {~~}
START P                         2  0.1000000000000002E+01 {~~}
START H     sofc                     2 -0.6077944726815711E+04 {~~}
START M     sofc                      4 -0.2712892558897801E+02 {~~}
START P                          4  0.1000000000000002E+01 {~~}
START H     sofc                      4  0.7460750684058085E+03 {~~}
START E     sofc                    201 -0.1000000000000002E+05 {~~}
START Q     sofc                    301  0.0000000000000000E+00 {~~}
START ZA    sofc                      1  0.9305205152080904E+05 {~~}
START ZA    sofc                      2  0.8334089162545065E+05 {~~}
START ZA    sofc                      3  0.1171736976840727E+06 {~~}
START ZA    sofc                      4  0.2887364309244900E+06 {~~}
START ZA    sofc                      5 -0.4395688774684369E+06 {~~}
START ZA    sofc                      6  0.6884847150125958E+00 {~~}
START ZA    sofc                      7  0.8454116292315869E+00 {~~}
START ZA    sofc                      8  0.8500000000000016E+00 {~~}
START ZA    sofc                      9  0.4947450369268662E+00 {~~}
START ZA    sofc                     10  0.4097249128244875E+00 {~~}
START ZA    sofc                     11  0.9452308098598988E+00 {~~}
START ZA    sofc                     12  0.1082124265828745E+00 {~~}
START ZA    sofc                     13  0.7147434745365793E-02 {~~}
START ZA    sofc                     14  0.3076182956811065E-01 {~~}
START ZA    sofc                     15  0.7991091189635479E+00 {~~}
START ZA    sofc                     16 -0.8462030083349127E+05 {~~}
START ZA    sofc                     17 -0.1885369880714485E+06 {~~}
START ZA    sofc                     18 -0.1824011893786647E+06 {~~}
START ZA    sofc                     19  0.2778328680585008E+00 {~~}
START ZA    sofc                     20  0.2335762988681631E-01 {~~}
START ZA    sofc                     21  0.4356137835365532E+05 {~~}
START ZA    sofc                     22  0.3000000000000006E+03 {~~}
START Y_J   USEDFUEL                  H2          0.4175231528646270E-01 {~~}
START Y_J   USEDFUEL                  CO          0.2943327774588393E-01 {~~}
START Y_J   USEDFUEL                  CO2         0.2739639104926799E+00 {~~}
START Y_J   USEDFUEL                  H2O-G       0.3590352285377990E+00 {~~}
START Y_J   USEDFUEL                  CH4         0.3577116348414438E-07 {~~}
START Y_J   USEDFUEL                  N2          0.2958152321660127E+00 {~~}
START Y_J   USEDAIR                   O2          0.1790704565457096E+00 {~~}
START Y_J   USEDAIR                   N2          0.8006264279316373E+00 {~~}
START Y_J   USEDAIR                   CO2         0.3107619722855365E-03 {~~}
```

```
START Y_J   USEDAIR                       H2O-G        0.1046231973361306E-01 {~~}
START Y_J   USEDAIR                       AR           0.9530033816756465E-02 {~~}
C ~~~~~~~~~~~~~~~~~~~~~~~~~~~~~~~~~~~~~~~~~~~~~~~~~~~~~~~~~~~~~~~~~~~~~~~~~~~~~~~~~~~~~~~~~~~~~~~~~
C ~~ End of generated initial guesses.
C ~~~~~~~~~~~~~~~~~~~~~~~~~~~~~~~~~~~~~~~~~~~~~~~~~~~~~~~~~~~~~~~~~~~~~~~~~~~~~~~~~~~~~~~~~~~~~~~~~
```

end

DNA Output for SOFC component test


```
SOFC component test
RUN NUMBER     1



ALGEBRAIC VARIABLES
 NO |      TO      |  MEDIA       |     M     |     T     |     P     |     H     |   ENERGY    |  X  |     S      |      V      |     U     |
 DE | COMPONENT    |              |  [kg/s]   |    [C]    |   [bar]   |  [kJ/kg]  |   [kJ/s]    |     | [kJ/kg K]  |   [m3/kg]   |  [kJ/kg]  |
--------------------------------------------------------------------------------------------------------------------------------
  1 |sofc        |FUEL          |      3.57 |  650.00 |    1.000 |  -3556.8 |  2.021E+04 |  -  |   10.5509 |      3.5354 |  -3910.3|
  3 |sofc        |STANDARD_AIR  |     28.21 |  600.00 |    1.000 |    519.4 |            |  -  |    8.0291 |      2.5159 |    267.8|
  2 |sofc        |USEDFUEL      |     -4.65 |  800.00 |    1.000 |  -6077.9 |            |  -  |    9.1127 |      3.2186 |  -6399.8|
  4 |sofc        |USEDAIR       |    -27.13 |  800.00 |    1.000 |    746.1 |            |  -  |    8.2703 |      3.1043 |    435.6|
201 |sofc        |ELECT_POWER   |           |         |          |          | -1.000E+04 |     |           |             |         |
301 |sofc        |HEAT          |           |         |          |          |  0.000E+00 |     |           |             |         |
--------------------------------------------------------------------------------------------------------------------------------

  ELEC. POWER PRODUCTION  =   10000.0000 kW
  NET POWER PRODUCTION    =   10000.0000 kW
  FUEL CONSUMPTION (LHV)  =   20212.4312 kJ/s
  FUEL CONSUMPTION (HHV)  =   41892.1896 kJ/s
  THERMAL EFFICIENCY (LHV)=       0.4947
  THERMAL EFFICIENCY (HHV)=       0.2387

  MAXIMUM RELATIVE ERROR = 2.1736E-14
  COMPUTER ACCURACY      = 1.0842E-19



IDEAL GAS COMPOSITION (MOLAR BASE):

                |FUEL        |STANDARD_AIR|USEDFUEL    |USEDAIR     |
--------------------------------------------------------------------
HYDROGEN        | 0.2614E+00 | 0.0000E+00 | 0.4175E-01 | 0.0000E+00 |
OXYGEN          | 0.0000E+00 | 0.2075E+00 | 0.0000E+00 | 0.1791E+00 |
NITROGEN        | 0.3020E+00 | 0.7729E+00 | 0.2958E+00 | 0.8006E+00 |
CARBON MONOXIDE | 0.1814E+00 | 0.0000E+00 | 0.2943E-01 | 0.0000E+00 |
CARBON DIOXIDE  | 0.1179E+00 | 0.3000E-03 | 0.2740E+00 | 0.3108E-03 |
WATER (I.G.)    | 0.1269E+00 | 0.1010E-01 | 0.3590E+00 | 0.1046E-01 |
METHANE         | 0.1042E-01 | 0.0000E+00 | 0.3577E-07 | 0.0000E+00 |
ARGON           | 0.0000E+00 | 0.9200E-02 | 0.0000E+00 | 0.9530E-02 |
--------------------------------------------------------------------
MEAN  MOLE  MASS| 0.2171E+02 | 0.2885E+02 | 0.2772E+02 | 0.2874E+02 |
NET CALORI VALUE| 0.5662E+04 | 0.0000E+00 | 0.6647E+03 | 0.0000E+00 |
GRS CALORI VALUE| 0.1173E+05 | 0.0000E+00 | 0.2453E+04 | 0.0000E+00 |
--------------------------------------------------------------------

MEDIUM 200 : ELECTRICAL POWER
MEDIUM 300 : HEAT
MEDIUM 301 : PRODUCT HEAT


NUMBER OF CLOSED INTERNAL LOOPS IN THE SYSTEM:    0

```

```
 SOLUTION FOR THE INDEPENDENT ALGEBRAIC VARIABLES :


 VARIABLE NO | COMPONENT  |    NAME     |    VALUE    |
------------------------------------------------------
      1     |sofc        |MULTIPLIER H|  0.9305E+05 |
      2     |sofc        |MULTIPLIER C|  0.8334E+05 |
      3     |sofc        |MULTIPLIER N|  0.1172E+06 |
      4     |sofc        |MULTIPLIER O|  0.2887E+06 |
      5     |sofc        |GIBBS ENERGY|  -.4396E+06 |
      6     |sofc        |ETAMAX      |  0.6885E+00 |
      7     |sofc        |ETASYS      |  0.8454E+00 |
      8     |sofc        |UF          |  0.8500E+00 |
      9     |sofc        |ETATOT      |  0.4947E+00 |
     10     |sofc        |STCR        |  0.4097E+00 |
     11     |sofc        |E_nernst    |  0.9452E+00 |
     12     |sofc        |V_act       |  0.1082E+00 |
     13     |sofc        |V_ohm       |  0.7147E-02 |
     14     |sofc        |V_conc      |  0.3076E-01 |
     15     |sofc        |V_cell      |  0.7991E+00 |
     16     |sofc        |GMAX        |  -.8462E+05 |
     17     |sofc        |G(T)        |  -.1885E+06 |
     18     |sofc        |G(p,T)      |  -.1824E+06 |
     19     |sofc        |p_H2eq      |  0.2778E+00 |
     20     |sofc        |R_e         |  0.2336E-01 |
     21     |sofc        |Area [cm^2] |  0.4356E+05 |
     22     |sofc        |i_load      |  0.3000E+03 |
     23     |sofc        |eta_DCAC    |  0.1000E+01 |
------------------------------------------------------

========================================================================================================================
########################################################################################################################
```

Appendix C MGT PLANT MODEL LISTING

Included in this Appendix are:

- Flow sheet of MGT scenario with node numbers (1 page)
- DNA Input for MGT scenario (9 pages)
- DNA Output for MGT scenario (6 pages)

The input and output data only represent one simulation using the reference conditions.

Flow sheet of MGT scenario with node numbers

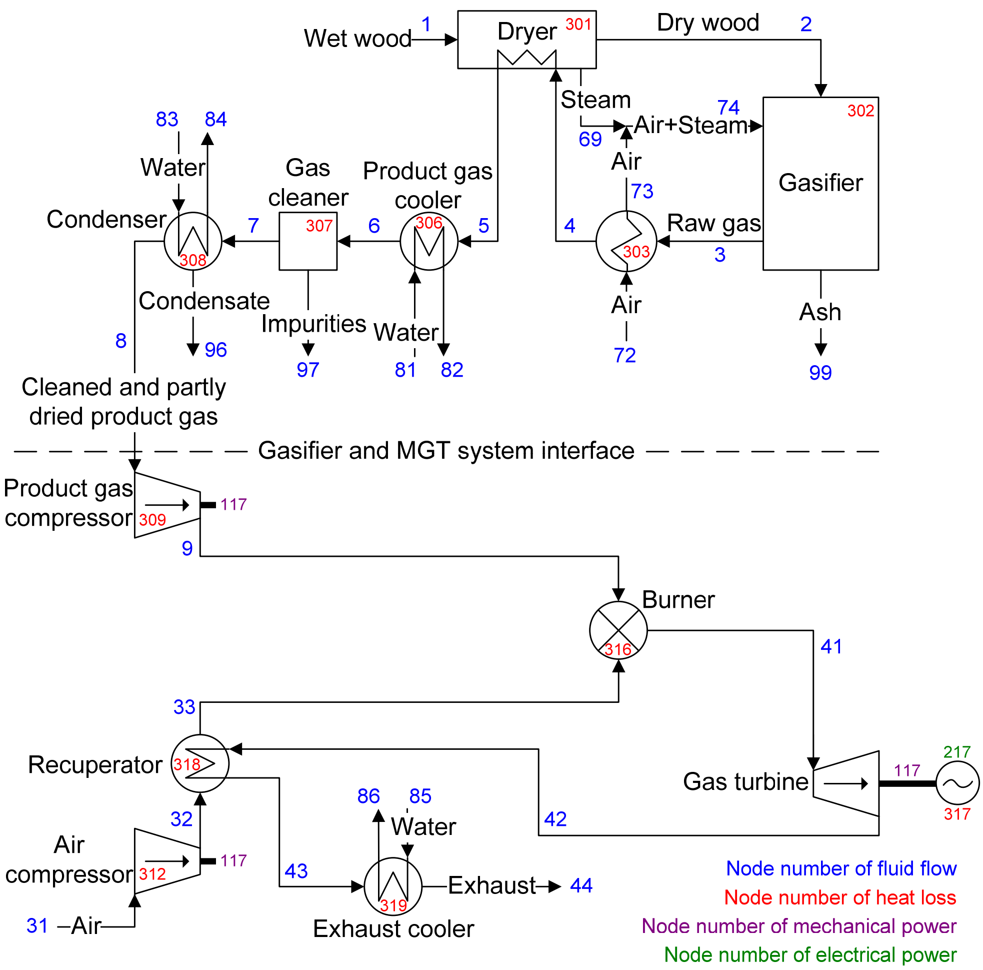

```
title Biomass gasification (Viking) + MGT incl. recuperation
C Wood is dried and gasified. The gasification is atmospheric,
C based on air, and almost reaches equilibrium. The produced
C product gas (PG) composition and the cold gas efficiency is
C similar to that from the Viking gasifier.
C Power and heat production by a MGT system.


C ###################################################
C ###################################################
C ###################################################
C -----------------GASIFIER PART---------------------
C ###################################################
C ###################################################
C ###################################################

C ##Media##
media 1 Wood 2 DryWood
media 73 STANDARD_AIR 3 raw_PG 99 Ash

C ##Fuel composition##
solid Wood C 0.488 H .062 O .439 S .0002 N 0.0017 ASH .0091
+ LHV 18280 CP 1.35 MOI .322
C [Ahrenfeldt, J. et al., Energy & Fuels 2006, 20, 2672-2680] without Cl.



C ###################################################
C -----------------------DRYER-----------------------
C ###################################################
struc Dryer DRYER_03 1 64 2 61 301  0.05 0.005

C Fuel input (plant size):
addco m Dryer 1 0.043

addco t Dryer 1 15 p 1 1.013
addco p 2 1.008 t Dryer 2 150
addco q Dryer 301 0



C ###################################################
C ---------------------GASIFIER----------------------
C ###################################################
struc Gasifier GASIFI_3 8  2 26 74 3 99 302  1 3 4 6 7 9 11 36 /
 0.998 800 0.005 0 1.0 0.01
C Variable constitution parameter: Number of calculated gas components 8
C Nodes: Inlet fuel 2; inlet water 26; inlet air 74; outlet PG 3,
C        outlet ash 99, heat loss 302
C Integer Parameters: Calculated gas compounds H2 (1), N2 (3), CO (4),
C                      CO2 (6), H2O (7), H2S (9), CH4 (11), Ar (36)
C Real parameter: Pressure 1 bar, Eq. temperature 800 degC, Pressure loss 0,
C                 Water-to-fuel ratio 0, carbon conversion factor 1,
C                 non-equilibrium methane 0.01.

addco t Gasifier 3 800
addco t Gasifier 26 150
addco p 99 1.013
addco q Gasifier 302 0



C ###################################################
C -------------GASIFIER AIR PREHEATER----------------
C ###################################################
struc airpreheat heatex_2 3 4 72 73 303 20 0.005 0.005
addco t airpreheat 72 15
addco q airpreheat 303 0



C ###################################################
C ------------------STEAM HEATER---------------------
C ###################################################
struc steamheater heatex_1 4 5 63 64 304 0.005 0.005

```

```
media 63 STEAM-HF

addco t steamheater 64 250
addco q steamheater 304 0



C ###################################################
C ------------------STEAM BLOWER---------------------
C ###################################################
struc steamblower COMPRE_1 61 62 305 105 0.6 0.98



C ###################################################
C --------------------SPLITTER-----------------------
C ###################################################
struc split1 SPLITTER 62 63 69



C ###################################################
C ----------------------MIXER------------------------
C ###################################################
struc mix1 MIXER_02 73 69 74

media 74 humid_air



C ###################################################
C --------------------GAS COOLER---------------------
C ###################################################
struc gascooler GASCOOL1 5 6 98 81 82 306 0.005 0.005

media 81 STEAM-HF 6 cold_PG

addco t gascooler 6 90
addco t gascooler 81 30 p 81 1.013
addco t gascooler 82 80
addco q gascooler 306 0



C ###################################################
C -------------------GAS CLEANING--------------------
C ###################################################
struc gasclean GASCLE_1 6 7 97 307 0.0049
C Pressure loss is taken from paper about Viking

media 7 clean_PG 97 impurities

addco q gasclean 307 0



C ###################################################
C --------------------CONDENSER----------------------
C ###################################################
struc condenser GASCOOL1 7 8 96 83 84 308 0.005 0.005

media 83 STEAM-HF 8 dry_PG

addco t condenser 8 50
addco t condenser 83 30 p 83 1.013
addco t condenser 84 80
addco q condenser 308 0



C ###################################################
C ###################################################
C ###################################################
C -------------------MGT PART-----------------------
C ###################################################
C ###################################################
```

```
C ###################################################



C ###################################################
C ----------------PG COMPRESSOR--------------------
C ###################################################
struc PGcompressor compre_1 8 9 309 117 0.75 0.98
C Isentropic efficiency from L. Fryda et al. (2008)



C ###################################################
C -----------------AIR COMPRESSOR--------------------
C ###################################################
struc aircompressor compre_1 31 32 312 117 0.75 0.98
C Isentropic efficiency from L. Fryda et al. (2008)

media 31 STANDARD_AIR

addco p 31 1.013 t aircompressor 31 15



C ###################################################
C ------------------RECUPERATOR---------------------
C ###################################################
struc recuperator heatex_4 42 43 32 33 318 0.85 0.01 0.01
addco q recuperator 318 0



C ###################################################
C ---------------------BURNER------------------------
C ###################################################
struc burner GASBUR_3 33 9 41 316 0.999374

media 41 FLUE_GAS

addco q burner 316 0

C BURNER OPERATING PRESSURE:
addco p 9 3.75



C ###################################################
C -------------------GAS TURBINE---------------------
C ###################################################
struc GT turbin_1 41 42 117 0.84
C Isentropic efficiency from L. Fryda et al. (2008)

addco t GT 41 900



C ###################################################
C --------------------GENERATOR----------------------
C ###################################################
struc generator sim_gene 217 317 117 0.95



C ###################################################
C ----------------DISTRICT HEATING-------------------
C ###################################################
struc exhaustcooler heatex_2 43 44 85 86 319 90 0.010 0.005

media 85 STEAM-HF

addco p 44 1.013
addco p 85 1.013 t exhaustcooler 85 30
addco t exhaustcooler 86 80
addco q exhaustcooler 319 0
```

```

C Reference conditions for exergy
xergy p 1 t 15




C ~~~~~~~~~~~~~~~~~~~~~~~~~~~~~~~~~~~~~~~~~~~~~~~~~~~~~~~~~~~~~~~~~~~~~~~~~~~~~~~~~~~~~~~~~~~~~~~~~~~~~
C ~~ Start of list of generated initial guesses.
C ~~ The values are the results of the latest simulation.
C ~~~~~~~~~~~~~~~~~~~~~~~~~~~~~~~~~~~~~~~~~~~~~~~~~~~~~~~~~~~~~~~~~~~~~~~~~~~~~~~~~~~~~~~~~~~~~~~~~~~~~
START M     Dryer                         1  0.4300000000000009E-01 {~~}
START P                              1  0.1013000000000002E+01 {~~}
START H     Dryer                         1 -0.8621618755529553E+04 {~~}
START M     Dryer                        64  0.2000459030657094E+00 {~~}
START P                             64  0.9980000000000021E+00 {~~}
START H     Dryer                        64 -0.1299653551379775E+05 {~~}
START M     Dryer                         2 -0.3068842105263164E-01 {~~}
START P                              2  0.1008000000000002E+01 {~~}
START H     Dryer                         2 -0.5497059220211011E+04 {~~}
START M     Dryer                        61 -0.2123574820130778E+00 {~~}
START P                             61  0.9930000000000021E+00 {~~}
START H     Dryer                        61 -0.1319443607829822E+05 {~~}
START Q     Dryer                       301  0.0000000000000000E+00 {~~}
START X_J   DryWood                  H2           0.5890000000000011E-01 {~~}
START X_J   DryWood                  O2           0.4170500000000009E+00 {~~}
START X_J   DryWood                  N2           0.1615000000000003E-02 {~~}
START X_J   DryWood                  CO           0.0000000000000000E+00 {~~}
START X_J   DryWood                  NO           0.0000000000000000E+00 {~~}
START X_J   DryWood                  CO2          0.0000000000000000E+00 {~~}
START X_J   DryWood                  H2O-L        0.5000000000000009E-01 {~~}
START X_J   DryWood                  NH3          0.0000000000000000E+00 {~~}
START X_J   DryWood                  H2S          0.0000000000000000E+00 {~~}
START X_J   DryWood                  SO2          0.0000000000000000E+00 {~~}
START X_J   DryWood                  CH4          0.0000000000000000E+00 {~~}
START X_J   DryWood                  C2H6         0.0000000000000000E+00 {~~}
START X_J   DryWood                  C3H8         0.0000000000000000E+00 {~~}
START X_J   DryWood                  C4H10-N      0.0000000000000000E+00 {~~}
START X_J   DryWood                  C4H10-I      0.0000000000000000E+00 {~~}
START X_J   DryWood                  C5H12        0.0000000000000000E+00 {~~}
START X_J   DryWood                  C6H14        0.0000000000000000E+00 {~~}
START X_J   DryWood                  C7H16        0.0000000000000000E+00 {~~}
START X_J   DryWood                  C8H18        0.0000000000000000E+00 {~~}
START X_J   DryWood                  C2H4         0.0000000000000000E+00 {~~}
START X_J   DryWood                  C3H6         0.0000000000000000E+00 {~~}
START X_J   DryWood                  C5H10        0.0000000000000000E+00 {~~}
START X_J   DryWood                  C6H12-1      0.0000000000000000E+00 {~~}
START X_J   DryWood                  C7H14        0.0000000000000000E+00 {~~}
START X_J   DryWood                  C2H2         0.0000000000000000E+00 {~~}
START X_J   DryWood                  C6H6         0.0000000000000000E+00 {~~}
START X_J   DryWood                  C6H12-C      0.0000000000000000E+00 {~~}
START X_J   DryWood                  C            0.4636000000000009E+00 {~~}
START X_J   DryWood                  S            0.1900000000000004E-03 {~~}
START X_J   DryWood                  NO2          0.0000000000000000E+00 {~~}
START X_J   DryWood                  HCN          0.0000000000000000E+00 {~~}
START X_J   DryWood                  COS          0.0000000000000000E+00 {~~}
START X_J   DryWood                  N2O          0.0000000000000000E+00 {~~}
START X_J   DryWood                  NO3          0.0000000000000000E+00 {~~}
START X_J   DryWood                  SO3          0.0000000000000000E+00 {~~}
START X_J   DryWood                  AR           0.0000000000000000E+00 {~~}
START X_J   DryWood                  ASH          0.8645000000000019E-02 {~~}
START X_J   DryWood                  TAR          0.0000000000000000E+00 {~~}
START M     Gasifier                      2  0.3068842105263164E-01 {~~}
START H     Gasifier                      2 -0.5497059220211011E+04 {~~}
START M     Gasifier                     26  0.0000000000000000E+00 {~~}
START P                             26  0.1003000000000002E+01 {~~}
START H     Gasifier                     26 -0.1319450918722708E+05 {~~}
START M     Gasifier                     74  0.5485206982616304E-01 {~~}
START P                             74  0.1003000000000002E+01 {~~}
START H     Gasifier                     74 -0.2398848478333938E+04 {~~}
START M     Gasifier                      3 -0.8527518947879467E-01 {~~}
START P                              3  0.9980000000000021E+00 {~~}
START H     Gasifier                      3 -0.3507877913073770E+04 {~~}
START M     Gasifier                     99 -0.2653014000000006E-03 {~~}
```

```
START P                          99  0.1013000000000002E+01 {~~}
START H     Gasifier              99 -0.4308000000000008E+04 {~~}
START Q     Gasifier             302  0.0000000000000000E+00 {~~}
START ZA    Gasifier               1  0.8500945239865259E+05 {~~}
START ZA    Gasifier               2  0.4363965291425181E+05 {~~}
START ZA    Gasifier               3  0.1172765217993688E+06 {~~}
START ZA    Gasifier               4  0.3124902840469579E+06 {~~}
START ZA    Gasifier               5  0.1827651987487792E+06 {~~}
START ZA    Gasifier               6  0.2292482774424775E+06 {~~}
START ZA    Gasifier               7 -0.3279719879436739E+06 {~~}
START Y_J   raw_PG               H2           0.2538114658675978E+00 {~~}
START Y_J   raw_PG               O2           0.0000000000000000E+00 {~~}
START Y_J   raw_PG               N2           0.2896541868376543E+00 {~~}
START Y_J   raw_PG               CO           0.1761818347160900E+00 {~~}
START Y_J   raw_PG               NO           0.0000000000000000E+00 {~~}
START Y_J   raw_PG               CO2          0.1144395150133745E+00 {~~}
START Y_J   raw_PG               H2O-G        0.1523098114753787E+00 {~~}
START Y_J   raw_PG               NH3          0.0000000000000000E+00 {~~}
START Y_J   raw_PG               H2S          0.4615796164902311E-04 {~~}
START Y_J   raw_PG               SO2          0.0000000000000000E+00 {~~}
START Y_J   raw_PG               CH4          0.1011293223314740E-01 {~~}
START Y_J   raw_PG               NO2          0.0000000000000000E+00 {~~}
START Y_J   raw_PG               HCN          0.0000000000000000E+00 {~~}
START Y_J   raw_PG               COS          0.0000000000000000E+00 {~~}
START Y_J   raw_PG               AR           0.3444095895110056E-02 {~~}
START X_J   Ash                  C            0.0000000000000000E+00 {~~}
START X_J   Ash                  ASH          0.1000000000000002E+01 {~~}
START M     airpreheat             3  0.8527518947879467E-01 {~~}
START H     airpreheat             3 -0.3507877913073770E+04 {~~}
START M     airpreheat             4 -0.8527518947879467E-01 {~~}
START P                           4  0.9930000000000021E+00 {~~}
START H     airpreheat             4 -0.3918630307677503E+04 {~~}
START M     airpreheat            72  0.4254049087879459E-01 {~~}
START P                          72  0.1008000000000002E+01 {~~}
START H     airpreheat            72 -0.9883454496688249E+02 {~~}
START M     airpreheat            73 -0.4254049087879459E-01 {~~}
START P                          73  0.1003000000000002E+01 {~~}
START H     airpreheat            73  0.7245454291500140E+03 {~~}
START Q     airpreheat           303  0.0000000000000000E+00 {~~}
START ZA    airpreheat             1  0.3502698827870191E+02 {~~}
START M     steamheater            4  0.8527518947879467E-01 {~~}
START H     steamheater            4 -0.3918630307677503E+04 {~~}
START M     steamheater            5 -0.8527518947879467E-01 {~~}
START P                           5  0.9880000000000021E+00 {~~}
START H     steamheater            5 -0.4375257198957321E+04 {~~}
START M     steamheater           63  0.2000459030657094E+00 {~~}
START P                          63  0.1003000000000002E+01 {~~}
START H     steamheater           63 -0.1319118556200298E+05 {~~}
START M     steamheater           64 -0.2000459030657094E+00 {~~}
START H     steamheater           64 -0.1299653551379775E+05 {~~}
START Q     steamheater          304  0.0000000000000000E+00 {~~}
START ZA    steamheater            1  0.3893894467499939E+02 {~~}
START M     steamblower           61  0.2123574820130778E+00 {~~}
START H     steamblower           61 -0.1319443607829822E+05 {~~}
START M     steamblower           62 -0.2123574820130778E+00 {~~}
START P                          62  0.1003000000000002E+01 {~~}
START H     steamblower           62 -0.1319118556200298E+05 {~~}
START Q     steamblower          305 -0.1408717256529193E-01 {~~}
START W     steamblower          105  0.7043586282645935E+00 {~~}
START M     split1                62  0.2123574820130778E+00 {~~}
START H     split1                62 -0.1319118556200298E+05 {~~}
START M     split1                63 -0.2000459030657094E+00 {~~}
START H     split1                63 -0.1319118556200298E+05 {~~}
START M     split1                69 -0.1231157894736844E-01 {~~}
START P                          69  0.1003000000000002E+01 {~~}
START H     split1                69 -0.1319118556200298E+05 {~~}
START M     mix1                  73  0.4254049087879459E-01 {~~}
START H     mix1                  73  0.7245454291500140E+03 {~~}
START M     mix1                  69  0.1231157894736844E-01 {~~}
START H     mix1                  69 -0.1319118556200299E+05 {~~}
START M     mix1                  74 -0.5485206982616304E-01 {~~}
START H     mix1                  74 -0.2398848478333938E+04 {~~}
START Y_J   humid_air            H2           0.0000000000000000E+00 {~~}
START Y_J   humid_air            O2           0.1417803964772677E+00 {~~}
START Y_J   humid_air            N2           0.5281063539146036E+00 {~~}
START Y_J   humid_air            CO           0.0000000000000000E+00 {~~}
```

```
START Y_J   humid_air            NO       0.0000000000000000E+00 {~~}
START Y_J   humid_air            CO2      0.2049837057502667E-03 {~~}
START Y_J   humid_air            H2O-G    0.3236220989260387E+00 {~~}
START Y_J   humid_air            NH3      0.0000000000000000E+00 {~~}
START Y_J   humid_air            H2S      0.0000000000000000E+00 {~~}
START Y_J   humid_air            SO2      0.0000000000000000E+00 {~~}
START Y_J   humid_air            CH4      0.0000000000000000E+00 {~~}
START Y_J   humid_air            C2H6     0.0000000000000000E+00 {~~}
START Y_J   humid_air            C3H8     0.0000000000000000E+00 {~~}
START Y_J   humid_air            C4H10-N  0.0000000000000000E+00 {~~}
START Y_J   humid_air            C4H10-I  0.0000000000000000E+00 {~~}
START Y_J   humid_air            C5H12    0.0000000000000000E+00 {~~}
START Y_J   humid_air            C6H14    0.0000000000000000E+00 {~~}
START Y_J   humid_air            C7H16    0.0000000000000000E+00 {~~}
START Y_J   humid_air            C8H18    0.0000000000000000E+00 {~~}
START Y_J   humid_air            C2H4     0.0000000000000000E+00 {~~}
START Y_J   humid_air            C3H6     0.0000000000000000E+00 {~~}
START Y_J   humid_air            C5H10    0.0000000000000000E+00 {~~}
START Y_J   humid_air            C6H12-1  0.0000000000000000E+00 {~~}
START Y_J   humid_air            C7H14    0.0000000000000000E+00 {~~}
START Y_J   humid_air            C2H2     0.0000000000000000E+00 {~~}
START Y_J   humid_air            C6H6     0.0000000000000000E+00 {~~}
START Y_J   humid_air            C6H12-C  0.0000000000000000E+00 {~~}
START Y_J   humid_air            C        0.0000000000000000E+00 {~~}
START Y_J   humid_air            S        0.0000000000000000E+00 {~~}
START Y_J   humid_air            NO2      0.0000000000000000E+00 {~~}
START Y_J   humid_air            HCN      0.0000000000000000E+00 {~~}
START Y_J   humid_air            COS      0.0000000000000000E+00 {~~}
START Y_J   humid_air            N2O      0.0000000000000000E+00 {~~}
START Y_J   humid_air            NO3      0.0000000000000000E+00 {~~}
START Y_J   humid_air            SO3      0.0000000000000000E+00 {~~}
START Y_J   humid_air            AR       0.6286166976341510E-02 {~~}
START Y_J   humid_air            ASH      0.0000000000000000E+00 {~~}
START Y_J   humid_air            TAR      0.0000000000000000E+00 {~~}
START Y_J   humid_air            CH3OH    0.0000000000000000E+00 {~~}
START M     gascooler              5  0.8527518947879467E-01 {~~}
START H     gascooler              5 -0.4375257198957321E+04 {~~}
START M     gascooler              6 -0.8527518947879467E-01 {~~}
START P                       6  0.9830000000000021E+00 {~~}
START H     gascooler              6 -0.4624611248324039E+04 {~~}
START M     gascooler             98  0.0000000000000000E+00 {~~}
START P                      98  0.9830000000000021E+00 {~~}
START H     gascooler             98 -0.1559408877861427E+05 {~~}
START M     gascooler             81  0.1016636501943091E+00 {~~}
START P                      81  0.1013000000000002E+01 {~~}
START H     gascooler             81 -0.1584524528596514E+05 {~~}
START M     gascooler             82 -0.1016636501943091E+00 {~~}
START P                      82  0.1008000000000002E+01 {~~}
START H     gascooler             82 -0.1563608779686839E+05 {~~}
START Q     gascooler            306  0.0000000000000000E+00 {~~}
START Y_J   cold_PG          H2          0.2538114658675980E+00 {~~}
START Y_J   cold_PG          O2          0.0000000000000000E+00 {~~}
START Y_J   cold_PG          N2          0.2896541868376545E+00 {~~}
START Y_J   cold_PG          CO          0.1761818347160902E+00 {~~}
START Y_J   cold_PG          NO          0.0000000000000000E+00 {~~}
START Y_J   cold_PG          CO2         0.1144395150133747E+00 {~~}
START Y_J   cold_PG          H2O-G       0.1523098114753787E+00 {~~}
START Y_J   cold_PG          NH3         0.0000000000000000E+00 {~~}
START Y_J   cold_PG          H2S         0.4615796164902315E-04 {~~}
START Y_J   cold_PG          SO2         0.0000000000000000E+00 {~~}
START Y_J   cold_PG          CH4         0.1011293223314741E-01 {~~}
START Y_J   cold_PG          C2H6        0.0000000000000000E+00 {~~}
START Y_J   cold_PG          C3H8        0.0000000000000000E+00 {~~}
START Y_J   cold_PG          C4H10-N     0.0000000000000000E+00 {~~}
START Y_J   cold_PG          C4H10-I     0.0000000000000000E+00 {~~}
START Y_J   cold_PG          C5H12       0.0000000000000000E+00 {~~}
START Y_J   cold_PG          C6H14       0.0000000000000000E+00 {~~}
START Y_J   cold_PG          C7H16       0.0000000000000000E+00 {~~}
START Y_J   cold_PG          C8H18       0.0000000000000000E+00 {~~}
START Y_J   cold_PG          C2H4        0.0000000000000000E+00 {~~}
START Y_J   cold_PG          C3H6        0.0000000000000000E+00 {~~}
START Y_J   cold_PG          C5H10       0.0000000000000000E+00 {~~}
START Y_J   cold_PG          C6H12-1     0.0000000000000000E+00 {~~}
START Y_J   cold_PG          C7H14       0.0000000000000000E+00 {~~}
START Y_J   cold_PG          C2H2        0.0000000000000000E+00 {~~}
START Y_J   cold_PG          C6H6        0.0000000000000000E+00 {~~}
```

```
START Y_J   cold_PG                  C6H12-C      0.0000000000000000E+00 {~~}
START Y_J   cold_PG                  C            0.0000000000000000E+00 {~~}
START Y_J   cold_PG                  S            0.0000000000000000E+00 {~~}
START Y_J   cold_PG                  NO2          0.0000000000000000E+00 {~~}
START Y_J   cold_PG                  HCN          0.0000000000000000E+00 {~~}
START Y_J   cold_PG                  COS          0.0000000000000000E+00 {~~}
START Y_J   cold_PG                  N2O          0.0000000000000000E+00 {~~}
START Y_J   cold_PG                  NO3          0.0000000000000000E+00 {~~}
START Y_J   cold_PG                  SO3          0.0000000000000000E+00 {~~}
START Y_J   cold_PG                  AR           0.3444095895110058E-02 {~~}
START M     gasclean                       6  0.8527518947879467E-01 {~~}
START H     gasclean                       6 -0.4624611248324039E+04 {~~}
START M     gasclean                       7 -0.8526899202586889E-01 {~~}
START P                              7  0.9781000000000021E+00 {~~}
START H     gasclean                       7 -0.4624908439609420E+04 {~~}
START M     gasclean                      97 -0.6197452925764206E-05 {~~}
START P                             97  0.9781000000000021E+00 {~~}
START H     gasclean                      97 -0.5356408846834947E+03 {~~}
START Q     gasclean                     307  0.0000000000000000E+00 {~~}
START Y_J   clean_PG                 H2           0.2538231818282903E+00 {~~}
START Y_J   clean_PG                 O2           0.0000000000000000E+00 {~~}
START Y_J   clean_PG                 N2           0.2896675573016551E+00 {~~}
START Y_J   clean_PG                 CO           0.1761899672858430E+00 {~~}
START Y_J   clean_PG                 NO           0.0000000000000000E+00 {~~}
START Y_J   clean_PG                 CO2          0.1144447975519509E+00 {~~}
START Y_J   clean_PG                 H2O-G        0.1523168421103353E+00 {~~}
START Y_J   clean_PG                 CH4          0.1011339904703275E-01 {~~}
START Y_J   clean_PG                 NO2          0.0000000000000000E+00 {~~}
START Y_J   clean_PG                 AR           0.3444254874894482E-02 {~~}
START Y_J   impurities                   H2O-G        0.0000000000000000E+00 {~~}
START Y_J   impurities                   NH3          0.0000000000000000E+00 {~~}
START Y_J   impurities                   H2S          0.1000000000000002E+01 {~~}
START Y_J   impurities                   SO2          0.0000000000000000E+00 {~~}
START Y_J   impurities                   HCN          0.0000000000000000E+00 {~~}
START Y_J   impurities                   COS          0.0000000000000000E+00 {~~}
START Y_J   impurities                   AR           0.0000000000000000E+00 {~~}
START Y_J   impurities                   ASH          0.0000000000000000E+00 {~~}
START M     condenser                      7  0.8526899202586889E-01 {~~}
START H     condenser                      7 -0.4624908439609421E+04 {~~}
START M     condenser                      8 -0.8320484335731924E-01 {~~}
START P                              8  0.9731000000000021E+00 {~~}
START H     condenser                      8 -0.4466561290262782E+04 {~~}
START M     condenser                     96 -0.2064148668549664E-02 {~~}
START P                             96  0.9731000000000021E+00 {~~}
START H     condenser                     96 -0.1576166949955456E+05 {~~}
START M     condenser                     83  0.4691527326491080E-01 {~~}
START P                             83  0.1013000000000002E+01 {~~}
START H     condenser                     83 -0.1584524528596514E+05 {~~}
START M     condenser                     84 -0.4691527326491080E-01 {~~}
START P                             84  0.1008000000000002E+01 {~~}
START H     condenser                     84 -0.1563608779686839E+05 {~~}
START Q     condenser                    308  0.0000000000000000E+00 {~~}
START Y_J   dry_PG                   H2           0.2614256920940560E+00 {~~}
START Y_J   dry_PG                   O2           0.0000000000000000E+00 {~~}
START Y_J   dry_PG                   N2           0.2983436780648677E+00 {~~}
START Y_J   dry_PG                   CO           0.1814672080223557E+00 {~~}
START Y_J   dry_PG                   NO           0.0000000000000000E+00 {~~}
START Y_J   dry_PG                   CO2          0.1178726473723852E+00 {~~}
START Y_J   dry_PG                   H2O-G        0.1269270417636808E+00 {~~}
START Y_J   dry_PG                   NH3          0.0000000000000000E+00 {~~}
START Y_J   dry_PG                   H2S          0.0000000000000000E+00 {~~}
START Y_J   dry_PG                   SO2          0.0000000000000000E+00 {~~}
START Y_J   dry_PG                   CH4          0.1041631550849633E-01 {~~}
START Y_J   dry_PG                   C2H6         0.0000000000000000E+00 {~~}
START Y_J   dry_PG                   C3H8         0.0000000000000000E+00 {~~}
START Y_J   dry_PG                   C4H10-N      0.0000000000000000E+00 {~~}
START Y_J   dry_PG                   C4H10-I      0.0000000000000000E+00 {~~}
START Y_J   dry_PG                   C5H12        0.0000000000000000E+00 {~~}
START Y_J   dry_PG                   C6H14        0.0000000000000000E+00 {~~}
START Y_J   dry_PG                   C7H16        0.0000000000000000E+00 {~~}
START Y_J   dry_PG                   C8H18        0.0000000000000000E+00 {~~}
START Y_J   dry_PG                   C2H4         0.0000000000000000E+00 {~~}
START Y_J   dry_PG                   C3H6         0.0000000000000000E+00 {~~}
START Y_J   dry_PG                   C5H10        0.0000000000000000E+00 {~~}
START Y_J   dry_PG                   C6H12-1      0.0000000000000000E+00 {~~}
START Y_J   dry_PG                   C7H14        0.0000000000000000E+00 {~~}
```

```
START Y_J   dry_PG           C2H2       0.0000000000000000E+00 {~~}
START Y_J   dry_PG           C6H6       0.0000000000000000E+00 {~~}
START Y_J   dry_PG           C6H12-C    0.0000000000000000E+00 {~~}
START Y_J   dry_PG           C          0.0000000000000000E+00 {~~}
START Y_J   dry_PG           S          0.0000000000000000E+00 {~~}
START Y_J   dry_PG           NO2        0.0000000000000000E+00 {~~}
START Y_J   dry_PG           HCN        0.0000000000000000E+00 {~~}
START Y_J   dry_PG           COS        0.0000000000000000E+00 {~~}
START Y_J   dry_PG           N2O        0.0000000000000000E+00 {~~}
START Y_J   dry_PG           NO3        0.0000000000000000E+00 {~~}
START Y_J   dry_PG           SO3        0.0000000000000000E+00 {~~}
START Y_J   dry_PG           AR         0.3547417174160010E-02 {~~}
START M     PGcompressor         8  0.8320484335731924E-01 {~~}
START H     PGcompressor         8 -0.4466561290262782E+04 {~~}
START M     PGcompressor         9 -0.8320484335731924E-01 {~~}
START P                      9  0.3750000000000007E+01 {~~}
START H     PGcompressor         9 -0.4199072570137568E+04 {~~}
START Q     PGcompressor       309 -0.4542113685279208E+00 {~~}
START W     PGcompressor       117  0.2271056842639615E+02 {~~}
START M     aircompressor        31  0.1018083234123910E+01 {~~}
START P                     31  0.1013000000000002E+01 {~~}
START H     aircompressor        31 -0.9883454496688249E+02 {~~}
START M     aircompressor        32 -0.1018083234123910E+01 {~~}
START P                     32  0.3760000000000006E+01 {~~}
START H     aircompressor        32  0.7718226301745642E+02 {~~}
START Q     aircompressor       312 -0.3657137982303304E+01 {~~}
START W     aircompressor       117  0.1828568991151661E+03 {~~}
START M     burner               33  0.1018083234123910E+01 {~~}
START P                     33  0.3750000000000007E+01 {~~}
START H     burner               33  0.4838361573740053E+03 {~~}
START M     burner                9  0.8320484335731924E-01 {~~}
START H     burner                9 -0.4199072570137567E+04 {~~}
START M     burner               41 -0.1101288077481229E+01 {~~}
START P                     41  0.3747652500000008E+01 {~~}
START H     burner               41  0.1300316487295679E+03 {~~}
START Q     burner              316  0.0000000000000000E+00 {~~}
START ZA    burner                1  0.7899556968713444E+01 {~~}
START Y_J   FLUE_GAS             O2         0.1671258083618115E+00 {~~}
START Y_J   FLUE_GAS             N2         0.7425665022970938E+00 {~~}
START Y_J   FLUE_GAS             NO         0.0000000000000000E+00 {~~}
START Y_J   FLUE_GAS             CO2        0.3124559018208463E-01 {~~}
START Y_J   FLUE_GAS             H2O-G      0.5022354879730917E-01 {~~}
START Y_J   FLUE_GAS             SO2        0.0000000000000000E+00 {~~}
START Y_J   FLUE_GAS             NO2        0.0000000000000000E+00 {~~}
START Y_J   FLUE_GAS             AR         0.8838550361702892E-02 {~~}
START M     GT                   41  0.1101288077481229E+01 {~~}
START H     GT                   41  0.1300316487295679E+03 {~~}
START M     GT                   42 -0.1101288077481229E+01 {~~}
START P                     42  0.1033000000000002E+01 {~~}
START H     GT                   42 -0.1851504231204904E+03 {~~}
START W     GT                  117 -0.3471062579643006E+03 {~~}
START E     generator           217 -0.1344618509016015E+03 {~~}
START Q     generator           317 -0.7076939521136913E+01 {~~}
START W     generator           117  0.1415387904227384E+03 {~~}
START M     recuperator          42  0.1101288077481229E+01 {~~}
START H     recuperator          42 -0.1851504231204904E+03 {~~}
START M     recuperator          43 -0.1101288077481229E+01 {~~}
START P                     43  0.1023000000000002E+01 {~~}
START H     recuperator          43 -0.5610806818793795E+03 {~~}
START M     recuperator          32  0.1018083234123910E+01 {~~}
START H     recuperator          32  0.7718226301745642E+02 {~~}
START M     recuperator          33 -0.1018083234123910E+01 {~~}
START H     recuperator          33  0.4838361573740053E+03 {~~}
START Q     recuperator         318  0.0000000000000000E+00 {~~}
START ZA    recuperator           1  0.4140075119355976E+03 {~~}
START M     exhaustcooler         43  0.1101288077481229E+01 {~~}
START H     exhaustcooler         43 -0.5610806818793795E+03 {~~}
START M     exhaustcooler         44 -0.1101288077481229E+01 {~~}
START P                     44  0.1013000000000002E+01 {~~}
START H     exhaustcooler         44 -0.7510747147930945E+03 {~~}
START M     exhaustcooler         85  0.1000385710041053E+01 {~~}
START P                     85  0.1013000000000002E+01 {~~}
START H     exhaustcooler         85 -0.1584524528596514E+05 {~~}
START M     exhaustcooler         86 -0.1000385710041053E+01 {~~}
START P                     86  0.1008000000000002E+01 {~~}
START H     exhaustcooler         86 -0.1563608779686839E+05 {~~}
```

```
START Q      exhaustcooler              319  0.0000000000000000E+00 {~~}
START ZA     exhaustcooler                1  0.2092381632404501E+03 {~~}
C ~~~~~~~~~~~~~~~~~~~~~~~~~~~~~~~~~~~~~~~~~~~~~~~~~~~~~~~~~~~~~~~~~~~~~~~~~~~~~~~~~~~~~~~~~~~~
~~~~~
C ~~ End of generated initial guesses.
C ~~~~~~~~~~~~~~~~~~~~~~~~~~~~~~~~~~~~~~~~~~~~~~~~~~~~~~~~~~~~~~~~~~~~~~~~~~~~~~~~~~~~~~~~~~~~
~~~~~
```

end

DNA Output for MGT scenario

Biomass gasification (Viking) + MGT incl. recuperation

RUN NUMBER 1

ALGEBRAIC VARIABLES

NODE	TO COMPONENT	MEDIA	M [kg/s]	T [C]	P [bar]	H [kJ/kg]	ENERGY [kJ/s]	X	S [kJ/kg K]	V [m3/kg]	U [kJ/kg]
1	Dryer	Wood	0.04	15.00	-	-8621.6	4.991E+02	-	0.4612	-	-8621.6
64	Dryer	STEAM-HF	0.20	250.00	0.998	-12996.5		-	11.5514	2.4110	-13237.2
2	Dryer	DryWood	-0.03	150.00	-	-5497.1		-	1.7075	-	-5497.1
61	Dryer	STEAM-HF	-0.21	150.00	0.993	-13194.4		-	11.1339	1.9505	-13388.1
301	Dryer	HEAT					0.000E+00				
2	Gasifier	DryWood	0.03	150.00	-	-5497.1		-	1.7075	-	-5497.1
26	Gasifier	STEAM-HF	0.00	150.00	1.003	-13194.5		-	11.1292	1.9309	-13388.2
74	Gasifier	humid_air	0.05	564.13	1.003	-2398.8		-	9.1937	2.7302	-2672.7
3	Gasifier	raw_PG	-0.09	800.00	0.998	-3507.9		-	10.8590	4.1308	-3920.1
99	Gasifier	Ash	0.00	800.00	-	-4308.0		-	0.0000	-	-4308.0
302	Gasifier	HEAT					0.000E+00				
3	airpreheat	raw_PG	0.09	800.00	0.998	-3507.9		-	10.8590	4.1308	-3920.1
4	airpreheat	raw_PG	-0.09	552.33	0.993	-3918.6		-	10.4262	3.1935	-4235.7
72	airpreheat	STANDARD_AIR	0.04	15.00	1.008	-98.8		-	6.8668	0.8237	-181.9
73	airpreheat	STANDARD_AIR	-0.04	780.00	1.003	724.5		-	8.2418	3.0255	421.1
303	airpreheat	HEAT					0.000E+00				
4	steamheater	raw_PG	0.09	552.33	0.993	-3918.6		-	10.4262	3.1935	-4235.7
5	steamheater	raw_PG	-0.09	259.48	0.988	-4375.3		-	9.7468	2.0710	-4579.9
63	steamheater	STEAM-HF	0.20	151.68	1.003	-13191.2		-	11.1370	1.9388	-13385.6
64	steamheater	STEAM-HF	-0.20	250.00	0.998	-12996.5		-	11.5514	2.4110	-13237.2
304	steamheater	HEAT					0.000E+00				
61	steamblower	STEAM-HF	0.21	150.00	0.993	-13194.4		-	11.1339	1.9505	-13388.1
62	steamblower	STEAM-HF	-0.21	151.68	1.003	-13191.2		-	11.1370	1.9388	-13385.6
305	steamblower	HEAT					-1.409E-02				
105	steamblower	MECH_POWER					7.044E-01				
62	split1	STEAM-HF	0.21	151.68	1.003	-13191.2		-	11.1370	1.9388	-13385.6
63	split1	STEAM-HF	-0.20	151.68	1.003	-13191.2		-	11.1370	1.9388	-13385.6
69	split1	STEAM-HF	-0.01	151.68	1.003	-13191.2		-	11.1370	1.9388	-13385.6
73	mix1	STANDARD_AIR	0.04	780.00	1.003	724.5		-	8.2418	3.0255	421.1
69	mix1	STEAM-HF	0.01	151.68	1.003	-13191.2		-	11.1370	1.9388	-13385.6
74	mix1	humid_air	-0.05	564.13	1.003	-2398.8		-	9.1937	2.7302	-2672.7
5	gascooler	raw_PG	0.09	259.48	0.988	-4375.3		-	9.7468	2.0710	-4579.9
6	gascooler	cold_PG	-0.09	90.00	0.983	-4624.6		-	9.1860	1.4192	-4764.1
98	gascooler	STEAM-HF	0.00	90.00	0.983	-15594.1		-	4.7085	0.0010	-15594.2
81	gascooler	STEAM-HF	0.10	30.02	1.013	-15845.2		-	3.9530	0.0010	-15845.3
82	gascooler	STEAM-HF	-0.10	80.00	1.008	-15636.1		-	4.5912	0.0010	-15636.2
306	gascooler	HEAT					0.000E+00				
6	gasclean	cold_PG	0.09	90.00	0.983	-4624.6		-	9.1860	1.4192	-4764.1
7	gasclean	clean_PG	-0.09	90.00	0.978	-4624.9		-	9.1879	1.4263	-4764.4
97	gasclean	impurities	0.00	90.00	0.978	-535.6		-	6.2438	0.9059	-624.2
307	gasclean	HEAT					0.000E+00				
7	condenser	clean_PG	0.09	90.00	0.978	-4624.9		-	9.1879	1.4263	-4764.4
8	condenser	dry_PG	-0.08	50.00	0.973	-4466.6		-	8.9598	1.2694	-4590.1
96	condenser	STEAM-HF	0.00	50.01	0.973	-15761.7		-	4.2198	0.0010	-15761.7
83	condenser	STEAM-HF	0.05	30.02	1.013	-15845.2		-	3.9530	0.0010	-15845.3

84	condenser	STEAM-HF	-0.05	80.00	1.008	-15636.1		-	4.5912	0.0010	-15636.2
308	condenser	HEAT					0.000E+00				
8	PGcompressor	dry_PG	0.08	50.00	0.973	-4466.6		-	8.9598	1.2694	-4590.1
9	PGcompressor	dry_PG	-0.08	234.69	3.750	-4199.1		-	9.0977	0.5176	-4393.2
309	PGcompressor	HEAT					-4.542E-01				
117	PGcompressor	MECH_POWER					2.271E+01				
31	aircompressor	STANDARD_AIR	1.02	15.00	1.013	-98.8		-	6.8653	0.8196	-181.9
32	aircompressor	STANDARD_AIR	-1.02	188.08	3.760	77.2		-	6.9655	0.3535	-55.7
312	aircompressor	HEAT					-3.657E+00				
117	aircompressor	MECH_POWER					1.829E+02				
42	recuperator	FLUE_GAS	1.10	635.23	1.033	-185.2		-	8.1694	2.5401	-447.5
43	recuperator	FLUE_GAS	-1.10	299.69	1.023	-561.1		-	7.6572	1.6175	-726.6
32	recuperator	STANDARD_AIR	1.02	188.08	3.760	77.2		-	6.9655	0.3535	-55.7
33	recuperator	STANDARD_AIR	-1.02	568.16	3.750	483.8		-	7.6068	0.6464	241.4
318	recuperator	HEAT					0.000E+00				
33	burner	STANDARD_AIR	1.02	568.16	3.750	483.8		-	7.6068	0.6464	241.4
9	burner	dry_PG	0.08	234.69	3.750	-4199.1		-	9.0977	0.5176	-4393.2
41	burner	FLUE_GAS	-1.10	900.00	3.748	130.0		-	8.1014	0.9042	-208.8
316	burner	HEAT					0.000E+00				
41	GT	FLUE_GAS	1.10	900.00	3.748	130.0		-	8.1014	0.9042	-208.8
42	GT	FLUE_GAS	-1.10	635.23	1.033	-185.2		-	8.1694	2.5401	-447.5
117	GT	MECH_POWER					-3.471E+02				
217	generator	ELECT_POWER					-1.345E+02				
317	generator	HEAT					-7.077E+00				
117	generator	MECH_POWER					1.415E+02				
43	exhaustcooler	FLUE_GAS	1.10	299.69	1.023	-561.1		-	7.6572	1.6175	-726.6
44	exhaustcooler	FLUE_GAS	-1.10	120.02	1.013	-751.1		-	7.2625	1.1211	-864.6
85	exhaustcooler	STEAM-HF	1.00	30.02	1.013	-15845.2		-	3.9530	0.0010	-15845.3
86	exhaustcooler	STEAM-HF	-1.00	80.00	1.008	-15636.1		-	4.5912	0.0010	-15636.2
319	exhaustcooler	HEAT					0.000E+00				

EXERGY

NO DE	TO COMPONENT	MEDIA	E_PH [kJ/kg]	E_CH [kJ/kg]	E [kJ/kg]	EX_PH [kJ/s]	EX_CH [kJ/s]	EX [kJ/s]
1	Dryer	Wood	0.00	13311.33	13311.33	0.00	572.39	572.39
64	Dryer	STEAM-HF	660.71	-	660.71	132.17	-	132.17
2	Dryer	DryWood	-54.56	18651.57	18597.01	1.67	-572.39	-570.71
61	Dryer	STEAM-HF	583.11	-	583.11	-123.83	-	-123.83
301	Dryer	HEAT	-	-	-	0.00	0.00	0.00
2	Gasifier	DryWood	-54.56	18651.57	18597.01	-1.67	572.39	570.71
26	Gasifier	STEAM-HF	584.41	-	584.41	0.00	-	0.00
74	Gasifier	humid_air	310.33	66.40	376.73	17.02	3.64	20.66
3	Gasifier	raw_PG	644.70	5438.32	6083.02	-54.98	-463.75	-518.73
99	Gasifier	Ash	785.00	-	785.00	-0.21	-	-0.21
302	Gasifier	HEAT	-	-	-	0.00	0.00	0.00
3	airpreheat	raw_PG	644.70	5438.32	6083.02	54.98	463.75	518.73
4	airpreheat	raw_PG	358.65	5438.32	5796.96	-30.58	-463.75	-494.34
72	airpreheat	STANDARD_AIR	0.66	3.73	4.39	0.03	0.16	0.19
73	airpreheat	STANDARD_AIR	427.84	3.73	431.57	-18.20	-0.16	-18.36

303	airpreheat	HEAT	-	-	-	0.00	0.00	0.00
4	steamheater	raw_PG	358.65	5438.32	5796.96	30.58	463.75	494.34
5	steamheater	raw_PG	97.80	5438.32	5536.12	-8.34	-463.75	-472.09
63	steamheater	STEAM-HF	585.47	-	585.47	117.12	-	117.12
64	steamheater	STEAM-HF	660.71	-	660.71	-132.17	-	-132.17
304	steamheater	HEAT	-	-	-	0.00	0.00	0.00
61	steamblower	STEAM-HF	583.11	-	583.11	123.83	-	123.83
62	steamblower	STEAM-HF	585.47	-	585.47	-124.33	-	-124.33
305	steamblower	HEAT	-	-	-	0.00	0.00	0.00
105	steamblower	MECH_POWER	-	-	-	0.70	0.00	0.70
62	split1	STEAM-HF	585.47	-	585.47	124.33	-	124.33
63	split1	STEAM-HF	585.47	-	585.47	-117.12	-	-117.12
69	split1	STEAM-HF	585.47	-	585.47	-7.21	-	-7.21
73	mix1	STANDARD_AIR	427.84	3.73	431.57	18.20	0.16	18.36
69	mix1	STEAM-HF	585.47	-	585.47	7.21	-	7.21
74	mix1	humid_air	310.33	66.40	376.73	-17.02	-3.64	-20.66
5	gascooler	raw_PG	97.80	5438.32	5536.12	8.34	463.75	472.09
6	gascooler	cold_PG	10.04	5438.32	5448.36	-0.86	-463.75	-464.61
98	gascooler	STEAM-HF	34.93	-	34.93	0.00	-	0.00
81	gascooler	STEAM-HF	1.49	-	1.49	0.15	-	0.15
82	gascooler	STEAM-HF	26.73	-	26.73	-2.72	-	-2.72
306	gascooler	HEAT	-	-	-	0.00	0.00	0.00
6	gasclean	cold_PG	10.04	5438.32	5448.36	0.86	463.75	464.61
7	gasclean	clean_PG	9.49	5437.03	5446.52	-0.81	-463.61	-464.42
97	gasclean	impurities	6.93	23829.09	23836.02	0.00	-0.15	-0.15
307	gasclean	HEAT	-	-	-	0.00	0.00	0.00
7	condenser	clean_PG	9.49	5437.03	5446.52	0.81	463.61	464.42
8	condenser	dry_PG	-0.23	5566.16	5565.93	0.02	-463.13	-463.11
96	condenser	STEAM-HF	8.19	-	8.19	-0.02	-	-0.02
83	condenser	STEAM-HF	1.49	-	1.49	0.07	-	0.07
84	condenser	STEAM-HF	26.73	-	26.73	-1.25	-	-1.25
308	condenser	HEAT	-	-	-	0.00	0.00	0.00
8	PGcompressor	dry_PG	-0.23	5566.16	5565.93	-0.02	463.13	463.11
9	PGcompressor	dry_PG	227.52	5566.16	5793.68	-18.93	-463.13	-482.06
309	PGcompressor	HEAT	-	-	-	0.00	0.00	0.00
117	PGcompressor	MECH_POWER	-	-	-	22.71	0.00	22.71
31	aircompressor	STANDARD_AIR	1.07	3.73	4.81	1.09	3.80	4.89
32	aircompressor	STANDARD_AIR	148.24	3.73	151.97	-150.92	-3.80	-154.72
312	aircompressor	HEAT	-	-	-	0.00	0.00	0.00
117	aircompressor	MECH_POWER	-	-	-	182.86	0.00	182.86
42	recuperator	FLUE_GAS	321.66	15.16	336.82	354.24	16.69	370.93
43	recuperator	FLUE_GAS	93.34	15.16	108.49	-102.79	-16.69	-119.48
32	recuperator	STANDARD_AIR	148.24	3.73	151.97	150.92	3.80	154.72
33	recuperator	STANDARD_AIR	370.10	3.73	373.84	-376.80	-3.80	-380.60
318	recuperator	HEAT	-	-	-	0.00	0.00	0.00
33	burner	STANDARD_AIR	370.10	3.73	373.84	376.80	3.80	380.60
9	burner	dry_PG	227.52	5566.16	5793.68	18.93	463.13	482.06
41	burner	FLUE_GAS	656.45	15.16	671.61	-722.94	-16.69	-739.63
316	burner	HEAT	-	-	-	0.00	0.00	0.00
41	GT	FLUE_GAS	656.45	15.16	671.61	722.94	16.69	739.63
42	GT	FLUE_GAS	321.66	15.16	336.82	-354.24	-16.69	-370.93
117	GT	MECH_POWER	-	-	-	-347.11	0.00	-347.11
217	generator	ELECT_POWER	-	-	-	-134.46	0.00	-134.46
317	generator	HEAT	-	-	-	0.00	0.00	0.00

117	generator	MECH_POWER	-	-	-	141.54	0.00	141.54
43	exhaustcooler	FLUE_GAS	93.34	15.16	108.49	102.79	16.69	119.48
44	exhaustcooler	FLUE_GAS	17.07	15.16	32.23	-18.80	-16.69	-35.49
85	exhaustcooler	STEAM-HF	1.49	-	1.49	1.50	-	1.50
86	exhaustcooler	STEAM-HF	26.73	-	26.73	-26.74	-	-26.74
319	exhaustcooler	HEAT	-	-	-	0.00	0.00	0.00

ELEC. POWER PRODUCTION = 134.4619 kW
TOTAL POWER CONSUMPTION = 0.7044 kW
NET POWER PRODUCTION = 133.7575 kW
FUEL CONSUMPTION (LHV) = 499.1161 kJ/s
FUEL CONSUMPTION (HHV) = 572.3872 kJ/s
THERMAL EFFICIENCY (LHV)= 0.2680
THERMAL EFFICIENCY (HHV)= 0.2337

MAXIMUM RELATIVE ERROR = 8.9184E-13
COMPUTER ACCURACY = 1.0842E-19

IDEAL GAS COMPOSITION (MOLAR BASE):

	humid_air	raw_PG	STANDARD_AIR	cold_PG	clean_PG
HYDROGEN	0.0000E+00	0.2538E+00	0.0000E+00	0.2538E+00	0.2538E+00
OXYGEN	0.1418E+00	0.0000E+00	0.2075E+00	0.0000E+00	0.0000E+00
NITROGEN	0.5281E+00	0.2897E+00	0.7729E+00	0.2897E+00	0.2897E+00
CARBON MONOXIDE	0.0000E+00	0.1762E+00	0.0000E+00	0.1762E+00	0.1762E+00
CARBON DIOXIDE	0.2050E-03	0.1144E+00	0.3000E-03	0.1144E+00	0.1144E+00
WATER (I.G.)	0.3236E+00	0.1523E+00	0.1010E-01	0.1523E+00	0.1523E+00
HYDROGEN SULFIDE	0.0000E+00	0.4616E-04	0.0000E+00	0.4616E-04	0.0000E+00
METHANE	0.0000E+00	0.1011E-01	0.0000E+00	0.1011E-01	0.1011E-01
ARGON	0.6286E-02	0.3444E-02	0.9200E-02	0.3444E-02	0.3444E-02
MEAN MOLE MASS	0.2542E+02	0.2164E+02	0.2885E+02	0.2164E+02	0.2164E+02
NET CALORI VALUE	0.0000E+00	0.5516E+04	0.0000E+00	0.5516E+04	0.5515E+04
GRS CALORI VALUE	0.0000E+00	0.1148E+05	0.0000E+00	0.1148E+05	0.1148E+05

IDEAL GAS COMPOSITION (MOLAR BASE):

	impurities	dry_PG	FLUE_GAS
HYDROGEN	0.0000E+00	0.2614E+00	0.0000E+00
OXYGEN	0.0000E+00	0.0000E+00	0.1671E+00
NITROGEN	0.0000E+00	0.2983E+00	0.7426E+00
CARBON MONOXIDE	0.0000E+00	0.1815E+00	0.0000E+00
CARBON DIOXIDE	0.0000E+00	0.1179E+00	0.3125E-01
WATER (I.G.)	0.0000E+00	0.1269E+00	0.5022E-01
HYDROGEN SULFIDE	0.1000E+01	0.0000E+00	0.0000E+00
METHANE	0.0000E+00	0.1042E-01	0.0000E+00
ARGON	0.0000E+00	0.3547E-02	0.8839E-02

```
-------------------------------------------------------
MEAN  MOLE  MASS| 0.3408E+02 | 0.2175E+02 | 0.2878E+02 |
NET CALORI VALUE| 0.1521E+05 | 0.5652E+04 | 0.0000E+00 |
GRS CALORI VALUE| 0.1650E+05 | 0.1172E+05 | 0.0000E+00 |
-------------------------------------------------------

NON-IDEAL FLUID AND SOLID COMPOSITION (MASS BASE):

                |Wood        |DryWood     |Ash         |
-------------------------------------------------------
HYDROGEN        | 0.4204E-01 | 0.5890E-01 | 0.0000E+00 |
OXYGEN          | 0.2976E+00 | 0.4171E+00 | 0.0000E+00 |
NITROGEN        | 0.1153E-02 | 0.1615E-02 | 0.0000E+00 |
CARBON (SOLID)  | 0.3309E+00 | 0.4636E+00 | 0.0000E+00 |
SULFUR (SOLID)  | 0.1356E-03 | 0.1900E-03 | 0.0000E+00 |
WATER (LIQUID)  | 0.3220E+00 | 0.5000E-01 | 0.0000E+00 |
ASHES           | 0.6170E-02 | 0.8645E-02 | 0.1000E+01 |
-------------------------------------------------------
MEAN  MOLE  MASS| 0.1321E+02 | 0.1193E+02 | 0.7600E+02 |
NET CALORI VALUE| 0.1161E+05 | 0.1724E+05 | 0.0000E+00 |
GRS CALORI VALUE| 0.1331E+05 | 0.1865E+05 | 0.0000E+00 |
-------------------------------------------------------

MEDIUM  97 : WATER FOR GAS APP
MEDIUM 300 : HEAT
MEDIUM 301 : PRODUCT HEAT


NUMBER OF CLOSED INTERNAL LOOPS IN THE SYSTEM:    0





 SOLUTION FOR THE INDEPENDENT ALGEBRAIC VARIABLES :


 VARIABLE NO | COMPONENT    |    NAME     |    VALUE   |
------------------------------------------------------
       1     |Gasifier      |MULTIPLIER H| 0.8501E+05 |
       2     |Gasifier      |MULTIPLIER C| 0.4364E+05 |
       3     |Gasifier      |MULTIPLIER N| 0.1173E+06 |
       4     |Gasifier      |MULTIPLIER O| 0.3125E+06 |
       5     |Gasifier      |MULTIPLIER S| 0.1828E+06 |
       6     |Gasifier      |MULTIPL Ar  | 0.2292E+06 |
       7     |Gasifier      |GIBBS ENERGY| -.3280E+06 |
       1     |airpreheat    |Transferred | 0.3503E+02 |
       1     |steamheater   |Transferred | 0.3894E+02 |
       1     |recuperator   |Transferred | 0.4140E+03 |
       1     |burner        |Lambda      | 0.7900E+01 |
       1     |exhaustcooler |Transferred | 0.2092E+03 |
------------------------------------------------------

========================================================================================================================
```

269 ##

end

Appendix D SOFC PLANT MODEL LISTING

Included in this Appendix are:

- Flow sheet of SOFC scenario with node numbers (1 page)
- DNA Input for SOFC scenario (9 pages)
- DNA Output for SOFC scenario (6 pages)

The input and output data only represent one simulation using the reference conditions.

Flow sheet of SOFC scenario with node numbers

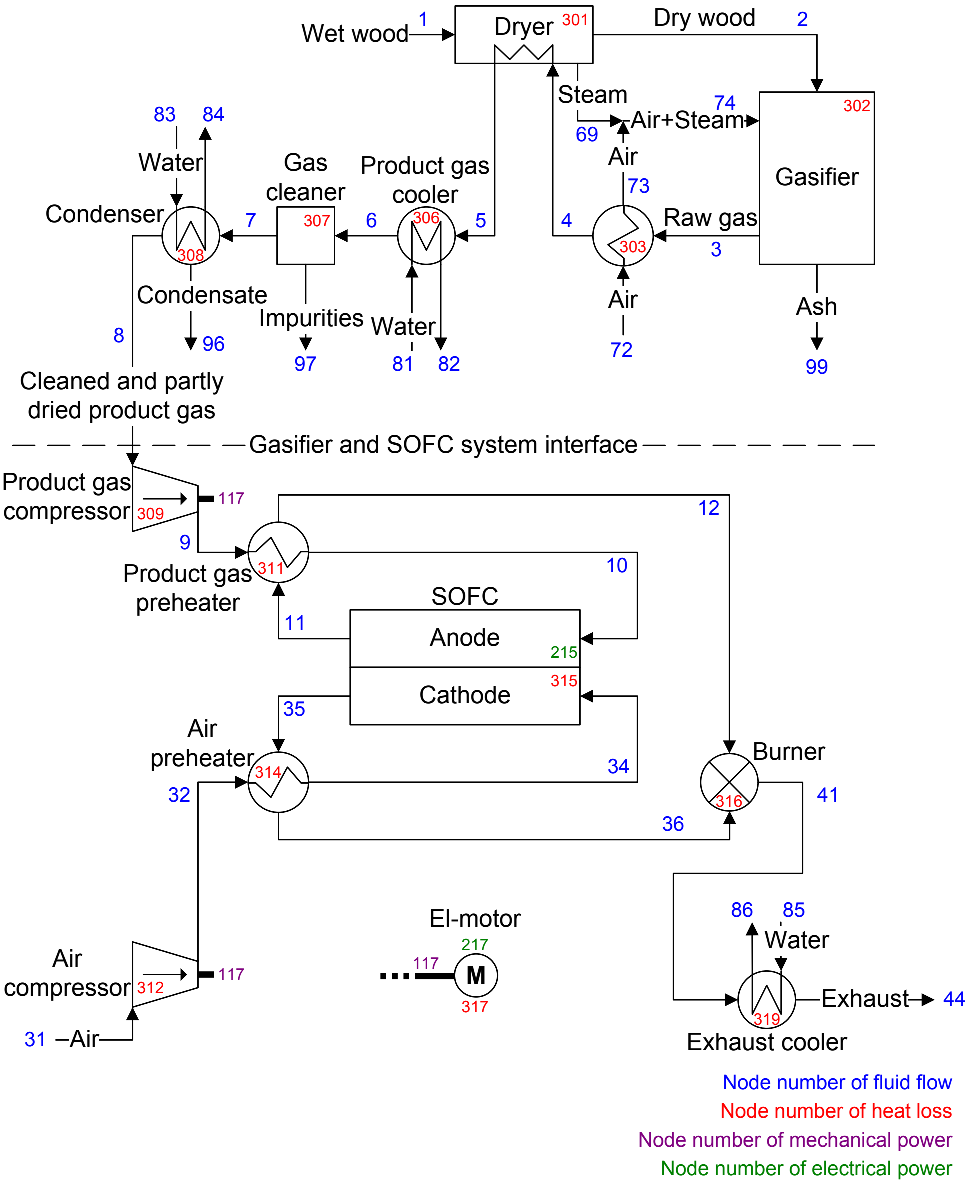

```
title Biomass gasification (Viking) + SOFC
C Wood is dried and gasified. The gasification is atmospheric,
C based on air, and almost reaches equilibrium. The produced
C product gas (PG) composition and the cold gas efficiency is
C similar to that from the Viking gasifier.
C Power and heat production by an SOFC system.


C ###################################################
C ###################################################
C ###################################################
C -----------------GASIFIER PART---------------------
C ###################################################
C ###################################################
C ###################################################

C ##Media##
media 1 Wood 2 DryWood
media 73 STANDARD_AIR 3 raw_PG 99 Ash

C ##Fuel composition##
solid Wood C 0.488 H .062 O .439 S .0002 N 0.0017 ASH .0091
+ LHV 18280 CP 1.35 MOI .322
C [Ahrenfeldt, J. et al., Energy & Fuels 2006, 20, 2672-2680] without Cl.



C ###################################################
C -----------------------DRYER-----------------------
C ###################################################
struc Dryer DRYER_03 1 64 2 61 301  0.05 0.005

C Fuel input (plant size):
addco m Dryer 1 0.043

addco t Dryer 1 15 p 1 1.013
addco p 2 1.008 t Dryer 2 150
addco q Dryer 301 0



C ###################################################
C ---------------------GASIFIER----------------------
C ###################################################
struc Gasifier GASIFI_3 8  2 26 74 3 99 302  1 3 4 6 7 9 11 36 /
 0.998 800 0.005 0 1.0 0.01
C Variable constitution parameter: Number of calculated gas components 8
C Nodes: Inlet fuel 2; inlet water 26; inlet air 74; outlet PG 3,
C        outlet ash 99, heat loss 302
C Integer Parameters: Calculated gas compounds H2 (1), N2 (3), CO (4),
C                     CO2 (6), H2O (7), H2S (9), CH4 (11), Ar (36)
C Real parameter: Pressure 1 bar, Eq. temperature 800 degC, Pressure loss 0,
C                 Water-to-fuel ratio 0, carbon conversion factor 1,
C                 non-equilibrium methane 0.01.

addco t Gasifier 3 800
addco t Gasifier 26 150
addco p 99 1.013
addco q Gasifier 302 0



C ###################################################
C -------------GASIFIER AIR PREHEATER----------------
C ###################################################
struc airpreheat heatex_2 3 4 72 73 303 20 0.005 0.005
addco t airpreheat 72 15
addco q airpreheat 303 0



C ###################################################
C ------------------STEAM HEATER---------------------
C ###################################################
struc steamheater heatex_1 4 5 63 64 304 0.005 0.005
```

```
media 63 STEAM-HF

addco t steamheater 64 250
addco q steamheater 304 0



C ###################################################
C ------------------STEAM BLOWER---------------------
C ###################################################
struc steamblower COMPRE_1 61 62 305 105 0.6 0.98



C ###################################################
C --------------------SPLITTER-----------------------
C ###################################################
struc split1 SPLITTER 62 63 69



C ###################################################
C ----------------------MIXER------------------------
C ###################################################
struc mix1 MIXER_02 73 69 74

media 74 humid_air



C ###################################################
C --------------------GAS COOLER---------------------
C ###################################################
struc gascooler GASCOOL1 5 6 98 81 82 306 0.005 0.005

media 81 STEAM-HF 6 cold_PG

addco t gascooler 6 90
addco t gascooler 81 30 p 81 1.013
addco t gascooler 82 80
addco q gascooler 306 0



C ###################################################
C -------------------GAS CLEANING--------------------
C ###################################################
struc gasclean GASCLE_1 6 7 97 307 0.0049
C Pressure loss is taken from paper about Viking

media 7 clean_PG 97 impurities

addco q gasclean 307 0



C ###################################################
C --------------------CONDENSER----------------------
C ###################################################
struc condenser GASCOOL1 7 8 96 83 84 308 0.005 0.005

media 83 STEAM-HF 8 dry_PG

addco t condenser 8 50
addco t condenser 83 30 p 83 1.013
addco t condenser 84 80
addco q condenser 308 0



C ###################################################
C ###################################################
C ###################################################
C -------------------SOFC PART-----------------------
C ###################################################
C ###################################################
```

```
C ###################################################

media 11 USEDFUEL 35 USEDAIR



C ###################################################
C -------------PRODUCT GAS COMPRESSOR----------------
C ###################################################
struc PGcompressor compre_1 8 9 309 117 0.6 0.98
C Isentropic efficiency from L. Fryda et al. (2008)



C ###################################################
C -------------PRODUCT GAS PREHEATING----------------
C ###################################################
struc PGpreheat heatex_2 11 12 9 10 311 150 0.005 0.005
addco q PGpreheat 311 0



C ###################################################
C -----------------AIR COMPRESSOR--------------------
C ###################################################
struc aircompressor compre_1 31 32 312 117 0.6 0.98

media 31 STANDARD_AIR
addco p 31 1.013 t aircompressor 31 15



C ###################################################
C -----------------AIR PREHEATING--------------------
C ###################################################
struc airpreheat2 heatex_2 35 36 32 34 314 200 0.01 0.01
addco q airpreheat2 314 0



C ###################################################
C ----------------------SOFC-------------------------
C ###################################################
struc sofc sofceq0d_CBM /
    {fuel and air inlets} 10 34 /
    {fuel and air outlets} 11 35  /
    {nodes for power and heat loss} 215 315 /
    {parameters: utilization, temperature} 0.85 800 /
    {pressure loss} 0.005 0.010 /
    {temperature difference between anode and cathode outlet} 0 /
    {current density [mA/cm^2]} 300 /
    {DC to AC conversion efficiency [-]} 0.95

addco q sofc 315 0

C SOFC OPERATING PRESSURE:
C addco p 10 2.5



C ###################################################
C --------------------EL-MOTOR-----------------------
C ###################################################
struc el-motor el-motor 217 317 117 0.95



C ###################################################
C ---------------------BURNER------------------------
C ###################################################
struc burner GASBUR_3 36 12 41 316 0.999374

media 41 FLUE_GAS

addco q burner 316 0

```

```


C ####################################################
C -----------------EXHAUST COOLING------------------
C ####################################################
struc exhaustcooler heatex_2 41 44 85 86 319 90 0.010 0.005

media 85 STEAM-HF

addco p 44 1.013
addco p 85 1.013 t exhaustcooler 85 30
addco t exhaustcooler 86 80
addco q exhaustcooler 319 0



C Reference conditions for exergy
xergy p 1 t 15




C ~~~~~~~~~~~~~~~~~~~~~~~~~~~~~~~~~~~~~~~~~~~~~~~~~~~~~~~~~~~~~~~~~~~~~~~~~~~~~~~~~~~~~~~~~~~~
~~~~~
C ~~ Start of list of generated initial guesses.
C ~~ The values are the results of the latest simulation.
C ~~~~~~~~~~~~~~~~~~~~~~~~~~~~~~~~~~~~~~~~~~~~~~~~~~~~~~~~~~~~~~~~~~~~~~~~~~~~~~~~~~~~~~~~~~~~
~~~~~
START M     Dryer                        1  0.4300000000000009E-01 {~~}
START P                             1  0.1013000000000002E+01 {~~}
START H     Dryer                        1 -0.8621618755529553E+04 {~~}
START M     Dryer                       64  0.2000459030657089E+00 {~~}
START P                            64  0.9980000000000021E+00 {~~}
START H     Dryer                       64 -0.1299653551379775E+05 {~~}
START M     Dryer                        2 -0.3068842105263164E-01 {~~}
START P                             2  0.1008000000000002E+01 {~~}
START H     Dryer                        2 -0.5497059220211011E+04 {~~}
START M     Dryer                       61 -0.2123574820130773E+00 {~~}
START P                            61  0.9930000000000021E+00 {~~}
START H     Dryer                       61 -0.1319443607829822E+05 {~~}
START Q     Dryer                      301  0.0000000000000000E+00 {~~}
START X_J   DryWood             H2          0.5890000000000011E-01 {~~}
START X_J   DryWood             O2          0.4170500000000009E+00 {~~}
START X_J   DryWood             N2          0.1615000000000003E-02 {~~}
START X_J   DryWood             CO          0.0000000000000000E+00 {~~}
START X_J   DryWood             NO          0.0000000000000000E+00 {~~}
START X_J   DryWood             CO2         0.0000000000000000E+00 {~~}
START X_J   DryWood             H2O-L       0.5000000000000009E-01 {~~}
START X_J   DryWood             NH3         0.0000000000000000E+00 {~~}
START X_J   DryWood             H2S         0.0000000000000000E+00 {~~}
START X_J   DryWood             SO2         0.0000000000000000E+00 {~~}
START X_J   DryWood             CH4         0.0000000000000000E+00 {~~}
START X_J   DryWood             C2H6        0.0000000000000000E+00 {~~}
START X_J   DryWood             C3H8        0.0000000000000000E+00 {~~}
START X_J   DryWood             C4H10-N     0.0000000000000000E+00 {~~}
START X_J   DryWood             C4H10-I     0.0000000000000000E+00 {~~}
START X_J   DryWood             C5H12       0.0000000000000000E+00 {~~}
START X_J   DryWood             C6H14       0.0000000000000000E+00 {~~}
START X_J   DryWood             C7H16       0.0000000000000000E+00 {~~}
START X_J   DryWood             C8H18       0.0000000000000000E+00 {~~}
START X_J   DryWood             C2H4        0.0000000000000000E+00 {~~}
START X_J   DryWood             C3H6        0.0000000000000000E+00 {~~}
START X_J   DryWood             C5H10       0.0000000000000000E+00 {~~}
START X_J   DryWood             C6H12-1     0.0000000000000000E+00 {~~}
START X_J   DryWood             C7H14       0.0000000000000000E+00 {~~}
START X_J   DryWood             C2H2        0.0000000000000000E+00 {~~}
START X_J   DryWood             C6H6        0.0000000000000000E+00 {~~}
START X_J   DryWood             C6H12-C     0.0000000000000000E+00 {~~}
START X_J   DryWood             C           0.4636000000000009E+00 {~~}
START X_J   DryWood             S           0.1900000000000004E-03 {~~}
START X_J   DryWood             NO2         0.0000000000000000E+00 {~~}
START X_J   DryWood             HCN         0.0000000000000000E+00 {~~}
START X_J   DryWood             COS         0.0000000000000000E+00 {~~}
START X_J   DryWood             N2O         0.0000000000000000E+00 {~~}
START X_J   DryWood             NO3         0.0000000000000000E+00 {~~}
START X_J   DryWood             SO3         0.0000000000000000E+00 {~~}
```

```
START X_J    DryWood                   AR          0.0000000000000000E+00 {~~}
START X_J    DryWood                   ASH         0.8645000000000019E-02 {~~}
START X_J    DryWood                   TAR         0.0000000000000000E+00 {~~}
START M      Gasifier                    2  0.3068842105263164E-01 {~~}
START H      Gasifier                    2 -0.5497059220211011E+04 {~~}
START M      Gasifier                   26  0.0000000000000000E+00 {~~}
START P                          26  0.1003000000000002E+01 {~~}
START H      Gasifier                   26 -0.1319450918722708E+05 {~~}
START M      Gasifier                   74  0.5485206982616303E-01 {~~}
START P                          74  0.1003000000000002E+01 {~~}
START H      Gasifier                   74 -0.2398848478333937E+04 {~~}
START M      Gasifier                    3 -0.8527518947879467E-01 {~~}
START P                           3  0.9980000000000021E+00 {~~}
START H      Gasifier                    3 -0.3507877913073770E+04 {~~}
START M      Gasifier                   99 -0.2653014000000006E-03 {~~}
START P                          99  0.1013000000000002E+01 {~~}
START H      Gasifier                   99 -0.4308000000000007E+04 {~~}
START Q      Gasifier                  302  0.0000000000000000E+00 {~~}
START ZA     Gasifier                    1  0.8500945239865259E+05 {~~}
START ZA     Gasifier                    2  0.4363965291425181E+05 {~~}
START ZA     Gasifier                    3  0.1172765217993688E+06 {~~}
START ZA     Gasifier                    4  0.3124902840469579E+06 {~~}
START ZA     Gasifier                    5  0.1827651987487792E+06 {~~}
START ZA     Gasifier                    6  0.2292482774424776E+06 {~~}
START ZA     Gasifier                    7 -0.3279719879436739E+06 {~~}
START Y_J    raw_PG                    H2          0.2538114658675977E+00 {~~}
START Y_J    raw_PG                    O2          0.0000000000000000E+00 {~~}
START Y_J    raw_PG                    N2          0.2896541868376543E+00 {~~}
START Y_J    raw_PG                    CO          0.1761818347160904E+00 {~~}
START Y_J    raw_PG                    NO          0.0000000000000000E+00 {~~}
START Y_J    raw_PG                    CO2         0.1144395150133743E+00 {~~}
START Y_J    raw_PG                    H2O-G       0.1523098114753791E+00 {~~}
START Y_J    raw_PG                    NH3         0.0000000000000000E+00 {~~}
START Y_J    raw_PG                    H2S         0.4615796164902312E-04 {~~}
START Y_J    raw_PG                    SO2         0.0000000000000000E+00 {~~}
START Y_J    raw_PG                    CH4         0.1011293223314740E-01 {~~}
START Y_J    raw_PG                    NO2         0.0000000000000000E+00 {~~}
START Y_J    raw_PG                    HCN         0.0000000000000000E+00 {~~}
START Y_J    raw_PG                    COS         0.0000000000000000E+00 {~~}
START Y_J    raw_PG                    AR          0.3444095895109989E-02 {~~}
START X_J    Ash                       C           0.0000000000000000E+00 {~~}
START X_J    Ash                       ASH         0.1000000000000002E+01 {~~}
START M      airpreheat                  3  0.8527518947879467E-01 {~~}
START H      airpreheat                  3 -0.3507877913073770E+04 {~~}
START M      airpreheat                  4 -0.8527518947879467E-01 {~~}
START P                           4  0.9930000000000021E+00 {~~}
START H      airpreheat                  4 -0.3918630307677503E+04 {~~}
START M      airpreheat                 72  0.4254049087879458E-01 {~~}
START P                          72  0.1008000000000002E+01 {~~}
START H      airpreheat                 72 -0.9883454496688249E+02 {~~}
START M      airpreheat                 73 -0.4254049087879458E-01 {~~}
START P                          73  0.1003000000000002E+01 {~~}
START H      airpreheat                 73  0.7245454291500147E+03 {~~}
START Q      airpreheat                303  0.0000000000000000E+00 {~~}
START ZA     airpreheat                  1  0.3502698827870192E+02 {~~}
START M      steamheater                 4  0.8527518947879467E-01 {~~}
START H      steamheater                 4 -0.3918630307677503E+04 {~~}
START M      steamheater                 5 -0.8527518947879467E-01 {~~}
START P                           5  0.9880000000000021E+00 {~~}
START H      steamheater                 5 -0.4375257198957320E+04 {~~}
START M      steamheater                63  0.2000459030657089E+00 {~~}
START P                          63  0.1003000000000002E+01 {~~}
START H      steamheater                63 -0.1319118556200298E+05 {~~}
START M      steamheater                64 -0.2000459030657089E+00 {~~}
START H      steamheater                64 -0.1299653551379775E+05 {~~}
START Q      steamheater               304  0.0000000000000000E+00 {~~}
START ZA     steamheater                 1  0.3893894467499928E+02 {~~}
START M      steamblower                61  0.2123574820130773E+00 {~~}
START H      steamblower                61 -0.1319443607829822E+05 {~~}
START M      steamblower                62 -0.2123574820130773E+00 {~~}
START P                          62  0.1003000000000002E+01 {~~}
START H      steamblower                62 -0.1319118556200298E+05 {~~}
START Q      steamblower               305 -0.1408717256529172E-01 {~~}
START W      steamblower               105  0.7043586282645917E+00 {~~}
START M      split1                     62  0.2123574820130773E+00 {~~}
START H      split1                     62 -0.1319118556200298E+05 {~~}
```

```
START M     split1                      63 -0.2000459030657089E+00 {~~}
START H     split1                      63 -0.1319118556200298E+05 {~~}
START M     split1                      69 -0.1231157894736844E-01 {~~}
START P                            69  0.1003000000000002E+01 {~~}
START H     split1                      69 -0.1319118556200298E+05 {~~}
START M     mix1                        73  0.4254049087879458E-01 {~~}
START H     mix1                        73  0.7245454291500147E+03 {~~}
START M     mix1                        69  0.1231157894736844E-01 {~~}
START H     mix1                        69 -0.1319118556200299E+05 {~~}
START M     mix1                        74 -0.5485206982616303E-01 {~~}
START H     mix1                        74 -0.2398848478333937E+04 {~~}
START Y_J   humid_air                  H2            0.0000000000000000E+00 {~~}
START Y_J   humid_air                  O2            0.1417803964772677E+00 {~~}
START Y_J   humid_air                  N2            0.5281063539146036E+00 {~~}
START Y_J   humid_air                  CO            0.0000000000000000E+00 {~~}
START Y_J   humid_air                  NO            0.0000000000000000E+00 {~~}
START Y_J   humid_air                  CO2           0.2049837057502667E-03 {~~}
START Y_J   humid_air                  H2O-G         0.3236220989260387E+00 {~~}
START Y_J   humid_air                  NH3           0.0000000000000000E+00 {~~}
START Y_J   humid_air                  H2S           0.0000000000000000E+00 {~~}
START Y_J   humid_air                  SO2           0.0000000000000000E+00 {~~}
START Y_J   humid_air                  CH4           0.0000000000000000E+00 {~~}
START Y_J   humid_air                  C2H6          0.0000000000000000E+00 {~~}
START Y_J   humid_air                  C3H8          0.0000000000000000E+00 {~~}
START Y_J   humid_air                  C4H10-N       0.0000000000000000E+00 {~~}
START Y_J   humid_air                  C4H10-I       0.0000000000000000E+00 {~~}
START Y_J   humid_air                  C5H12         0.0000000000000000E+00 {~~}
START Y_J   humid_air                  C6H14         0.0000000000000000E+00 {~~}
START Y_J   humid_air                  C7H16         0.0000000000000000E+00 {~~}
START Y_J   humid_air                  C8H18         0.0000000000000000E+00 {~~}
START Y_J   humid_air                  C2H4          0.0000000000000000E+00 {~~}
START Y_J   humid_air                  C3H6          0.0000000000000000E+00 {~~}
START Y_J   humid_air                  C5H10         0.0000000000000000E+00 {~~}
START Y_J   humid_air                  C6H12-1       0.0000000000000000E+00 {~~}
START Y_J   humid_air                  C7H14         0.0000000000000000E+00 {~~}
START Y_J   humid_air                  C2H2          0.0000000000000000E+00 {~~}
START Y_J   humid_air                  C6H6          0.0000000000000000E+00 {~~}
START Y_J   humid_air                  C6H12-C       0.0000000000000000E+00 {~~}
START Y_J   humid_air                  C             0.0000000000000000E+00 {~~}
START Y_J   humid_air                  S             0.0000000000000000E+00 {~~}
START Y_J   humid_air                  NO2           0.0000000000000000E+00 {~~}
START Y_J   humid_air                  HCN           0.0000000000000000E+00 {~~}
START Y_J   humid_air                  COS           0.0000000000000000E+00 {~~}
START Y_J   humid_air                  N2O           0.0000000000000000E+00 {~~}
START Y_J   humid_air                  NO3           0.0000000000000000E+00 {~~}
START Y_J   humid_air                  SO3           0.0000000000000000E+00 {~~}
START Y_J   humid_air                  AR            0.6286166976341510E-02 {~~}
START Y_J   humid_air                  ASH           0.0000000000000000E+00 {~~}
START Y_J   humid_air                  TAR           0.0000000000000000E+00 {~~}
START Y_J   humid_air                  CH3OH         0.0000000000000000E+00 {~~}
START M     gascooler                    5  0.8527518947879467E-01 {~~}
START H     gascooler                    5 -0.4375257198957320E+04 {~~}
START M     gascooler                    6 -0.8527518947879467E-01 {~~}
START P                             6  0.9830000000000021E+00 {~~}
START H     gascooler                    6 -0.4624611248324039E+04 {~~}
START M     gascooler                   98  0.0000000000000000E+00 {~~}
START P                            98  0.9830000000000021E+00 {~~}
START H     gascooler                   98 -0.1559408877861427E+05 {~~}
START M     gascooler                   81  0.1016636501943104E+00 {~~}
START P                            81  0.1013000000000002E+01 {~~}
START H     gascooler                   81 -0.1584524528596514E+05 {~~}
START M     gascooler                   82 -0.1016636501943104E+00 {~~}
START P                            82  0.1008000000000002E+01 {~~}
START H     gascooler                   82 -0.1563608779686839E+05 {~~}
START Q     gascooler                  306  0.0000000000000000E+00 {~~}
START Y_J   cold_PG                H2            0.2538114658675973E+00 {~~}
START Y_J   cold_PG                O2            0.0000000000000000E+00 {~~}
START Y_J   cold_PG                N2            0.2896541868376540E+00 {~~}
START Y_J   cold_PG                CO            0.1761818347160902E+00 {~~}
START Y_J   cold_PG                NO            0.0000000000000000E+00 {~~}
START Y_J   cold_PG                CO2           0.1144395150133742E+00 {~~}
START Y_J   cold_PG                H2O-G         0.1523098114753791E+00 {~~}
START Y_J   cold_PG                NH3           0.0000000000000000E+00 {~~}
START Y_J   cold_PG                H2S           0.4615796164902307E-04 {~~}
START Y_J   cold_PG                SO2           0.0000000000000000E+00 {~~}
START Y_J   cold_PG                CH4           0.1011293223314739E-01 {~~}
```

```
START Y_J    cold_PG               C2H6        0.0000000000000000E+00 {~~}
START Y_J    cold_PG               C3H8        0.0000000000000000E+00 {~~}
START Y_J    cold_PG               C4H10-N     0.0000000000000000E+00 {~~}
START Y_J    cold_PG               C4H10-I     0.0000000000000000E+00 {~~}
START Y_J    cold_PG               C5H12       0.0000000000000000E+00 {~~}
START Y_J    cold_PG               C6H14       0.0000000000000000E+00 {~~}
START Y_J    cold_PG               C7H16       0.0000000000000000E+00 {~~}
START Y_J    cold_PG               C8H18       0.0000000000000000E+00 {~~}
START Y_J    cold_PG               C2H4        0.0000000000000000E+00 {~~}
START Y_J    cold_PG               C3H6        0.0000000000000000E+00 {~~}
START Y_J    cold_PG               C5H10       0.0000000000000000E+00 {~~}
START Y_J    cold_PG               C6H12-1     0.0000000000000000E+00 {~~}
START Y_J    cold_PG               C7H14       0.0000000000000000E+00 {~~}
START Y_J    cold_PG               C2H2        0.0000000000000000E+00 {~~}
START Y_J    cold_PG               C6H6        0.0000000000000000E+00 {~~}
START Y_J    cold_PG               C6H12-C     0.0000000000000000E+00 {~~}
START Y_J    cold_PG               C           0.0000000000000000E+00 {~~}
START Y_J    cold_PG               S           0.0000000000000000E+00 {~~}
START Y_J    cold_PG               NO2         0.0000000000000000E+00 {~~}
START Y_J    cold_PG               HCN         0.0000000000000000E+00 {~~}
START Y_J    cold_PG               COS         0.0000000000000000E+00 {~~}
START Y_J    cold_PG               N2O         0.0000000000000000E+00 {~~}
START Y_J    cold_PG               NO3         0.0000000000000000E+00 {~~}
START Y_J    cold_PG               SO3         0.0000000000000000E+00 {~~}
START Y_J    cold_PG               AR          0.3444095895109983E-02 {~~}
START M      gasclean                   6   0.8527518947879467E-01 {~~}
START H      gasclean                   6  -0.4624611248324039E+04 {~~}
START M      gasclean                   7  -0.8526899202586889E-01 {~~}
START P                            7  0.9781000000000021E+00 {~~}
START H      gasclean                   7  -0.4624908439609422E+04 {~~}
START M      gasclean                  97  -0.6197452925764206E-05 {~~}
START P                           97  0.9781000000000021E+00 {~~}
START H      gasclean                  97  -0.5356408846834938E+03 {~~}
START Q      gasclean                 307   0.0000000000000000E+00 {~~}
START Y_J    clean_PG              H2          0.2538231818282900E+00 {~~}
START Y_J    clean_PG              O2          0.0000000000000000E+00 {~~}
START Y_J    clean_PG              N2          0.2896675573016551E+00 {~~}
START Y_J    clean_PG              CO          0.1761899672858432E+00 {~~}
START Y_J    clean_PG              NO          0.0000000000000000E+00 {~~}
START Y_J    clean_PG              CO2         0.1144447975519506E+00 {~~}
START Y_J    clean_PG              H2O-G       0.1523168421103358E+00 {~~}
START Y_J    clean_PG              CH4         0.1011339904703275E-01 {~~}
START Y_J    clean_PG              NO2         0.0000000000000000E+00 {~~}
START Y_J    clean_PG              AR          0.3444254874894413E-02 {~~}
START Y_J    impurities                H2O-G       0.0000000000000000E+00 {~~}
START Y_J    impurities                NH3         0.0000000000000000E+00 {~~}
START Y_J    impurities                H2S         0.1000000000000002E+01 {~~}
START Y_J    impurities                SO2         0.0000000000000000E+00 {~~}
START Y_J    impurities                HCN         0.0000000000000000E+00 {~~}
START Y_J    impurities                COS         0.0000000000000000E+00 {~~}
START Y_J    impurities                AR          0.0000000000000000E+00 {~~}
START Y_J    impurities                ASH         0.0000000000000000E+00 {~~}
START M      condenser                  7   0.8526899202586889E-01 {~~}
START H      condenser                  7  -0.4624908439609422E+04 {~~}
START M      condenser                  8  -0.8320484335731876E-01 {~~}
START P                            8  0.9731000000000021E+00 {~~}
START H      condenser                  8  -0.4466561290262733E+04 {~~}
START M      condenser                 96  -0.2064148668550151E-02 {~~}
START P                           96  0.9731000000000021E+00 {~~}
START H      condenser                 96  -0.1576166949955456E+05 {~~}
START M      condenser                 83   0.4691527326491761E-01 {~~}
START P                           83  0.1013000000000002E+01 {~~}
START H      condenser                 83  -0.1584524528596514E+05 {~~}
START M      condenser                 84  -0.4691527326491761E-01 {~~}
START P                           84  0.1008000000000002E+01 {~~}
START H      condenser                 84  -0.1563608779686839E+05 {~~}
START Q      condenser                308   0.0000000000000000E+00 {~~}
START Y_J    dry_PG                H2          0.2614256920940575E+00 {~~}
START Y_J    dry_PG                O2          0.0000000000000000E+00 {~~}
START Y_J    dry_PG                N2          0.2983436780648697E+00 {~~}
START Y_J    dry_PG                CO          0.1814672080223573E+00 {~~}
START Y_J    dry_PG                NO          0.0000000000000000E+00 {~~}
START Y_J    dry_PG                CO2         0.1178726473723858E+00 {~~}
START Y_J    dry_PG                H2O-G       0.1269270417636751E+00 {~~}
START Y_J    dry_PG                NH3         0.0000000000000000E+00 {~~}
START Y_J    dry_PG                H2S         0.0000000000000000E+00 {~~}
```

```
START Y_J   dry_PG                   SO2           0.0000000000000000E+00 {~~}
START Y_J   dry_PG                   CH4           0.1041631550849640E-01 {~~}
START Y_J   dry_PG                   C2H6          0.0000000000000000E+00 {~~}
START Y_J   dry_PG                   C3H8          0.0000000000000000E+00 {~~}
START Y_J   dry_PG                   C4H10-N       0.0000000000000000E+00 {~~}
START Y_J   dry_PG                   C4H10-I       0.0000000000000000E+00 {~~}
START Y_J   dry_PG                   C5H12         0.0000000000000000E+00 {~~}
START Y_J   dry_PG                   C6H14         0.0000000000000000E+00 {~~}
START Y_J   dry_PG                   C7H16         0.0000000000000000E+00 {~~}
START Y_J   dry_PG                   C8H18         0.0000000000000000E+00 {~~}
START Y_J   dry_PG                   C2H4          0.0000000000000000E+00 {~~}
START Y_J   dry_PG                   C3H6          0.0000000000000000E+00 {~~}
START Y_J   dry_PG                   C5H10         0.0000000000000000E+00 {~~}
START Y_J   dry_PG                   C6H12-1       0.0000000000000000E+00 {~~}
START Y_J   dry_PG                   C7H14         0.0000000000000000E+00 {~~}
START Y_J   dry_PG                   C2H2          0.0000000000000000E+00 {~~}
START Y_J   dry_PG                   C6H6          0.0000000000000000E+00 {~~}
START Y_J   dry_PG                   C6H12-C       0.0000000000000000E+00 {~~}
START Y_J   dry_PG                   C             0.0000000000000000E+00 {~~}
START Y_J   dry_PG                   S             0.0000000000000000E+00 {~~}
START Y_J   dry_PG                   NO2           0.0000000000000000E+00 {~~}
START Y_J   dry_PG                   HCN           0.0000000000000000E+00 {~~}
START Y_J   dry_PG                   COS           0.0000000000000000E+00 {~~}
START Y_J   dry_PG                   N2O           0.0000000000000000E+00 {~~}
START Y_J   dry_PG                   NO3           0.0000000000000000E+00 {~~}
START Y_J   dry_PG                   SO3           0.0000000000000000E+00 {~~}
START Y_J   dry_PG                   AR            0.3547417174159966E-02 {~~}
START M     PGcompressor                  8   0.8320484335731876E-01 {~~}
START H     PGcompressor                  8  -0.4466561290262733E+04 {~~}
START M     PGcompressor                  9  -0.8320484335731876E-01 {~~}
START P                              9  0.1038640799140263E+01 {~~}
START H     PGcompressor                  9  -0.4453023621827175E+04 {~~}
START Q     PGcompressor                309  -0.2298774656334687E-01 {~~}
START W     PGcompressor                117   0.1149387328167349E+01 {~~}
START M     PGpreheat                    11   0.1084136464468039E+00 {~~}
START P                             11  0.1028640799140263E+01 {~~}
START H     PGpreheat                    11  -0.6150749955252332E+04 {~~}
START M     PGpreheat                    12  -0.1084136464468039E+00 {~~}
START P                             12  0.1023640799140263E+01 {~~}
START H     PGpreheat                    12  -0.6842868464426251E+04 {~~}
START M     PGpreheat                     9   0.8320484335731876E-01 {~~}
START H     PGpreheat                     9  -0.4453023621827175E+04 {~~}
START M     PGpreheat                    10  -0.8320484335731876E-01 {~~}
START P                             10  0.1033640799140263E+01 {~~}
START H     PGpreheat                    10  -0.3551212040611453E+04 {~~}
START Q     PGpreheat                   311   0.0000000000000000E+00 {~~}
START ZA    PGpreheat                     1   0.7503509135286993E+02 {~~}
START M     aircompressor                  31   0.7441554834157872E+00 {~~}
START P                             31  0.1013000000000002E+01 {~~}
START H     aircompressor                  31  -0.9883454496688249E+02 {~~}
START M     aircompressor                  32  -0.7441554834157872E+00 {~~}
START P                             32  0.1053640799140263E+01 {~~}
START H     aircompressor                  32  -0.9336060792260105E+02 {~~}
START Q     aircompressor                 312  -0.8313184219132176E-01 {~~}
START W     aircompressor                 117   0.4156592109566154E+01 {~~}
START M     airpreheat2                    35   0.7189466803263022E+00 {~~}
START P                             35  0.1033640799140263E+01 {~~}
START H     airpreheat2                    35   0.7462773132386449E+03 {~~}
START M     airpreheat2                    36  -0.7189466803263022E+00 {~~}
START P                             36  0.1023640799140263E+01 {~~}
START H     airpreheat2                    36   0.1120243700978561E+03 {~~}
START M     airpreheat2                    32   0.7441554834157872E+00 {~~}
START H     airpreheat2                    32  -0.9336060792260105E+02 {~~}
START M     airpreheat2                    34  -0.7441554834157872E+00 {~~}
START P                             34  0.1043640799140263E+01 {~~}
START H     airpreheat2                    34   0.5194065598541849E+03 {~~}
START Q     airpreheat2                   314   0.0000000000000000E+00 {~~}
START ZA    airpreheat2                     1   0.4559940479582562E+03 {~~}
START M     sofc                           10   0.8320484335731876E-01 {~~}
START H     sofc                           10  -0.3551212040611453E+04 {~~}
START M     sofc                           34   0.7441554834157872E+00 {~~}
START H     sofc                           34   0.5194065598541849E+03 {~~}
START M     sofc                           11  -0.1084136464468039E+00 {~~}
START H     sofc                           11  -0.6150749955252332E+04 {~~}
START M     sofc                           35  -0.7189466803263022E+00 {~~}
START H     sofc                           35   0.7462773132386449E+03 {~~}
```

```
START E     sofc                         215 -0.2213328321455869E+03 {~~}
START Q     sofc                         315  0.0000000000000000E+00 {~~}
START ZA    sofc                           1  0.9348775972877994E+05 {~~}
START ZA    sofc                           2  0.8550154548146646E+05 {~~}
START ZA    sofc                           3  0.1170862073421318E+06 {~~}
START ZA    sofc                           4  0.2874558030874020E+06 {~~}
START ZA    sofc                           5 -0.4425649794871430E+06 {~~}
START ZA    sofc                           6  0.6890776990028493E+00 {~~}
START ZA    sofc                           7  0.8458535404752862E+00 {~~}
START ZA    sofc                           8  0.8500000000000016E+00 {~~}
START ZA    sofc                           9  0.4954299896595041E+00 {~~}
START ZA    sofc                          10  0.4097643685146286E+00 {~~}
START ZA    sofc                          11  0.9450055454564674E+00 {~~}
START ZA    sofc                          12  0.1080954241372454E+00 {~~}
START ZA    sofc                          13  0.7147434745365802E-02 {~~}
START ZA    sofc                          14  0.3042640018072583E-01 {~~}
START ZA    sofc                          15  0.7993362863931303E+00 {~~}
START ZA    sofc                          16 -0.8470853341704197E+05 {~~}
START ZA    sofc                          17 -0.1885369880714485E+06 {~~}
START ZA    sofc                          18 -0.1823577201067346E+06 {~~}
START ZA    sofc                          19  0.2821703056799879E+00 {~~}
START ZA    sofc                          20  0.2335762988681635E-01 {~~}
START ZA    sofc                          21  0.1013478073726874E+04 {~~}
START ZA    sofc                          22  0.3000000000000006E+03 {~~}
START ZA    sofc                          23  0.9500000000000016E+00 {~~}
START Y_J   USEDFUEL                     H2            0.3681288480481491E-01 {~~}
START Y_J   USEDFUEL                     CO            0.2592619821632520E-01 {~~}
START Y_J   USEDFUEL                     CO2           0.2785667382357346E+00 {~~}
START Y_J   USEDFUEL                     H2O-G         0.3654197752201502E+00 {~~}
START Y_J   USEDFUEL                     CH4           0.2245244540724863E-07 {~~}
START Y_J   USEDFUEL                     N2            0.2932743810705314E+00 {~~}
START Y_J   USEDAIR                      O2            0.1825295746533185E+00 {~~}
START Y_J   USEDAIR                      N2            0.7972528602529357E+00 {~~}
START Y_J   USEDAIR                      CO2           0.3094525269451167E-03 {~~}
START Y_J   USEDAIR                      H2O-G         0.1041823507381893E-01 {~~}
START Y_J   USEDAIR                      AR            0.9489877492983592E-02 {~~}
START M     burner                        36  0.7189466803263022E+00 {~~}
START H     burner                        36  0.1120243700978561E+03 {~~}
START M     burner                        12  0.1084136464468039E+00 {~~}
START H     burner                        12 -0.6842868464426250E+04 {~~}
START M     burner                        41 -0.8273603267731059E+00 {~~}
START P                              41 0.1023000000000002E+01 {~~}
START H     burner                        41 -0.7993140980860109E+03 {~~}
START Q     burner                       316  0.0000000000000000E+00 {~~}
START ZA    burner                         1  0.3738435658349209E+02 {~~}
START Y_J   FLUE_GAS                     O2            0.1543733815328906E+00 {~~}
START Y_J   FLUE_GAS                     N2            0.7324705619747473E+00 {~~}
START Y_J   FLUE_GAS                     NO            0.0000000000000000E+00 {~~}
START Y_J   FLUE_GAS                     CO2           0.4145268848345668E-01 {~~}
START Y_J   FLUE_GAS                     H2O-G         0.6345676680902396E-01 {~~}
START Y_J   FLUE_GAS                     SO2           0.0000000000000000E+00 {~~}
START Y_J   FLUE_GAS                     NO2           0.0000000000000000E+00 {~~}
START Y_J   FLUE_GAS                     AR            0.8246601199883187E-02 {~~}
START E     el-motor                     217  0.5585241513403690E+01 {~~}
START Q     el-motor                     317 -0.2792620756701864E+00 {~~}
START W     el-motor                     117 -0.5305979437733503E+01 {~~}
START M     exhaustcooler                  41  0.8273603267731059E+00 {~~}
START H     exhaustcooler                  41 -0.7993140980860109E+03 {~~}
START M     exhaustcooler                  44 -0.8273603267731059E+00 {~~}
START P                              44 0.1013000000000002E+01 {~~}
START H     exhaustcooler                  44 -0.1002214102959687E+04 {~~}
START M     exhaustcooler                  85  0.8026077146914962E+00 {~~}
START P                              85 0.1013000000000002E+01 {~~}
START H     exhaustcooler                  85 -0.1584524528596514E+05 {~~}
START M     exhaustcooler                  86 -0.8026077146914962E+00 {~~}
START P                              86 0.1008000000000002E+01 {~~}
START H     exhaustcooler                  86 -0.1563608779686839E+05 {~~}
START Q     exhaustcooler                 319  0.0000000000000000E+00 {~~}
START ZA    exhaustcooler                   1  0.1678714143345494E+03 {~~}
C ~~~~~~~~~~~~~~~~~~~~~~~~~~~~~~~~~~~~~~~~~~~~~~~~~~~~~~~~~~~~~~~~~~~~~~~~~~~~~~~~~~~~~~~~~~~~~~~~~~~
C ~~ End of generated initial guesses.
C ~~~~~~~~~~~~~~~~~~~~~~~~~~~~~~~~~~~~~~~~~~~~~~~~~~~~~~~~~~~~~~~~~~~~~~~~~~~~~~~~~~~~~~~~~~~~~~~~~~~
```

end

Biomass gasification (Viking) + SOFC

RUN NUMBER 1

ALGEBRAIC VARIABLES

NO DE	TO COMPONENT	MEDIA	M [kg/s]	T [C]	P [bar]	H [kJ/kg]	ENERGY [kJ/s]	X	S [kJ/kg K]	V [m3/kg]	U [kJ/kg]
1	Dryer	Wood	0.04	15.00	-	-8621.6	4.991E+02	-	0.4612	-	-8621.6
64	Dryer	STEAM-HF	0.20	250.00	0.998	-12996.5		-	11.5514	2.4110	-13237.2
2	Dryer	DryWood	-0.03	150.00	-	-5497.1		-	1.7075	-	-5497.1
61	Dryer	STEAM-HF	-0.21	150.00	0.993	-13194.4		-	11.1339	1.9505	-13388.1
301	Dryer	HEAT					0.000E+00				
2	Gasifier	DryWood	0.03	150.00	-	-5497.1		-	1.7075	-	-5497.1
26	Gasifier	STEAM-HF	0.00	150.00	1.003	-13194.5		-	11.1292	1.9309	-13388.2
74	Gasifier	humid_air	0.05	564.13	1.003	-2398.8		-	9.1937	2.7302	-2672.7
3	Gasifier	raw_PG	-0.09	800.00	0.998	-3507.9		-	10.8590	4.1308	-3920.1
99	Gasifier	Ash	0.00	800.00	-	-4308.0		-	0.0000	-	-4308.0
302	Gasifier	HEAT					0.000E+00				
3	airpreheat	raw_PG	0.09	800.00	0.998	-3507.9		-	10.8590	4.1308	-3920.1
4	airpreheat	raw_PG	-0.09	552.33	0.993	-3918.6		-	10.4262	3.1935	-4235.7
72	airpreheat	STANDARD_AIR	0.04	15.00	1.008	-98.8		-	6.8668	0.8237	-181.9
73	airpreheat	STANDARD_AIR	-0.04	780.00	1.003	724.5		-	8.2418	3.0255	421.1
303	airpreheat	HEAT					0.000E+00				
4	steamheater	raw_PG	0.09	552.33	0.993	-3918.6		-	10.4262	3.1935	-4235.7
5	steamheater	raw_PG	-0.09	259.48	0.988	-4375.3		-	9.7468	2.0710	-4579.9
63	steamheater	STEAM-HF	0.20	151.68	1.003	-13191.2		-	11.1370	1.9388	-13385.6
64	steamheater	STEAM-HF	-0.20	250.00	0.998	-12996.5		-	11.5514	2.4110	-13237.2
304	steamheater	HEAT					0.000E+00				
61	steamblower	STEAM-HF	0.21	150.00	0.993	-13194.4		-	11.1339	1.9505	-13388.1
62	steamblower	STEAM-HF	-0.21	151.68	1.003	-13191.2		-	11.1370	1.9388	-13385.6
305	steamblower	HEAT					-1.409E-02				
105	steamblower	MECH_POWER					7.044E-01				
62	split1	STEAM-HF	0.21	151.68	1.003	-13191.2		-	11.1370	1.9388	-13385.6
63	split1	STEAM-HF	-0.20	151.68	1.003	-13191.2		-	11.1370	1.9388	-13385.6
69	split1	STEAM-HF	-0.01	151.68	1.003	-13191.2		-	11.1370	1.9388	-13385.6
73	mix1	STANDARD_AIR	0.04	780.00	1.003	724.5		-	8.2418	3.0255	421.1
69	mix1	STEAM-HF	0.01	151.68	1.003	-13191.2		-	11.1370	1.9388	-13385.6
74	mix1	humid_air	-0.05	564.13	1.003	-2398.8		-	9.1937	2.7302	-2672.7
5	gascooler	raw_PG	0.09	259.48	0.988	-4375.3		-	9.7468	2.0710	-4579.9
6	gascooler	cold_PG	-0.09	90.00	0.983	-4624.6		-	9.1860	1.4192	-4764.1
98	gascooler	STEAM-HF	0.00	90.00	0.983	-15594.1		-	4.7085	0.0010	-15594.2
81	gascooler	STEAM-HF	0.10	30.02	1.013	-15845.2		-	3.9530	0.0010	-15845.3
82	gascooler	STEAM-HF	-0.10	80.00	1.008	-15636.1		-	4.5912	0.0010	-15636.2
306	gascooler	HEAT					0.000E+00				
6	gasclean	cold_PG	0.09	90.00	0.983	-4624.6		-	9.1860	1.4192	-4764.1
7	gasclean	clean_PG	-0.09	90.00	0.978	-4624.9		-	9.1879	1.4263	-4764.4
97	gasclean	impurities	0.00	90.00	0.978	-535.6		-	6.2438	0.9059	-624.2
307	gasclean	HEAT					0.000E+00				
7	condenser	clean_PG	0.09	90.00	0.978	-4624.9		-	9.1879	1.4263	-4764.4
8	condenser	dry_PG	-0.08	50.00	0.973	-4466.6		-	8.9598	1.2694	-4590.1
96	condenser	STEAM-HF	0.00	50.01	0.973	-15761.7		-	4.2198	0.0010	-15761.7
83	condenser	STEAM-HF	0.05	30.02	1.013	-15845.2		-	3.9530	0.0010	-15845.3
84	condenser	STEAM-HF	-0.05	80.00	1.008	-15636.1		-	4.5912	0.0010	-15636.2
308	condenser	HEAT					0.000E+00				
8	PGcompressor	dry_PG	0.08	50.00	0.973	-4466.6		-	8.9598	1.2694	-4590.1

9	PGcompressor	dry_PG	-0.08	59.55	1.039	-4453.0		-	8.9761	1.2244	-4580.2
309	PGcompressor	HEAT					-2.299E-02				
117	PGcompressor	MECH_POWER					1.149E+00				
11	PGpreheat	USEDFUEL	0.11	800.00	1.029	-6150.7		-	9.0717	3.1135	-6471.0
12	PGpreheat	USEDFUEL	-0.11	316.78	1.024	-6842.9		-	8.2220	1.7199	-7018.9
9	PGpreheat	dry_PG	0.08	59.55	1.039	-4453.0		-	8.9761	1.2244	-4580.2
10	PGpreheat	dry_PG	-0.08	650.00	1.034	-3551.2		-	10.5180	3.4139	-3904.1
311	PGpreheat	HEAT					0.000E+00				
31	aircompressor	STANDARD_AIR	0.74	15.00	1.013	-98.8		-	6.8653	0.8196	-181.9
32	aircompressor	STANDARD_AIR	-0.74	20.42	1.054	-93.4		-	6.8728	0.8028	-178.0
312	aircompressor	HEAT					-8.313E-02				
117	aircompressor	MECH_POWER					4.157E+00				
35	airpreheat2	USEDAIR	0.72	800.00	1.034	746.3		-	8.2601	3.0019	436.0
36	airpreheat2	USEDAIR	-0.72	224.33	1.024	112.0		-	7.4222	1.4052	-31.8
32	airpreheat2	STANDARD_AIR	0.74	20.42	1.054	-93.4		-	6.8728	0.8028	-178.0
34	airpreheat2	STANDARD_AIR	-0.74	600.00	1.044	519.4		-	8.0168	2.4107	267.8
314	airpreheat2	HEAT					0.000E+00				
10	sofc	dry_PG	0.08	650.00	1.034	-3551.2		-	10.5180	3.4139	-3904.1
34	sofc	STANDARD_AIR	0.74	600.00	1.044	519.4		-	8.0168	2.4107	267.8
11	sofc	USEDFUEL	-0.11	800.00	1.029	-6150.7		-	9.0717	3.1135	-6471.0
35	sofc	USEDAIR	-0.72	800.00	1.034	746.3		-	8.2601	3.0019	436.0
215	sofc	ELECT_POWER					-2.213E+02				
315	sofc	HEAT					0.000E+00				
217	el-motor	ELECT_POWER					5.585E+00				
317	el-motor	HEAT					-2.793E-01				
117	el-motor	MECH_POWER					-5.306E+00				
36	burner	USEDAIR	0.72	224.33	1.024	112.0		-	7.4222	1.4052	-31.8
12	burner	USEDFUEL	0.11	316.78	1.024	-6842.9		-	8.2220	1.7199	-7018.9
41	burner	FLUE_GAS	-0.83	310.20	1.023	-799.3		-	7.7021	1.6487	-968.0
316	burner	HEAT					0.000E+00				
41	exhaustcooler	FLUE_GAS	0.83	310.20	1.023	-799.3		-	7.7021	1.6487	-968.0
44	exhaustcooler	FLUE_GAS	-0.83	120.02	1.013	-1002.2		-	7.2845	1.1222	-1115.9
85	exhaustcooler	STEAM-HF	0.80	30.02	1.013	-15845.2		-	3.9530	0.0010	-15845.3
86	exhaustcooler	STEAM-HF	-0.80	80.00	1.008	-15636.1		-	4.5912	0.0010	-15636.2
319	exhaustcooler	HEAT					0.000E+00				

EXERGY

NO DE	TO COMPONENT	MEDIA	E_PH [kJ/kg]	E_CH [kJ/kg]	E [kJ/kg]	EX_PH [kJ/s]	EX_CH [kJ/s]	EX [kJ/s]
1	Dryer	Wood	0.00	13311.33	13311.33	0.00	572.39	572.39
64	Dryer	STEAM-HF	660.71	-	660.71	132.17	-	132.17
2	Dryer	DryWood	-54.56	18651.57	18597.01	1.67	-572.39	-570.71
61	Dryer	STEAM-HF	583.11	-	583.11	-123.83	-	-123.83
301	Dryer	HEAT	-	-	-	0.00	0.00	0.00
2	Gasifier	DryWood	-54.56	18651.57	18597.01	-1.67	572.39	570.71
26	Gasifier	STEAM-HF	584.41	-	584.41	0.00	-	0.00
74	Gasifier	humid_air	310.33	66.40	376.73	17.02	3.64	20.66
3	Gasifier	raw_PG	644.70	5438.32	6083.02	-54.98	-463.75	-518.73
99	Gasifier	Ash	785.00	-	785.00	-0.21	-	-0.21
302	Gasifier	HEAT	-	-	-	0.00	0.00	0.00
3	airpreheat	raw_PG	644.70	5438.32	6083.02	54.98	463.75	518.73
4	airpreheat	raw_PG	358.65	5438.32	5796.96	-30.58	-463.75	-494.34
72	airpreheat	STANDARD_AIR	0.66	3.73	4.39	0.03	0.16	0.19

73	airpreheat	STANDARD_AIR	427.84	3.73	431.57	-18.20	-0.16	-18.36
303	airpreheat	HEAT	-	-	-	0.00	0.00	0.00
4	steamheater	raw_PG	358.65	5438.32	5796.96	30.58	463.75	494.34
5	steamheater	raw_PG	97.80	5438.32	5536.12	-8.34	-463.75	-472.09
63	steamheater	STEAM-HF	585.47	-	585.47	117.12	-	117.12
64	steamheater	STEAM-HF	660.71	-	660.71	-132.17	-	-132.17
304	steamheater	HEAT	-	-	-	0.00	0.00	0.00
61	steamblower	STEAM-HF	583.11	-	583.11	123.83	-	123.83
62	steamblower	STEAM-HF	585.47	-	585.47	-124.33	-	-124.33
305	steamblower	HEAT	-	-	-	0.00	0.00	0.00
105	steamblower	MECH_POWER	-	-	-	0.70	0.00	0.70
62	split1	STEAM-HF	585.47	-	585.47	124.33	-	124.33
63	split1	STEAM-HF	585.47	-	585.47	-117.12	-	-117.12
69	split1	STEAM-HF	585.47	-	585.47	-7.21	-	-7.21
73	mix1	STANDARD_AIR	427.84	3.73	431.57	18.20	0.16	18.36
69	mix1	STEAM-HF	585.47	-	585.47	7.21	-	7.21
74	mix1	humid_air	310.33	66.40	376.73	-17.02	-3.64	-20.66
5	gascooler	raw_PG	97.80	5438.32	5536.12	8.34	463.75	472.09
6	gascooler	cold_PG	10.04	5438.32	5448.36	-0.86	-463.75	-464.61
98	gascooler	STEAM-HF	34.93	-	34.93	0.00	-	0.00
81	gascooler	STEAM-HF	1.49	-	1.49	0.15	-	0.15
82	gascooler	STEAM-HF	26.73	-	26.73	-2.72	-	-2.72
306	gascooler	HEAT	-	-	-	0.00	0.00	0.00
6	gasclean	cold_PG	10.04	5438.32	5448.36	0.86	463.75	464.61
7	gasclean	clean_PG	9.49	5437.03	5446.52	-0.81	-463.61	-464.42
97	gasclean	impurities	6.93	23829.09	23836.02	0.00	-0.15	-0.15
307	gasclean	HEAT	-	-	-	0.00	0.00	0.00
7	condenser	clean_PG	9.49	5437.03	5446.52	0.81	463.61	464.42
8	condenser	dry_PG	-0.23	5566.16	5565.93	0.02	-463.13	-463.11
96	condenser	STEAM-HF	8.19	-	8.19	-0.02	-	-0.02
83	condenser	STEAM-HF	1.49	-	1.49	0.07	-	0.07
84	condenser	STEAM-HF	26.73	-	26.73	-1.25	-	-1.25
308	condenser	HEAT	-	-	-	0.00	0.00	0.00
8	PGcompressor	dry_PG	-0.23	5566.16	5565.93	-0.02	463.13	463.11
9	PGcompressor	dry_PG	8.60	5566.16	5574.75	-0.72	-463.13	-463.85
309	PGcompressor	HEAT	-	-	-	0.00	0.00	0.00
117	PGcompressor	MECH_POWER	-	-	-	1.15	0.00	1.15
11	PGpreheat	USEDFUEL	570.75	787.09	1357.84	61.88	85.33	147.21
12	PGpreheat	USEDFUEL	123.47	787.09	910.56	-13.39	-85.33	-98.72
9	PGpreheat	dry_PG	8.60	5566.16	5574.75	0.72	463.13	463.85
10	PGpreheat	dry_PG	466.12	5566.16	6032.28	-38.78	-463.13	-501.92
311	PGpreheat	HEAT	-	-	-	0.00	0.00	0.00
31	aircompressor	STANDARD_AIR	1.07	3.73	4.81	0.80	2.78	3.58
32	aircompressor	STANDARD_AIR	4.39	3.73	8.12	-3.27	-2.78	-6.04
312	aircompressor	HEAT	-	-	-	0.00	0.00	0.00
117	aircompressor	MECH_POWER	-	-	-	4.16	0.00	4.16
35	airpreheat2	USEDAIR	448.07	3.78	451.85	322.14	2.72	324.86
36	airpreheat2	USEDAIR	55.27	3.78	59.05	-39.73	-2.72	-42.45
32	airpreheat2	STANDARD_AIR	4.39	3.73	8.12	3.27	2.78	6.04
34	airpreheat2	STANDARD_AIR	287.52	3.73	291.25	-213.96	-2.78	-216.74
314	airpreheat2	HEAT	-	-	-	0.00	0.00	0.00
10	sofc	dry_PG	466.12	5566.16	6032.28	38.78	463.13	501.92
34	sofc	STANDARD_AIR	287.52	3.73	291.25	213.96	2.78	216.74
11	sofc	USEDFUEL	570.75	787.09	1357.84	-61.88	-85.33	-147.21
35	sofc	USEDAIR	448.07	3.78	451.85	-322.14	-2.72	-324.86

215	sofc	ELECT_POWER	-	-	-	-221.33	0.00	-221.33
315	sofc	HEAT	-	-	-	0.00	0.00	0.00
217	el-motor	ELECT_POWER	-	-	-	5.59	0.00	5.59
317	el-motor	HEAT	-	-	-	0.00	0.00	0.00
117	el-motor	MECH_POWER	-	-	-	-5.31	0.00	-5.31
36	burner	USEDAIR	55.27	3.78	59.05	39.73	2.72	42.45
12	burner	USEDFUEL	123.47	787.09	910.56	13.39	85.33	98.72
41	burner	FLUE_GAS	99.77	20.90	120.66	-82.54	-17.29	-99.83
316	burner	HEAT	-	-	-	0.00	0.00	0.00
41	exhaustcooler	FLUE_GAS	99.77	20.90	120.66	82.54	17.29	99.83
44	exhaustcooler	FLUE_GAS	17.18	20.90	38.08	-14.21	-17.29	-31.50
85	exhaustcooler	STEAM-HF	1.49	-	1.49	1.20	-	1.20
86	exhaustcooler	STEAM-HF	26.73	-	26.73	-21.45	-	-21.45
319	exhaustcooler	HEAT	-	-	-	0.00	0.00	0.00

```
ELEC. POWER PRODUCTION  =     221.3328 kW
TOTAL POWER CONSUMPTION =       6.2896 kW
NET POWER PRODUCTION    =     215.0432 kW
FUEL CONSUMPTION (LHV)  =     499.1161 kJ/s
FUEL CONSUMPTION (HHV)  =     572.3872 kJ/s
THERMAL EFFICIENCY (LHV)=       0.4308
THERMAL EFFICIENCY (HHV)=       0.3757

MAXIMUM RELATIVE ERROR = 8.8267E-13
COMPUTER ACCURACY      = 1.0842E-19
```

IDEAL GAS COMPOSITION (MOLAR BASE):

	humid_air	raw_PG	STANDARD_AIR	cold_PG	clean_PG
HYDROGEN	0.0000E+00	0.2538E+00	0.0000E+00	0.2538E+00	0.2538E+00
OXYGEN	0.1418E+00	0.0000E+00	0.2075E+00	0.0000E+00	0.0000E+00
NITROGEN	0.5281E+00	0.2897E+00	0.7729E+00	0.2897E+00	0.2897E+00
CARBON MONOXIDE	0.0000E+00	0.1762E+00	0.0000E+00	0.1762E+00	0.1762E+00
CARBON DIOXIDE	0.2050E-03	0.1144E+00	0.3000E-03	0.1144E+00	0.1144E+00
WATER (I.G.)	0.3236E+00	0.1523E+00	0.1010E-01	0.1523E+00	0.1523E+00
HYDROGEN SULFIDE	0.0000E+00	0.4616E-04	0.0000E+00	0.4616E-04	0.0000E+00
METHANE	0.0000E+00	0.1011E-01	0.0000E+00	0.1011E-01	0.1011E-01
ARGON	0.6286E-02	0.3444E-02	0.9200E-02	0.3444E-02	0.3444E-02
MEAN MOLE MASS	0.2542E+02	0.2164E+02	0.2885E+02	0.2164E+02	0.2164E+02
NET CALORI VALUE	0.0000E+00	0.5516E+04	0.0000E+00	0.5516E+04	0.5515E+04
GRS CALORI VALUE	0.0000E+00	0.1148E+05	0.0000E+00	0.1148E+05	0.1148E+05

IDEAL GAS COMPOSITION (MOLAR BASE):

	impurities	dry_PG	USEDFUEL	USEDAIR	FLUE_GAS
HYDROGEN	0.0000E+00	0.2614E+00	0.3681E-01	0.0000E+00	0.0000E+00
OXYGEN	0.0000E+00	0.0000E+00	0.0000E+00	0.1825E+00	0.1544E+00
NITROGEN	0.0000E+00	0.2983E+00	0.2933E+00	0.7973E+00	0.7325E+00
CARBON MONOXIDE	0.0000E+00	0.1815E+00	0.2593E-01	0.0000E+00	0.0000E+00
CARBON DIOXIDE	0.0000E+00	0.1179E+00	0.2786E+00	0.3095E-03	0.4145E-01
WATER (I.G.)	0.0000E+00	0.1269E+00	0.3654E+00	0.1042E-01	0.6346E-01
HYDROGEN SULFIDE	0.1000E+01	0.0000E+00	0.0000E+00	0.0000E+00	0.0000E+00

```
METHANE          | 0.0000E+00 | 0.1042E-01 | 0.2245E-07 | 0.0000E+00 | 0.0000E+00 |
ARGON            | 0.0000E+00 | 0.3547E-02 | 0.0000E+00 | 0.9490E-02 | 0.8247E-02 |
---------------------------------------------------------------------------------
MEAN  MOLE  MASS| 0.3408E+02 | 0.2175E+02 | 0.2786E+02 | 0.2875E+02 | 0.2876E+02 |
NET CALORI VALUE| 0.1521E+05 | 0.5652E+04 | 0.5829E+03 | 0.0000E+00 | 0.0000E+00 |
GRS CALORI VALUE| 0.1650E+05 | 0.1172E+05 | 0.2279E+04 | 0.0000E+00 | 0.0000E+00 |
---------------------------------------------------------------------------------

NON-IDEAL FLUID AND SOLID COMPOSITION (MASS BASE):

                |Wood        |DryWood     |Ash         |
-------------------------------------------------------
HYDROGEN        | 0.4204E-01 | 0.5890E-01 | 0.0000E+00 |
OXYGEN          | 0.2976E+00 | 0.4171E+00 | 0.0000E+00 |
NITROGEN        | 0.1153E-02 | 0.1615E-02 | 0.0000E+00 |
CARBON (SOLID)  | 0.3309E+00 | 0.4636E+00 | 0.0000E+00 |
SULFUR (SOLID)  | 0.1356E-03 | 0.1900E-03 | 0.0000E+00 |
WATER (LIQUID)  | 0.3220E+00 | 0.5000E-01 | 0.0000E+00 |
ASHES           | 0.6170E-02 | 0.8645E-02 | 0.1000E+01 |
-------------------------------------------------------
MEAN  MOLE  MASS| 0.1321E+02 | 0.1193E+02 | 0.7600E+02 |
NET CALORI VALUE| 0.1161E+05 | 0.1724E+05 | 0.0000E+00 |
GRS CALORI VALUE| 0.1331E+05 | 0.1865E+05 | 0.0000E+00 |
-------------------------------------------------------

MEDIUM  97 : WATER FOR GAS APP
MEDIUM 300 : HEAT
MEDIUM 301 : PRODUCT HEAT


NUMBER OF CLOSED INTERNAL LOOPS IN THE SYSTEM:    0





 SOLUTION FOR THE INDEPENDENT ALGEBRAIC VARIABLES :


 VARIABLE NO | COMPONENT    |    NAME    |    VALUE   |
------------------------------------------------------
       1     |Gasifier      |MULTIPLIER H| 0.8501E+05 |
       2     |Gasifier      |MULTIPLIER C| 0.4364E+05 |
       3     |Gasifier      |MULTIPLIER N| 0.1173E+06 |
       4     |Gasifier      |MULTIPLIER O| 0.3125E+06 |
       5     |Gasifier      |MULTIPLIER S| 0.1828E+06 |
       6     |Gasifier      |MULTIPL Ar  | 0.2292E+06 |
       7     |Gasifier      |GIBBS ENERGY| -.3280E+06 |
       1     |airpreheat    |Transferred | 0.3503E+02 |
       1     |steamheater   |Transferred | 0.3894E+02 |
       1     |PGpreheat     |Transferred | 0.7504E+02 |
       1     |airpreheat2   |Transferred | 0.4560E+03 |
       1     |sofc          |MULTIPLIER H| 0.9349E+05 |
       2     |sofc          |MULTIPLIER C| 0.8550E+05 |
       3     |sofc          |MULTIPLIER N| 0.1171E+06 |
       4     |sofc          |MULTIPLIER O| 0.2875E+06 |
       5     |sofc          |GIBBS ENERGY| -.4426E+06 |
       6     |sofc          |ETAMAX      | 0.6891E+00 |
       7     |sofc          |ETASYS      | 0.8459E+00 |
       8     |sofc          |UF          | 0.8500E+00 |
       9     |sofc          |ETATOT      | 0.4954E+00 |
```

```
       10     |sofc          |STCR         | 0.4098E+00 |
       11     |sofc          |E_nernst     | 0.9450E+00 |
       12     |sofc          |V_act        | 0.1081E+00 |
       13     |sofc          |V_ohm        | 0.7147E-02 |
       14     |sofc          |V_conc       | 0.3043E-01 |
       15     |sofc          |V_cell       | 0.7993E+00 |
       16     |sofc          |GMAX         | -.8471E+05 |
       17     |sofc          |G(T)         | -.1885E+06 |
       18     |sofc          |G(p,T)       | -.1824E+06 |
       19     |sofc          |p_H2eq       | 0.2822E+00 |
       20     |sofc          |R_e          | 0.2336E-01 |
       21     |sofc          |Area [cm^2]  | 0.1013E+04 |
       22     |sofc          |i_load       | 0.3000E+03 |
       23     |sofc          |eta_DCAC     | 0.9500E+00 |
        1     |burner        |Lambda       | 0.3738E+02 |
        1     |exhaustcooler |Transferred  | 0.1679E+03 |
-------------------------------------------------------

========================================================================================================================
########################################################################################################################
```

Appendix E SOFC-MGT PLANT MODEL LISTING

Included in this Appendix are:

- Flow sheet of SOFC-MGT scenario with node numbers (1 page)
- DNA Input for SOFC-MGT scenario (10 pages)
- DNA Output for SOFC-MGT scenario (7 pages)

The input and output data only represent one simulation using the reference conditions.

Flow sheet of SOFC-MGT scenario with node numbers

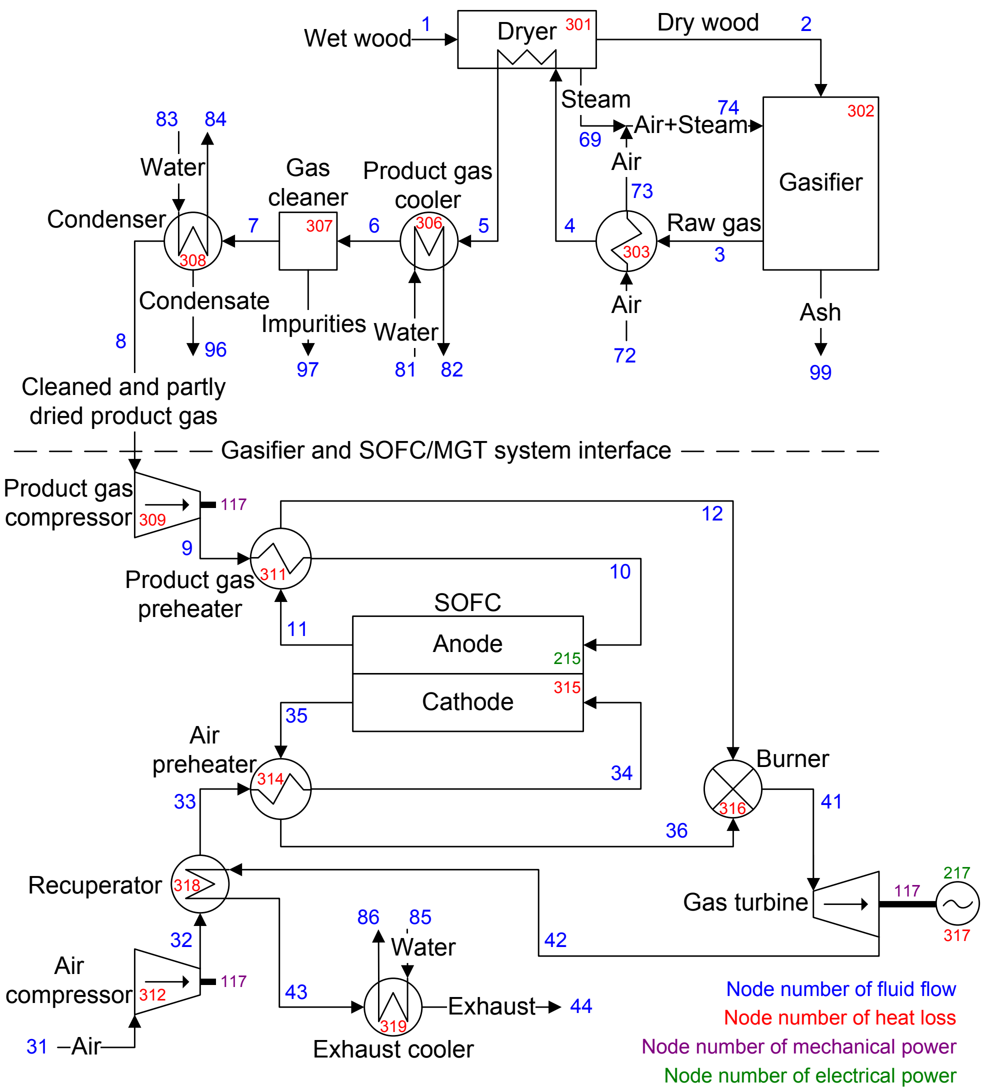

```
title Biomass gasification (Viking) + SOFC/MGT incl. recuperation
C Wood is dried and gasified. The gasification is atmospheric,
C based on air, and almost reaches equilibrium. The produced
C product gas (PG) composition and the cold gas efficiency is
C similar to that from the Viking gasifier.
C Power and heat production by a hybrid SOFC/MGT system.


C ###################################################
C ###################################################
C ###################################################
C -----------------GASIFIER PART---------------------
C ###################################################
C ###################################################
C ###################################################

C ##Media##
media 1 Wood 2 DryWood
media 73 STANDARD_AIR 3 raw_PG 99 Ash

C ##Fuel composition##
solid Wood C 0.488 H .062 O .439 S .0002 N 0.0017 ASH .0091
+ LHV 18280 CP 1.35 MOI .322
C [Ahrenfeldt, J. et al., Energy & Fuels 2006, 20, 2672-2680] without Cl.



C ###################################################
C -----------------------DRYER-----------------------
C ###################################################
struc Dryer DRYER_03 1 64 2 61 301  0.05 0.005

C Fuel input (plant size):
addco m Dryer 1 0.043

addco t Dryer 1 15 p 1 1.013
addco p 2 1.008 t Dryer 2 150
addco q Dryer 301 0



C ###################################################
C ---------------------GASIFIER----------------------
C ###################################################
struc Gasifier GASIFI_3 8  2 26 74 3 99 302  1 3 4 6 7 9 11 36 /
 0.998 800 0.005 0 1.0 0.01
C Variable constitution parameter: Number of calculated gas components 8
C Nodes: Inlet fuel 2; inlet water 26; inlet air 74; outlet PG 3,
C        outlet ash 99, heat loss 302
C Integer Parameters: Calculated gas compounds H2 (1), N2 (3), CO (4),
C                      CO2 (6), H2O (7), H2S (9), CH4 (11), Ar (36)
C Real parameter: Pressure 1 bar, Eq. temperature 800 degC, Pressure loss 0,
C                 Water-to-fuel ratio 0, carbon conversion factor 1,
C                 non-equilibrium methane 0.01.

addco t Gasifier 3 800
addco t Gasifier 26 150
addco p 99 1.013
addco q Gasifier 302 0



C ###################################################
C -------------GASIFIER AIR PREHEATER----------------
C ###################################################
struc airpreheat heatex_2 3 4 72 73 303 20 0.005 0.005
addco t airpreheat 72 15
addco q airpreheat 303 0



C ###################################################
C ------------------STEAM HEATER---------------------
C ###################################################
struc steamheater heatex_1 4 5 63 64 304 0.005 0.005
```

```
media 63 STEAM-HF

addco t steamheater 64 250
addco q steamheater 304 0



C ###################################################
C ------------------STEAM BLOWER---------------------
C ###################################################
struc steamblower COMPRE_1 61 62 305 105 0.6 0.98



C ###################################################
C --------------------SPLITTER-----------------------
C ###################################################
struc split1 SPLITTER 62 63 69



C ###################################################
C ----------------------MIXER------------------------
C ###################################################
struc mix1 MIXER_02 73 69 74

media 74 humid_air



C ###################################################
C --------------------GAS COOLER---------------------
C ###################################################
struc gascooler GASCOOL1 5 6 98 81 82 306 0.005 0.005

media 81 STEAM-HF 6 cold_PG

addco t gascooler 6 90
addco t gascooler 81 30 p 81 1.013
addco t gascooler 82 80
addco q gascooler 306 0



C ###################################################
C -------------------GAS CLEANING--------------------
C ###################################################
struc gasclean GASCLE_1 6 7 97 307 0.0049
C Pressure loss is taken from paper about Viking

media 7 clean_PG 97 impurities

addco q gasclean 307 0



C ###################################################
C --------------------CONDENSER----------------------
C ###################################################
struc condenser GASCOOL1 7 8 96 83 84 308 0.005 0.005

media 83 STEAM-HF 8 dry_PG

addco t condenser 8 50
addco t condenser 83 30 p 83 1.013
addco t condenser 84 80
addco q condenser 308 0



C ###################################################
C ###################################################
C ###################################################
C -----------------SOFC/MGT PART---------------------
C ###################################################
C ###################################################
```

```
C ###################################################

media 11 USEDFUEL 35 USEDAIR


C ###################################################
C ------------PRODUCT GAS COMPRESSOR---------------
C ###################################################
struc PGcompressor compre_1 8 9 309 117 0.75 0.98
C Isentropic efficiency from L. Fryda et al. (2008)


C ###################################################
C ------------PRODUCT GAS PREHEATING---------------
C ###################################################
struc PGpreheat heatex_2 11 12 9 10 311 150 0.005 0.005
addco q PGpreheat 311 0


C ###################################################
C ----------------AIR COMPRESSOR-------------------
C ###################################################
struc aircompressor compre_1 31 32 312 117 0.75 0.98
C Isentropic efficiency from L. Fryda et al. (2008)

media 31 STANDARD_AIR

addco p 31 1.013 t aircompressor 31 15


C ###################################################
C ------------------RECUPERATOR--------------------
C ###################################################
struc recuperator heatex_4 42 43 32 33 318 0.85 0.01 0.01
addco q recuperator 318 0


C ###################################################
C -------------SOFC AIR PREHEATING-----------------
C ###################################################
struc airpreheat2 heatex_2 35 36 33 34 314 200 0.01 0.01
addco q airpreheat2 314 0


C ###################################################
C ---------------------SOFC------------------------
C ###################################################
struc sofc sofceq0d_CBM /
    {fuel and air inlets} 10 34 /
    {fuel and air outlets} 11 35  /
    {nodes for power and heat loss} 215 315 /
    {parameters: utilization, temperature} 0.85 800 /
    {pressure loss} 0.005 0.010 /
    {temperature difference between anode and cathode outlet} 0 /
    {current density [mA/cm^2]} 300 /
    {DC to AC conversion efficiency [-]} 0.95

addco q sofc 315 0

C SOFC OPERATING PRESSURE:
addco p 10 2.5


C ###################################################
C --------------------BURNER-----------------------
C ###################################################
struc burner GASBUR_3 36 12 41 316 0.999374

media 41 FLUE_GAS
```

```
addco q burner 316 0


C ####################################################
C -------------------GAS TURBINE---------------------
C ####################################################
struc GT turbin_1 41 42 117 0.84
C Isentropic efficiency from L. Fryda et al. (2008)



C ####################################################
C --------------------GENERATOR---------------------
C ####################################################
struc generator sim_gene 217 317 117 0.95



C ####################################################
C -----------------EXHAUST COOLING------------------
C ####################################################
struc exhaustcooler heatex_2 43 44 85 86 319 90 0.010 0.005

media 85 STEAM-HF

addco p 44 1.013
addco p 85 1.013 t exhaustcooler 85 30
addco t exhaustcooler 86 80
addco q exhaustcooler 319 0



C Reference conditions for exergy
xergy p 1 t 15





C ~~~~~~~~~~~~~~~~~~~~~~~~~~~~~~~~~~~~~~~~~~~~~~~~~~~~~~~~~~~~~~~~~~~~~~~~~~~~~~~~~~~~~~~~~~~~~~~
~~~~~
C ~~ Start of list of generated initial guesses.
C ~~ The values are the results of the latest simulation.
C ~~~~~~~~~~~~~~~~~~~~~~~~~~~~~~~~~~~~~~~~~~~~~~~~~~~~~~~~~~~~~~~~~~~~~~~~~~~~~~~~~~~~~~~~~~~~~~~
~~~~~
START M     Dryer                      1   0.43000000000000013E-01 {~~}
START P                           1  0.10130000000000003E+01 {~~}
START H     Dryer                      1  -0.86216187555295 60E+04 {~~}
START M     Dryer                     64   0.20004590306570 81E+00 {~~}
START P                          64  0.99800000000000029E+00 {~~}
START H     Dryer                     64  -0.12996535513797 76E+05 {~~}
START M     Dryer                      2  -0.30688421052631 66E-01 {~~}
START P                           2  0.10080000000000003E+01 {~~}
START H     Dryer                      2  -0.54970592202110 16E+04 {~~}
START M     Dryer                     61  -0.21235748201307 65E+00 {~~}
START P                          61  0.99300000000000029E+00 {~~}
START H     Dryer                     61  -0.13194436078298 23E+05 {~~}
START Q     Dryer                    301   0.00000000000000000E+00 {~~}
START X_J   DryWood                   H2          0.58900000000000016E-01 {~~}
START X_J   DryWood                   O2          0.41705000000000013E+00 {~~}
START X_J   DryWood                   N2          0.16150000000000005E-02 {~~}
START X_J   DryWood                   CO          0.00000000000000000E+00 {~~}
START X_J   DryWood                   NO          0.00000000000000000E+00 {~~}
START X_J   DryWood                   CO2         0.00000000000000000E+00 {~~}
START X_J   DryWood                   H2O-L       0.50000000000000014E-01 {~~}
START X_J   DryWood                   NH3         0.00000000000000000E+00 {~~}
START X_J   DryWood                   H2S         0.00000000000000000E+00 {~~}
START X_J   DryWood                   SO2         0.00000000000000000E+00 {~~}
START X_J   DryWood                   CH4         0.00000000000000000E+00 {~~}
START X_J   DryWood                   C2H6        0.00000000000000000E+00 {~~}
START X_J   DryWood                   C3H8        0.00000000000000000E+00 {~~}
START X_J   DryWood                   C4H10-N     0.00000000000000000E+00 {~~}
START X_J   DryWood                   C4H10-I     0.00000000000000000E+00 {~~}
START X_J   DryWood                   C5H12       0.00000000000000000E+00 {~~}
```

```
START X_J   DryWood                     C6H14       0.0000000000000000E+00 {~~}
START X_J   DryWood                     C7H16       0.0000000000000000E+00 {~~}
START X_J   DryWood                     C8H18       0.0000000000000000E+00 {~~}
START X_J   DryWood                     C2H4        0.0000000000000000E+00 {~~}
START X_J   DryWood                     C3H6        0.0000000000000000E+00 {~~}
START X_J   DryWood                     C5H10       0.0000000000000000E+00 {~~}
START X_J   DryWood                     C6H12-1     0.0000000000000000E+00 {~~}
START X_J   DryWood                     C7H14       0.0000000000000000E+00 {~~}
START X_J   DryWood                     C2H2        0.0000000000000000E+00 {~~}
START X_J   DryWood                     C6H6        0.0000000000000000E+00 {~~}
START X_J   DryWood                     C6H12-C     0.0000000000000000E+00 {~~}
START X_J   DryWood                     C           0.4636000000000013E+00 {~~}
START X_J   DryWood                     S           0.1900000000000006E-03 {~~}
START X_J   DryWood                     NO2         0.0000000000000000E+00 {~~}
START X_J   DryWood                     HCN         0.0000000000000000E+00 {~~}
START X_J   DryWood                     COS         0.0000000000000000E+00 {~~}
START X_J   DryWood                     N2O         0.0000000000000000E+00 {~~}
START X_J   DryWood                     NO3         0.0000000000000000E+00 {~~}
START X_J   DryWood                     SO3         0.0000000000000000E+00 {~~}
START X_J   DryWood                     AR          0.0000000000000000E+00 {~~}
START X_J   DryWood                     ASH         0.8645000000000028E-02 {~~}
START X_J   DryWood                     TAR         0.0000000000000000E+00 {~~}
START M     Gasifier                      2   0.3068842105263166E-01 {~~}
START H     Gasifier                      2  -0.5497059220211016E+04 {~~}
START M     Gasifier                     26   0.0000000000000000E+00 {~~}
START P                              26  0.1003000000000003E+01 {~~}
START H     Gasifier                     26  -0.1319450918722709E+05 {~~}
START M     Gasifier                     74   0.5485206982616307E-01 {~~}
START P                              74  0.1003000000000003E+01 {~~}
START H     Gasifier                     74  -0.2398848478333941E+04 {~~}
START M     Gasifier                      3  -0.8527518947879474E-01 {~~}
START P                               3  0.9980000000000029E+00 {~~}
START H     Gasifier                      3  -0.3507877913073774E+04 {~~}
START M     Gasifier                     99  -0.2653014000000009E-03 {~~}
START P                              99  0.1013000000000003E+01 {~~}
START H     Gasifier                     99  -0.4308000000000012E+04 {~~}
START Q     Gasifier                    302   0.0000000000000000E+00 {~~}
START ZA    Gasifier                      1   0.8500945239865266E+05 {~~}
START ZA    Gasifier                      2   0.4363965291425185E+05 {~~}
START ZA    Gasifier                      3   0.1172765217993689E+06 {~~}
START ZA    Gasifier                      4   0.3124902840469581E+06 {~~}
START ZA    Gasifier                      5   0.1827651987487794E+06 {~~}
START ZA    Gasifier                      6   0.2292482774424778E+06 {~~}
START ZA    Gasifier                      7  -0.3279719879436743E+06 {~~}
START Y_J   raw_PG                      H2          0.2538114658675982E+00 {~~}
START Y_J   raw_PG                      O2          0.0000000000000000E+00 {~~}
START Y_J   raw_PG                      N2          0.2896541868376543E+00 {~~}
START Y_J   raw_PG                      CO          0.1761818347160904E+00 {~~}
START Y_J   raw_PG                      NO          0.0000000000000000E+00 {~~}
START Y_J   raw_PG                      CO2         0.1144395150133747E+00 {~~}
START Y_J   raw_PG                      H2O-G       0.1523098114753788E+00 {~~}
START Y_J   raw_PG                      NH3         0.0000000000000000E+00 {~~}
START Y_J   raw_PG                      H2S         0.4615796164902317E-04 {~~}
START Y_J   raw_PG                      SO2         0.0000000000000000E+00 {~~}
START Y_J   raw_PG                      CH4         0.1011293223314741E-01 {~~}
START Y_J   raw_PG                      NO2         0.0000000000000000E+00 {~~}
START Y_J   raw_PG                      HCN         0.0000000000000000E+00 {~~}
START Y_J   raw_PG                      COS         0.0000000000000000E+00 {~~}
START Y_J   raw_PG                      AR          0.3444095895110012E-02 {~~}
START X_J   Ash                         C           0.0000000000000000E+00 {~~}
START X_J   Ash                         ASH         0.1000000000000003E+01 {~~}
START M     airpreheat                    3   0.8527518947879474E-01 {~~}
START H     airpreheat                    3  -0.3507877913073774E+04 {~~}
START M     airpreheat                    4  -0.8527518947879474E-01 {~~}
START P                               4  0.9930000000000029E+00 {~~}
START H     airpreheat                    4  -0.3918630307677507E+04 {~~}
START M     airpreheat                   72   0.4254049087879462E-01 {~~}
START P                              72  0.1008000000000003E+01 {~~}
START H     airpreheat                   72  -0.9883454496688256E+02 {~~}
START M     airpreheat                   73  -0.4254049087879462E-01 {~~}
START P                              73  0.1003000000000003E+01 {~~}
START H     airpreheat                   73   0.7245454291500146E+03 {~~}
START Q     airpreheat                  303   0.0000000000000000E+00 {~~}
START ZA    airpreheat                    1   0.3502698827870191E+02 {~~}
START M     steamheater                   4   0.8527518947879474E-01 {~~}
START H     steamheater                   4  -0.3918630307677508E+04 {~~}
```

```
START M     steamheater                  5 -0.8527518947879474E-01 {~~}
START P                           5  0.9880000000000029E+00 {~~}
START H     steamheater                  5 -0.4375257198957320E+04 {~~}
START M     steamheater                 63  0.2000459030657081E+00 {~~}
START P                          63  0.1003000000000003E+01 {~~}
START H     steamheater                 63 -0.1319118556200299E+05 {~~}
START M     steamheater                 64 -0.2000459030657081E+00 {~~}
START H     steamheater                 64 -0.1299653551379776E+05 {~~}
START Q     steamheater                304  0.0000000000000000E+00 {~~}
START ZA    steamheater                  1  0.3893894467499886E+02 {~~}
START M     steamblower                 61  0.2123574820130765E+00 {~~}
START H     steamblower                 61 -0.1319443607829823E+05 {~~}
START M     steamblower                 62 -0.2123574820130765E+00 {~~}
START P                          62  0.1003000000000003E+01 {~~}
START H     steamblower                 62 -0.1319118556200299E+05 {~~}
START Q     steamblower                305 -0.1408717256529157E-01 {~~}
START W     steamblower                105  0.7043586282645840E+00 {~~}
START M     split1                      62  0.2123574820130765E+00 {~~}
START H     split1                      62 -0.1319118556200299E+05 {~~}
START M     split1                      63 -0.2000459030657081E+00 {~~}
START H     split1                      63 -0.1319118556200299E+05 {~~}
START M     split1                      69 -0.1231157894736845E-01 {~~}
START P                          69  0.1003000000000003E+01 {~~}
START H     split1                      69 -0.1319118556200299E+05 {~~}
START M     mix1                        73  0.4254049087879462E-01 {~~}
START H     mix1                        73  0.7245454291500146E+03 {~~}
START M     mix1                        69  0.1231157894736845E-01 {~~}
START H     mix1                        69 -0.1319118556200300E+05 {~~}
START M     mix1                        74 -0.5485206982616307E-01 {~~}
START H     mix1                        74 -0.2398848478333941E+04 {~~}
START Y_J   humid_air           H2            0.0000000000000000E+00 {~~}
START Y_J   humid_air           O2            0.1417803964772678E+00 {~~}
START Y_J   humid_air           N2            0.5281063539146039E+00 {~~}
START Y_J   humid_air           CO            0.0000000000000000E+00 {~~}
START Y_J   humid_air           NO            0.0000000000000000E+00 {~~}
START Y_J   humid_air           CO2           0.2049837057502668E-03 {~~}
START Y_J   humid_air           H2O-G         0.3236220989260391E+00 {~~}
START Y_J   humid_air           NH3           0.0000000000000000E+00 {~~}
START Y_J   humid_air           H2S           0.0000000000000000E+00 {~~}
START Y_J   humid_air           SO2           0.0000000000000000E+00 {~~}
START Y_J   humid_air           CH4           0.0000000000000000E+00 {~~}
START Y_J   humid_air           C2H6          0.0000000000000000E+00 {~~}
START Y_J   humid_air           C3H8          0.0000000000000000E+00 {~~}
START Y_J   humid_air           C4H10-N       0.0000000000000000E+00 {~~}
START Y_J   humid_air           C4H10-I       0.0000000000000000E+00 {~~}
START Y_J   humid_air           C5H12         0.0000000000000000E+00 {~~}
START Y_J   humid_air           C6H14         0.0000000000000000E+00 {~~}
START Y_J   humid_air           C7H16         0.0000000000000000E+00 {~~}
START Y_J   humid_air           C8H18         0.0000000000000000E+00 {~~}
START Y_J   humid_air           C2H4          0.0000000000000000E+00 {~~}
START Y_J   humid_air           C3H6          0.0000000000000000E+00 {~~}
START Y_J   humid_air           C5H10         0.0000000000000000E+00 {~~}
START Y_J   humid_air           C6H12-1       0.0000000000000000E+00 {~~}
START Y_J   humid_air           C7H14         0.0000000000000000E+00 {~~}
START Y_J   humid_air           C2H2          0.0000000000000000E+00 {~~}
START Y_J   humid_air           C6H6          0.0000000000000000E+00 {~~}
START Y_J   humid_air           C6H12-C       0.0000000000000000E+00 {~~}
START Y_J   humid_air           C             0.0000000000000000E+00 {~~}
START Y_J   humid_air           S             0.0000000000000000E+00 {~~}
START Y_J   humid_air           NO2           0.0000000000000000E+00 {~~}
START Y_J   humid_air           HCN           0.0000000000000000E+00 {~~}
START Y_J   humid_air           COS           0.0000000000000000E+00 {~~}
START Y_J   humid_air           N2O           0.0000000000000000E+00 {~~}
START Y_J   humid_air           NO3           0.0000000000000000E+00 {~~}
START Y_J   humid_air           SO3           0.0000000000000000E+00 {~~}
START Y_J   humid_air           AR            0.6286166976341515E-02 {~~}
START Y_J   humid_air           ASH           0.0000000000000000E+00 {~~}
START Y_J   humid_air           TAR           0.0000000000000000E+00 {~~}
START Y_J   humid_air           CH3OH         0.0000000000000000E+00 {~~}
START M     gascooler                    5  0.8527518947879474E-01 {~~}
START H     gascooler                    5 -0.4375257198957320E+04 {~~}
START M     gascooler                    6 -0.8527518947879474E-01 {~~}
START P                           6  0.9830000000000029E+00 {~~}
START H     gascooler                    6 -0.4624611248324044E+04 {~~}
START M     gascooler                   98  0.0000000000000000E+00 {~~}
START P                          98  0.9830000000000029E+00 {~~}
```

```
START H     gascooler                          98 -0.1559408877861429E+05 {~~}
START M     gascooler                          81  0.1016636501943121E+00 {~~}
START P                                   81  0.1013000000000003E+01 {~~}
START H     gascooler                          81 -0.1584524528596515E+05 {~~}
START M     gascooler                          82 -0.1016636501943121E+00 {~~}
START P                                   82  0.1008000000000003E+01 {~~}
START H     gascooler                          82 -0.1563608779686840E+05 {~~}
START Q     gascooler                         306  0.0000000000000000E+00 {~~}
START Y_J   cold_PG                       H2           0.2538114658675977E+00 {~~}
START Y_J   cold_PG                       O2           0.0000000000000000E+00 {~~}
START Y_J   cold_PG                       N2           0.2896541868376540E+00 {~~}
START Y_J   cold_PG                       CO           0.1761818347160901E+00 {~~}
START Y_J   cold_PG                       NO           0.0000000000000000E+00 {~~}
START Y_J   cold_PG                       CO2          0.1144395150133745E+00 {~~}
START Y_J   cold_PG                       H2O-G        0.1523098114753788E+00 {~~}
START Y_J   cold_PG                       NH3          0.0000000000000000E+00 {~~}
START Y_J   cold_PG                       H2S          0.4615796164902310E-04 {~~}
START Y_J   cold_PG                       SO2          0.0000000000000000E+00 {~~}
START Y_J   cold_PG                       CH4          0.1011293223314739E-01 {~~}
START Y_J   cold_PG                       C2H6         0.0000000000000000E+00 {~~}
START Y_J   cold_PG                       C3H8         0.0000000000000000E+00 {~~}
START Y_J   cold_PG                       C4H10-N      0.0000000000000000E+00 {~~}
START Y_J   cold_PG                       C4H10-I      0.0000000000000000E+00 {~~}
START Y_J   cold_PG                       C5H12        0.0000000000000000E+00 {~~}
START Y_J   cold_PG                       C6H14        0.0000000000000000E+00 {~~}
START Y_J   cold_PG                       C7H16        0.0000000000000000E+00 {~~}
START Y_J   cold_PG                       C8H18        0.0000000000000000E+00 {~~}
START Y_J   cold_PG                       C2H4         0.0000000000000000E+00 {~~}
START Y_J   cold_PG                       C3H6         0.0000000000000000E+00 {~~}
START Y_J   cold_PG                       C5H10        0.0000000000000000E+00 {~~}
START Y_J   cold_PG                       C6H12-1      0.0000000000000000E+00 {~~}
START Y_J   cold_PG                       C7H14        0.0000000000000000E+00 {~~}
START Y_J   cold_PG                       C2H2         0.0000000000000000E+00 {~~}
START Y_J   cold_PG                       C6H6         0.0000000000000000E+00 {~~}
START Y_J   cold_PG                       C6H12-C      0.0000000000000000E+00 {~~}
START Y_J   cold_PG                       C            0.0000000000000000E+00 {~~}
START Y_J   cold_PG                       S            0.0000000000000000E+00 {~~}
START Y_J   cold_PG                       NO2          0.0000000000000000E+00 {~~}
START Y_J   cold_PG                       HCN          0.0000000000000000E+00 {~~}
START Y_J   cold_PG                       COS          0.0000000000000000E+00 {~~}
START Y_J   cold_PG                       N2O          0.0000000000000000E+00 {~~}
START Y_J   cold_PG                       NO3          0.0000000000000000E+00 {~~}
START Y_J   cold_PG                       SO3          0.0000000000000000E+00 {~~}
START Y_J   cold_PG                       AR           0.3444095895110008E-02 {~~}
START M     gasclean                            6  0.8527518947879474E-01 {~~}
START H     gasclean                            6 -0.4624611248324044E+04 {~~}
START M     gasclean                            7 -0.8526899202586896E-01 {~~}
START P                                    7  0.9781000000000029E+00 {~~}
START H     gasclean                            7 -0.4624908439609428E+04 {~~}
START M     gasclean                           97 -0.6197452925764212E-05 {~~}
START P                                   97  0.9781000000000029E+00 {~~}
START H     gasclean                           97 -0.5356408846834941E+03 {~~}
START Q     gasclean                          307  0.0000000000000000E+00 {~~}
START Y_J   clean_PG                      H2           0.2538231818282905E+00 {~~}
START Y_J   clean_PG                      O2           0.0000000000000000E+00 {~~}
START Y_J   clean_PG                      N2           0.2896675573016552E+00 {~~}
START Y_J   clean_PG                      CO           0.1761899672858432E+00 {~~}
START Y_J   clean_PG                      NO           0.0000000000000000E+00 {~~}
START Y_J   clean_PG                      CO2          0.1144447975519510E+00 {~~}
START Y_J   clean_PG                      H2O-G        0.1523168421103356E+00 {~~}
START Y_J   clean_PG                      CH4          0.1011339904703276E-01 {~~}
START Y_J   clean_PG                      NO2          0.0000000000000000E+00 {~~}
START Y_J   clean_PG                      AR           0.3444254874894436E-02 {~~}
START Y_J   impurities                        H2O-G        0.0000000000000000E+00 {~~}
START Y_J   impurities                        NH3          0.0000000000000000E+00 {~~}
START Y_J   impurities                        H2S          0.1000000000000003E+01 {~~}
START Y_J   impurities                        SO2          0.0000000000000000E+00 {~~}
START Y_J   impurities                        HCN          0.0000000000000000E+00 {~~}
START Y_J   impurities                        COS          0.0000000000000000E+00 {~~}
START Y_J   impurities                        AR           0.0000000000000000E+00 {~~}
START Y_J   impurities                        ASH          0.0000000000000000E+00 {~~}
START M     condenser                           7  0.8526899202586896E-01 {~~}
START H     condenser                           7 -0.4624908439609428E+04 {~~}
START M     condenser                           8 -0.8320484335731909E-01 {~~}
START P                                    8  0.9731000000000029E+00 {~~}
START H     condenser                           8 -0.4466561290262767E+04 {~~}
```

```
START M      condenser                    96 -0.2064148668549882E-02 {~~}
START P                              96  0.9731000000000029E+00 {~~}
START H      condenser                    96 -0.1576166949955457E+05 {~~}
START M      condenser                    83  0.4691527326491425E-01 {~~}
START P                              83  0.1013000000000003E+01 {~~}
START H      condenser                    83 -0.1584524528596515E+05 {~~}
START M      condenser                    84 -0.4691527326491425E-01 {~~}
START P                              84  0.1008000000000003E+01 {~~}
START H      condenser                    84 -0.1563608779686840E+05 {~~}
START Q      condenser                   308  0.0000000000000000E+00 {~~}
START Y_J    dry_PG                  H2             0.2614256920940570E+00 {~~}
START Y_J    dry_PG                  O2             0.0000000000000000E+00 {~~}
START Y_J    dry_PG                  N2             0.2983436780648686E+00 {~~}
START Y_J    dry_PG                  CO             0.1814672080223565E+00 {~~}
START Y_J    dry_PG                  NO             0.0000000000000000E+00 {~~}
START Y_J    dry_PG                  CO2            0.1178726473723857E+00 {~~}
START Y_J    dry_PG                  H2O-G          0.1269270417636784E+00 {~~}
START Y_J    dry_PG                  NH3            0.0000000000000000E+00 {~~}
START Y_J    dry_PG                  H2S            0.0000000000000000E+00 {~~}
START Y_J    dry_PG                  SO2            0.0000000000000000E+00 {~~}
START Y_J    dry_PG                  CH4            0.1041631550849636E-01 {~~}
START Y_J    dry_PG                  C2H6           0.0000000000000000E+00 {~~}
START Y_J    dry_PG                  C3H8           0.0000000000000000E+00 {~~}
START Y_J    dry_PG                  C4H10-N        0.0000000000000000E+00 {~~}
START Y_J    dry_PG                  C4H10-I        0.0000000000000000E+00 {~~}
START Y_J    dry_PG                  C5H12          0.0000000000000000E+00 {~~}
START Y_J    dry_PG                  C6H14          0.0000000000000000E+00 {~~}
START Y_J    dry_PG                  C7H16          0.0000000000000000E+00 {~~}
START Y_J    dry_PG                  C8H18          0.0000000000000000E+00 {~~}
START Y_J    dry_PG                  C2H4           0.0000000000000000E+00 {~~}
START Y_J    dry_PG                  C3H6           0.0000000000000000E+00 {~~}
START Y_J    dry_PG                  C5H10          0.0000000000000000E+00 {~~}
START Y_J    dry_PG                  C6H12-1        0.0000000000000000E+00 {~~}
START Y_J    dry_PG                  C7H14          0.0000000000000000E+00 {~~}
START Y_J    dry_PG                  C2H2           0.0000000000000000E+00 {~~}
START Y_J    dry_PG                  C6H6           0.0000000000000000E+00 {~~}
START Y_J    dry_PG                  C6H12-C        0.0000000000000000E+00 {~~}
START Y_J    dry_PG                  C              0.0000000000000000E+00 {~~}
START Y_J    dry_PG                  S              0.0000000000000000E+00 {~~}
START Y_J    dry_PG                  NO2            0.0000000000000000E+00 {~~}
START Y_J    dry_PG                  HCN            0.0000000000000000E+00 {~~}
START Y_J    dry_PG                  COS            0.0000000000000000E+00 {~~}
START Y_J    dry_PG                  N2O            0.0000000000000000E+00 {~~}
START Y_J    dry_PG                  NO3            0.0000000000000000E+00 {~~}
START Y_J    dry_PG                  SO3            0.0000000000000000E+00 {~~}
START Y_J    dry_PG                  AR             0.3547417174159975E-02 {~~}
START M      PGcompressor                8  0.8320484335731909E-01 {~~}
START H      PGcompressor                8 -0.4466561290262767E+04 {~~}
START M      PGcompressor                9 -0.8320484335731909E-01 {~~}
START P                               9  0.2505000000000006E+01 {~~}
START H      PGcompressor                9 -0.4289316158106304E+04 {~~}
START Q      PGcompressor              309 -0.3009725195290968E+00 {~~}
START W      PGcompressor              117  0.1504862597645489E+02 {~~}
START M      PGpreheat                  11  0.1084136464468042E+00 {~~}
START P                              11  0.2495000000000006E+01 {~~}
START H      PGpreheat                  11 -0.6150750931339399E+04 {~~}
START M      PGpreheat                  12 -0.1084136464468042E+00 {~~}
START P                              12  0.2490000000000006E+01 {~~}
START H      PGpreheat                  12 -0.6717227933915665E+04 {~~}
START M      PGpreheat                   9  0.8320484335731909E-01 {~~}
START H      PGpreheat                   9 -0.4289316158106304E+04 {~~}
START M      PGpreheat                  10 -0.8320484335731909E-01 {~~}
START P                              10  0.2500000000000006E+01 {~~}
START H      PGpreheat                  10 -0.3551212040611485E+04 {~~}
START Q      PGpreheat                 311  0.0000000000000000E+00 {~~}
START ZA     PGpreheat                   1  0.6141383747754848E+02 {~~}
START M      aircompressor                31  0.7206544633491334E+00 {~~}
START P                              31  0.1013000000000003E+01 {~~}
START H      aircompressor                31 -0.9883454496688256E+02 {~~}
START M      aircompressor                32 -0.7206544633491334E+00 {~~}
START P                              32  0.2530000000000007E+01 {~~}
START H      aircompressor                32  0.1694338091721306E+02 {~~}
START Q      aircompressor               312 -0.1702773041748533E+01 {~~}
START W      aircompressor               117  0.8513865208742698E+02 {~~}
START M      airpreheat2                  35  0.6954456602596484E+00 {~~}
START P                              35  0.2500000000000006E+01 {~~}
```

```
START H     airpreheat2               35  0.7462281704415040E+03 {~~}
START M     airpreheat2               36 -0.6954456602596484E+00 {~~}
START P                          36  0.2490000000000006E+01 {~~}
START H     airpreheat2               36  0.6125054264003596E+03 {~~}
START M     airpreheat2               33  0.7206544633491334E+00 {~~}
START P                          33  0.2520000000000007E+01 {~~}
START H     airpreheat2               33  0.3903614949152461E+03 {~~}
START M     airpreheat2               34 -0.7206544633491334E+00 {~~}
START P                          34  0.2510000000000007E+01 {~~}
START H     airpreheat2               34  0.5194065598541856E+03 {~~}
START Q     airpreheat2              314  0.0000000000000000E+00 {~~}
START ZA    airpreheat2                1  0.9299690202142516E+02 {~~}
START M     sofc                      10  0.8320484335731909E-01 {~~}
START H     sofc                      10 -0.3551212040611485E+04 {~~}
START M     sofc                      34  0.7206544633491334E+00 {~~}
START H     sofc                      34  0.5194065598541854E+03 {~~}
START M     sofc                      11 -0.1084136464468042E+00 {~~}
START H     sofc                      11 -0.6150750931339399E+04 {~~}
START M     sofc                      35 -0.6954456602596484E+00 {~~}
START H     sofc                      35  0.7462281704415040E+03 {~~}
START E     sofc                     215 -0.2266988082395728E+03 {~~}
START Q     sofc                     315  0.0000000000000000E+00 {~~}
START ZA    sofc                       1  0.8953504439170833E+05 {~~}
START ZA    sofc                       2  0.7759617742337787E+05 {~~}
START ZA    sofc                       3  0.1131334605653419E+06 {~~}
START ZA    sofc                       4  0.2874557392272268E+06 {~~}
START ZA    sofc                       5 -0.4346595838206942E+06 {~~}
START ZA    sofc                       6  0.7031243231141652E+00 {~~}
START ZA    sofc                       7  0.8490526863609010E+00 {~~}
START ZA    sofc                       8  0.8500000000000023E+00 {~~}
START ZA    sofc                       9  0.5074411560779050E+00 {~~}
START ZA    sofc                      10  0.4097643685146410E+00 {~~}
START ZA    sofc                      11  0.9653081902361105E+00 {~~}
START ZA    sofc                      12  0.1081368457960910E+00 {~~}
START ZA    sofc                      13  0.7147434745365800E-02 {~~}
START ZA    sofc                      14  0.3042639760850667E-01 {~~}
START ZA    sofc                      15  0.8195975120861470E+00 {~~}
START ZA    sofc                      16 -0.8643528923812226E+05 {~~}
START ZA    sofc                      17 -0.1885369880714487E+06 {~~}
START ZA    sofc                      18 -0.1862755214698623E+06 {~~}
START ZA    sofc                      19  0.6834375642423529E+00 {~~}
START ZA    sofc                      20  0.2335762988681633E-01 {~~}
START ZA    sofc                      21  0.1013478073726875E+04 {~~}
START ZA    sofc                      22  0.3000000000000009E+03 {~~}
START ZA    sofc                      23  0.9500000000000024E+00 {~~}
START Y_J   USEDFUEL            H2           0.3681263343705554E-01 {~~}
START Y_J   USEDFUEL            CO           0.2592602480079992E-01 {~~}
START Y_J   USEDFUEL            CO2          0.2785668687819785E+00 {~~}
START Y_J   USEDFUEL            H2O-G        0.3654198955141020E+00 {~~}
START Y_J   USEDFUEL            CH4          0.1320885926659904E-06 {~~}
START Y_J   USEDFUEL            N2           0.2932744453774739E+00 {~~}
START Y_J   USEDAIR             O2           0.1816887511884419E+00 {~~}
START Y_J   USEDAIR             N2           0.7980728885885872E+00 {~~}
START Y_J   USEDAIR             CO2          0.3097708197393921E-03 {~~}
START Y_J   USEDAIR             H2O-G        0.1042895093122620E-01 {~~}
START Y_J   USEDAIR             AR           0.9499638472008036E-02 {~~}
START M     burner                    36  0.6954456602596484E+00 {~~}
START H     burner                    36  0.6125054264003596E+03 {~~}
START M     burner                    12  0.1084136464468042E+00 {~~}
START H     burner                    12 -0.6717227933915663E+04 {~~}
START M     burner                    41 -0.8038593067064525E+00 {~~}
START P                          41  0.2488441260000007E+01 {~~}
START H     burner                    41 -0.3760296498811286E+03 {~~}
START Q     burner                   316  0.0000000000000000E+00 {~~}
START ZA    burner                     1  0.3599992793955970E+02 {~~}
START Y_J   FLUE_GAS            O2           0.1528256566367803E+00 {~~}
START Y_J   FLUE_GAS            N2           0.7312927409586391E+00 {~~}
START Y_J   FLUE_GAS            NO           0.0000000000000000E+00 {~~}
START Y_J   FLUE_GAS            CO2          0.4265157978005395E-01 {~~}
START Y_J   FLUE_GAS            H2O-G        0.6501119656074644E-01 {~~}
START Y_J   FLUE_GAS            SO2          0.0000000000000000E+00 {~~}
START Y_J   FLUE_GAS            NO2          0.0000000000000000E+00 {~~}
START Y_J   FLUE_GAS            AR           0.8218826063782632E-02 {~~}
START M     GT                        41  0.8038593067064525E+00 {~~}
START H     GT                        41 -0.3760296498811286E+03 {~~}
START M     GT                        42 -0.8038593067064525E+00 {~~}
```

```
START P                          42  0.1033000000000003E+01 {~~}
START H    GT                         42 -0.5641539005908002E+03 {~~}
START W    GT                        117 -0.1512254297501471E+03 {~~}
START E    generator                 217 -0.4848624410195209E+02 {~~}
START Q    generator                 317 -0.2551907584313264E+01 {~~}
START W    generator                 117  0.5103815168626537E+02 {~~}
START M    recuperator                42  0.8038593067064525E+00 {~~}
START H    recuperator                42 -0.5641539005908002E+03 {~~}
START M    recuperator                43 -0.8038593067064525E+00 {~~}
START P                          43  0.1023000000000003E+01 {~~}
START H    recuperator                43 -0.8989207289437225E+03 {~~}
START M    recuperator                32  0.7206544633491334E+00 {~~}
START H    recuperator                32  0.1694338091721306E+02 {~~}
START M    recuperator                33 -0.7206544633491334E+00 {~~}
START H    recuperator                33  0.3903614949152461E+03 {~~}
START Q    recuperator               318  0.0000000000000000E+00 {~~}
START ZA   recuperator                 1  0.2691054305480973E+03 {~~}
START M    exhaustcooler               43  0.8038593067064525E+00 {~~}
START H    exhaustcooler               43 -0.8989207289437225E+03 {~~}
START M    exhaustcooler               44 -0.8038593067064525E+00 {~~}
START P                          44  0.1013000000000003E+01 {~~}
START H    exhaustcooler               44 -0.1031734334544724E+04 {~~}
START M    exhaustcooler               85  0.5104452792040437E+00 {~~}
START P                          85  0.1013000000000003E+01 {~~}
START H    exhaustcooler               85 -0.1584524528596515E+05 {~~}
START M    exhaustcooler               86 -0.5104452792040437E+00 {~~}
START P                          86  0.1008000000000003E+01 {~~}
START H    exhaustcooler               86 -0.1563608779686840E+05 {~~}
START Q    exhaustcooler              319  0.0000000000000000E+00 {~~}
START ZA   exhaustcooler                1  0.1067634529196043E+03 {~~}
C ~~~~~~~~~~~~~~~~~~~~~~~~~~~~~~~~~~~~~~~~~~~~~~~~~~~~~~~~~~~~~~~~~~~~~~~~~~~~~~~~~~~~~~~~~~~~~~~~~~~
C ~~ End of generated initial guesses.
C ~~~~~~~~~~~~~~~~~~~~~~~~~~~~~~~~~~~~~~~~~~~~~~~~~~~~~~~~~~~~~~~~~~~~~~~~~~~~~~~~~~~~~~~~~~~~~~~~~~~
```

end

Biomass gasification (Viking) + SOFC/MGT incl. recuperation

RUN NUMBER 1

ALGEBRAIC VARIABLES

NO DE	TO COMPONENT	MEDIA	M [kg/s]	T [C]	P [bar]	H [kJ/kg]	ENERGY [kJ/s]	X	S [kJ/kg K]	V [m3/kg]	U [kJ/kg]
1	Dryer	Wood	0.04	15.00	-	-8621.6	4.991E+02	-	0.4612	-	-8621.6
64	Dryer	STEAM-HF	0.20	250.00	0.998	-12996.5		-	11.5514	2.4110	-13237.2
2	Dryer	DryWood	-0.03	150.00	-	-5497.1		-	1.7075	-	-5497.1
61	Dryer	STEAM-HF	-0.21	150.00	0.993	-13194.4		-	11.1339	1.9505	-13388.1
301	Dryer	HEAT					0.000E+00				
2	Gasifier	DryWood	0.03	150.00	-	-5497.1		-	1.7075	-	-5497.1
26	Gasifier	STEAM-HF	0.00	150.00	1.003	-13194.5		-	11.1292	1.9309	-13388.2
74	Gasifier	humid_air	0.05	564.13	1.003	-2398.8		-	9.1937	2.7302	-2672.7
3	Gasifier	raw_PG	-0.09	800.00	0.998	-3507.9		-	10.8590	4.1308	-3920.1
99	Gasifier	Ash	0.00	800.00	-	-4308.0		-	0.0000	-	-4308.0
302	Gasifier	HEAT					0.000E+00				
3	airpreheat	raw_PG	0.09	800.00	0.998	-3507.9		-	10.8590	4.1308	-3920.1
4	airpreheat	raw_PG	-0.09	552.33	0.993	-3918.6		-	10.4262	3.1935	-4235.7
72	airpreheat	STANDARD_AIR	0.04	15.00	1.008	-98.8		-	6.8668	0.8237	-181.9
73	airpreheat	STANDARD_AIR	-0.04	780.00	1.003	724.5		-	8.2418	3.0255	421.1
303	airpreheat	HEAT					0.000E+00				
4	steamheater	raw_PG	0.09	552.33	0.993	-3918.6		-	10.4262	3.1935	-4235.7
5	steamheater	raw_PG	-0.09	259.48	0.988	-4375.3		-	9.7468	2.0710	-4579.9
63	steamheater	STEAM-HF	0.20	151.68	1.003	-13191.2		-	11.1370	1.9388	-13385.6
64	steamheater	STEAM-HF	-0.20	250.00	0.998	-12996.5		-	11.5514	2.4110	-13237.2
304	steamheater	HEAT					0.000E+00				
61	steamblower	STEAM-HF	0.21	150.00	0.993	-13194.4		-	11.1339	1.9505	-13388.1
62	steamblower	STEAM-HF	-0.21	151.68	1.003	-13191.2		-	11.1370	1.9388	-13385.6
305	steamblower	HEAT					-1.409E-02				
105	steamblower	MECH_POWER					7.044E-01				
62	split1	STEAM-HF	0.21	151.68	1.003	-13191.2		-	11.1370	1.9388	-13385.6
63	split1	STEAM-HF	-0.20	151.68	1.003	-13191.2		-	11.1370	1.9388	-13385.6
69	split1	STEAM-HF	-0.01	151.68	1.003	-13191.2		-	11.1370	1.9388	-13385.6
73	mix1	STANDARD_AIR	0.04	780.00	1.003	724.5		-	8.2418	3.0255	421.1
69	mix1	STEAM-HF	0.01	151.68	1.003	-13191.2		-	11.1370	1.9388	-13385.6
74	mix1	humid_air	-0.05	564.13	1.003	-2398.8		-	9.1937	2.7302	-2672.7
5	gascooler	raw_PG	0.09	259.48	0.988	-4375.3		-	9.7468	2.0710	-4579.9
6	gascooler	cold_PG	-0.09	90.00	0.983	-4624.6		-	9.1860	1.4192	-4764.1
98	gascooler	STEAM-HF	0.00	90.00	0.983	-15594.1		-	4.7085	0.0010	-15594.2
81	gascooler	STEAM-HF	0.10	30.02	1.013	-15845.2		-	3.9530	0.0010	-15845.3
82	gascooler	STEAM-HF	-0.10	80.00	1.008	-15636.1		-	4.5912	0.0010	-15636.2
306	gascooler	HEAT					0.000E+00				
6	gasclean	cold_PG	0.09	90.00	0.983	-4624.6		-	9.1860	1.4192	-4764.1
7	gasclean	clean_PG	-0.09	90.00	0.978	-4624.9		-	9.1879	1.4263	-4764.4
97	gasclean	impurities	0.00	90.00	0.978	-535.6		-	6.2438	0.9059	-624.2
307	gasclean	HEAT					0.000E+00				
7	condenser	clean_PG	0.09	90.00	0.978	-4624.9		-	9.1879	1.4263	-4764.4
8	condenser	dry_PG	-0.08	50.00	0.973	-4466.6		-	8.9598	1.2694	-4590.1
96	condenser	STEAM-HF	0.00	50.01	0.973	-15761.7		-	4.2198	0.0010	-15761.7
83	condenser	STEAM-HF	0.05	30.02	1.013	-15845.2		-	3.9530	0.0010	-15845.3

84	condenser	STEAM-HF	-0.05	80.00	1.008	-15636.1		-	4.5912	0.0010	-15636.2
308	condenser	HEAT					0.000E+00				
8	PGcompressor	dry_PG	0.08	50.00	0.973	-4466.6		-	8.9598	1.2694	-4590.1
9	PGcompressor	dry_PG	-0.08	173.32	2.505	-4289.3		-	9.0626	0.6813	-4460.0
309	PGcompressor	HEAT					-3.010E-01				
117	PGcompressor	MECH_POWER					1.505E+01				
11	PGpreheat	USEDFUEL	0.11	800.00	2.495	-6150.8		-	8.8073	1.2836	-6471.0
12	PGpreheat	USEDFUEL	-0.11	409.82	2.490	-6717.2		-	8.1544	0.8186	-6921.1
9	PGpreheat	dry_PG	0.08	173.32	2.505	-4289.3		-	9.0626	0.6813	-4460.0
10	PGpreheat	dry_PG	-0.08	650.00	2.500	-3551.2		-	10.1804	1.4115	-3904.1
311	PGpreheat	HEAT					0.000E+00				
31	aircompressor	STANDARD_AIR	0.72	15.00	1.013	-98.8		-	6.8653	0.8196	-181.9
32	aircompressor	STANDARD_AIR	-0.72	129.26	2.530	16.9		-	6.9399	0.4583	-99.0
312	aircompressor	HEAT					-1.703E+00				
117	aircompressor	MECH_POWER					8.514E+01				
42	recuperator	FLUE_GAS	0.80	546.00	1.033	-564.2		-	8.0822	2.2930	-801.0
43	recuperator	FLUE_GAS	-0.80	245.28	1.023	-898.9		-	7.5771	1.4654	-1048.8
32	recuperator	STANDARD_AIR	0.72	129.26	2.530	16.9		-	6.9399	0.4583	-99.0
33	recuperator	STANDARD_AIR	-0.72	483.49	2.520	390.4		-	7.6042	0.8652	172.3
318	recuperator	HEAT					0.000E+00				
35	airpreheat2	USEDAIR	0.70	800.00	2.500	746.2		-	8.0049	1.2413	435.9
36	airpreheat2	USEDAIR	-0.70	683.95	2.490	612.5		-	7.8742	1.1115	335.7
33	airpreheat2	STANDARD_AIR	0.72	483.49	2.520	390.4		-	7.6042	0.8652	172.3
34	airpreheat2	STANDARD_AIR	-0.72	600.00	2.510	519.4		-	7.7639	1.0024	267.8
314	airpreheat2	HEAT					0.000E+00				
10	sofc	dry_PG	0.08	650.00	2.500	-3551.2		-	10.1804	1.4115	-3904.1
34	sofc	STANDARD_AIR	0.72	600.00	2.510	519.4		-	7.7639	1.0024	267.8
11	sofc	USEDFUEL	-0.11	800.00	2.495	-6150.8		-	8.8073	1.2836	-6471.0
35	sofc	USEDAIR	-0.70	800.00	2.500	746.2		-	8.0049	1.2413	435.9
215	sofc	ELECT_POWER					-2.267E+02				
315	sofc	HEAT					0.000E+00				
36	burner	USEDAIR	0.70	683.95	2.490	612.5		-	7.8742	1.1115	335.7
12	burner	USEDFUEL	0.11	409.82	2.490	-6717.2		-	8.1544	0.8186	-6921.1
41	burner	FLUE_GAS	-0.80	706.46	2.488	-376.0		-	8.0376	1.1383	-659.3
316	burner	HEAT					0.000E+00				
41	GT	FLUE_GAS	0.80	706.46	2.488	-376.0		-	8.0376	1.1383	-659.3
42	GT	FLUE_GAS	-0.80	546.00	1.033	-564.2		-	8.0822	2.2930	-801.0
117	GT	MECH_POWER					-1.512E+02				
217	generator	ELECT_POWER					-4.849E+01				
317	generator	HEAT					-2.552E+00				
117	generator	MECH_POWER					5.104E+01				
43	exhaustcooler	FLUE_GAS	0.80	245.28	1.023	-898.9		-	7.5771	1.4654	-1048.8
44	exhaustcooler	FLUE_GAS	-0.80	120.02	1.013	-1031.7		-	7.2869	1.1223	-1145.4
85	exhaustcooler	STEAM-HF	0.51	30.02	1.013	-15845.2		-	3.9530	0.0010	-15845.3
86	exhaustcooler	STEAM-HF	-0.51	80.00	1.008	-15636.1		-	4.5912	0.0010	-15636.2
319	exhaustcooler	HEAT					0.000E+00				

EXERGY

NO	TO	MEDIA	E_PH	E_CH	E	EX_PH	EX_CH	EX
DE	COMPONENT		[kJ/kg]	[kJ/kg]	[kJ/kg]	[kJ/s]	[kJ/s]	[kJ/s]

1	Dryer	Wood	0.00	13311.33	13311.33	0.00	572.39	572.39
64	Dryer	STEAM-HF	660.71	-	660.71	132.17	-	132.17
2	Dryer	DryWood	-54.56	18651.57	18597.01	1.67	-572.39	-570.71
61	Dryer	STEAM-HF	583.11	-	583.11	-123.83	-	-123.83
301	Dryer	HEAT	-	-	-	0.00	0.00	0.00
2	Gasifier	DryWood	-54.56	18651.57	18597.01	-1.67	572.39	570.71
26	Gasifier	STEAM-HF	584.41	-	584.41	0.00	-	0.00
74	Gasifier	humid_air	310.33	66.40	376.73	17.02	3.64	20.66
3	Gasifier	raw_PG	644.70	5438.32	6083.02	-54.98	-463.75	-518.73
99	Gasifier	Ash	785.00	-	785.00	-0.21	-	-0.21
302	Gasifier	HEAT	-	-	-	0.00	0.00	0.00
3	airpreheat	raw_PG	644.70	5438.32	6083.02	54.98	463.75	518.73
4	airpreheat	raw_PG	358.65	5438.32	5796.96	-30.58	-463.75	-494.34
72	airpreheat	STANDARD_AIR	0.66	3.73	4.39	0.03	0.16	0.19
73	airpreheat	STANDARD_AIR	427.84	3.73	431.57	-18.20	-0.16	-18.36
303	airpreheat	HEAT	-	-	-	0.00	0.00	0.00
4	steamheater	raw_PG	358.65	5438.32	5796.96	30.58	463.75	494.34
5	steamheater	raw_PG	97.80	5438.32	5536.12	-8.34	-463.75	-472.09
63	steamheater	STEAM-HF	585.47	-	585.47	117.12	-	117.12
64	steamheater	STEAM-HF	660.71	-	660.71	-132.17	-	-132.17
304	steamheater	HEAT	-	-	-	0.00	0.00	0.00
61	steamblower	STEAM-HF	583.11	-	583.11	123.83	-	123.83
62	steamblower	STEAM-HF	585.47	-	585.47	-124.33	-	-124.33
305	steamblower	HEAT	-	-	-	0.00	0.00	0.00
105	steamblower	MECH_POWER	-	-	-	0.70	0.00	0.70
62	split1	STEAM-HF	585.47	-	585.47	124.33	-	124.33
63	split1	STEAM-HF	585.47	-	585.47	-117.12	-	-117.12
69	split1	STEAM-HF	585.47	-	585.47	-7.21	-	-7.21
73	mix1	STANDARD_AIR	427.84	3.73	431.57	18.20	0.16	18.36
69	mix1	STEAM-HF	585.47	-	585.47	7.21	-	7.21
74	mix1	humid_air	310.33	66.40	376.73	-17.02	-3.64	-20.66
5	gascooler	raw_PG	97.80	5438.32	5536.12	8.34	463.75	472.09
6	gascooler	cold_PG	10.04	5438.32	5448.36	-0.86	-463.75	-464.61
98	gascooler	STEAM-HF	34.93	-	34.93	0.00	-	0.00
81	gascooler	STEAM-HF	1.49	-	1.49	0.15	-	0.15
82	gascooler	STEAM-HF	26.73	-	26.73	-2.72	-	-2.72
306	gascooler	HEAT	-	-	-	0.00	0.00	0.00
6	gasclean	cold_PG	10.04	5438.32	5448.36	0.86	463.75	464.61
7	gasclean	clean_PG	9.49	5437.03	5446.52	-0.81	-463.61	-464.42
97	gasclean	impurities	6.93	23829.09	23836.02	0.00	-0.15	-0.15
307	gasclean	HEAT	-	-	-	0.00	0.00	0.00
7	condenser	clean_PG	9.49	5437.03	5446.52	0.81	463.61	464.42
8	condenser	dry_PG	-0.23	5566.16	5565.93	0.02	-463.13	-463.11
96	condenser	STEAM-HF	8.19	-	8.19	-0.02	-	-0.02
83	condenser	STEAM-HF	1.49	-	1.49	0.07	-	0.07
84	condenser	STEAM-HF	26.73	-	26.73	-1.25	-	-1.25
308	condenser	HEAT	-	-	-	0.00	0.00	0.00
8	PGcompressor	dry_PG	-0.23	5566.16	5565.93	-0.02	463.13	463.11
9	PGcompressor	dry_PG	147.40	5566.16	5713.56	-12.26	-463.13	-475.40
309	PGcompressor	HEAT	-	-	-	0.00	0.00	0.00
117	PGcompressor	MECH_POWER	-	-	-	15.05	0.00	15.05
11	PGpreheat	USEDFUEL	646.94	787.09	1434.03	70.14	85.33	155.47
12	PGpreheat	USEDFUEL	268.59	787.09	1055.68	-29.12	-85.33	-114.45

9	PGpreheat	dry_PG	147.40	5566.16	5713.56	12.26	463.13	475.40
10	PGpreheat	dry_PG	563.40	5566.16	6129.56	-46.88	-463.13	-510.01
311	PGpreheat	HEAT	-	-	-	0.00	0.00	0.00
31	aircompressor	STANDARD_AIR	1.07	3.73	4.81	0.77	2.69	3.46
32	aircompressor	STANDARD_AIR	95.36	3.73	99.09	-68.72	-2.69	-71.41
312	aircompressor	HEAT	-	-	-	0.00	0.00	0.00
117	aircompressor	MECH_POWER	-	-	-	85.14	0.00	85.14
42	recuperator	FLUE_GAS	255.61	21.61	277.21	205.47	17.37	222.84
43	recuperator	FLUE_GAS	66.38	21.61	87.98	-53.36	-17.37	-70.73
32	recuperator	STANDARD_AIR	95.36	3.73	99.09	68.72	2.69	71.41
33	recuperator	STANDARD_AIR	277.36	3.73	281.10	-199.88	-2.69	-202.57
318	recuperator	HEAT	-	-	-	0.00	0.00	0.00
35	airpreheat2	USEDAIR	521.69	3.79	525.48	362.81	2.63	365.44
36	airpreheat2	USEDAIR	425.63	3.79	429.42	-296.00	-2.63	-298.64
33	airpreheat2	STANDARD_AIR	277.36	3.73	281.10	199.88	2.69	202.57
34	airpreheat2	STANDARD_AIR	360.38	3.73	364.12	-259.71	-2.69	-262.40
314	airpreheat2	HEAT	-	-	-	0.00	0.00	0.00
10	sofc	dry_PG	563.40	5566.16	6129.56	46.88	463.13	510.01
34	sofc	STANDARD_AIR	360.38	3.73	364.12	259.71	2.69	262.40
11	sofc	USEDFUEL	646.94	787.09	1434.03	-70.14	-85.33	-155.47
35	sofc	USEDAIR	521.69	3.79	525.48	-362.81	-2.63	-365.44
215	sofc	ELECT_POWER	-	-	-	-226.70	0.00	-226.70
315	sofc	HEAT	-	-	-	0.00	0.00	0.00
36	burner	USEDAIR	425.63	3.79	429.42	296.00	2.63	298.64
12	burner	USEDFUEL	268.59	787.09	1055.68	29.12	85.33	114.45
41	burner	FLUE_GAS	456.58	21.61	478.19	-367.03	-17.37	-384.40
316	burner	HEAT	-	-	-	0.00	0.00	0.00
41	GT	FLUE_GAS	456.58	21.61	478.19	367.03	17.37	384.40
42	GT	FLUE_GAS	255.61	21.61	277.21	-205.47	-17.37	-222.84
117	GT	MECH_POWER	-	-	-	-151.23	0.00	-151.23
217	generator	ELECT_POWER	-	-	-	-48.49	0.00	-48.49
317	generator	HEAT	-	-	-	0.00	0.00	0.00
117	generator	MECH_POWER	-	-	-	51.04	0.00	51.04
43	exhaustcooler	FLUE_GAS	66.38	21.61	87.98	53.36	17.37	70.73
44	exhaustcooler	FLUE_GAS	17.19	21.61	38.80	-13.82	-17.37	-31.19
85	exhaustcooler	STEAM-HF	1.49	-	1.49	0.76	-	0.76
86	exhaustcooler	STEAM-HF	26.73	-	26.73	-13.64	-	-13.64
319	exhaustcooler	HEAT	-	-	-	0.00	0.00	0.00

```
ELEC. POWER PRODUCTION  =     275.1851 kW
TOTAL POWER CONSUMPTION =       0.7044 kW
NET POWER PRODUCTION    =     274.4807 kW
FUEL CONSUMPTION (LHV)  =     499.1161 kJ/s
FUEL CONSUMPTION (HHV)  =     572.3872 kJ/s
THERMAL EFFICIENCY (LHV)=       0.5499
THERMAL EFFICIENCY (HHV)=       0.4795

MAXIMUM RELATIVE ERROR = 8.6715E-13
COMPUTER ACCURACY      = 1.0842E-19
```

IDEAL GAS COMPOSITION (MOLAR BASE):

	humid_air	raw_PG	STANDARD_AIR	cold_PG	clean_PG
HYDROGEN	0.0000E+00	0.2538E+00	0.0000E+00	0.2538E+00	0.2538E+00
OXYGEN	0.1418E+00	0.0000E+00	0.2075E+00	0.0000E+00	0.0000E+00
NITROGEN	0.5281E+00	0.2897E+00	0.7729E+00	0.2897E+00	0.2897E+00
CARBON MONOXIDE	0.0000E+00	0.1762E+00	0.0000E+00	0.1762E+00	0.1762E+00
CARBON DIOXIDE	0.2050E-03	0.1144E+00	0.3000E-03	0.1144E+00	0.1144E+00
WATER (I.G.)	0.3236E+00	0.1523E+00	0.1010E-01	0.1523E+00	0.1523E+00
HYDROGEN SULFIDE	0.0000E+00	0.4616E-04	0.0000E+00	0.4616E-04	0.0000E+00
METHANE	0.0000E+00	0.1011E-01	0.0000E+00	0.1011E-01	0.1011E-01
ARGON	0.6286E-02	0.3444E-02	0.9200E-02	0.3444E-02	0.3444E-02
MEAN MOLE MASS	0.2542E+02	0.2164E+02	0.2885E+02	0.2164E+02	0.2164E+02
NET CALORI VALUE	0.0000E+00	0.5516E+04	0.0000E+00	0.5516E+04	0.5515E+04
GRS CALORI VALUE	0.0000E+00	0.1148E+05	0.0000E+00	0.1148E+05	0.1148E+05

IDEAL GAS COMPOSITION (MOLAR BASE):

	impurities	dry_PG	USEDFUEL	FLUE_GAS	USEDAIR
HYDROGEN	0.0000E+00	0.2614E+00	0.3681E-01	0.0000E+00	0.0000E+00
OXYGEN	0.0000E+00	0.0000E+00	0.0000E+00	0.1528E+00	0.1817E+00
NITROGEN	0.0000E+00	0.2983E+00	0.2933E+00	0.7313E+00	0.7981E+00
CARBON MONOXIDE	0.0000E+00	0.1815E+00	0.2593E-01	0.0000E+00	0.0000E+00
CARBON DIOXIDE	0.0000E+00	0.1179E+00	0.2786E+00	0.4265E-01	0.3098E-03
WATER (I.G.)	0.0000E+00	0.1269E+00	0.3654E+00	0.6501E-01	0.1043E-01
HYDROGEN SULFIDE	0.1000E+01	0.0000E+00	0.0000E+00	0.0000E+00	0.0000E+00
METHANE	0.0000E+00	0.1042E-01	0.1321E-06	0.0000E+00	0.0000E+00
ARGON	0.0000E+00	0.3547E-02	0.0000E+00	0.8219E-02	0.9500E-02
MEAN MOLE MASS	0.3408E+02	0.2175E+02	0.2786E+02	0.2875E+02	0.2875E+02
NET CALORI VALUE	0.1521E+05	0.5652E+04	0.5829E+03	0.0000E+00	0.0000E+00
GRS CALORI VALUE	0.1650E+05	0.1172E+05	0.2279E+04	0.0000E+00	0.0000E+00

NON-IDEAL FLUID AND SOLID COMPOSITION (MASS BASE):

	Wood	DryWood	Ash
HYDROGEN	0.4204E-01	0.5890E-01	0.0000E+00
OXYGEN	0.2976E+00	0.4171E+00	0.0000E+00
NITROGEN	0.1153E-02	0.1615E-02	0.0000E+00
CARBON (SOLID)	0.3309E+00	0.4636E+00	0.0000E+00
SULFUR (SOLID)	0.1356E-03	0.1900E-03	0.0000E+00
WATER (LIQUID)	0.3220E+00	0.5000E-01	0.0000E+00
ASHES	0.6170E-02	0.8645E-02	0.1000E+01
MEAN MOLE MASS	0.1321E+02	0.1193E+02	0.7600E+02
NET CALORI VALUE	0.1161E+05	0.1724E+05	0.0000E+00
GRS CALORI VALUE	0.1331E+05	0.1865E+05	0.0000E+00

```
MEDIUM  97 : WATER FOR GAS APP
MEDIUM 300 : HEAT
MEDIUM 301 : PRODUCT HEAT


NUMBER OF CLOSED INTERNAL LOOPS IN THE SYSTEM:    0




 SOLUTION FOR THE INDEPENDENT ALGEBRAIC VARIABLES :


 VARIABLE NO | COMPONENT    |     NAME     |    VALUE    |
-------------------------------------------------------
       1     |Gasifier      |MULTIPLIER H| 0.8501E+05 |
       2     |Gasifier      |MULTIPLIER C| 0.4364E+05 |
       3     |Gasifier      |MULTIPLIER N| 0.1173E+06 |
       4     |Gasifier      |MULTIPLIER O| 0.3125E+06 |
       5     |Gasifier      |MULTIPLIER S| 0.1828E+06 |
       6     |Gasifier      |MULTIPL Ar  | 0.2292E+06 |
       7     |Gasifier      |GIBBS ENERGY| -.3280E+06 |
       1     |airpreheat    |Transferred | 0.3503E+02 |
       1     |steamheater   |Transferred | 0.3894E+02 |
       1     |PGpreheat     |Transferred | 0.6141E+02 |
       1     |recuperator   |Transferred | 0.2691E+03 |
       1     |airpreheat2   |Transferred | 0.9300E+02 |
       1     |sofc          |MULTIPLIER H| 0.8954E+05 |
       2     |sofc          |MULTIPLIER C| 0.7760E+05 |
       3     |sofc          |MULTIPLIER N| 0.1131E+06 |
       4     |sofc          |MULTIPLIER O| 0.2875E+06 |
       5     |sofc          |GIBBS ENERGY| -.4347E+06 |
       6     |sofc          |ETAMAX      | 0.7031E+00 |
       7     |sofc          |ETASYS      | 0.8491E+00 |
       8     |sofc          |UF          | 0.8500E+00 |
       9     |sofc          |ETATOT      | 0.5074E+00 |
      10     |sofc          |STCR        | 0.4098E+00 |
      11     |sofc          |E_nernst    | 0.9653E+00 |
      12     |sofc          |V_act       | 0.1081E+00 |
      13     |sofc          |V_ohm       | 0.7147E-02 |
      14     |sofc          |V_conc      | 0.3043E-01 |
      15     |sofc          |V_cell      | 0.8196E+00 |
      16     |sofc          |GMAX        | -.8644E+05 |
      17     |sofc          |G(T)        | -.1885E+06 |
      18     |sofc          |G(p,T)      | -.1863E+06 |
      19     |sofc          |p_H2eq      | 0.6834E+00 |
      20     |sofc          |R_e         | 0.2336E-01 |
      21     |sofc          |Area [cm^2] | 0.1013E+04 |
      22     |sofc          |i_load      | 0.3000E+03 |
      23     |sofc          |eta_DCAC    | 0.9500E+00 |
       1     |burner        |Lambda      | 0.3600E+02 |
       1     |exhaustcooler |Transferred | 0.1068E+03 |
```

```
------------------------------------------------------

======================================================================================================================
######################################################################################################################
```

end

Appendix F OPTIMIZED SOFC-MGT PLANT MODEL LISTING

Included in this Appendix are:

- Flow sheet of optimized SOFC-MGT scenario with node numbers (1 page)
- DNA Input for optimized SOFC-MGT scenario (10 pages)
- DNA Output for optimized SOFC-MGT scenario (7 pages)

The input and output data only represent one simulation using the reference conditions.

Flow sheet of optimized SOFC-MGT scenario with node numbers

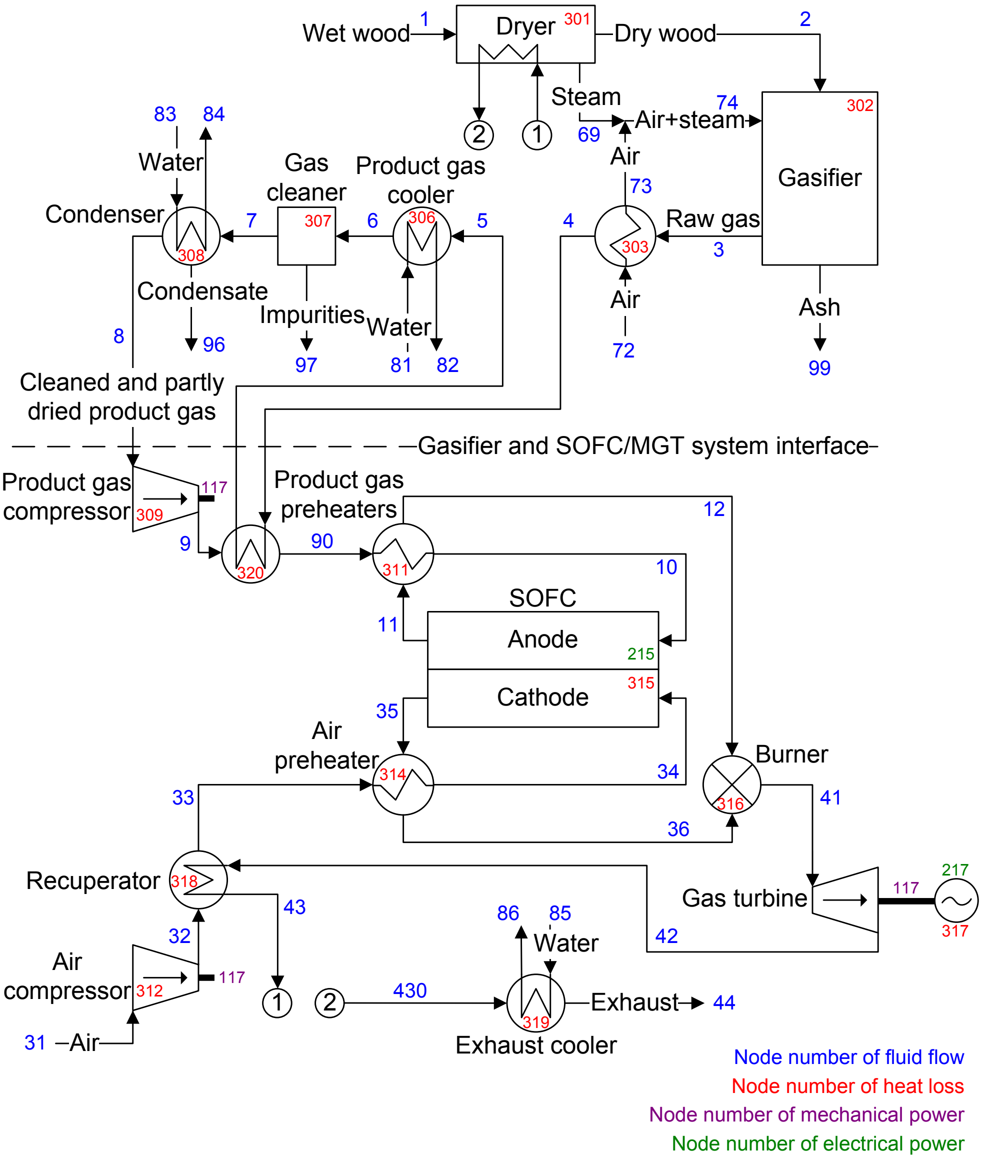

```
title Optimized Biomass gasification (Viking) + SOFC/MGT incl. recuperation
C Wood is dried and gasified. The gasification is atmospheric,
C based on air, and almost reaches equilibrium. The produced
C product gas (PG) composition and the cold gas efficiency is
C similar to that from the Viking gasifier.
C Power and heat production by a hybrid SOFC/MGT system.


C ###################################################
C ###################################################
C ###################################################
C -----------------GASIFIER PART---------------------
C ###################################################
C ###################################################
C ###################################################

C ##Media##
media 1 Wood 2 DryWood
media 73 STANDARD_AIR 3 raw_PG 99 Ash

C ##Fuel composition##
solid Wood C 0.488 H .062 O .439 S .0002 N 0.0017 ASH .0091
+ LHV 18280 CP 1.35 MOI .322
C [Ahrenfeldt, J. et al., Energy & Fuels 2006, 20, 2672-2680] without Cl.



C ###################################################
C -----------------------DRYER-----------------------
C ###################################################
struc Dryer DRYER_03 1 64 2 61 301  0.05 0.005

C Fuel input (plant size):
addco m Dryer 1 0.043

addco t Dryer 1 15 p 1 1.013
addco p 2 1.008 t Dryer 2 150
addco q Dryer 301 0



C ###################################################
C ---------------------GASIFIER----------------------
C ###################################################
struc Gasifier GASIFI_3 8  2 26 74 3 99 302  1 3 4 6 7 9 11 36 /
 0.998 800 0.005 0 1.0 0.01
C Variable constitution parameter: Number of calculated gas components 8
C Nodes: Inlet fuel 2; inlet water 26; inlet air 74; outlet PG 3,
C        outlet ash 99, heat loss 302
C Integer Parameters: Calculated gas compounds H2 (1), N2 (3), CO (4),
C                     CO2 (6), H2O (7), H2S (9), CH4 (11), Ar (36)
C Real parameter: Pressure 1 bar, Eq. temperature 800 degC, Pressure loss 0,
C                 Water-to-fuel ratio 0, carbon conversion factor 1,
C                 non-equilibrium methane 0.01.

addco t Gasifier 3 800
addco t Gasifier 26 150
addco p 99 1.013
addco q Gasifier 302 0



C ###################################################
C -------------GASIFIER AIR PREHEATER----------------
C ###################################################
struc airpreheat heatex_2 3 4 72 73 303 20 0.005 0.005
addco t airpreheat 72 15
addco q airpreheat 303 0



C ###################################################
C ------------------STEAM HEATER---------------------
C ###################################################
struc steamheater heatex_1 43 430 63 64 304 0.005 0.005

```

```
media 63 STEAM-HF

addco t steamheater 64 250
addco q steamheater 304 0



C ###################################################
C ------------------STEAM BLOWER---------------------
C ###################################################
struc steamblower COMPRE_1 61 62 305 105 0.6 0.98



C ###################################################
C --------------------SPLITTER-----------------------
C ###################################################
struc split1 SPLITTER 62 63 69



C ###################################################
C ----------------------MIXER------------------------
C ###################################################
struc mix1 MIXER_02 73 69 74

media 74 humid_air



C ###################################################
C --------------------GAS COOLER---------------------
C ###################################################
struc gascooler GASCOOL1 5 6 98 81 82 306 0.005 0.005

media 81 STEAM-HF 6 cold_PG

addco t gascooler 6 90
addco t gascooler 81 30 p 81 1.013
addco t gascooler 82 80
addco q gascooler 306 0



C ###################################################
C -------------------GAS CLEANING--------------------
C ###################################################
struc gasclean GASCLE_1 6 7 97 307 0.0049
C Pressure loss is taken from paper about Viking

media 7 clean_PG 97 impurities

addco q gasclean 307 0



C ###################################################
C --------------------CONDENSER----------------------
C ###################################################
struc condenser GASCOOL1 7 8 96 83 84 308 0.005 0.005

media 83 STEAM-HF 8 dry_PG

addco t condenser 8 50
addco t condenser 83 30 p 83 1.013
addco t condenser 84 80
addco q condenser 308 0



C ###################################################
C ###################################################
C ###################################################
C -------------------SOFC PART-----------------------
C ###################################################
C ###################################################
```

```
C ###################################################

media 11 USEDFUEL 35 USEDAIR



C ###################################################
C -------------PRODUCT GAS COMPRESSOR----------------
C ###################################################
struc PGcompressor compre_1 8 9 309 117 0.75 0.98
C Isentropic efficiency from L. Fryda et al. (2008)



C ###################################################
C -------FIRST STEP PRODUCT GAS PREHEATING-----------
C ###################################################
struc PGpreheat0 heatex_4 4 5 9 90 320 0.85 0.005 0.005
addco q PGpreheat0 320 0



C ###################################################
C -------SECOND STEP PRODUCT GAS PREHEATING----------
C ###################################################
struc PGpreheat heatex_2 11 12 90 10 311 150 0.005 0.005
addco q PGpreheat 311 0



C ###################################################
C -----------------AIR COMPRESSOR--------------------
C ###################################################
struc aircompressor compre_1 31 32 312 117 0.75 0.98
C Isentropic efficiency from L. Fryda et al. (2008)

media 31 STANDARD_AIR
addco p 31 1.013 t aircompressor 31 15



C ###################################################
C ------------------RECUPERATOR---------------------
C ###################################################
struc recuperator heatex_4 42 43 32 33 318 0.85 0.01 0.01
addco q recuperator 318 0



C ###################################################
C --------------SOFC AIR PREHEATING------------------
C ###################################################
struc airpreheat2 heatex_2 35 36 33 34 314 200 0.01 0.01
addco q airpreheat2 314 0



C ###################################################
C ----------------------SOFC-------------------------
C ###################################################
struc sofc sofceq0d_CBM /
    {fuel and air inlets} 10 34 /
    {fuel and air outlets} 11 35  /
    {nodes for power and heat loss} 215 315 /
    {parameters: utilization, temperature} 0.85 800 /
    {pressure loss} 0.005 0.010 /
    {temperature difference between anode and cathode outlet} 0 /
    {current density [mA/cm^2]} 300 /
    {DC to AC conversion efficiency [-]} 0.95

addco q sofc 315 0

C SOFC OPERATING PRESSURE:
addco p 10 2.75
```

```

C ################################################
C ---------------------BURNER-----------------------
C ################################################
struc burner GASBUR_3 36 12 41 316 0.999374

media 41 FLUE_GAS

addco q burner 316 0



C ################################################
C ------------------GAS TURBINE--------------------
C ################################################
struc GT turbin_1 41 42 117 0.84
C Isentropic efficiency from L. Fryda et al. (2008)



C ################################################
C --------------------GENERATOR--------------------
C ################################################
struc generator sim_gene 217 317 117 0.95



C ################################################
C -----------------EXHAUST COOLING------------------
C ################################################
struc exhaustcooler heatex_2 430 44 85 86 319 60 0.010 0.005

media 85 STEAM-HF

addco p 44 1.013
addco p 85 1.013 t exhaustcooler 85 30
addco t exhaustcooler 86 80
addco q exhaustcooler 319 0



C Reference conditions for exergy
xergy p 1 t 15





C ~~~~~~~~~~~~~~~~~~~~~~~~~~~~~~~~~~~~~~~~~~~~~~~~~~~~~~~~~~~~~~~~~~~~~~~~~~~~~~~~~~~~~~~~~~~~~~~
C ~~ Start of list of generated initial guesses.
C ~~ The values are the results of the latest simulation.
C ~~~~~~~~~~~~~~~~~~~~~~~~~~~~~~~~~~~~~~~~~~~~~~~~~~~~~~~~~~~~~~~~~~~~~~~~~~~~~~~~~~~~~~~~~~~~~~~
START M     Dryer                     1  0.4300000000000001E-01 {~~}
START P                          1  0.1013000000000000E+01 {~~}
START H     Dryer                     1 -0.8621618755529536E+04 {~~}
START M     Dryer                    64  0.2000459030657078E+00 {~~}
START P                         64  0.9980000000000002E+00 {~~}
START H     Dryer                    64 -0.1299653551379773E+05 {~~}
START M     Dryer                     2 -0.3068842105263158E-01 {~~}
START P                          2  0.1008000000000000E+01 {~~}
START H     Dryer                     2 -0.5497059220211002E+04 {~~}
START M     Dryer                    61 -0.2123574820130763E+00 {~~}
START P                         61  0.9930000000000002E+00 {~~}
START H     Dryer                    61 -0.1319443607829820E+05 {~~}
START Q     Dryer                   301  0.0000000000000000E+00 {~~}
START X_J   DryWood                 H2          0.5890000000000001E-01 {~~}
START X_J   DryWood                 O2          0.4170500000000001E+00 {~~}
START X_J   DryWood                 N2          0.1615000000000000E-02 {~~}
START X_J   DryWood                 CO          0.0000000000000000E+00 {~~}
START X_J   DryWood                 NO          0.0000000000000000E+00 {~~}
START X_J   DryWood                 CO2         0.0000000000000000E+00 {~~}
START X_J   DryWood                 H2O-L       0.5000000000000000E-01 {~~}
START X_J   DryWood                 NH3         0.0000000000000000E+00 {~~}
START X_J   DryWood                 H2S         0.0000000000000000E+00 {~~}
```

```
START X_J   DryWood                      SO2         0.0000000000000000E+00 {~~}
START X_J   DryWood                      CH4         0.0000000000000000E+00 {~~}
START X_J   DryWood                      C2H6        0.0000000000000000E+00 {~~}
START X_J   DryWood                      C3H8        0.0000000000000000E+00 {~~}
START X_J   DryWood                      C4H10-N     0.0000000000000000E+00 {~~}
START X_J   DryWood                      C4H10-I     0.0000000000000000E+00 {~~}
START X_J   DryWood                      C5H12       0.0000000000000000E+00 {~~}
START X_J   DryWood                      C6H14       0.0000000000000000E+00 {~~}
START X_J   DryWood                      C7H16       0.0000000000000000E+00 {~~}
START X_J   DryWood                      C8H18       0.0000000000000000E+00 {~~}
START X_J   DryWood                      C2H4        0.0000000000000000E+00 {~~}
START X_J   DryWood                      C3H6        0.0000000000000000E+00 {~~}
START X_J   DryWood                      C5H10       0.0000000000000000E+00 {~~}
START X_J   DryWood                      C6H12-1     0.0000000000000000E+00 {~~}
START X_J   DryWood                      C7H14       0.0000000000000000E+00 {~~}
START X_J   DryWood                      C2H2        0.0000000000000000E+00 {~~}
START X_J   DryWood                      C6H6        0.0000000000000000E+00 {~~}
START X_J   DryWood                      C6H12-C     0.0000000000000000E+00 {~~}
START X_J   DryWood                      C           0.4636000000000001E+00 {~~}
START X_J   DryWood                      S           0.1900000000000000E-03 {~~}
START X_J   DryWood                      NO2         0.0000000000000000E+00 {~~}
START X_J   DryWood                      HCN         0.0000000000000000E+00 {~~}
START X_J   DryWood                      COS         0.0000000000000000E+00 {~~}
START X_J   DryWood                      N2O         0.0000000000000000E+00 {~~}
START X_J   DryWood                      NO3         0.0000000000000000E+00 {~~}
START X_J   DryWood                      SO3         0.0000000000000000E+00 {~~}
START X_J   DryWood                      AR          0.0000000000000000E+00 {~~}
START X_J   DryWood                      ASH         0.8645000000000003E-02 {~~}
START X_J   DryWood                      TAR         0.0000000000000000E+00 {~~}
START M     Gasifier                       2   0.3068842105263158E-01 {~~}
START H     Gasifier                       2  -0.5497059220211002E+04 {~~}
START M     Gasifier                      26   0.0000000000000000E+00 {~~}
START P                              26  0.1003000000000000E+01 {~~}
START H     Gasifier                      26  -0.1319450918722706E+05 {~~}
START M     Gasifier                      74   0.5485206982616295E-01 {~~}
START P                              74  0.1003000000000000E+01 {~~}
START H     Gasifier                      74  -0.2398848478333933E+04 {~~}
START M     Gasifier                       3  -0.8527518947879453E-01 {~~}
START P                               3  0.9980000000000002E+00 {~~}
START H     Gasifier                       3  -0.3507877913073764E+04 {~~}
START M     Gasifier                      99  -0.2653014000000001E-03 {~~}
START P                              99  0.1013000000000000E+01 {~~}
START H     Gasifier                      99  -0.4307999999999999E+04 {~~}
START Q     Gasifier                     302   0.0000000000000000E+00 {~~}
START ZA    Gasifier                       1   0.8500945239865246E+05 {~~}
START ZA    Gasifier                       2   0.4363965291425175E+05 {~~}
START ZA    Gasifier                       3   0.1172765217993686E+06 {~~}
START ZA    Gasifier                       4   0.3124902840469573E+06 {~~}
START ZA    Gasifier                       5   0.1827651987487788E+06 {~~}
START ZA    Gasifier                       6   0.2292482774424771E+06 {~~}
START ZA    Gasifier                       7  -0.3279719879436734E+06 {~~}
START Y_J   raw_PG                       H2          0.2538114658675973E+00 {~~}
START Y_J   raw_PG                       O2          0.0000000000000000E+00 {~~}
START Y_J   raw_PG                       N2          0.2896541868376537E+00 {~~}
START Y_J   raw_PG                       CO          0.1761818347160896E+00 {~~}
START Y_J   raw_PG                       NO          0.0000000000000000E+00 {~~}
START Y_J   raw_PG                       CO2         0.1144395150133744E+00 {~~}
START Y_J   raw_PG                       H2O-G       0.1523098114753785E+00 {~~}
START Y_J   raw_PG                       NH3         0.0000000000000000E+00 {~~}
START Y_J   raw_PG                       H2S         0.4615796164902303E-04 {~~}
START Y_J   raw_PG                       SO2         0.0000000000000000E+00 {~~}
START Y_J   raw_PG                       CH4         0.1011293223314738E-01 {~~}
START Y_J   raw_PG                       NO2         0.0000000000000000E+00 {~~}
START Y_J   raw_PG                       HCN         0.0000000000000000E+00 {~~}
START Y_J   raw_PG                       COS         0.0000000000000000E+00 {~~}
START Y_J   raw_PG                       AR          0.3444095895110029E-02 {~~}
START X_J   Ash                          C           0.0000000000000000E+00 {~~}
START X_J   Ash                          ASH         0.1000000000000000E+01 {~~}
START M     airpreheat                     3   0.8527518947879453E-01 {~~}
START H     airpreheat                     3  -0.3507877913073763E+04 {~~}
START M     airpreheat                     4  -0.8527518947879453E-01 {~~}
START P                               4  0.9930000000000002E+00 {~~}
START H     airpreheat                     4  -0.3918630307677496E+04 {~~}
START M     airpreheat                    72   0.4254049087879453E-01 {~~}
START P                              72  0.1008000000000000E+01 {~~}
START H     airpreheat                    72  -0.9883454496688232E+02 {~~}
```

```
START M     airpreheat                 73 -0.4254049087879453E-01 {~~}
START P                              73  0.1003000000000000E+01 {~~}
START H     airpreheat                 73  0.7245454291500130E+03 {~~}
START Q     airpreheat                303  0.0000000000000000E+00 {~~}
START ZA    airpreheat                  1  0.3502698827870186E+02 {~~}
START M     steamheater                43  0.8013142818653432E+00 {~~}
START P                              43  0.1028000000000000E+01 {~~}
START H     steamheater                43 -0.8735921928420305E+03 {~~}
START M     steamheater               430 -0.8013142818653432E+00 {~~}
START P                             430  0.1023000000000000E+01 {~~}
START H     steamheater               430 -0.9221860411687504E+03 {~~}
START M     steamheater                63  0.2000459030657078E+00 {~~}
START P                              63  0.1003000000000000E+01 {~~}
START H     steamheater                63 -0.1319118556200296E+05 {~~}
START M     steamheater                64 -0.2000459030657078E+00 {~~}
START H     steamheater                64 -0.1299653551379773E+05 {~~}
START Q     steamheater               304  0.0000000000000000E+00 {~~}
START ZA    steamheater                 1  0.3893894467499903E+02 {~~}
START M     steamblower                61  0.2123574820130763E+00 {~~}
START H     steamblower                61 -0.1319443607829820E+05 {~~}
START M     steamblower                62 -0.2123574820130763E+00 {~~}
START P                              62  0.1003000000000000E+01 {~~}
START H     steamblower                62 -0.1319118556200296E+05 {~~}
START Q     steamblower               305 -0.1408717256529214E-01 {~~}
START W     steamblower               105  0.7043586282646008E+00 {~~}
START M     split1                     62  0.2123574820130763E+00 {~~}
START H     split1                     62 -0.1319118556200296E+05 {~~}
START M     split1                     63 -0.2000459030657078E+00 {~~}
START H     split1                     63 -0.1319118556200296E+05 {~~}
START M     split1                     69 -0.1231157894736842E-01 {~~}
START P                              69  0.1003000000000000E+01 {~~}
START H     split1                     69 -0.1319118556200296E+05 {~~}
START M     mix1                       73  0.4254049087879453E-01 {~~}
START H     mix1                       73  0.7245454291500130E+03 {~~}
START M     mix1                       69  0.1231157894736842E-01 {~~}
START H     mix1                       69 -0.1319118556200297E+05 {~~}
START M     mix1                       74 -0.5485206982616295E-01 {~~}
START H     mix1                       74 -0.2398848478333933E+04 {~~}
START Y_J   humid_air          H2           0.0000000000000000E+00 {~~}
START Y_J   humid_air          O2           0.1417803964772675E+00 {~~}
START Y_J   humid_air          N2           0.5281063539146027E+00 {~~}
START Y_J   humid_air          CO           0.0000000000000000E+00 {~~}
START Y_J   humid_air          NO           0.0000000000000000E+00 {~~}
START Y_J   humid_air          CO2          0.2049837057502663E-03 {~~}
START Y_J   humid_air          H2O-G        0.3236220989260379E+00 {~~}
START Y_J   humid_air          NH3          0.0000000000000000E+00 {~~}
START Y_J   humid_air          H2S          0.0000000000000000E+00 {~~}
START Y_J   humid_air          SO2          0.0000000000000000E+00 {~~}
START Y_J   humid_air          CH4          0.0000000000000000E+00 {~~}
START Y_J   humid_air          C2H6         0.0000000000000000E+00 {~~}
START Y_J   humid_air          C3H8         0.0000000000000000E+00 {~~}
START Y_J   humid_air          C4H10-N      0.0000000000000000E+00 {~~}
START Y_J   humid_air          C4H10-I      0.0000000000000000E+00 {~~}
START Y_J   humid_air          C5H12        0.0000000000000000E+00 {~~}
START Y_J   humid_air          C6H14        0.0000000000000000E+00 {~~}
START Y_J   humid_air          C7H16        0.0000000000000000E+00 {~~}
START Y_J   humid_air          C8H18        0.0000000000000000E+00 {~~}
START Y_J   humid_air          C2H4         0.0000000000000000E+00 {~~}
START Y_J   humid_air          C3H6         0.0000000000000000E+00 {~~}
START Y_J   humid_air          C5H10        0.0000000000000000E+00 {~~}
START Y_J   humid_air          C6H12-1      0.0000000000000000E+00 {~~}
START Y_J   humid_air          C7H14        0.0000000000000000E+00 {~~}
START Y_J   humid_air          C2H2         0.0000000000000000E+00 {~~}
START Y_J   humid_air          C6H6         0.0000000000000000E+00 {~~}
START Y_J   humid_air          C6H12-C      0.0000000000000000E+00 {~~}
START Y_J   humid_air          C            0.0000000000000000E+00 {~~}
START Y_J   humid_air          S            0.0000000000000000E+00 {~~}
START Y_J   humid_air          NO2          0.0000000000000000E+00 {~~}
START Y_J   humid_air          HCN          0.0000000000000000E+00 {~~}
START Y_J   humid_air          COS          0.0000000000000000E+00 {~~}
START Y_J   humid_air          N2O          0.0000000000000000E+00 {~~}
START Y_J   humid_air          NO3          0.0000000000000000E+00 {~~}
START Y_J   humid_air          SO3          0.0000000000000000E+00 {~~}
START Y_J   humid_air          AR           0.6286166976341500E-02 {~~}
START Y_J   humid_air          ASH          0.0000000000000000E+00 {~~}
START Y_J   humid_air          TAR          0.0000000000000000E+00 {~~}
```

```
START Y_J   humid_air              CH3OH       0.0000000000000000E+00 {~~}
START M     gascooler                5   0.8527518947879453E-01 {~~}
START P                          5  0.9880000000000002E+00 {~~}
START H     gascooler                5 -0.4379339392033765E+04 {~~}
START M     gascooler                6 -0.8527518947879453E-01 {~~}
START P                          6  0.9830000000000002E+00 {~~}
START H     gascooler                6 -0.4624611248324029E+04 {~~}
START M     gascooler               98   0.0000000000000000E+00 {~~}
START P                         98  0.9830000000000002E+00 {~~}
START H     gascooler               98 -0.1559408877861425E+05 {~~}
START M     gascooler               81   0.9999930726503181E-01 {~~}
START P                         81  0.1013000000000000E+01 {~~}
START H     gascooler               81 -0.1584524528596511E+05 {~~}
START M     gascooler               82 -0.9999930726503181E-01 {~~}
START P                         82  0.1008000000000000E+01 {~~}
START H     gascooler               82 -0.1563608779686837E+05 {~~}
START Q     gascooler              306   0.0000000000000000E+00 {~~}
START Y_J   cold_PG             H2          0.2538114658675976E+00 {~~}
START Y_J   cold_PG             O2          0.0000000000000000E+00 {~~}
START Y_J   cold_PG             N2          0.2896541868376540E+00 {~~}
START Y_J   cold_PG             CO          0.1761818347160898E+00 {~~}
START Y_J   cold_PG             NO          0.0000000000000000E+00 {~~}
START Y_J   cold_PG             CO2         0.1144395150133745E+00 {~~}
START Y_J   cold_PG             H2O-G       0.1523098114753785E+00 {~~}
START Y_J   cold_PG             NH3         0.0000000000000000E+00 {~~}
START Y_J   cold_PG             H2S         0.4615796164902308E-04 {~~}
START Y_J   cold_PG             SO2         0.0000000000000000E+00 {~~}
START Y_J   cold_PG             CH4         0.1011293223314739E-01 {~~}
START Y_J   cold_PG             C2H6        0.0000000000000000E+00 {~~}
START Y_J   cold_PG             C3H8        0.0000000000000000E+00 {~~}
START Y_J   cold_PG             C4H10-N     0.0000000000000000E+00 {~~}
START Y_J   cold_PG             C4H10-I     0.0000000000000000E+00 {~~}
START Y_J   cold_PG             C5H12       0.0000000000000000E+00 {~~}
START Y_J   cold_PG             C6H14       0.0000000000000000E+00 {~~}
START Y_J   cold_PG             C7H16       0.0000000000000000E+00 {~~}
START Y_J   cold_PG             C8H18       0.0000000000000000E+00 {~~}
START Y_J   cold_PG             C2H4        0.0000000000000000E+00 {~~}
START Y_J   cold_PG             C3H6        0.0000000000000000E+00 {~~}
START Y_J   cold_PG             C5H10       0.0000000000000000E+00 {~~}
START Y_J   cold_PG             C6H12-1     0.0000000000000000E+00 {~~}
START Y_J   cold_PG             C7H14       0.0000000000000000E+00 {~~}
START Y_J   cold_PG             C2H2        0.0000000000000000E+00 {~~}
START Y_J   cold_PG             C6H6        0.0000000000000000E+00 {~~}
START Y_J   cold_PG             C6H12-C     0.0000000000000000E+00 {~~}
START Y_J   cold_PG             C           0.0000000000000000E+00 {~~}
START Y_J   cold_PG             S           0.0000000000000000E+00 {~~}
START Y_J   cold_PG             NO2         0.0000000000000000E+00 {~~}
START Y_J   cold_PG             HCN         0.0000000000000000E+00 {~~}
START Y_J   cold_PG             COS         0.0000000000000000E+00 {~~}
START Y_J   cold_PG             N2O         0.0000000000000000E+00 {~~}
START Y_J   cold_PG             NO3         0.0000000000000000E+00 {~~}
START Y_J   cold_PG             SO3         0.0000000000000000E+00 {~~}
START Y_J   cold_PG             AR          0.3444095895110033E-02 {~~}
START M     gasclean                 6   0.8527518947879453E-01 {~~}
START H     gasclean                 6 -0.4624611248324028E+04 {~~}
START M     gasclean                 7 -0.8526899202586877E-01 {~~}
START P                          7  0.9781000000000002E+00 {~~}
START H     gasclean                 7 -0.4624908439609411E+04 {~~}
START M     gasclean                97 -0.6197452925764196E-05 {~~}
START P                         97  0.9781000000000002E+00 {~~}
START H     gasclean                97 -0.5356408846834924E+03 {~~}
START Q     gasclean               307   0.0000000000000000E+00 {~~}
START Y_J   clean_PG            H2          0.2538231818282898E+00 {~~}
START Y_J   clean_PG            O2          0.0000000000000000E+00 {~~}
START Y_J   clean_PG            N2          0.2896675573016547E+00 {~~}
START Y_J   clean_PG            CO          0.1761899672858426E+00 {~~}
START Y_J   clean_PG            NO          0.0000000000000000E+00 {~~}
START Y_J   clean_PG            CO2         0.1144447975519507E+00 {~~}
START Y_J   clean_PG            H2O-G       0.1523168421103350E+00 {~~}
START Y_J   clean_PG            CH4         0.1011339904703273E-01 {~~}
START Y_J   clean_PG            NO2         0.0000000000000000E+00 {~~}
START Y_J   clean_PG            AR          0.3444254874894455E-02 {~~}
START Y_J   impurities             H2O-G       0.0000000000000000E+00 {~~}
START Y_J   impurities             NH3         0.0000000000000000E+00 {~~}
START Y_J   impurities             H2S         0.1000000000000000E+01 {~~}
START Y_J   impurities             SO2         0.0000000000000000E+00 {~~}
```

```
START Y_J   impurities           HCN        0.0000000000000000E+00 {~~}
START Y_J   impurities           COS        0.0000000000000000E+00 {~~}
START Y_J   impurities           AR         0.0000000000000000E+00 {~~}
START Y_J   impurities           ASH        0.0000000000000000E+00 {~~}
START M     condenser              7  0.8526899202586877E-01 {~~}
START H     condenser              7 -0.4624908439609411E+04 {~~}
START M     condenser              8 -0.8320484335731894E-01 {~~}
START P                        8  0.9731000000000002E+00 {~~}
START H     condenser              8 -0.4466561290262755E+04 {~~}
START M     condenser             96 -0.2064148668549822E-02 {~~}
START P                       96  0.9731000000000002E+00 {~~}
START H     condenser             96 -0.1576166949955454E+05 {~~}
START M     condenser             83  0.4691527326491256E-01 {~~}
START P                       83  0.1013000000000000E+01 {~~}
START H     condenser             83 -0.1584524528596511E+05 {~~}
START M     condenser             84 -0.4691527326491256E-01 {~~}
START P                       84  0.1008000000000000E+01 {~~}
START H     condenser             84 -0.1563608779686837E+05 {~~}
START Q     condenser            308  0.0000000000000000E+00 {~~}
START Y_J   dry_PG            H2           0.2614256920940565E+00 {~~}
START Y_J   dry_PG            O2           0.0000000000000000E+00 {~~}
START Y_J   dry_PG            N2           0.2983436780648683E+00 {~~}
START Y_J   dry_PG            CO           0.1814672080223560E+00 {~~}
START Y_J   dry_PG            NO           0.0000000000000000E+00 {~~}
START Y_J   dry_PG            CO2          0.1178726473723855E+00 {~~}
START Y_J   dry_PG            H2O-G        0.1269270417636784E+00 {~~}
START Y_J   dry_PG            NH3          0.0000000000000000E+00 {~~}
START Y_J   dry_PG            H2S          0.0000000000000000E+00 {~~}
START Y_J   dry_PG            SO2          0.0000000000000000E+00 {~~}
START Y_J   dry_PG            CH4          0.1041631550849635E-01 {~~}
START Y_J   dry_PG            C2H6         0.0000000000000000E+00 {~~}
START Y_J   dry_PG            C3H8         0.0000000000000000E+00 {~~}
START Y_J   dry_PG            C4H10-N      0.0000000000000000E+00 {~~}
START Y_J   dry_PG            C4H10-I      0.0000000000000000E+00 {~~}
START Y_J   dry_PG            C5H12        0.0000000000000000E+00 {~~}
START Y_J   dry_PG            C6H14        0.0000000000000000E+00 {~~}
START Y_J   dry_PG            C7H16        0.0000000000000000E+00 {~~}
START Y_J   dry_PG            C8H18        0.0000000000000000E+00 {~~}
START Y_J   dry_PG            C2H4         0.0000000000000000E+00 {~~}
START Y_J   dry_PG            C3H6         0.0000000000000000E+00 {~~}
START Y_J   dry_PG            C5H10        0.0000000000000000E+00 {~~}
START Y_J   dry_PG            C6H12-1      0.0000000000000000E+00 {~~}
START Y_J   dry_PG            C7H14        0.0000000000000000E+00 {~~}
START Y_J   dry_PG            C2H2         0.0000000000000000E+00 {~~}
START Y_J   dry_PG            C6H6         0.0000000000000000E+00 {~~}
START Y_J   dry_PG            C6H12-C      0.0000000000000000E+00 {~~}
START Y_J   dry_PG            C            0.0000000000000000E+00 {~~}
START Y_J   dry_PG            S            0.0000000000000000E+00 {~~}
START Y_J   dry_PG            NO2          0.0000000000000000E+00 {~~}
START Y_J   dry_PG            HCN          0.0000000000000000E+00 {~~}
START Y_J   dry_PG            COS          0.0000000000000000E+00 {~~}
START Y_J   dry_PG            N2O          0.0000000000000000E+00 {~~}
START Y_J   dry_PG            NO3          0.0000000000000000E+00 {~~}
START Y_J   dry_PG            SO3          0.0000000000000000E+00 {~~}
START Y_J   dry_PG            AR           0.3547417174159995E-02 {~~}
START M     PGcompressor         8  0.8320484335731894E-01 {~~}
START H     PGcompressor         8 -0.4466561290262755E+04 {~~}
START M     PGcompressor         9 -0.8320484335731894E-01 {~~}
START P                        9  0.2760000000000000E+01 {~~}
START H     PGcompressor         9 -0.4268497982768156E+04 {~~}
START Q     PGcompressor       309 -0.3363229892840937E+00 {~~}
START W     PGcompressor       117  0.1681614946420476E+02 {~~}
START M     PGpreheat0           4  0.8527518947879453E-01 {~~}
START H     PGpreheat0           4 -0.3918630307677496E+04 {~~}
START M     PGpreheat0           5 -0.8527518947879453E-01 {~~}
START H     PGpreheat0           5 -0.4379339392033766E+04 {~~}
START M     PGpreheat0           9  0.8320484335731894E-01 {~~}
START H     PGpreheat0           9 -0.4268497982768156E+04 {~~}
START M     PGpreheat0          90 -0.8320484335731894E-01 {~~}
START P                       90  0.2755000000000000E+01 {~~}
START H     PGpreheat0          90 -0.3796325295724367E+04 {~~}
START Q     PGpreheat0         320  0.0000000000000000E+00 {~~}
START ZA    PGpreheat0           1  0.3928705446308283E+02 {~~}
START M     PGpreheat           11  0.1084136464468040E+00 {~~}
START P                       11  0.2745000000000000E+01 {~~}
START H     PGpreheat           11 -0.6150751178803807E+04 {~~}
```

```
START M     PGpreheat                 12 -0.1084136464468040E+00 {~~}
START P                            12  0.2740000000000000E+01 {~~}
START H     PGpreheat                 12 -0.6338869655258502E+04 {~~}
START M     PGpreheat                 90  0.8320484335731894E-01 {~~}
START H     PGpreheat                 90 -0.3796325295724366E+04 {~~}
START M     PGpreheat                 10 -0.8320484335731894E-01 {~~}
START P                            10  0.2750000000000000E+01 {~~}
START H     PGpreheat                 10 -0.3551212040611476E+04 {~~}
START Q     PGpreheat                311  0.0000000000000000E+00 {~~}
START ZA    PGpreheat                  1  0.2039460999647063E+02 {~~}
START M     aircompressor               31  0.7181094385080242E+00 {~~}
START P                            31  0.1013000000000000E+01 {~~}
START H     aircompressor               31 -0.9883454496688232E+02 {~~}
START M     aircompressor               32 -0.7181094385080242E+00 {~~}
START P                            32  0.2780000000000000E+01 {~~}
START H     aircompressor               32  0.3066441581850383E+02 {~~}
START Q     aircompressor              312 -0.1897845428917670E+01 {~~}
START W     aircompressor              117  0.9489227144588396E+02 {~~}
START M     airpreheat2                 35  0.6929006354185392E+00 {~~}
START P                            35  0.2750000000000000E+01 {~~}
START H     airpreheat2                 35  0.7462226485113632E+03 {~~}
START M     airpreheat2                 36 -0.6929006354185392E+00 {~~}
START P                            36  0.2740000000000000E+01 {~~}
START H     airpreheat2                 36  0.6693894914039743E+03 {~~}
START M     airpreheat2                 33  0.7181094385080242E+00 {~~}
START P                            33  0.2770000000000000E+01 {~~}
START H     airpreheat2                 33  0.4452705848535890E+03 {~~}
START M     airpreheat2                 34 -0.7181094385080242E+00 {~~}
START P                            34  0.2760000000000000E+01 {~~}
START H     airpreheat2                 34  0.5194065598541840E+03 {~~}
START Q     airpreheat2                314  0.0000000000000000E+00 {~~}
START ZA    airpreheat2                  1  0.5323774338092223E+02 {~~}
START M     sofc                        10  0.8320484335731894E-01 {~~}
START H     sofc                        10 -0.3551212040611476E+04 {~~}
START M     sofc                        34  0.7181094385080242E+00 {~~}
START H     sofc                        34  0.5194065598541839E+03 {~~}
START M     sofc                        11 -0.1084136464468040E+00 {~~}
START H     sofc                        11 -0.6150751178803807E+04 {~~}
START M     sofc                        35 -0.6929006354185392E+00 {~~}
START H     sofc                        35  0.7462226485113632E+03 {~~}
START E     sofc                       215 -0.2272799278504398E+03 {~~}
START Q     sofc                       315  0.0000000000000000E+00 {~~}
START ZA    sofc                         1  0.8910905268625762E+05 {~~}
START ZA    sofc                         2  0.7674420988740612E+05 {~~}
START ZA    sofc                         3  0.1127074608890391E+06 {~~}
START ZA    sofc                         4  0.2874557230368785E+06 {~~}
START ZA    sofc                         5 -0.4338076091026879E+06 {~~}
START ZA    sofc                         6  0.7046466791463556E+00 {~~}
START ZA    sofc                         7  0.8493901070235544E+00 {~~}
START ZA    sofc                         8  0.8500000000000001E+00 {~~}
START ZA    sofc                         9  0.5087419304818280E+00 {~~}
START ZA    sofc                        10  0.4097643685146409E+00 {~~}
START ZA    sofc                        11  0.9675017630887374E+00 {~~}
START ZA    sofc                        12  0.1081415052915717E+00 {~~}
START ZA    sofc                        13  0.7147434745365779E-02 {~~}
START ZA    sofc                        14  0.3042639695637969E-01 {~~}
START ZA    sofc                        15  0.8217864260954202E+00 {~~}
START ZA    sofc                        16 -0.8662243293325575E+05 {~~}
START ZA    sofc                        17 -0.1885369880714480E+06 {~~}
START ZA    sofc                        18 -0.1866988152232337E+06 {~~}
START ZA    sofc                        19  0.7518497376280033E+00 {~~}
START ZA    sofc                        20  0.2335762988681627E-01 {~~}
START ZA    sofc                        21  0.1013478073726872E+04 {~~}
START ZA    sofc                        22  0.3000000000000000E+03 {~~}
START ZA    sofc                        23  0.9500000000000001E+00 {~~}
START Y_J   USEDFUEL                 H2           0.3681256970852961E-01 {~~}
START Y_J   USEDFUEL                 CO           0.2592598083526594E-01 {~~}
START Y_J   USEDFUEL                 CO2          0.2785669018789887E+00 {~~}
START Y_J   USEDFUEL                 H2O-G        0.3654199260118688E+00 {~~}
START Y_J   USEDFUEL                 CH4          0.1598843230450034E-06 {~~}
START Y_J   USEDFUEL                 N2           0.2932744616810239E+00 {~~}
START Y_J   USEDAIR                  O2           0.1815942842608005E+00 {~~}
START Y_J   USEDAIR                  N2           0.7981650191732836E+00 {~~}
START Y_J   USEDAIR                  CO2          0.3098065800905487E-03 {~~}
START Y_J   USEDAIR                  H2O-G        0.1043015486304847E-01 {~~}
START Y_J   USEDAIR                  AR           0.9500735122776839E-02 {~~}
```

```
START M     burner                    36  0.6929006354185392E+00 {~~}
START H     burner                    36  0.6693894914039743E+03 {~~}
START M     burner                    12  0.1084136464468040E+00 {~~}
START H     burner                    12 -0.6338869655258501E+04 {~~}
START M     burner                    41 -0.8013142818653432E+00 {~~}
START P                          41  0.2738284760000001E+01 {~~}
START H     burner                    41 -0.2787914489945458E+03 {~~}
START Q     burner                   316  0.0000000000000000E+00 {~~}
START ZA    burner                     1  0.3585000230706632E+02 {~~}
START Y_J   FLUE_GAS                 O2          0.1526526181100374E+00 {~~}
START Y_J   FLUE_GAS                 N2          0.7311610583748572E+00 {~~}
START Y_J   FLUE_GAS                 NO          0.0000000000000000E+00 {~~}
START Y_J   FLUE_GAS                 CO2         0.4278561806047913E-01 {~~}
START Y_J   FLUE_GAS                 H2O-G       0.6518498470280273E-01 {~~}
START Y_J   FLUE_GAS                 SO2         0.0000000000000000E+00 {~~}
START Y_J   FLUE_GAS                 NO2         0.0000000000000000E+00 {~~}
START Y_J   FLUE_GAS                 AR          0.8215720751823488E-02 {~~}
START M     GT                        41  0.8013142818653432E+00 {~~}
START H     GT                        41 -0.2787914489945458E+03 {~~}
START M     GT                        42 -0.8013142818653432E+00 {~~}
START P                          42  0.1038000000000000E+01 {~~}
START H     GT                        42 -0.5020368493447578E+03 {~~}
START W     GT                       117 -0.1788897276613712E+03 {~~}
START E     generator                217 -0.6382224141371830E+02 {~~}
START Q     generator                317 -0.3359065337564116E+01 {~~}
START W     generator                117  0.6718130675128242E+02 {~~}
START M     recuperator               42  0.8013142818653432E+00 {~~}
START H     recuperator               42 -0.5020368493447578E+03 {~~}
START M     recuperator               43 -0.8013142818653432E+00 {~~}
START H     recuperator               43 -0.8735921928420305E+03 {~~}
START M     recuperator               32  0.7181094385080242E+00 {~~}
START H     recuperator               32  0.3066441581850383E+02 {~~}
START M     recuperator               33 -0.7181094385080242E+00 {~~}
START H     recuperator               33  0.4452705848535890E+03 {~~}
START Q     recuperator              318  0.0000000000000000E+00 {~~}
START ZA    recuperator                1  0.2977326032477479E+03 {~~}
START M     exhaustcooler             430  0.8013142818653432E+00 {~~}
START H     exhaustcooler             430 -0.9221860411687504E+03 {~~}
START M     exhaustcooler              44 -0.8013142818653432E+00 {~~}
START P                          44  0.1013000000000000E+01 {~~}
START H     exhaustcooler              44 -0.1066378943833518E+04 {~~}
START M     exhaustcooler              85  0.5524250302864077E+00 {~~}
START P                          85  0.1013000000000000E+01 {~~}
START H     exhaustcooler              85 -0.1584524528596511E+05 {~~}
START M     exhaustcooler              86 -0.5524250302864077E+00 {~~}
START P                          86  0.1008000000000000E+01 {~~}
START H     exhaustcooler              86 -0.1563608779686837E+05 {~~}
START Q     exhaustcooler             319  0.0000000000000000E+00 {~~}
START ZA    exhaustcooler               1  0.1155438322488978E+03 {~~}
C ~~~~~~~~~~~~~~~~~~~~~~~~~~~~~~~~~~~~~~~~~~~~~~~~~~~~~~~~~~~~~~~~~~~~~~~~~~~~~~~~~~~~~~~~~~~~~~~~~
~~~~~
C ~~ End of generated initial guesses.
C ~~~~~~~~~~~~~~~~~~~~~~~~~~~~~~~~~~~~~~~~~~~~~~~~~~~~~~~~~~~~~~~~~~~~~~~~~~~~~~~~~~~~~~~~~~~~~~~~~
~~~~~
```

end

Optimized Biomass gasification (Viking) + SOFC/MGT incl. recuperation

RUN NUMBER 1

ALGEBRAIC VARIABLES

NO DE	TO COMPONENT	MEDIA	M [kg/s]	T [C]	P [bar]	H [kJ/kg]	ENERGY [kJ/s]	X	S [kJ/kg K]	V [m3/kg]	U [kJ/kg]
1	Dryer	Wood	0.04	15.00	-	-8621.6	4.991E+02	-	0.4612	-	-8621.6
64	Dryer	STEAM-HF	0.20	250.00	0.998	-12996.5		-	11.5514	2.4110	-13237.2
2	Dryer	DryWood	-0.03	150.00	-	-5497.1		-	1.7075	-	-5497.1
61	Dryer	STEAM-HF	-0.21	150.00	0.993	-13194.4		-	11.1339	1.9505	-13388.1
301	Dryer	HEAT					0.000E+00				
2	Gasifier	DryWood	0.03	150.00	-	-5497.1		-	1.7075	-	-5497.1
26	Gasifier	STEAM-HF	0.00	150.00	1.003	-13194.5		-	11.1292	1.9309	-13388.2
74	Gasifier	humid_air	0.05	564.13	1.003	-2398.8		-	9.1937	2.7302	-2672.7
3	Gasifier	raw_PG	-0.09	800.00	0.998	-3507.9		-	10.8590	4.1308	-3920.1
99	Gasifier	Ash	0.00	800.00	-	-4308.0		-	0.0000	-	-4308.0
302	Gasifier	HEAT					0.000E+00				
3	airpreheat	raw_PG	0.09	800.00	0.998	-3507.9		-	10.8590	4.1308	-3920.1
4	airpreheat	raw_PG	-0.09	552.33	0.993	-3918.6		-	10.4262	3.1935	-4235.7
72	airpreheat	STANDARD_AIR	0.04	15.00	1.008	-98.8		-	6.8668	0.8237	-181.9
73	airpreheat	STANDARD_AIR	-0.04	780.00	1.003	724.5		-	8.2418	3.0255	421.1
303	airpreheat	HEAT					0.000E+00				
43	steamheater	FLUE_GAS	0.80	271.83	1.028	-873.6		-	7.6298	1.5330	-1031.2
430	steamheater	FLUE_GAS	-0.80	226.65	1.023	-922.2		-	7.5381	1.4127	-1066.7
63	steamheater	STEAM-HF	0.20	151.68	1.003	-13191.2		-	11.1370	1.9388	-13385.6
64	steamheater	STEAM-HF	-0.20	250.00	0.998	-12996.5		-	11.5514	2.4110	-13237.2
304	steamheater	HEAT					0.000E+00				
61	steamblower	STEAM-HF	0.21	150.00	0.993	-13194.4		-	11.1339	1.9505	-13388.1
62	steamblower	STEAM-HF	-0.21	151.68	1.003	-13191.2		-	11.1370	1.9388	-13385.6
305	steamblower	HEAT					-1.409E-02				
105	steamblower	MECH_POWER					7.044E-01				
62	split1	STEAM-HF	0.21	151.68	1.003	-13191.2		-	11.1370	1.9388	-13385.6
63	split1	STEAM-HF	-0.20	151.68	1.003	-13191.2		-	11.1370	1.9388	-13385.6
69	split1	STEAM-HF	-0.01	151.68	1.003	-13191.2		-	11.1370	1.9388	-13385.6
73	mix1	STANDARD_AIR	0.04	780.00	1.003	724.5		-	8.2418	3.0255	421.1
69	mix1	STEAM-HF	0.01	151.68	1.003	-13191.2		-	11.1370	1.9388	-13385.6
74	mix1	humid_air	-0.05	564.13	1.003	-2398.8		-	9.1937	2.7302	-2672.7
5	gascooler	raw_PG	0.09	256.76	0.988	-4379.3		-	9.7391	2.0604	-4582.9
6	gascooler	cold_PG	-0.09	90.00	0.983	-4624.6		-	9.1860	1.4192	-4764.1
98	gascooler	STEAM-HF	0.00	90.00	0.983	-15594.1		-	4.7085	0.0010	-15594.2
81	gascooler	STEAM-HF	0.10	30.02	1.013	-15845.2		-	3.9530	0.0010	-15845.3
82	gascooler	STEAM-HF	-0.10	80.00	1.008	-15636.1		-	4.5912	0.0010	-15636.2
306	gascooler	HEAT					0.000E+00				
6	gasclean	cold_PG	0.09	90.00	0.983	-4624.6		-	9.1860	1.4192	-4764.1
7	gasclean	clean_PG	-0.09	90.00	0.978	-4624.9		-	9.1879	1.4263	-4764.4
97	gasclean	impurities	0.00	90.00	0.978	-535.6		-	6.2438	0.9059	-624.2
307	gasclean	HEAT					0.000E+00				
7	condenser	clean_PG	0.09	90.00	0.978	-4624.9		-	9.1879	1.4263	-4764.4
8	condenser	dry_PG	-0.08	50.00	0.973	-4466.6		-	8.9598	1.2694	-4590.1
96	condenser	STEAM-HF	0.00	50.01	0.973	-15761.7		-	4.2198	0.0010	-15761.7
83	condenser	STEAM-HF	0.05	30.02	1.013	-15845.2		-	3.9530	0.0010	-15845.3

84	condenser	STEAM-HF	-0.05	80.00	1.008	-15636.1		-	4.5912	0.0010	-15636.2
308	condenser	HEAT					0.000E+00				
8	PGcompressor	dry_PG	0.08	50.00	0.973	-4466.6		-	8.9598	1.2694	-4590.1
9	PGcompressor	dry_PG	-0.08	187.57	2.760	-4268.5		-	9.0714	0.6381	-4444.6
309	PGcompressor	HEAT					-3.363E-01				
117	PGcompressor	MECH_POWER					1.682E+01				
4	PGpreheat0	raw_PG	0.09	552.33	0.993	-3918.6		-	10.4262	3.1935	-4235.7
5	PGpreheat0	raw_PG	-0.09	256.76	0.988	-4379.3		-	9.7391	2.0604	-4582.9
9	PGpreheat0	dry_PG	0.08	187.57	2.760	-4268.5		-	9.0714	0.6381	-4444.6
90	PGpreheat0	dry_PG	-0.08	497.61	2.755	-3796.3		-	9.8532	1.0694	-4090.9
320	PGpreheat0	HEAT					0.000E+00				
11	PGpreheat	USEDFUEL	0.11	800.00	2.745	-6150.8		-	8.7788	1.1667	-6471.0
12	PGpreheat	USEDFUEL	-0.11	674.84	2.740	-6338.9		-	8.5930	1.0325	-6621.8
90	PGpreheat	dry_PG	0.08	497.61	2.755	-3796.3		-	9.8532	1.0694	-4090.9
10	PGpreheat	dry_PG	-0.08	650.00	2.750	-3551.2		-	10.1440	1.2832	-3904.1
311	PGpreheat	HEAT					0.000E+00				
31	aircompressor	STANDARD_AIR	0.72	15.00	1.013	-98.8		-	6.8653	0.8196	-181.9
32	aircompressor	STANDARD_AIR	-0.72	142.70	2.780	30.7		-	6.9463	0.4310	-89.2
312	aircompressor	HEAT					-1.898E+00				
117	aircompressor	MECH_POWER					9.489E+01				
42	recuperator	FLUE_GAS	0.80	602.36	1.038	-502.0		-	8.1583	2.4389	-755.2
43	recuperator	FLUE_GAS	-0.80	271.83	1.028	-873.6		-	7.6298	1.5330	-1031.2
32	recuperator	STANDARD_AIR	0.72	142.70	2.780	30.7		-	6.9463	0.4310	-89.2
33	recuperator	STANDARD_AIR	-0.72	533.41	2.770	445.3		-	7.6472	0.8390	212.9
318	recuperator	HEAT					0.000E+00				
35	airpreheat2	USEDAIR	0.69	800.00	2.750	746.2		-	7.9773	1.1285	435.9
36	airpreheat2	USEDAIR	-0.69	733.60	2.740	669.4		-	7.9045	1.0625	378.3
33	airpreheat2	STANDARD_AIR	0.72	533.41	2.770	445.3		-	7.6472	0.8390	212.9
34	airpreheat2	STANDARD_AIR	-0.72	600.00	2.760	519.4		-	7.7366	0.9116	267.8
314	airpreheat2	HEAT					0.000E+00				
10	sofc	dry_PG	0.08	650.00	2.750	-3551.2		-	10.1440	1.2832	-3904.1
34	sofc	STANDARD_AIR	0.72	600.00	2.760	519.4		-	7.7366	0.9116	267.8
11	sofc	USEDFUEL	-0.11	800.00	2.745	-6150.8		-	8.7788	1.1667	-6471.0
35	sofc	USEDAIR	-0.69	800.00	2.750	746.2		-	7.9773	1.1285	435.9
215	sofc	ELECT_POWER					-2.273E+02				
315	sofc	HEAT					0.000E+00				
36	burner	USEDAIR	0.69	733.60	2.740	669.4		-	7.9045	1.0625	378.3
12	burner	USEDFUEL	0.11	674.84	2.740	-6338.9		-	8.5930	1.0325	-6621.8
41	burner	FLUE_GAS	-0.80	790.13	2.738	-278.8		-	8.1087	1.1228	-586.2
316	burner	HEAT					0.000E+00				
41	GT	FLUE_GAS	0.80	790.13	2.738	-278.8		-	8.1087	1.1228	-586.2
42	GT	FLUE_GAS	-0.80	602.36	1.038	-502.0		-	8.1583	2.4389	-755.2
117	GT	MECH_POWER					-1.789E+02				
217	generator	ELECT_POWER					-6.382E+01				
317	generator	HEAT					-3.359E+00				
117	generator	MECH_POWER					6.718E+01				
430	exhaustcooler	FLUE_GAS	0.80	226.65	1.023	-922.2		-	7.5381	1.4127	-1066.7
44	exhaustcooler	FLUE_GAS	-0.80	90.02	1.013	-1066.4		-	7.2042	1.0367	-1171.4
85	exhaustcooler	STEAM-HF	0.55	30.02	1.013	-15845.2		-	3.9530	0.0010	-15845.3
86	exhaustcooler	STEAM-HF	-0.55	80.00	1.008	-15636.1		-	4.5912	0.0010	-15636.2
319	exhaustcooler	HEAT					0.000E+00				

EXERGY

NO DE	TO COMPONENT	MEDIA	E_PH [kJ/kg]	E_CH [kJ/kg]	E [kJ/kg]	EX_PH [kJ/s]	EX_CH [kJ/s]	EX [kJ/s]
1	Dryer	Wood	0.00	13311.33	13311.33	0.00	572.39	572.39
64	Dryer	STEAM-HF	660.71	-	660.71	132.17	-	132.17
2	Dryer	DryWood	-54.56	18651.57	18597.01	1.67	-572.39	-570.71
61	Dryer	STEAM-HF	583.11	-	583.11	-123.83	-	-123.83
301	Dryer	HEAT	-	-	-	0.00	0.00	0.00
2	Gasifier	DryWood	-54.56	18651.57	18597.01	-1.67	572.39	570.71
26	Gasifier	STEAM-HF	584.41	-	584.41	0.00	-	0.00
74	Gasifier	humid_air	310.33	66.40	376.73	17.02	3.64	20.66
3	Gasifier	raw_PG	644.70	5438.32	6083.02	-54.98	-463.75	-518.73
99	Gasifier	Ash	785.00	-	785.00	-0.21	-	-0.21
302	Gasifier	HEAT	-	-	-	0.00	0.00	0.00
3	airpreheat	raw_PG	644.70	5438.32	6083.02	54.98	463.75	518.73
4	airpreheat	raw_PG	358.65	5438.32	5796.96	-30.58	-463.75	-494.34
72	airpreheat	STANDARD_AIR	0.66	3.73	4.39	0.03	0.16	0.19
73	airpreheat	STANDARD_AIR	427.84	3.73	431.57	-18.20	-0.16	-18.36
303	airpreheat	HEAT	-	-	-	0.00	0.00	0.00
43	steamheater	FLUE_GAS	79.89	21.69	101.58	64.02	17.38	81.40
430	steamheater	FLUE_GAS	57.71	21.69	79.40	-46.25	-17.38	-63.62
63	steamheater	STEAM-HF	585.47	-	585.47	117.12	-	117.12
64	steamheater	STEAM-HF	660.71	-	660.71	-132.17	-	-132.17
304	steamheater	HEAT	-	-	-	0.00	0.00	0.00
61	steamblower	STEAM-HF	583.11	-	583.11	123.83	-	123.83
62	steamblower	STEAM-HF	585.47	-	585.47	-124.33	-	-124.33
305	steamblower	HEAT	-	-	-	0.00	0.00	0.00
105	steamblower	MECH_POWER	-	-	-	0.70	0.00	0.70
62	split1	STEAM-HF	585.47	-	585.47	124.33	-	124.33
63	split1	STEAM-HF	585.47	-	585.47	-117.12	-	-117.12
69	split1	STEAM-HF	585.47	-	585.47	-7.21	-	-7.21
73	mix1	STANDARD_AIR	427.84	3.73	431.57	18.20	0.16	18.36
69	mix1	STEAM-HF	585.47	-	585.47	7.21	-	7.21
74	mix1	humid_air	310.33	66.40	376.73	-17.02	-3.64	-20.66
5	gascooler	raw_PG	95.93	5438.32	5534.25	8.18	463.75	471.93
6	gascooler	cold_PG	10.04	5438.32	5448.36	-0.86	-463.75	-464.61
98	gascooler	STEAM-HF	34.93	-	34.93	0.00	-	0.00
81	gascooler	STEAM-HF	1.49	-	1.49	0.15	-	0.15
82	gascooler	STEAM-HF	26.73	-	26.73	-2.67	-	-2.67
306	gascooler	HEAT	-	-	-	0.00	0.00	0.00
6	gasclean	cold_PG	10.04	5438.32	5448.36	0.86	463.75	464.61
7	gasclean	clean_PG	9.49	5437.03	5446.52	-0.81	-463.61	-464.42
97	gasclean	impurities	6.93	23829.09	23836.02	0.00	-0.15	-0.15
307	gasclean	HEAT	-	-	-	0.00	0.00	0.00
7	condenser	clean_PG	9.49	5437.03	5446.52	0.81	463.61	464.42
8	condenser	dry_PG	-0.23	5566.16	5565.93	0.02	-463.13	-463.11
96	condenser	STEAM-HF	8.19	-	8.19	-0.02	-	-0.02
83	condenser	STEAM-HF	1.49	-	1.49	0.07	-	0.07
84	condenser	STEAM-HF	26.73	-	26.73	-1.25	-	-1.25
308	condenser	HEAT	-	-	-	0.00	0.00	0.00
8	PGcompressor	dry_PG	-0.23	5566.16	5565.93	-0.02	463.13	463.11

9	PGcompressor	dry_PG	165.67	5566.16	5731.83	-13.78	-463.13	-476.92
309	PGcompressor	HEAT	-	-	-	0.00	0.00	0.00
117	PGcompressor	MECH_POWER	-	-	-	16.82	0.00	16.82
4	PGpreheat0	raw_PG	358.65	5438.32	5796.96	30.58	463.75	494.34
5	PGpreheat0	raw_PG	95.93	5438.32	5534.25	-8.18	-463.75	-471.93
9	PGpreheat0	dry_PG	165.67	5566.16	5731.83	13.78	463.13	476.92
90	PGpreheat0	dry_PG	412.56	5566.16	5978.72	-34.33	-463.13	-497.46
320	PGpreheat0	HEAT	-	-	-	0.00	0.00	0.00
11	PGpreheat	USEDFUEL	655.16	787.09	1442.25	71.03	85.33	156.36
12	PGpreheat	USEDFUEL	520.57	787.09	1307.66	-56.44	-85.33	-141.77
90	PGpreheat	dry_PG	412.56	5566.16	5978.72	34.33	463.13	497.46
10	PGpreheat	dry_PG	573.90	5566.16	6140.06	-47.75	-463.13	-510.88
311	PGpreheat	HEAT	-	-	-	0.00	0.00	0.00
31	aircompressor	STANDARD_AIR	1.07	3.73	4.81	0.77	2.68	3.45
32	aircompressor	STANDARD_AIR	107.24	3.73	110.97	-77.01	-2.68	-79.69
312	aircompressor	HEAT	-	-	-	0.00	0.00	0.00
117	aircompressor	MECH_POWER	-	-	-	94.89	0.00	94.89
42	recuperator	FLUE_GAS	299.17	21.69	320.85	239.73	17.38	257.11
43	recuperator	FLUE_GAS	79.89	21.69	101.58	-64.02	-17.38	-81.40
32	recuperator	STANDARD_AIR	107.24	3.73	110.97	77.01	2.68	79.69
33	recuperator	STANDARD_AIR	319.88	3.73	323.61	-229.71	-2.68	-232.39
318	recuperator	HEAT	-	-	-	0.00	0.00	0.00
35	airpreheat2	USEDAIR	529.64	3.79	533.43	366.99	2.63	369.61
36	airpreheat2	USEDAIR	473.80	3.79	477.59	-328.29	-2.63	-330.92
33	airpreheat2	STANDARD_AIR	319.88	3.73	323.61	229.71	2.68	232.39
34	airpreheat2	STANDARD_AIR	368.27	3.73	372.00	-264.46	-2.68	-267.14
314	airpreheat2	HEAT	-	-	-	0.00	0.00	0.00
10	sofc	dry_PG	573.90	5566.16	6140.06	47.75	463.13	510.88
34	sofc	STANDARD_AIR	368.27	3.73	372.00	264.46	2.68	267.14
11	sofc	USEDFUEL	655.16	787.09	1442.25	-71.03	-85.33	-156.36
35	sofc	USEDAIR	529.64	3.79	533.43	-366.99	-2.63	-369.61
215	sofc	ELECT_POWER	-	-	-	-227.28	0.00	-227.28
315	sofc	HEAT	-	-	-	0.00	0.00	0.00
36	burner	USEDAIR	473.80	3.79	477.59	328.29	2.63	330.92
12	burner	USEDFUEL	520.57	787.09	1307.66	56.44	85.33	141.77
41	burner	FLUE_GAS	536.71	21.69	558.40	-430.07	-17.38	-447.45
316	burner	HEAT	-	-	-	0.00	0.00	0.00
41	GT	FLUE_GAS	536.71	21.69	558.40	430.07	17.38	447.45
42	GT	FLUE_GAS	299.17	21.69	320.85	-239.73	-17.38	-257.11
117	GT	MECH_POWER	-	-	-	-178.89	0.00	-178.89
217	generator	ELECT_POWER	-	-	-	-63.82	0.00	-63.82
317	generator	HEAT	-	-	-	0.00	0.00	0.00
117	generator	MECH_POWER	-	-	-	67.18	0.00	67.18
430	exhaustcooler	FLUE_GAS	57.71	21.69	79.40	46.25	17.38	63.62
44	exhaustcooler	FLUE_GAS	9.74	21.69	31.43	-7.81	-17.38	-25.19
85	exhaustcooler	STEAM-HF	1.49	-	1.49	0.83	-	0.83
86	exhaustcooler	STEAM-HF	26.73	-	26.73	-14.77	-	-14.77
319	exhaustcooler	HEAT	-	-	-	0.00	0.00	0.00

```
ELEC. POWER PRODUCTION  =     291.1022 kW
TOTAL POWER CONSUMPTION =       0.7044 kW
NET POWER PRODUCTION    =     290.3978 kW
```

```
  FUEL CONSUMPTION (LHV)  =     499.1161 kJ/s
  FUEL CONSUMPTION (HHV)  =     572.3872 kJ/s
  THERMAL EFFICIENCY (LHV)=       0.5818
  THERMAL EFFICIENCY (HHV)=       0.5073

  MAXIMUM RELATIVE ERROR = 9.0091E-13
  COMPUTER ACCURACY      = 1.0842E-19



IDEAL GAS COMPOSITION (MOLAR BASE):

                |humid_air   |raw_PG      |STANDARD_AIR|FLUE_GAS    |cold_PG     |
---------------------------------------------------------------------------------
HYDROGEN        | 0.0000E+00 | 0.2538E+00 | 0.0000E+00 | 0.0000E+00 | 0.2538E+00 |
OXYGEN          | 0.1418E+00 | 0.0000E+00 | 0.2075E+00 | 0.1527E+00 | 0.0000E+00 |
NITROGEN        | 0.5281E+00 | 0.2897E+00 | 0.7729E+00 | 0.7312E+00 | 0.2897E+00 |
CARBON MONOXIDE | 0.0000E+00 | 0.1762E+00 | 0.0000E+00 | 0.0000E+00 | 0.1762E+00 |
CARBON DIOXIDE  | 0.2050E-03 | 0.1144E+00 | 0.3000E-03 | 0.4279E-01 | 0.1144E+00 |
WATER (I.G.)    | 0.3236E+00 | 0.1523E+00 | 0.1010E-01 | 0.6518E-01 | 0.1523E+00 |
HYDROGEN SULFIDE| 0.0000E+00 | 0.4616E-04 | 0.0000E+00 | 0.0000E+00 | 0.4616E-04 |
METHANE         | 0.0000E+00 | 0.1011E-01 | 0.0000E+00 | 0.0000E+00 | 0.1011E-01 |
ARGON           | 0.6286E-02 | 0.3444E-02 | 0.9200E-02 | 0.8216E-02 | 0.3444E-02 |
---------------------------------------------------------------------------------
MEAN  MOLE  MASS| 0.2542E+02 | 0.2164E+02 | 0.2885E+02 | 0.2875E+02 | 0.2164E+02 |
NET CALORI VALUE| 0.0000E+00 | 0.5516E+04 | 0.0000E+00 | 0.0000E+00 | 0.5516E+04 |
GRS CALORI VALUE| 0.0000E+00 | 0.1148E+05 | 0.0000E+00 | 0.0000E+00 | 0.1148E+05 |
---------------------------------------------------------------------------------

IDEAL GAS COMPOSITION (MOLAR BASE):

                |clean_PG    |impurities  |dry_PG      |USEDFUEL    |USEDAIR     |
---------------------------------------------------------------------------------
HYDROGEN        | 0.2538E+00 | 0.0000E+00 | 0.2614E+00 | 0.3681E-01 | 0.0000E+00 |
OXYGEN          | 0.0000E+00 | 0.0000E+00 | 0.0000E+00 | 0.0000E+00 | 0.1816E+00 |
NITROGEN        | 0.2897E+00 | 0.0000E+00 | 0.2983E+00 | 0.2933E+00 | 0.7982E+00 |
CARBON MONOXIDE | 0.1762E+00 | 0.0000E+00 | 0.1815E+00 | 0.2593E-01 | 0.0000E+00 |
CARBON DIOXIDE  | 0.1144E+00 | 0.0000E+00 | 0.1179E+00 | 0.2786E+00 | 0.3098E-03 |
WATER (I.G.)    | 0.1523E+00 | 0.0000E+00 | 0.1269E+00 | 0.3654E+00 | 0.1043E-01 |
HYDROGEN SULFIDE| 0.0000E+00 | 0.1000E+01 | 0.0000E+00 | 0.0000E+00 | 0.0000E+00 |
METHANE         | 0.1011E-01 | 0.0000E+00 | 0.1042E-01 | 0.1599E-06 | 0.0000E+00 |
ARGON           | 0.3444E-02 | 0.0000E+00 | 0.3547E-02 | 0.0000E+00 | 0.9501E-02 |
---------------------------------------------------------------------------------
MEAN  MOLE  MASS| 0.2164E+02 | 0.3408E+02 | 0.2175E+02 | 0.2786E+02 | 0.2875E+02 |
NET CALORI VALUE| 0.5515E+04 | 0.1521E+05 | 0.5652E+04 | 0.5829E+03 | 0.0000E+00 |
GRS CALORI VALUE| 0.1148E+05 | 0.1650E+05 | 0.1172E+05 | 0.2279E+04 | 0.0000E+00 |
---------------------------------------------------------------------------------

NON-IDEAL FLUID AND SOLID COMPOSITION (MASS BASE):

                |Wood        |DryWood     |Ash         |
--------------------------------------------------------
HYDROGEN        | 0.4204E-01 | 0.5890E-01 | 0.0000E+00 |
OXYGEN          | 0.2976E+00 | 0.4171E+00 | 0.0000E+00 |
```

```
NITROGEN         | 0.1153E-02 | 0.1615E-02 | 0.0000E+00 |
CARBON (SOLID)   | 0.3309E+00 | 0.4636E+00 | 0.0000E+00 |
SULFUR (SOLID)   | 0.1356E-03 | 0.1900E-03 | 0.0000E+00 |
WATER (LIQUID)   | 0.3220E+00 | 0.5000E-01 | 0.0000E+00 |
ASHES            | 0.6170E-02 | 0.8645E-02 | 0.1000E+01 |
--------------------------------------------------------
MEAN  MOLE  MASS| 0.1321E+02 | 0.1193E+02 | 0.7600E+02 |
NET CALORI VALUE| 0.1161E+05 | 0.1724E+05 | 0.0000E+00 |
GRS CALORI VALUE| 0.1331E+05 | 0.1865E+05 | 0.0000E+00 |
--------------------------------------------------------

MEDIUM  97 : WATER FOR GAS APP
MEDIUM 300 : HEAT
MEDIUM 301 : PRODUCT HEAT


NUMBER OF CLOSED INTERNAL LOOPS IN THE SYSTEM:    0





 SOLUTION FOR THE INDEPENDENT ALGEBRAIC VARIABLES :


 VARIABLE NO | COMPONENT    |    NAME     |    VALUE   |
-------------------------------------------------------
       1     |Gasifier      |MULTIPLIER H| 0.8501E+05 |
       2     |Gasifier      |MULTIPLIER C| 0.4364E+05 |
       3     |Gasifier      |MULTIPLIER N| 0.1173E+06 |
       4     |Gasifier      |MULTIPLIER O| 0.3125E+06 |
       5     |Gasifier      |MULTIPLIER S| 0.1828E+06 |
       6     |Gasifier      |MULTIPL Ar  | 0.2292E+06 |
       7     |Gasifier      |GIBBS ENERGY| -.3280E+06 |
       1     |airpreheat    |Transferred | 0.3503E+02 |
       1     |steamheater   |Transferred | 0.3894E+02 |
       1     |PGpreheat0    |Transferred | 0.3929E+02 |
       1     |PGpreheat     |Transferred | 0.2039E+02 |
       1     |recuperator   |Transferred | 0.2977E+03 |
       1     |airpreheat2   |Transferred | 0.5324E+02 |
       1     |sofc          |MULTIPLIER H| 0.8911E+05 |
       2     |sofc          |MULTIPLIER C| 0.7674E+05 |
       3     |sofc          |MULTIPLIER N| 0.1127E+06 |
       4     |sofc          |MULTIPLIER O| 0.2875E+06 |
       5     |sofc          |GIBBS ENERGY| -.4338E+06 |
       6     |sofc          |ETAMAX      | 0.7046E+00 |
       7     |sofc          |ETASYS      | 0.8494E+00 |
       8     |sofc          |UF          | 0.8500E+00 |
       9     |sofc          |ETATOT      | 0.5087E+00 |
      10     |sofc          |STCR        | 0.4098E+00 |
      11     |sofc          |E_nernst    | 0.9675E+00 |
      12     |sofc          |V_act       | 0.1081E+00 |
      13     |sofc          |V_ohm       | 0.7147E-02 |
      14     |sofc          |V_conc      | 0.3043E-01 |
```

```

       15     |sofc         |V_cell      | 0.8218E+00 |
       16     |sofc         |GMAX        | -.8662E+05 |
       17     |sofc         |G(T)        | -.1885E+06 |
       18     |sofc         |G(p,T)      | -.1867E+06 |
       19     |sofc         |p_H2eq      | 0.7518E+00 |
       20     |sofc         |R_e         | 0.2336E-01 |
       21     |sofc         |Area [cm^2] | 0.1013E+04 |
       22     |sofc         |i_load      | 0.3000E+03 |
       23     |sofc         |eta_DCAC    | 0.9500E+00 |
        1     |burner       |Lambda      | 0.3585E+02 |
        1     |exhaustcooler |Transferred | 0.1155E+03 |
------------------------------------------------------

========================================================================================================================
########################################################################################################################
```

Appendix G PAPER I

ISI Journal Paper

Bang-Møller C., Rokni M. Thermodynamic Performance Study of Biomass Gasification, Solid Oxide Fuel Cell and Micro Gas Turbine Hybrid Systems. Energy Conversion and Management. 2010, vol. 51, issue 11, pp. 2330-2339. doi:10.1016/j.enconman.2010.04.006.

Energy Conversion and Management 51 (2010) 2330–2339

Contents lists available at ScienceDirect

Energy Conversion and Management

journal homepage: www.elsevier.com/locate/enconman

Thermodynamic performance study of biomass gasification, solid oxide fuel cell and micro gas turbine hybrid systems

C. Bang-Møller *, M. Rokni

Department of Mechanical Engineering, The Technical University of Denmark, Nils Koppels Allé 403, 2800 Kgs. Lyngby, Denmark

ARTICLE INFO

Article history:
Received 17 August 2009
Received in revised form 30 March 2010
Accepted 8 April 2010
Available online 18 May 2010

Keywords:
System design
Combined heat and power
Biomass gasification
Solid oxide fuel cells
Micro gas turbine
Electrochemical model

ABSTRACT

A system level modelling study of three combined heat and power systems based on biomass gasification is presented. Product gas is converted in a micro gas turbine (MGT) in the first system, in a solid oxide fuel cell (SOFC) in the second system and in a combined SOFC–MGT arrangement in the third system. An electrochemical model of the SOFC has been developed and calibrated against published data from Topsoe Fuel Cells A/S and the Risø National Laboratory. The modelled gasifier is based on an up scaled version (~500 kW$_{th}$) of the demonstrated low tar gasifier, Viking, situated at the Technical University of Denmark. The SOFC converts the syngas more efficiently than the MGT, which is reflected by the energetic electrical efficiency of the gasifier and MGT system in opposition to the gasifier and SOFC configuration – η_{el} = 28.1% versus η_{el} = 36.4%. By combining the SOFC and MGT, the unconverted syngas from the SOFC is utilised in the MGT to produce more power and the SOFC is pressurised, which improves the efficiency to as much as η_{el} = 50.3%. Variation of the different operating conditions reveals an optimum for the chosen pressure ratio with respect to the resulting electrical efficiency. Furthermore, the SOFC operating temperature should be kept high and the cathode temperature gradient maximised.

1. Introduction

Development of sustainable and efficient production plants with combined heat and power (CHP) have gained more attention as climate change and the security of the supply and depletion of fossil fuels have become increasingly well-known issues. The share of biomass in CHP production is expected to increase in the future and decentralised CHP plants are of interest to avoid the cost associated with biomass transportation. Efficient power producing technologies for small scale production typically include gas engines, micro gas turbines (MGT) and fuel cells – all of which require gaseous fuel. Gasification can deliver biomass-based gaseous fuel. Therefore, combining biomass gasification and efficient syngas conversion may enable the design of a sustainable and efficient CHP plant.

Solid oxide fuel cells (SOFCs) can electrochemically convert H_2 and CO as well as internally reform CH_4 into more H_2 and CO due to their high operating temperature and the presence of a nickel catalyst. These conversions make SOFCs very fuel flexible and ideal for syngas conversion compared to other fuel cell types.

The performance and system design of integrated biomass gasifier and SOFC systems have been investigated by several researchers – first by Alderucci et al. in 1994 [1] and later by others [2–4]. An alternative design including heat pipes to thermally integrate an SOFC stack and an allothermal gasifier have also been published [5–8]. A major issue of combining gasification and SOFCs has proved to be gas cleaning, as SOFCs have strict requirements for fuel cleanliness [9,10].

Usage of gas turbine technology in combination with biomass gasification and SOFCs to improve system performance has also been shown. Efficiencies near 60% (LHV) should be achievable for large scale plants in the 5 MW$_e$ class [11]. A few researchers have looked at small scale plants using MGTs [7,12,13], but Fryda et al. [13] was the only group to compare the performance of a hybrid CHP system consisting of an autothermal gasifier feeding either an MGT, an SOFC or both combined. The best performing coupling used both the SOFC and MGT and obtained an electrical efficiency of approximately 40% (LHV).

This study focus on the potential of using the concept of a demonstrated two stage autothermal (air blown) fixed bed biomass gasifier in a small scale CHP plant (~500 kW$_{th}$) together with an SOFC and/or MGT. This gasifier plant, named Viking, produces a very clean gas, avoiding the need for advanced gas cleaning, and performs with a high cold gas efficiency of 93%. Viking was developed at the Technical University of Denmark and is demonstrated in a size of 75 kW$_{th}$ integrated with a gas engine performing with a biomass to electricity efficiency of approximately 25% (LHV). Details of this plant can be found in [14,15]. Hofmann et al. [16] operated an SOFC on cleaned syngas from the Viking gasifier for 150 h

* Corresponding author. Tel.: +45 45254123; fax: +45 45935215.
E-mail address: cbm@mek.dtu.dk (C. Bang-Møller).

0196-8904/$ - see front matter © 2010 Elsevier Ltd. All rights reserved.
doi:10.1016/j.enconman.2010.04.006

Nomenclature

a_{ohm}	coefficient (kΩ cm)
b_{ohm}	coefficient (K)
CC	carbon conversion factor (–)
E_{act}	activation energy (J mol^{-1})
E	reversible open circuit voltage (V)
ex	exergy (W)
F	Faradays constant (C mol^{-1})
g_f	Gibbs free energy (J mol^{-1})
h_f	enthalpy of formation (J mol^{-1})
i	current density (mA cm^{-2})
i_n	internal current density (mA cm^{-2})
i_0	exchange current density (mA cm^{-2})
LHV	lower heating value (kJ kg^{-1})
$\dot{m}$	mass flow (kg s^{-1})
$METH$	fraction of non-equilibrium methane (–)
$\dot{n}$	molar flow (mol s^{-1})
n_e	number of transferred electrons for each molecule of fuel (–)
p	pressure (bar)
P	power production (W)
PR	pressure ratio (–)
Q_{DH}	district heating production (J s^{-1})
r	area specific resistance of one or all layers (kΩ cm^2)
R	universal gas constant (J K^{-1} mol^{-1})
T	temperature (K)
U_F	fuel utilisation factor for fuel cell (%)
V	potential/overpotential (V)
x	mass fraction (–)
y	molar fraction (–)

Greek letters

δ	fuel cell layer thickness (cm)
Δ	change/difference
η_{CHP}	energy based combined heat and power efficiency (%)
η_{cg}	cold gas efficiency of gasifier (%)
η_{el}	energy based electrical efficiency (%)
$\eta_{ex,CHP}$	exergy based combined heat and power efficiency (%)
$\eta_{ex,el}$	exergy based electrical efficiency (%)
η_{rev}	reversible fuel cell efficiency (%)
η_v	voltage efficiency of fuel cell (%)
γ	exchange current density constant (mA cm^{-2})
ρ	resistivity (kΩ cm)

Superscript

0	standard conditions

Subscripts

a	anode
act	activation
c	cathode
C	carbon
cell	single fuel cell
con	consumption
e	electrolyte
elec	electrode
i	interconnect
in	inlet stream
ohm	ohmic
out	outlet stream
th	thermal
tot	total

without degradation. Furthermore, the impacts of varying the operating conditions of the SOFC and MGT are studied and discussed and the sensitivity of the total electrical system efficiency to these operating conditions are examined. From an electrical efficiency point of view, the optimal operating conditions are clarified. Economic aspects will influence the feasibility of the studied plant concepts, but economics are without the scope of this work and, as SOFCs are not fully commercialised, the future cost of SOFCs is uncertain.

The present study is based on steady-state process modelling combining zero-dimensional component models using the simulation tool Dynamic Network Analysis (DNA) [17]. DNA, which was developed at The Technical University of Denmark, is a component-based tool that incorporates thermodynamic property data.

A component model of the SOFC has been developed for the purpose of this study. The SOFC model includes an electrochemical model and takes the operating conditions of the SOFC, e.g., the operating temperature and pressure as well as the gas composition, fuel utilisation and load (current density), into account when predicting the SOFC performance.

2. System description

Three combined heat and power system configurations are investigated in this study. They are based on syngas production from an up scaled Viking gasifier. A flow sheet of the three systems is depicted in Fig. 1. The modelled gasifier system is slightly simplified, but it aims at the same resulting gas composition and cold gas efficiency as the Viking gasifier. In the modelled gasifier, the dryer is heated by hot syngas. The steam production from the dryer is added to the preheated air, and dry wood together with mixed air and steam are fed to the gasifier. The raw product gas is cooled to 90 °C in three steps, including air preheating, wood drying and syngas cooling, which produce hot water for district heating. The cooled syngas is then cleaned to remove impurities, such as particles, before some of the water in the gas is condensed through cooling to 50 °C. The cleaned and partly dried syngas is then converted into electricity and heat in a bottoming cycle consisting of an SOFC, an MGT or a combination of both the SOFC and the MGT. These three system configurations will be referred as the Gasifier–MGT, Gasifier–SOFC and Gasifier–SOFC–MGT configuration, respectively. In the Gasifier–SOFC–MGT configuration, all of the components in the flow sheet are in use, see Fig. 1. With respect to Fig. 1, the recuperator and gas turbine expander are bypassed in the Gasifier–SOFC case, whereas the SOFC and preheaters are bypassed in the Gasifier–MGT arrangement. Thus, the syngas and air compressors work as blowers in the Gasifier–SOFC case due to the lack of pressurisation. In addition, the syngas compressor works as a suction blower for the gasifier system. A generator (not illustrated) is situated on the axis of the gas turbine and it produces the net electric MGT power. In the Gasifier–SOFC configuration, the syngas and air blowers are driven by an electric motor.

3. Plant model

3.1. Gasifier model

The gasifier component calculates the produced syngas composition and produced ashes based on the inlet media composition and the operating conditions. The input parameters defining the

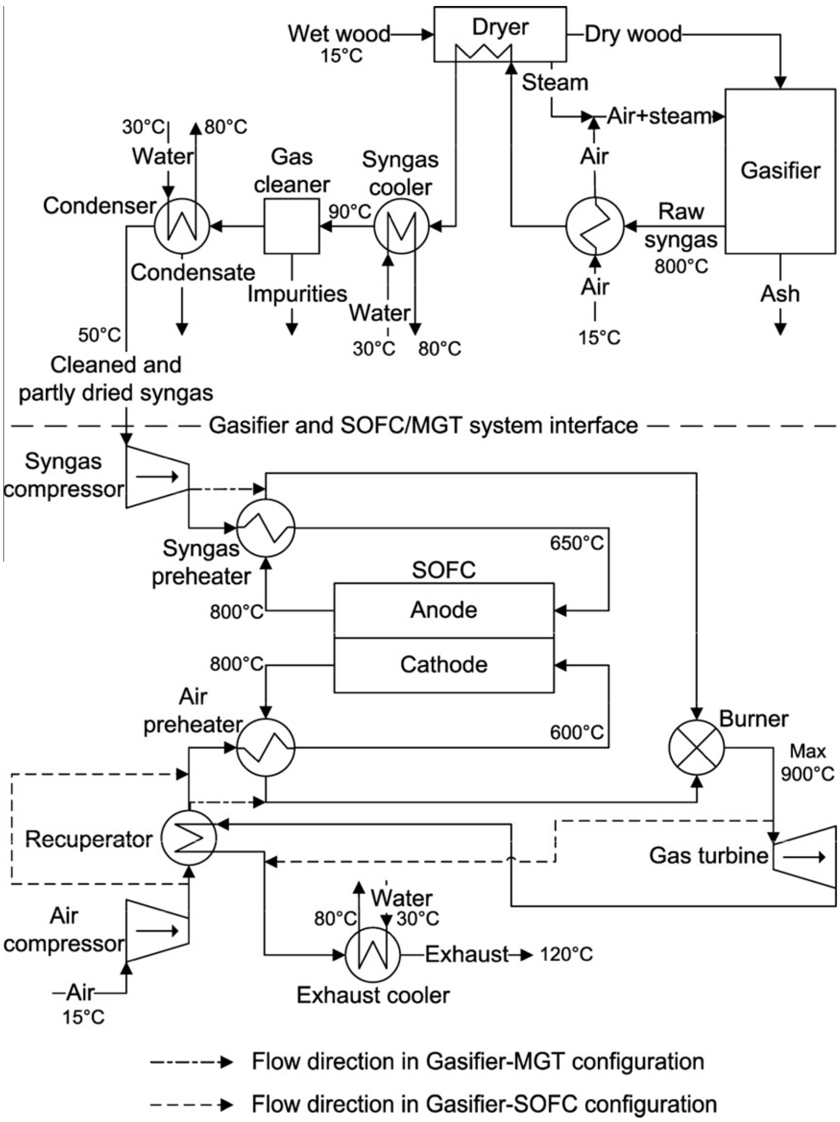

Fig. 1. Flow sheet of the gasifier system with SOFC and/or MGT.

Table 1
Inputs to the gasifier submodel.

Operating pressure	$p_{gasifier}$ [a]	0.998 bar
Operating temperature	$T_{gasifier}$ [a]	800 °C
Pressure loss	$\Delta p_{gasifier}$	5 mbar
Carbon conversion factor	*CC*	1
Non-equilibrium methane	*METH*	0.01

[a] Equals the gasifier outlet.

operating conditions for the gasifier submodel are given in Table 1. The gasifier pressure loss is defined as the difference between the inlet air and steam mixture and the outlet syngas.

In the gasifier, the incoming flows are converted into syngas and ashes. The ashes are represented by SiO_2 and unconverted carbon. SiO_2 originates from a defined content in the inlet biomass, while the unconverted carbon is controlled by a defined carbon conversion factor (*CC*). The amount and composition of ash are calculated by the following equations:

$$\dot{m}_{ash,out} = \dot{m}_{wood,in}[x_{SiO_2,in} + x_{C,in}(1 - CC)] \quad (1)$$

$$x_{SiO_{2,out}} = \frac{\dot{m}_{wood,in} x_{SiO_2,in}}{\dot{m}_{ash,out}} \quad (2)$$

$$x_{C,out} = 1 - x_{SiO_2,out} \quad (3)$$

The syngas can consist of the following species: H_2, N_2, CO, CO_2, H_2O, CH_4, H_2S and Ar. It is assumed that chemical equilibrium is reached at the operating temperature and pressure, where the total Gibbs free energy is minimised. With this assumption, the syngas outlet composition can be found by the Gibbs free energy minimisation method [18]. An option for bypassing methane in the equilibrium calculations is included in order to reach syngas compositions, which contain more methane than in the corresponding composition at equilibrium. Thus, the syngas composition can be adjusted to match realistic syngas compositions, e.g., from the Viking gasifier. The input parameter *METH* is used for this bypass option and is defined as the fraction of methane that is not included in the equilibrium calculations and instead appears in the outlet syngas.

3.1.1. Gasifier model validation

Model validation for the gasifier is done for the entire gasification plant, from the biomass input to the cleaned and dried syngas. Thus, data from the Viking gasifier plant can be used for validation.

Wood chips from beech with small amounts of oak are used in the model, which is in line with the wood chips used in the Viking gasifier reported in Ahrenfeldt et al. [15]. As seen in Table 2, the

Table 2
Dry syngas composition, LHV and cold gas efficiency for the Viking gasifier and the modelled gasifier.

	Viking gasifier [15]	Gasifier model
H_2 (vol.%)	30.5	29.9
CO (vol.%)	19.6	20.8
CO_2 (vol.%)	15.4	13.5
CH_4 (vol.%)	1.16	1.19
N_2 (vol.%)	33.3	34.2
LHV (MJ kg^{-1})	6.2	6.3
Cold gas efficiency (%)	93	94

produced syngas composition and the lower heating value (LHV) from the gasifier model are close to the Viking data. The CO_2 content shows the greatest variance, whereas the resulting LHVs are similar. The overall performance of the modelled gasifier is also similar to that of the Viking gasifier, as indicated by the cold gas efficiencies. The cold gas efficiency is defined in Eq. (4). The value of the cold gas efficiency is higher than traditional downdraft gasifiers, but it is ensured by the two stage design [15].

$$\eta_{\text{cold gas}} = \frac{\dot{m}_{\text{cold product gas}} \text{LHV}_{\text{cold product gas}}}{\dot{m}_{\text{biomass}} \text{LHV}_{\text{biomass}}} \tag{4}$$

3.2. Solid oxide fuel cell model

The SOFC stack component calculates the air and fuel outlet compositions and the power production. The calculations are based on the inlet air and fuel compositions and flow rates as well as the other operating conditions of the SOFC. The SOFC submodel includes an electrochemical model for predicting the performance of the SOFC. The operating conditions are partly described by input parameters given to the SOFC submodel. These parameters are presented in Table 3.

In the submodel only H_2 is electrochemically converted in the SOFC anode, but the model takes into account that CO produces an extra H_2 molecule through the water–gas–shift (WGS) reaction, while four additional H_2 molecules are produced from CH_4 through internal steam reforming and WGS of produced CO (full conversion is assumed). The total molar flow of H_2 on the anode after internal steam reforming and WGS is expressed in the following equation:

$$\dot{n}_{H_2,\text{tot}} = \dot{n}_{H_2,\text{in}} + \dot{n}_{\text{CO,in}} + 4\dot{n}_{CH_4,\text{in}} \tag{5}$$

$$H_2 + O^{2-} \rightarrow H_2O + 2e^- \tag{6}$$

$$\frac{1}{2}O_2 + 2e^- \rightarrow O^{2-} \tag{7}$$

$$H_2 + \frac{1}{2}O_2 \rightarrow H_2O \tag{8}$$

The amount of H_2 that is electrochemically converted depends on the fuel utilisation factor (U_F). The electrode reactions and the overall fuel cell reaction are as shown in Eqs. (6)–(8).

The overall fuel cell reaction reveals that the amount of consumed O_2 is half the amount of consumed H_2. The cathode outlet composition is calculated by the following equations; the only species taken into account are O_2, N_2, CO_2, H_2O and Ar.

Table 3
Inputs to the SOFC submodel.

Fuel utilisation factor	U_F	0.85
Operating temperature	T_{SOFC}[a]	800 °C
Anode pressure loss	Δp_a	5 mbar
Cathode pressure loss	Δp_c	10 mbar
Current density	i	300 mA cm^{-2}

[a] Equals the SOFC anode and cathode outlets.

$$\dot{n}_{O_2,\text{con}} = \frac{U_F \dot{n}_{H_2,\text{in}}}{2} \tag{9}$$

$$\dot{n}_{\text{c,out}} = \dot{n}_{\text{c,in}} - \dot{n}_{O_2,\text{con}} \tag{10}$$

$$y_{O_2,\text{out}} = \frac{\dot{n}_{\text{c,in}} y_{O_2,\text{in}} - \dot{n}_{O_2,\text{con}}}{\dot{n}_{\text{c,out}}} \tag{11}$$

$$y_{j,out} = \frac{\dot{n}_{\text{c,in}} y_{j,in}}{\dot{n}_{\text{c,out}}}, \quad j = \{N_2, CO_2, H_2O\} \tag{12}$$

$$y_{\text{Ar,out}} = 1 - y_{O_2,\text{out}} - y_{N_2,\text{out}} - y_{CO_2,\text{out}} - y_{H_2O,\text{out}} \tag{13}$$

The fuel composition leaving the anode is calculated by the Gibbs free energy minimisation method [18] as described for the gasifier submodel. Chemical equilibrium at the anode outlet temperature and pressure is assumed for the following species: H_2, CO, CO_2, H_2O, CH_4 and N_2. The equilibrium assumption is fair because the methane content in this study is low.

Power production from the SOFC depends on the amount of chemical energy fed to the anode, the reversible efficiency (η_{rev}), the voltage efficiency (η_v) and the fuel utilisation factor (U_F). It is defined in mathematical form in the following equation:

$$P_{\text{SOFC}} = [(\Delta\bar{h}_f)_{H_2} \dot{n}_{H_2,\text{in}} + (\Delta\bar{h}_f)_{\text{CO}} \dot{n}_{\text{CO,in}} + (\Delta\bar{h}_f)_{CH_4} \dot{n}_{CH_4,\text{in}}] \eta_{\text{rev}} \eta_v U_F \tag{14}$$

The reversible efficiency is the maximum possible efficiency defined as the relationship between the maximum available electrical energy (change in Gibbs free energy) and the change in enthalpy of formation, both of which are associated with full oxidation of the fuel. This relationship is shown in the following equation:

$$\eta_{\text{rev}} = \frac{(\Delta\bar{g}_f)_{\text{fuel}}}{(\Delta\bar{h}_f)_{\text{fuel}}} \tag{15}$$

In this model, the change in enthalpy of formation is the LHV. The voltage efficiency expresses the electrochemical performance of the SOFC. The calculation of voltage efficiency is described in the following section.

3.2.1. Electrochemical model

The electrochemical model is used to calculate the cell potential and voltage efficiency of the SOFC. Both of these values depend on the operating conditions, including the temperature, pressure, gas compositions, fuel utilisation and load (current density). The cell potential and voltage efficiency are defined in Eqs. (16) and (17), respectively.

$$V_{\text{cell}} = E - V_{\text{act}} - V_{\text{ohm}} \tag{16}$$

$$\eta_v = \frac{V_{\text{cell}}}{E} \tag{17}$$

In the following part of the section, the reversible open circuit voltage (E), activation overpotential (V_{act}) and ohmic overpotential (V_{ohm}) are calculated. The concentration overpotential due to the limitation of gas diffusion between the gas channel and the active cell area is neglected in this study because operation at high current densities is not examined. The concentration overpotential does not normally contribute to excessive voltage loss unless the current density approaches the limiting current density [19].

E can be calculated from the Nernst equation:

$$E = \frac{-\Delta\bar{g}_f^0}{n_e F} + \frac{RT}{n_e F} \ln\left(\frac{\bar{p}_{H_2,\text{tot}} \sqrt{\bar{p}_{O_2}}}{\bar{p}_{H_2O}}\right) \tag{18}$$

Because it is assumed that all CO and CH_4 are converted to H_2 before the electrochemical reactions take place, the change in standard Gibbs free energy ($\Delta\bar{g}_f^0$) and the number of electrons transferred for each molecule of fuel (n_e) are determined for the reaction of H_2 only. Thus, $n_e = 2$ and $\Delta\bar{g}_f^0 = (\bar{g}_f^0)_{H_2O} - (\bar{g}_f^0)_{H_2} - 1/2(\bar{g}_f^0)_{O_2}$. The partial pressure of species j is an average across the respective electrode and is defined as an arithmetic mean between the inlet and outlet shown in Eqs. (19) and (20). The average partial pressure of the available hydrogen after internal steam reforming and water gas shift of CH_4 and CO is defined in Eq. (21).

$$\bar{p}_j = \left(\frac{y_{j,out} - y_{j,in}}{2}\right)\bar{p}_a, \quad j = \{H_2, CO, CH_4, CO_2, H_2O, N_2\} \tag{19}$$

$$\bar{p}_{O_2} = \left(\frac{y_{O_2,out} - y_{O_2,in}}{2}\right)\bar{p}_c \tag{20}$$

$$\bar{p}_{H_2,tot} = \bar{p}_{H_2} + \bar{p}_{CO} + 4\bar{p}_{CH_4} \tag{21}$$

The activation overpotential is due to an energy barrier (activation energy) that the reactants must overcome in order to drive the electrochemical reactions. The activation overpotential is non-linear and is dominant at low current densities (i). The activation overpotential is defined as (cf. [20]):

$$V_{act} = V_{act,a} + V_{act,c} = \frac{2RT}{n_e F}\left[\sinh^{-1}\left(\frac{i + i_n}{2i_{0,a}}\right) + \sinh^{-1}\left(\frac{i + i_n}{2i_{0,c}}\right)\right] \tag{22}$$

The internal current density (i_n) is added to the actual fuel cell current density in order to account for the mixed potential caused by fuel crossover. The importance of the internal current density in the case of SOFCs is much less than that for low temperature fuel cells. Moreover, the value of i_n is usually very small for SOFCs [21]. In this study, the value of i_n is 2 mA cm^{-2} [22]. The exchange current density (i_0) is a measure of the level of activity on the electrode at i = 0 mA cm^{-2} and is defined for the anode and cathode, respectively, as (cf. [23–25]):

$$i_{0,a} = \gamma_a \left(\frac{\bar{p}_{H_2,tot}}{\bar{p}_a}\right)\left(\frac{\bar{p}_{H_2O}}{\bar{p}_a}\right)\exp\left(\frac{-E_{act,a}}{RT}\right) \tag{23}$$

$$i_{0,c} = \gamma_c \left(\frac{\bar{p}_{O_2}}{\bar{p}_c}\right)^{0.25}\exp\left(\frac{-E_{act,c}}{RT}\right) \tag{24}$$

The values of γ and E_{act} can be found in Table 4.

The ohmic overpotential is caused by the electrical resistance towards the ions passing through the electrolyte and the electrons passing through the electrodes and interconnects. The ohmic overpotential is defined below.

$$V_{ohm} = i\,r_{tot} \tag{25}$$

$$r_{tot} = r_a + r_c + r_e + r_i \tag{26}$$

$$r_j = \delta_j \rho_j, \quad j = \{a, c, e, i\} \tag{27}$$

$$\rho_j = a_{ohm,j}\exp\left(\frac{b_{ohm,j}}{T}\right), \quad j = \{a, c, e, i\} \tag{28}$$

Table 4
Inputs for the electrochemical model.

R	8.314 J K^{-1} mol^{-1}	
F	96 485 C mol^{-1}	
n_e	2	
i_n	2 mA cm^{-2}	[22]
γ_a	2.13×10^7 mA cm^{-2}	[22]
γ_c	1.49×10^7 mA cm^{-2}	[22]
$E_{act,a}$	110,000 J mol^{-1}	[22]
$E_{act,c}$	110,000 J mol^{-1}	[22]
δ_a	750×10^{-4} cm	[19]
δ_c	50×10^{-4} cm	[19]
δ_e	40×10^{-4} cm	[19]
δ_i	100×10^{-4} cm	[26]
$a_{ohm,a}$	0.00298×10^{-3} kΩ cm	[27]
$b_{ohm,a}$	−1392 K	[27]
$a_{ohm,c}$	0.00811×10^{-3} kΩ cm	[27]
$b_{ohm,c}$	600 K	[27]
$a_{ohm,e}$	0.00294×10^{-3} kΩ cm	[27]
$b_{ohm,e}$	10,350 K	[27]
$a_{ohm,i}$	0.1256×10^{-3} kΩ cm	[27]
$b_{ohm,i}$	4690 K	[27]

The thicknesses of the different layers (δ) and the constants a_{ohm} and b_{ohm} used for calculating the temperature-dependent resistivity (ρ) are listed in Table 4.

3.2.2. Electrochemical model calibration

The electrochemical performance predicted by the model has been calibrated against experimental data. Because the model aims to represent the performance of 2nd generation SOFCs from Topsoe Fuel Cell A/S (TOFC) and Risø National Laboratory, published data for this SOFC have been used. The model has been calibrated against a polarisation curve (75-cell stack, 12 × 12 cm^2, 800 °C and fuelled with H_2 and N_2) published by Linderoth et al. in [28]. An active cell area of 81 cm^2 has been assumed. Both modelled and experimental data as well as the error relative to the experimental data are presented in Fig. 2. The calibration was done at atmospheric pressure.

The model shows excellent agreement with the experimental data above a current density of 100 mA cm^{-2}. A current density of 300 mA cm^{-2} was chosen to represent the SOFC load in the following results.

3.3. Micro gas turbine

Modelling of gas turbines is well described in the literature. The reader is referred to Saravanamuttoo et al. [29] for details. Characteristics of the turbomachinery and other components connected to the MGT are listed in Table 5.

The turbine inlet temperature (TIT) is limited to 900 °C in the Gasifier–MGT case, while it varied in the Gasifier–SOFC–MGT arrangement. The performance of the compressors and the MGT expander corresponds to common performance data for an MGT of this scale, e.g., see [13]. The outlet pressure from the MGT depends on the total pressure loss downstream of the MGT because of the exhaust pressure, which is fixed at 1.013 bar. The outlet pressure from the MGT is slightly higher (1.033 bar) than the exhaust pressure due to the pressure drop in the recuperator and exhaust cooler.

3.4. Peripheral equipment

Modelling of peripheral components like heat exchangers is standard and therefore not described in detail.

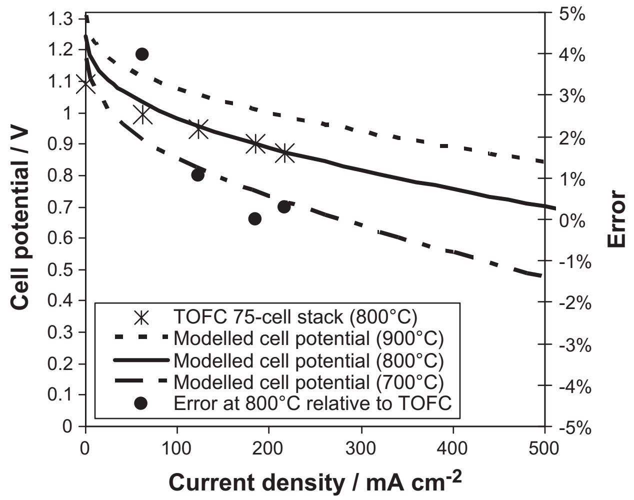

Fig. 2. Single cell polarisation curves based on a 75-cell stack at 800 °C and the SOFC model, respectively. The modelled performance is shown for 700, 800 and 900 °C and the relative error between the modelled and experimental performance is shown at 800 °C.

Table 5
Inputs related to the MGT.

Isentropic efficiency of expander	84%
Isentropic efficiency of compressor	75%
Mechanical efficiency of compressor	98%
Maximum turbine inlet temperature[a]	900 °C
Recuperator effectiveness	85%
Generator efficiency	99%

[a] Only an input in the Gasifier–MGT case.

The throughput of wet biomass is 154.8 kg h^{-1} (corresponds to 499.2 kW_{th} (LHV)). Thus, it is assumed that the Viking gasifier can be scaled up from its nominal thermal input, which is ~75 kW_{th} [15]. The hot product gas preheats the ambient air for the gasifier from 15 °C to 780 °C before the syngas is used to dry the wet biomass. The biomass dryer reduces the water content in the biomass from 32.2 wt.% to 5 wt.% by heating it to 150 °C. During the drying process, the biomass and hot syngas streams are separated. Because no drying component with separated streams exists in DNA, the modelling of this drying process is done by introducing a steam loop to transfer the heat from the syngas to the biomass as illustrated in Fig. 3 The superheated steam dries the biomass and the moisture from the biomass leaves the dryer together with the hot steam. The excess steam is separated from the steam loop and is exactly equal to the amount that evaporates from the biomass. No pressure losses are introduced in the steam loop and the steam blower is assumed to be ideal.

The gas cleaner is a bag filter that removes particulates and condensed impurities. It is assumed that the cleaned syngas can be directly used in an SOFC. The condenser removes some of the water from the syngas, resulting in a water content of 12.7 vol.% in the cleaned and dried syngas. The resulting steam to carbon ratio (S/C) is 0.41, which is somewhat low, but it is justified by the very low tar content in the Viking syngas.

The inlet temperatures to the SOFC anode and cathode are maintained at 150 °C and 200 °C below the outlet temperature, respectively. Thus, it is assumed that a cathode inlet temperature of 200 °C lower than the SOFC operating temperature is possible.

The pressure loss in every component in the SOFC air supply stream and burner exhaust stream is assumed to be 10 mbar, whereas the pressure loss in each of the remaining components is assumed to be 5 mbar; the exception is the burner, which has a pressure loss of 0.6‰ (equals 1.5 mbar if 2.5 bar is present at the inlet). In [14], a pressure loss of 4.9 mbar is reported for the gas cleaner in the Viking gasifier, which fits well with the 5 mbar assumption used here.

The pressure ratio (defined over the air compressor) is different in the three scenarios; being close to 1 in the Gasifier–SOFC configuration, 3.7 in the Gasifier–MGT configuration and 2.5 in the Gasifier–SOFC–MGT case. The pressure ratio is varied for the two pressurised systems as shown below.

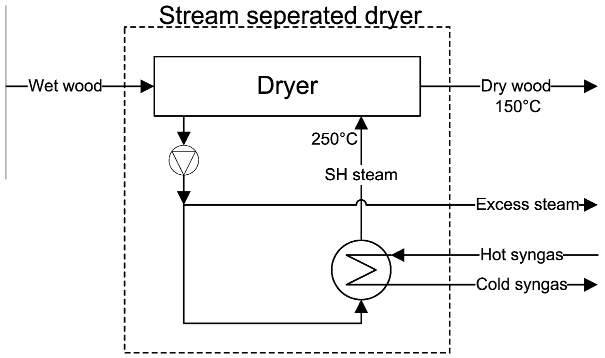

Fig. 3. Layout of the modelled dryer.

No heat losses are taken into account. Introducing heat losses from the gas cleaner will only affect the heat production from the condenser because the temperature after the condenser is fixed at 50 °C.

The district heating water is assumed to be 30 °C at the inlet and 80 °C at the outlet.

4. Results and discussion

In this section, the inputs presented in the previous sections are used unless otherwise stated. The different system configurations are described in detail in Section 2.

The performance of the different system configurations vary greatly with the operating conditions and the chosen pressure ratio

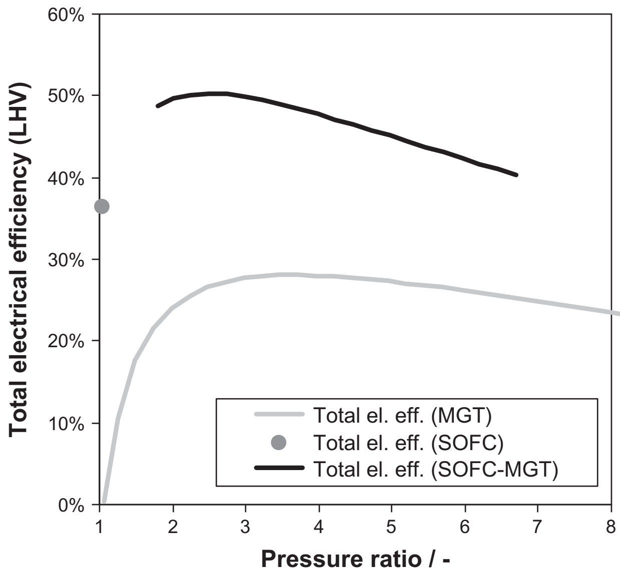

Fig. 4a. Energetic electric efficiency at different operating pressure ratios. The operating pressure ratio is defined over the air compressor.

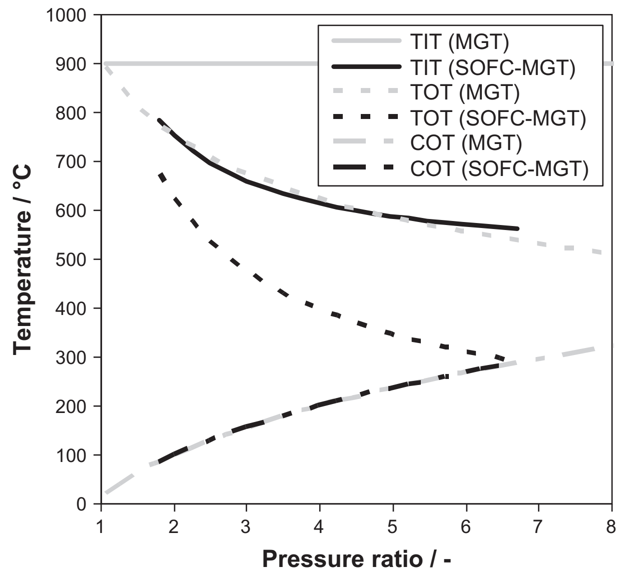

Fig. 4b. Turbine inlet temperature (TIT), turbine outlet temperature (TOT) and air compressor outlet temperature (COT) at different operating pressure ratios. Only the two pressurised system scenarios are illustrated.

is of great importance to the resulting system performance. The different system configurations have different optima with regard to this operating pressure ratio. This relationship can be seen in Fig. 4a. In Fig. 4b, the corresponding turbine inlet temperatures (TIT), turbine outlet temperatures (TOT) and air compressor outlet temperatures (COT) are shown. When operating at a constant TIT of 900 °C, the Gasifier–MGT configuration shows an optimum at a pressure ratio of 3.7, performing with an electric efficiency of 28.1% (energetic and based on LHV). The recuperator ensures an optimum at a relatively low pressure ratio. Obviously, the pressure in the Gasifier–SOFC case is constantly near atmospheric pressure. This system performs at an electrical efficiency of 36.4%. The Gasifier–SOFC configuration has a higher efficiency because conversion in the SOFC is more efficient than that in the MGT, but the SOFC cannot utilise all of the fuel. With a fuel utilisation rate of 85%, a substantial portion of the fuel passes through the anode and is converted to heat in the burner. By combining the SOFC and MGT in the Gasifier–SOFC–MGT configuration, this heat can be used for further electricity production. At the optimum operating pressure ratio of 2.5, the combined system configuration reaches an electrical efficiency of 50.3%, thereby outperforming the two simpler configurations. The substantial increase in efficiency is mainly the result of better utilisation of unconverted fuel from the SOFC, but it is also due to the pressurised operation of the SOFC.

In the Gasifier–SOFC–MGT arrangement, the TIT decreases with an increasing pressure ratio. This relationship is due to the fact that an increasing *PR* increases the COT and reduces the TOT, which means that less heat is transferred in the recuperator. Therefore, more heat must be transferred in the SOFC air preheater to reach the same cathode inlet temperature. More heat transfer in the SOFC air preheater results in a lower temperature of the cathode off gas fed to the burner, thus decreasing the TIT. Furthermore, the TIT is lower in the Gasifier–SOFC–MGT case compared to the Gasifier–MGT scenario because less fuel is used to produce heat. A TIT of 697 °C is reached at a *PR* = 2.5. The optimal *PR* is lower in the Gasifier–SOFC–MGT scenario relative to the Gasifier–MGT arrangement due to the lower TIT. Characteristically, lowering the TIT of a recuperated gas turbine will lower the optimal *PR*. The slight increase in the SOFC efficiency observed with increasing pressure is not sufficient to change the resulting electrical efficiency trend of the hybrid system. Note that above a *PR* of approximately 6.7 in the Gasifier–SOFC–MGT case, the TOT becomes lower than the COT, making it impossible to use a recuperator. Below a *PR* = 1.8, the heat transfer in the recuperator is sufficiently high to heat the air above the desired cathode inlet temperature.

The Gasifier–MGT system performance is also dependent on the allowed TIT as depicted in Fig. 5. Decreasing the TIT by 100 °C to 800 °C lowers the electrical efficiency to 25.4% – a drop of 2.7 percentage points. Considering the Gasifier–SOFC case, the sensitivity to the SOFC operating temperature is even greater. Lowering the SOFC operating temperature by 100 °C to 700 °C decreases the electrical efficiency to 28.8% – a drop of 7.6 percentage points. This differential effect indicates that the SOFC operating temperature has a greater influence on SOFC performance than the TIT has on MGT performance. In the Gasifier–SOFC–MGT configuration, a drop in the SOFC operating temperature by 100–700 °C decreases the electrical efficiency to 44.4% – a drop of 5.9 percentage points. The resulting TIT in the Gasifier–SOFC–MGT scenario shows dampened sensitivity to the chosen SOFC operating temperature because the SOFC air and fuel preheaters transfer more heat at higher SOFC operating temperatures to ensure maintenance of the temperature gradients across the anode and cathode. Therefore, temperatures of the SOFC off gases fed to the burner are not significantly affected by variation of the SOFC operating temperature.

The progress in research and development aimed at lowering the SOFC operating temperature may facilitate the use of cheaper materials, but will also influence system performance. If this is the case, other bottoming cycles could be beneficial, e.g., a Rankine cycle. An MGT development that allows for a higher TIT and an SOFC development that enables lowering of the SOFC temperature could lessen the gap between the electrical efficiencies of the Gasifier–MGT and the Gasifier–SOFC configurations.

An important aspect of SOFC systems is SOFC cooling. Given that the SOFC inlet and outlet temperatures are fixed, air flow through the cathode is determined by the cooling requirement of the SOFC in order to maintain a certain operating temperature. In Fig. 6, the cathode inlet temperature is varied. It is equivalent to changing the temperature gradient across the cathode (ΔT_c). A higher inlet temperature (a lower ΔT_c) decreases the electrical efficiency of the system. This effect is more pronounced in the Gasifier–SOFC–MGT configuration than in the Gasifier–SOFC configuration. An increase in the cathode inlet temperature from 600 to

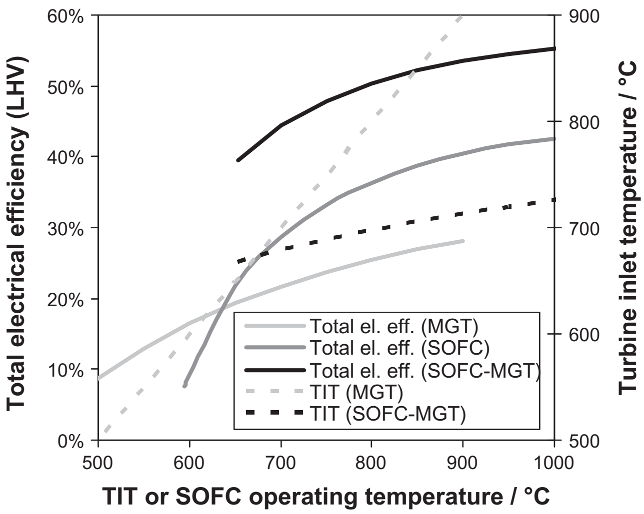

Fig. 5. Energetic electric efficiency and TIT at different TIT or SOFC operating temperatures. The TIT in the Gasifier–MGT case is defined at the gas turbine inlet and the SOFC operating temperature in the two other configurations is defined at the anode/cathode outlets. The maximum allowed TIT is 900 °C.

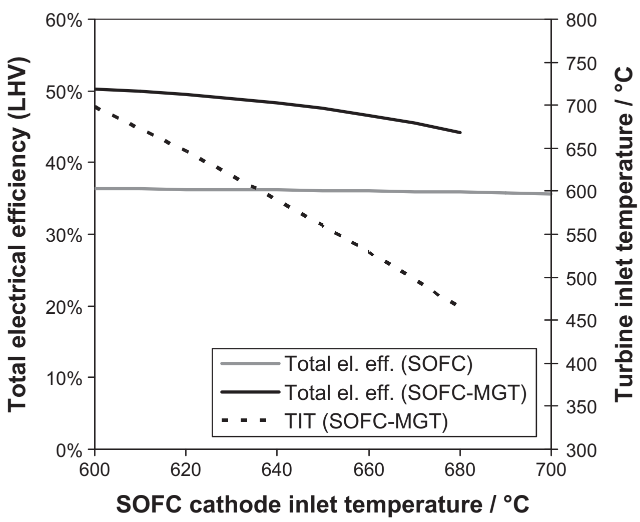

Fig. 6. Energetic electrical efficiency and TIT as a function of SOFC cathode inlet temperature.

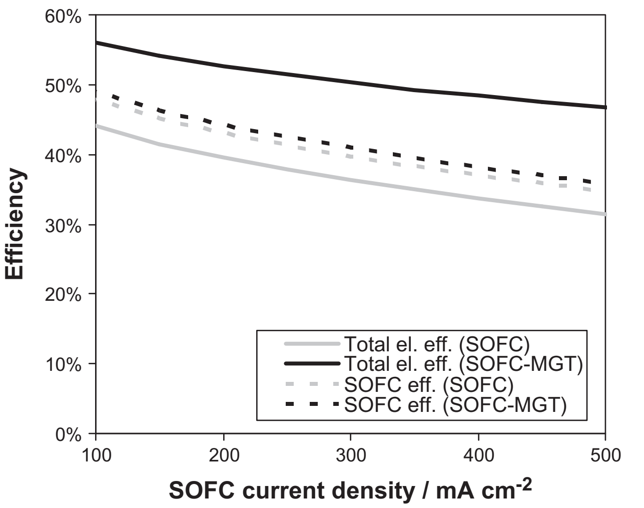

Fig. 7. System electrical efficiency and SOFC efficiency as a function of SOFC current density.

Table 6
Key data for the studied system configurations.

	Gasifier–MGT	Gasifier–SOFC	Gasifier–SOFC–MGT
Biomass throughput/kg h^{-1}	154.8	154.8	154.8
Energetic biomass input/kW$_{th}$ (LHV)	499.2	499.2	499.2
Exergetic biomass input ($ex_{biomass}$)/kW	572.4	572.4	572.4
Exergetic air input (ex_{air})/kW	6.6	6.6	6.6
PR/–	3.7	1.04	2.5
MGT net power production/kW$_{el}$	140.1	–	59.2
SOFC net power production/kW$_{el}$	–	181.5	191.8
Total net power production/kW$_{el}$	140.1	181.5	251.0
District heating production/kJ s^{-1}	239.7	216.6	146.7
η_{el}/% (LHV)	28.1	36.4	50.3
η_{CHP}/% (LHV)	76.1	79.7	79.7
$\eta_{ex,el}$/%[a]	24.2	31.3	43.4
$\eta_{ex,CHP}$/%[b]	65.6	68.8	68.7

[a] Defined as $\eta_{ex,el} = P_{net,tot}/(ex_{biomass} + ex_{air})$.
[b] Defined as $\eta_{ex,CHP} = (P_{net,tot} + Q_{DH})/(ex_{biomass} + ex_{air})$.

680 °C results in a decrease in the electrical efficiency of the Gasifier–SOFC–MGT arrangement from 50.3% to 44.1%, while it only drops from 36.4% to 35.9% in the Gasifier–SOFC configuration. In the Gasifier–SOFC scenario, the air compressor (working as a blower) consumes more power when the ΔT_c is decreased because a higher mass flow of air must be fed to the cathode to ensure a

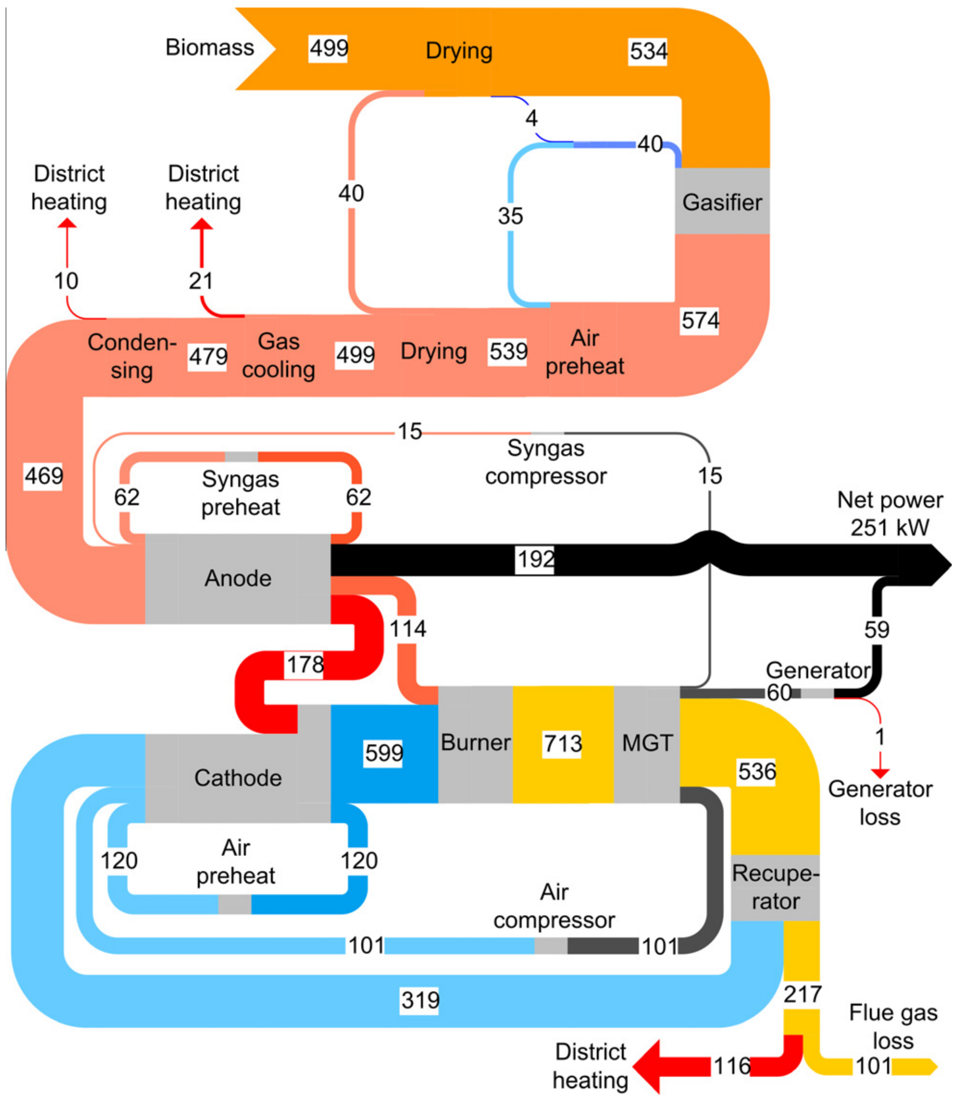

Fig. 8. Sankey diagram of the energy flows (rounded values in [kJ s^{-1}]) in the Gasifier–SOFC–MGT arrangement.

constant SOFC operating temperature. Thus, the parasitic losses increase, which in turn, slightly lower the electrical efficiency of the system. In the Gasifier–SOFC–MGT arrangement, the higher mass flow of air also passes through the MGT expander, thereby compensating for the greater air compressor work. The higher sensitivity to the chosen cathode inlet temperature in the Gasifier–SOFC–MGT scenario is explained by the following two facts: one, a lower ΔT_c results in a lower temperature of the cathode off gas fed to the burner (more heat transfer in the SOFC air preheater) and thus results in a lower TIT; and two, a lower ΔT_c necessitates a higher mass flow of air to maintain the same SOFC operating temperature, which ensures a more lean mixture in the burner and thereby decreases the TIT. Therefore, lowering the ΔT_c lowers the TIT, which decreases the MGT output and hence the electrical efficiency of the Gasifier–SOFC–MGT system.

The sensitivity of the model results to the chosen SOFC current density is shown in Fig. 7. At the reference current density value of 300 mA cm^{-2}, the total SOFC efficiency ($= \eta_{rev}\eta_v U_F$) is 39.6% in the Gasifier–SOFC arrangement and 40.8% in the Gasifier–SOFC–MGT case. The difference in SOFC efficiencies is due to the higher SOFC operating pressure in the Gasifier–SOFC–MGT case. Raising the SOFC load to 500 mA cm^{-2} reduces the SOFC efficiencies to 34.6% and 35.7% in the Gasifier–SOFC and Gasifier–SOFC–MGT cases, respectively. These decreases result in reductions in the total electrical efficiencies to 31.5% and 46.7%, respectively – equivalent to respective losses of 4.9% and 3.6 percentage points. These losses cause relative changes in electrical efficiency of 13.5% and 7.2%, respectively, for a 66.7% increase in current density. Therefore, the model is only moderately sensitive to the chosen current density. Furthermore, it is evident that a downstream MGT can raise the electrical efficiency of the total system above the performance of the SOFC alone. As mentioned earlier, this benefit is due to the utilisation of excess fuel from the SOFC.

Key data for the three studied system configurations are presented in Table 6. The respective optimal pressure ratio is used in each configuration as well as the reference input values presented in the previous sections. The Gasifier–SOFC–MGT configuration clearly has the best energetic- and exergetic-based electrical efficiency, while the CHP efficiencies do not significantly differ. In the Gasifier–SOFC–MGT case, power production is mainly derived from the SOFC, which produces 76.4% of the power. The exact efficiencies will be slightly lower when incorporating heat losses. Despite the neglected of heat losses, the comparisons of the systems' performances are still valid.

A Sankey diagram of the energy flows in the Gasifier–SOFC–MGT configuration is presented in Fig. 8. The Sankey diagram clearly shows the flow of energy, e.g. it clearly shows that heat is transferred from the anode to the cathode and that the flue gas loss from the exhaust of the hybrid system is approximately 100 kJ s^{-1}. In addition, it is evident that approximately 50% of the fuel is converted into electric power, while about 29% of it is used for district heating.

5. Conclusion

A study on the system performance of an up scaled Viking gasifier (~500 kW$_{th}$) with either a downstream MGT, SOFC or both has been conducted by process modelling combining zero-dimensional component models. An SOFC submodel has been developed, including an electrochemical model, which predicts the SOFC performance at different operating conditions. This submodel has been calibrated against published stack performance data from Topsoe Fuel Cell A/S.

For the two pressurised system configurations, the optimal operating pressure ratio was found to be 3.7 when using a recuperated MGT and 2.5 when using an SOFC–MGT combination. Inclusion of an SOFC lowers the TIT (less fuel is converted to heat), thereby lowering the optimal pressure ratio. Operation of the syngas fuelled SOFC alone was performed at atmospheric pressure. The SOFC converted the syngas more efficiently than the MGT, which is reflected in the efficiency of the gasifier and MGT system configuration in opposition to the efficiency of the gasifier and SOFC configuration – η_{el} = 28.1% ($\eta_{ex,el}$ = 24.2%) versus η_{el} = 36.4% ($\eta_{ex,el}$ = 31.3%). Combining the two technologies achieved the highest efficiency of η_{el} = 50.3% ($\eta_{ex,el}$ = 43.4%) due to the efficient SOFC, utilisation of unconverted syngas from the SOFC in the MGT and pressurisation of the SOFC.

The calculated efficiencies were very sensitive to the chosen pressure ratio and SOFC operating temperature (or TIT in the Gasifier–MGT arrangement), whereas only moderate sensitivity to the temperature difference across the SOFC cathode and the SOFC current density was observed. From a system efficiency point of view, it is concluded that inclusion of an SOFC necessitates maintaining a high SOFC operating temperature and maximising the cathode temperature gradient and that inclusion of a recuperated MGT permits determination of the optimal pressure ratio.

Acknowledgement

The authors would like to thank Dr. Braun, Colorado School of Mines, for his contribution to the development of the SOFC electrochemical model.

References

[1] Alderucci V, Antonucci PL, Maggio G, Giordano N, Antonucci V. Thermodynamic analysis of SOFC fuelled by biomass-derived gas. Int J Hydrogen Energy 1994;19:369–76.
[2] Hutton PN, Musich MA, Patel N, Schmidt DD, Timpe RC. Feasibility study of a thermally integrated SOFC-gasification system for biomass power generation, US Department of Energy, National Energy Technology Laboratory Cooperative Agreement, Phase 1, Interim report, No. DE-FC26-98FT40321, Energy and Environmental Research Center, University of North Dakota; 2003.
[3] Omosuna AO, Bauen A, Brandon NP, Adjiman CS, Hart D. Modelling system efficiencies and costs of two biomass-fuelled SOFC systems. J Power Sources 2004;131:96–106.
[4] Cordiner S, Feola M, Mulone V, Romanelli F. Analysis of a SOFC energy generation system fuelled with biomass reformate. Appl Therm Eng 2007;27:738–47.
[5] Panopoulos KD, Fryda LE, Karl J, Poulou S, Kakaras E. High temperature solid oxide fuel cell integrated with novel allothermal biomass gasification Part I: modelling and feasibility study. J Power Sources 2006;159:570–85.
[6] Panopoulos KD, Fryda L, Karl J, Poulou S, Kakaras E. High temperature solid oxide fuel cell integrated with novel allothermal biomass gasification Part II: exergy analysis. J Power Sources 2006;159:586–94.
[7] Karellas S, Karl J, Kakaras E. An innovative biomass gasification process and its coupling with microturbine and fuel cell systems. Energy 2008;33:284–91.
[8] Fryda L, Panopoulos KD, Karl J, Kakaras E. Exergetic analysis of solid oxide fuel cell and biomass gasification integration with heat pipes. Energy 2008;33:292–9.
[9] Dayton DC, Ratcliff M, Bain R. Fuel cell integration – a study of the impacts of gas quality and impurities, US Department of Energy Report, NREL/MP-510-30298; 2001. p. 16.
[10] Rasmussen JFB, Hagen A. The effect of H_2S on the performance of Ni-YSZ anodes in solid oxide fuel cells. J Power Sources 2009;191:534–41.
[11] Barchewitz L, Palsson J. Design of an SOFC system combined to the gasification of biomass. In: McEvoy AJ, editor. Proceedings of the 4th European SOFC Forum, Lucerne, vol. 1; 2000. p. 59–68.
[12] Sucipta M, Kimijima S, Suzuki K. Performance analysis of the SOFC–MGT hybrid system with gasified biomass fuel. J Power Sources 2007;174:124–35.
[13] Fryda L, Panopoulos KD, Kakaras E. Integrated CHP with autothermal biomass gasification and SOFC–MGT. Energy Convers Manage 2008;49:281–90.
[14] Henriksen U, Ahrenfeldt J, Jensen TK, Gøbel B, Bentzen JD, Hindsgaul C, et al. The design, construction and operation of a 75 kW two-stage gasifier. Energy 2006;31:1542–53.
[15] Ahrenfeldt J, Henriksen U, Jensen TK, Gøbel B, Wiese L, Kather A, et al. Validation of a Continuous Combined Heat and Power (CHP) Operation of a Two-Stage Biomass Gasifier. Energy Fuels 2006;20:2672–80.
[16] Hofmann P, Schweiger A, Fryda L, Panopoulos KD, Hohenwarter U, Bentzen JD, et al. High temperature electrolyte supported Ni-GDC/YSZ/LSM SOFC operation on two-stage Viking gasifier product gas. J Power Sources 2007;173:357–66.

[17] Elmegaard B, Houbak N. DNA – a general energy system simulation tool. In: Amundsen J et al., editors. SIMS 2005 46th conference on simulation and modeling. Trondheim: Tapir Academic Press; 2005. p. 43–52.
[18] Smith JM, Van Ness HC, Abbott MM. Introduction to chemical engineering thermodynamics, 7th ed.. Boston: McGraw-Hill; 2005.
[19] Chan SH, Khor KA, Xia ZT. A complete polarization model of a solid oxide fuel cell and its sensitivity to the change of cell component thickness. J Power Sources 2001;93:130–40.
[20] Aloui T, Halouani K. Analytical modeling of polarizations in a solid oxide fuel cell using biomass syngas product as fuel. Appl Therm Eng 2007;27:731–7.
[21] Larminie J, Dicks A. Fuel cell systems explained, 2nd ed. West Sussex: John Wiley & Sons Ltd.; 2003.
[22] Calise F, Dentice d'Accadia M, Palombo A, Vanoli L. Simulation and exergy analysis of a hybrid Solid Oxide Fuel Cell (SOFC)–Gas Turbine System. Energy 2006;31:3278–99.
[23] Mogensen M, Lindegaard T. The kinetics of hydrogen oxidation on a Ni-YSZ SOFC electrode at 1000degC. In: Singal SC, Iwahara T, editors. Solid oxide fuel cells, 3. International symposium on solid oxide fuel cells, Honolulu, USA, The Electrochemical Society Proceedings Series, Pennington, NJ; 1993. p. 484–93.
[24] Mogensen M. Electrode kinetics of SOFC anodes and cathodes. In: Poulsen FW, et al., editors. Proceedings of the 14th Risø international symposium on material science, high temperature electrochemical behaviour of fast ion and mixed conductors, Risø National Laboratory, Roskilde, Denmark; 1993. p. 117–35.
[25] Achenbach E. Three-dimensional and time-dependent simulation of a planar solid oxide fuel cell stack. J Power Sources 1994;49:333–48.
[26] Chan SH, Low CF, Ding OL. Energy and exergy analysis of simple solid-oxide fuel-cell power systems. J Power Sources 2002;103:188–200.
[27] Bessette II NF, Wepfer WJ, Winnick J. A mathematical model of a solid oxide fuel cell. J Electrochem Soc 2005;142:3792–800.
[28] Linderoth S, Larsen PH, Mogensen M, Hendriksen PV, Christiansen N, Holm-Larsen H. Solid Oxide Fuel Cell (SOFC) Development in Denmark. Mater Sci Forum 2007;539–543:1309–14.
[29] Saravanamuttoo HIH, Rogers GFC, Cohen H, Straznicky PV. Gas turbine theory, 6th ed.. Essex, Berlin: Pearson Education Ltd.; 2009 [ISBN 978-0-12-222437-6].

Appendix H PAPER II

Proceedings Paper - Peer Reviewed Manuscript
Bang-Møller C., Rokni M. Modelling a Combined Heat and Power Plant based on Gasification, Micro Gas Turbine and Solid Oxide Fuel Cells. In: Elmegaard B., Veje C., Nielsen M.P., Mølbak T. (eds.), *Proceedings of SIMS 50: Modelling of Energy Technology*. ISBN 978-87-89502-88-5. The Technical University of Denmark. Fredericia, Denmark. 2009, pp. 189-196.

Presented at the SIMS 50 Conference in October 2009 in Fredericia, Denmark.

Proceedings of SIMS 50
Fredericia, Denmark
October 7–8, 2009

MODELLING A COMBINED HEAT AND POWER PLANT BASED ON GASIFICATION, MICRO GAS TURBINE AND SOLID OXIDE FUEL CELLS

Christian Bang-Møller* **and Masoud Rokni**
Technical University of Denmark
Department of Mechanical Engineering
2800 Kgs. Lyngby
Denmark

ABSTRACT

A system level modelling study on two combined heat and power (CHP) systems both based on biomass gasification. One system converts the product gas in a micro gas turbine (MGT) and the other in a combined solid oxide fuel cell (SOFC) and MGT arrangement. An electrochemical model of the SOFC has been developed and calibrated against published data from Topsoe Fuel Cells A/S (TOFC) and Risø National Laboratory, and the modelled gasifier is based on an up scaled version of the demonstrated low tar gasifier, Viking, situated at the Technical University of Denmark. The SOFC converts the syngas more efficient than the MGT reflected in the electrical efficiency of the gasifier and MGT system in opposition to the gasifier and SOFC-MGT configuration - η_{el}=28.1% versus η_{el}=50.3%.

Keywords: System modelling, biomass gasification, micro gas turbine, SOFC

NOMENCLATURE

a_{ohm}, b_{ohm}	coefficients for Eq. (24)
ASR	area specific resistance
E	reversible open circuit voltage
F	Faradays constant
g_f	Gibbs free energy of formation
i	current density
LHV	lower heating value
$\dot{n}$	molar flow
n_e	transferred electrons per molecule of fuel
p	pressure/partial pressure
P	power production
R	universal gas constant
T	temperature
UF	fuel utilization factor for SOFC
V	potential/overpotential
y	molar fraction
δ	SOFC layer thickness
η	efficiency

Subscripts:

a	anode
c	cathode
con	consumption
e	electrolyte
i	interconnect

INTRODUCTION

Development of sustainable and efficient production plants of combined heat and power (CHP) tends to gain more attention as climate changes, security of supply and depletion of fossil fuels have become well known issues. The share of biomass in CHP production are expected to increase in the future and decentralized CHP plants are also of interest to avoid costs of biomass transportation. Efficient power producing technologies for small scale productions are typically gas engines, micro gas turbines (MGT) and fuel cells – all requiring gaseous fuel. Gasification can deliver biomass based gaseous fuel so the combination of biomass gasification and efficient syngas conversion are potentially a sustainable and efficient CHP plant.

Solid oxide fuel cells (SOFCs) can electrochemically convert H_2 and CO as well as internally reform CH_4 into more H_2 and CO due to their high operating temperature. This makes SOFCs very fuel flexible and ideal for converting syngas compared to other fuel cell types.

The performance and system design of integrated biomass gasifier and SOFC systems in the 100-

* Corresponding author: Email: chrbm@win.dtu.dk Phone: +45 45254123

$1000kW_e$ class have been investigated by several. An innovative design including heat pipes between a SOFC stack and an allothermal gasifier is described in [1]. Fryda et al. [2] studies the performance of a CHP system of less than $1MW_e$ and consisting of an autothermal gasifier combined with a MGT and/or SOFC.

This study focus on the performance of a system combining an up scaled version (~$500kW_{th}$) of the two-stage gasifier named Viking and a MGT or a SOFC-MGT system. Viking is a $75kW_{th}$ autothermal (air blown) fixed bed biomass gasifier demonstrated at the Technical University of Denmark and it is described in detail in [3]. The Viking gasifier produces almost no tars, which is favourable for downstream SOFC operation. Hofmann et al. [4] has operated a SOFC on cleaned syngas from the Viking gasifier for 150 hours without degradation.

The present study is based on zero dimensional and steady-state modelling in the simulation tool DNA [5]. DNA has incorporated thermodynamic property data, is component based and is developed at The Technical University of Denmark.

SYSTEM DESCRIPTION

Two different combined heat and power systems are investigated in this study, both based on syngas production from an up scaled Viking gasifier. A flow sheet of the two systems is depicted in Figure 1. The modelled gasifier system is slightly simplified, but aims at the same resulting gas composition and cold gas efficiency as for the Viking gasifier. In the gasifier model the dryer is heated by hot syngas. The steam production from the dryer is added to the preheated air and dry wood and mixed air and steam are fed to the gasifier. The raw product gas are cooled to 90°C in three steps; air preheating, wood drying and syngas cooling producing hot water for district heating. The cooled syngas are then cleaned from impurities as particles and sulphur compounds before some of the water in the gas are condensed through cooling to 50°C. The cleaned and partly dried syngas are then converted into electricity and heat in a bottoming cycle consisting of a MGT or both a SOFC and a MGT. These two system configurations will from now on be referred as the Gasifier-MGT and the Gasifier-SOFC-MGT configuration, respectively. In the Gasifier-SOFC-MGT configuration all the components in the flow sheet are in use. With respect to Figure 1 the SOFC and preheaters are bypassed in the Gasifier-MGT arrangement. In addition the syngas compressor works as a roots blower for the gasifier system and not illustrated is a generator.

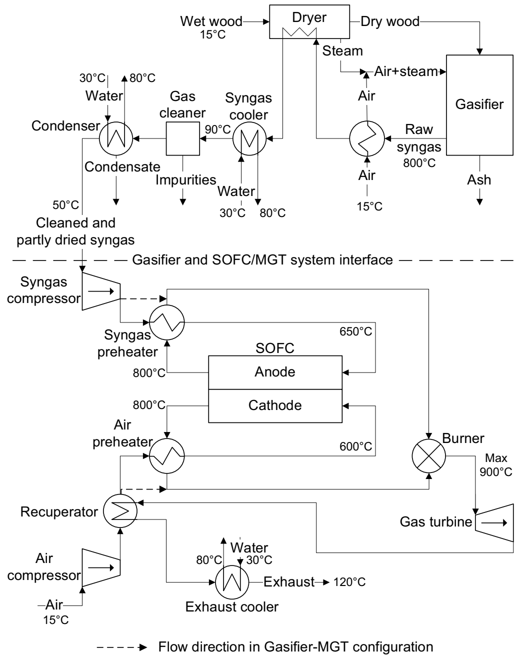

Figure 1: Flow sheet of the hybrid systems

Operating pressure	$p_{gasifier}$	0.998 bar
Operating temperature	$T_{gasifier}$	800°C
Pressure loss	$\Delta p_{gasifier}$	5 mbar
Non-equilibrium methane	*METH*	0.01

Table 1: Inputs to the gasifier submodel

GASIFIER MODEL

The gasifier component calculates the produced syngas composition as well as the produced ashes based on the inlet media composition and the operating conditions. The input parameters defining the operating conditions for the gasifier submodel are given in Table 1. The gasifier pressure loss is defined as the difference between the inlet air and steam mixture and the outlet syngas.

In the gasifier the incoming flows are converted into a syngas and ashes. The ashes come from a defined content in the biomass. The syngas can consist of the following species: H_2, O_2, N_2, CO, NO, CO_2, H_2O, NH_3, H_2S, SO_2, CH_4, NO_2, HCN, COS and Ar. It is assumed that equilibrium is reached at the operating temperature and pressure, where the total Gibbs energy has its minimum value. With this assumption the syngas outlet composition can be found by the Gibbs minimization method [6]. A possibility for bypassing an amount of methane from the equilibrium calculations is added in order to reach syngas compositions, which contain more methane than the corresponding one at equilibrium. Thus the syngas composition can be adjusted to match real syngas compositions, e.g. from the Viking gasifier. The input parameter *METH* is used for this bypassing and is defined as the fraction of the methane that is not included in the equilibrium calculations and instead flows through the gasifier and appears in the outlet syngas.

Gasifier model validation

The model validation for the gasifier is done for all of the gasification plant from the biomass input to the cleaned and dried syngas. Thus the data from the Viking gasifier plant can be used for validation.

Wood chips from beech with small amounts of oak are used in the modelling as for the Viking gasifier reported in Ahrenfeldt et al. [3].

As seen in Table 2 the produced syngas composition and the lower heating value (LHV) from the gasifier model is close to the Viking data. The overall performance of the modelled gasifier is also similar to the Viking gasifier expressed in the cold gas efficiencies.

	Viking [3]	Gasifier model
H_2 (vol-%)	30.5	29.9
CO (vol-%)	19.6	20.8
CO_2 (vol-%)	15.4	13.5
CH_4 (vol-%)	1.16	1.19
N_2 (vol-%)	33.3	34.2
LHV (MJ/kg)	6.2	6.3
Cold gas eff.	93%	94%

Table 2: Dry syngas composition, lower heating value as well as cold gas efficiency for the Viking gasifier and the modelled gasifier, respectively

SOLID OXIDE FUEL CELL MODEL

The SOFC stack component calculates the air and fuel outlet compositions as well as the power production. The calculations are based on the inlet air and fuel compositions and flow rates as well as the other operating conditions of the SOFC. The SOFC submodel includes an electrochemical model for predicting the performance of the SOFC. The operating conditions are partly described by input parameters given to the SOFC submodel and these are presented in Table 3.

Fuel utilization factor	*UF*	0.85
Operating temperature	T_{SOFC}	800°C
Anode pressure loss	Δp_a	5 mbar
Cathode pressure loss	Δp_c	10 mbar
Current density	*i*	300 mA cm^{-2}

Table 3: Inputs to the SOFC submodel

In the submodel only H_2 is electrochemically converted in the SOFC anode, but the model takes into account that CO produces an extra H_2 through the water-gas-shift (WGS) reaction, while four additional H_2 molecules are produced from CH_4 through internal steam reforming and WGS of produced CO (full conversion is assumed). The total mole flow of H_2 on the anode after internal steam reforming and WGS is expressed in Eq. (1).

$$\dot{n}_{H_2,tot} = \dot{n}_{H_2,in} + \dot{n}_{CO,in} + 4\dot{n}_{CH_4,in} \tag{1}$$

$$H_2 + O^{2-} \rightarrow H_2O + 2e^- \tag{2}$$

$$\tfrac{1}{2}O_2 + 2e^- \rightarrow O^{2-} \tag{3}$$

$$H_2 + \tfrac{1}{2}O_2 \rightarrow H_2O \tag{4}$$

The amount of hydrogen that is converted depends on the fuel utilization factor (*UF*) and this amount is electrochemically converted in the anode. The electrode reactions and the overall fuel cell reaction are as shown in Eq. (2) to (4).

From the overall fuel cell reaction it is seen that the amount of consumed oxygen is half the amount of consumed hydrogen. The cathode outlet composition can then be found by the following equations if the only species taking into account are O_2, N_2, CO_2, H_2O and Ar.

$$\dot{n}_{O_2,con} = \frac{UF\dot{n}_{H_2,in}}{2} \tag{5}$$

$$\dot{n}_{c,out} = \dot{n}_{c,in} - \dot{n}_{O_2,con} \tag{6}$$

$$y_{O_2,out} = \frac{\dot{n}_{c,in} y_{O_2,in} - \dot{n}_{O_2,con}}{\dot{n}_{c,out}} \quad (7)$$

$$y_{j,out} = \frac{\dot{n}_{c,in} y_{j,in}}{\dot{n}_{c,out}},\ j = \{N_2, CO_2, H_2O\} \quad (8)$$

$$y_{Ar,out} = 1 - y_{O_2,out} - y_{N_2,out} - y_{CO_2,out} - y_{H_2O,out} \quad (9)$$

The fuel composition leaving the anode is calculated by the Gibbs minimization method [6] as described for the gasifier submodel. Equilibrium at the anode outlet temperature and pressure is assumed for the following species: H_2, CO, CO_2, H_2O, CH_4 and N_2. The equilibrium assumption is fair since the methane content in this study is low enough for such kind of assumption to be made. The heat consumed by the endothermic internal reforming reactions is taken into account by the Gibbs minimization method. More internal reforming means more cooling of the SOFC.

The power production from the SOFC depends on the amount of chemical energy fed to the anode, the reversible efficiency (η_{rev}), the voltage efficiency (η_v) and the fuel utilization factor (UF). It is defined in mathematical form in Eq. (10).

$$P_{SOFC} = \begin{bmatrix} LHV_{H_2}\dot{n}_{H_2,in} \\ + LHV_{CO}\dot{n}_{CO,in} \\ + LHV_{CH_4}\dot{n}_{CH_4,in} \end{bmatrix} \eta_{rev}\eta_v UF \quad (10)$$

The reversible efficiency is the maximum possible efficiency defined as the relationship between the maximum electrical energy available (change in Gibbs free energy) and the fuels LHV. This is shown in Eq. (11) and the definition of the change in Gibbs free energy is shown in Eq. (12). The voltage efficiency express the electrochemical performance of the SOFC and the calculation of the voltage efficiency is described in the following subsection.

$$\eta_{rev} = \frac{(\Delta \bar{g}_f)_{fuel}}{LHV_{fuel}} \quad (11)$$

$$\begin{aligned}(\Delta \bar{g}_f)_{fuel} &= \left[(\bar{g}_f)_{H_2O} - (\bar{g}_f)_{H_2} - \tfrac{1}{2}(\bar{g}_f)_{O_2}\right] y_{H_2,in} \quad (12)\\ &+ \left[(\bar{g}_f)_{CO_2} - (\bar{g}_f)_{CO} - \tfrac{1}{2}(\bar{g}_f)_{O_2}\right] y_{CO,in} \\ &+ \left[(\bar{g}_f)_{CO_2} + 2(\bar{g}_f)_{H_2O} - (\bar{g}_f)_{CH_4} - 2(\bar{g}_f)_{O_2}\right] y_{CH_4,in}\end{aligned}$$

Electrochemical model

The electrochemical model is used to calculate the cell potential and the voltage efficiency of the SOFC. Both depend on the operating conditions such as temperature, pressure, gas compositions, fuel utilization and load (current density). The cell potential and voltage efficiency is defined in Eq. (13) and (14), respectively.

$$V_{cell} = E - V_{act} - V_{ohm} \quad (13)$$

$$\eta_v = \frac{V_{cell}}{E} \quad (14)$$

In the following the reversible open circuit voltage (E), the activation overpotential (V_{act}) and the ohmic overpotential (V_{ohm}) are calculated. Traditionally a concentration overpotential term is included in Eq. (13). The concentration overpotential is a result of the limitations of transporting the reactants to the active cell area. In Larminie et. al. [7] it is described as a voltage drop caused by the pressure change associated with the consumption of reactants. As a result of the current being drawn from the cell the average partial pressure of reactants is lower than at the inlet. Thus, in this study the concentration overvoltage is taken into account by using average partial pressures when calculating E and V_{act}.

E can be calculated from the Nernst equation:

$$E = \frac{-\Delta \bar{g}_f^{\,0}}{n_e F} + \frac{RT}{n_e F}\ln\left(\frac{\bar{p}_{H_2,tot}\sqrt{\bar{p}_{O_2}}}{\bar{p}_{H_2O}}\right) \quad (15)$$

Since it is assumed that all CO and CH_4 are converted to H_2 before the electrochemical reactions takes place, the change in standard Gibbs free energy ($\Delta \bar{g}_f^{\,0}$) and the number of electrons transferred for each molecule of fuel (n_e) is determined for the reaction of H_2 only. Thus, n_e = 2 and $\Delta \bar{g}_f^{\,0} = (\bar{g}_f^{\,0})_{H_2O} - (\bar{g}_f^{\,0})_{H_2} - \frac{1}{2}(\bar{g}_f^{\,0})_{O_2}$. The partial pressure of species j is an average across the respective electrode and is here defined as an arithmetic mean between inlet and outlet as shown in Eq. (16) and (17). The average partial pressure of available hydrogen after internal steam reforming and WGS of CH_4 and CO can be determined from the overall steam reforming and WGS reaction including all species. It is defined in Eq. (18):

$$\overline{p}_j = \left(\frac{y_{j,\text{out}} - y_{j,\text{in}}}{2} \right) p_\text{a}, \quad (16)$$

$$j = \{\text{H}_2, \text{CO}, \text{CH}_4, \text{CO}_2, \text{H}_2\text{O}, \text{N}_2\}$$

$$\overline{p}_{\text{O}_2} = \left(\frac{y_{\text{O}_2,\text{out}} - y_{\text{O}_2,\text{in}}}{2} \right) p_\text{c} \quad (17)$$

$$\overline{p}_{\text{H}_2,\text{tot}} = \left(\frac{\overline{p}_{\text{H}_2} + \overline{p}_\text{CO} + 4\overline{p}_{\text{CH}_4}}{\overline{p}_{\text{H}_2} + \overline{p}_\text{CO} + 3\overline{p}_{\text{CH}_4} + \overline{p}_{\text{CO}_2} + \overline{p}_{\text{H}_2\text{O}} + \overline{p}_{\text{N}_2}} \right) p_\text{a} \quad (18)$$

The activation overpotential is due to an energy barrier (activation energy) that the reactants must overcome in order to drive the electrochemical reactions. The activation overpotential is non-linear and is dominant at low current density (i). The activation overpotential is defined as (cf. [8]):

$$V_\text{act} = V_\text{act,a} + V_\text{act,c} = \frac{2RT}{n_\text{e}F} \left[\sinh^{-1}\left(\frac{i + i_\text{n}}{2i_\text{0,a}} \right) + \sinh^{-1}\left(\frac{i + i_\text{n}}{2i_\text{0,c}} \right) \right] \quad (19)$$

The internal current density (i_n) is added to the actual fuel cell current density in order to account for the mixed potential caused by fuel crossover. The importance of the internal current density in the case of SOFCs is much less than for low temperature fuel cells and the value of i_n is usually very small [7]. The exchange current density (i_0) is a measure of the level of activity on the electrode at i=0 mA cm^{-2} and is defined as (cf. [9]):

$$i_\text{0,a} = 2.13 \times 10^7 \left(\frac{\overline{p}_{\text{H}_2,\text{tot}} \overline{p}_{\text{H}_2\text{O}}}{p_\text{a}^2} \right) \exp\left(\frac{-110000}{RT} \right) \quad (20)$$

$$i_\text{0,c} = 1.49 \times 10^7 \left(\frac{\overline{p}_{\text{O}_2}}{p_\text{c}} \right)^{0.25} \exp\left(\frac{-110000}{RT} \right) \quad (21)$$

The ohmic overpotential is caused by the electrical resistance for the ions passing through the electrolyte as well as for the electrons passing through the electrodes and interconnects. The

R	8.314 J K^{-1} mol^{-1}	
F	96485 C mol^{-1}	
n_e	2	
i_n	2 mA cm^{-2}	[9]
δ_a	750×10^{-4} cm	[10]
δ_c	50×10^{-4} cm	[10]
δ_e	40×10^{-4} cm	[10]
δ_i	100×10^{-4} cm	[11]
$a_\text{ohm,a}$	0.00298×10^{-3} kΩcm	[12]
$b_\text{ohm,a}$	-1392 K	[12]
$a_\text{ohm,c}$	0.00811×10^{-3} kΩcm	[12]
$b_\text{ohm,c}$	600 K	[12]
$a_\text{ohm,e}$	0.00294×10^{-3} kΩcm	[12]
$b_\text{ohm,e}$	10350 K	[12]
$a_\text{ohm,i}$	0.1256×10^{-3} kΩcm	[12]
$b_\text{ohm,i}$	4690 K	[12]

Table 4: Inputs for the electrochemical model

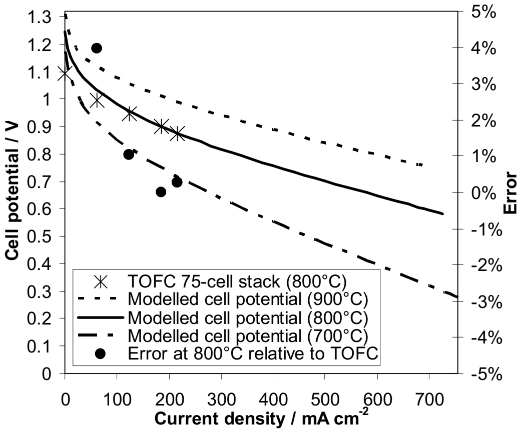

Figure 2: Single cell polarization curves based on a 75-cell stack and the SOFC model, respectively.

ohmic overpotential is defined below (cf. [9] and [12]).

$$V_\text{ohm} = i \, ASR \quad (22)$$

$$ASR = ASR_\text{a} + ASR_\text{c} + ASR_\text{e} + ASR_\text{i} \quad (23)$$

$$ASR_j = \delta_j a_{\text{ohm},j} \exp\left(\frac{b_{\text{ohm},j}}{T} \right), \; j = \{\text{a}, \text{c}, \text{e}, \text{i}\} \quad (24)$$

The thicknesses of the different layers (δ) and the constants a_ohm and b_ohm used are listed in Table 4.

SOFC model calibration

The described electrochemical model has been calibrated against experimental data. Since the model aims at the performance of 2nd generation SOFCs from Topsoe Fuel Cell A/S (TOFC) and Risø National Laboratory, published data from this SOFC type has been used. The *ASR* has been calibrated against a value of 0.15 Ω cm^2 at 850°C as published by [13] and the resulting cell potential has been calibrated against a polarization curve (800°C and fuelled with H_2 and N_2) published by [14]. An active cell area of 81 cm^2 has been assumed. Both modelled and experimental data as well as the error relative to the experimental data are presented in Figure 2.

The model shows excellent agreement with the experimental data above a current density of 100 mA cm^{-2}. The current density of 300 mA cm^{-2} is chosen to represent the SOFC load in the following results.

PERIPHERAL EQUIPMENT

Modelling of peripheral components like compressors, turbines and heat exchangers are standard and therefore not described in detail.

The throughput of wet biomass is 154.8 kg h^{-1} (corresponds to 499.2 kW_{th} (LHV)). Thus it is assumed that the Viking gasifier can be scaled up from a nominal ~75 kW_{th} [3]. The biomass dryer reduces the water content in the biomass from 32.2 wt-% to 5 wt-% by heating it to 150°C and the air for the gasifier is preheated to 780°C by the hot product gas.

The inlet temperature to the SOFC anode and cathode are maintained at 150°C and 200°C below the outlet temperature, respectively.

The pressure loss in every component in the SOFC air supply stream and burner exhaust stream is assumed to be 10 mbar, while the pressure loss in each of the rest of the components is assumed to be 5 mbar, except the burner that has a pressure loss of 0.6‰ (equals 1.5 mbar when 2.5 bar at inlet).

The gas cleaner is a baghouse filter removing particulates and it is assumed that the cleaned syngas can be used directly in a SOFC. The condenser removes some of the water content in the syngas resulting in a content of water in the cleaned and dried syngas of 12.7 vol-%. The resulting steam to carbon ratio (S/C) is 0.41, which is somewhat low, but is justified by the very low tar content in the Viking syngas.

The isentropic and mechanical efficiency of the compressors are 75% and 98%, respectively, and the isentropic efficiency of the MGT expander is 84%. The turbine inlet temperature (TIT) is limited to 900°C in the Gasifier-MGT case, while varied in the Gasifier-SOFC-MGT arrangement. The performance of the compressors and the MGT expander are taken from Fryda et al. [2] and corresponds to common performance data for a MGT of this scale. The recuperator effectiveness is assumed to be 85% and the generator efficiency is assumed to be 99%. In the Gasifier-MGT configuration the burner operating pressure is 3.75 bar and in the Gasifier-SOFC-MGT case the SOFC operating pressure is 2.5 bar (these pressures are varied in the results section).

No heat losses are taken into account. Introducing heat losses from the gas cleaner will only affect the heat production from the condenser since the temperature after the condenser is fixed to 50°C.

The outlet pressure from the MGT depends on the total pressure loss downstream the MGT, since it is the exhaust pressure which is fixed to 1.013 bar. Because of the recuperator and exhaust cooler the outlet pressure from the MGT is 1.033 bar. The district heating (DH) water is assumed to be 30°C at inlet and 80°C at outlet.

RESULTS AND DISCUSSION

In the following results the inputs presented in the previous sections are used unless something else is stated. The system configurations are previously described in detail.

The performance of the different system configurations vary greatly with the operating conditions and namely the pressure ratio of the MGT (in the Gasifier-MGT case) and the operating pressure of the SOFC (in the Gasifier-SOFC-MGT case) are of great importance to the resulting system performance. The two system configurations have different optimum with regard to their operating pressure and these can be seen in Figure 3. When operating at a constant TIT of 900°C the Gasifier-MGT configuration shows an optimum at 3.75 bar performing an electric efficiency of 28.1%. It is the recuperator that ensures an optimum at a relatively low operating pressure. By combining the SOFC and MGT in the Gasifier-SOFC-MGT configuration the electrical efficiency reaches 50.3% at an optimum operating pressure of 2.5 bar. This is a substantial increase in efficiency caused by the efficient SOFC. With a fuel utilization of 85% a part of the fuel passes through the anode, but this amount is used in the MGT. In this case the TIT is varying with the SOFC operating pressure and has a value of 697°C at 2.5 bar.

The Gasifier-MGT system performance also depend on the allowed TIT as depicted in Figure 4. Decreasing the TIT by 100°C to 800°C lowers the electrical efficiency to 25.4% - a drop of 2.7 percentage points. In the Gasifier-SOFC-MGT configuration a drop in SOFC operating temperature by 100°C to 700°C decreases the electrical efficiency to 44.4% - a drop of 5.9 percentage points. This indicates that the SOFC operating temperature has more influence on the SOFC performance than the TIT has on the MGT performance. The research and development working on lowering the SOFC operating temperature in order to use cheaper materials will influence the system performance presented here and potentially other bottoming cycles could be beneficial, e.g. a Rankine cycle.

The sensitivity of the model results to the chosen SOFC current density is shown in Figure 5. At the reference current density value of 300 mA cm^{-2} the SOFC voltage efficiency (defined in Eq. (14)) is 40.8%. Raising the SOFC load to 500 mA cm^{-2} lowers the voltage efficiency to 35.7% meaning a reduction in the total electrical efficiency to 46.7% - a drop of 3.6 percentage points. This is a relative change in electrical efficiency of 7% for a 66.7% increase in current density.

Key data for the two system configurations studied are presented in Table 5 and the respective optimal operating pressure is used in each configuration as well as the reference input values presented in the previous sections. The Gasifier-SOFC-MGT configuration clearly has the best electrical efficiency, while the CHP efficiencies do not differ significantly. In the Gasifier-SOFC-MGT case, the power production is mainly from the SOFC producing 76.4% of the power. The exact values of the efficiencies will be slightly lower when incorporating heat losses, a more accurate efficiency of the gasifier system and possible more extensive gas cleaning, but the comparison of the systems performance is still valid.

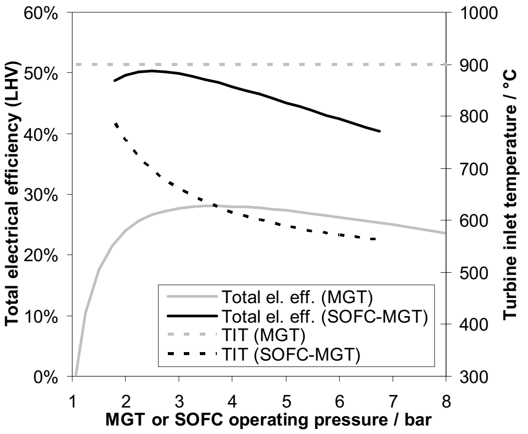

Figure 3: Electric efficiency and TIT at different MGT or SOFC operating pressures

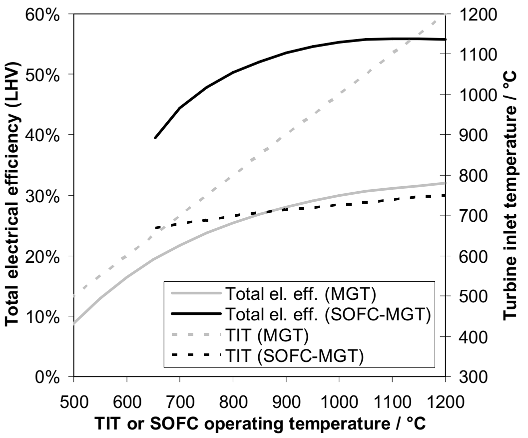

Figure 4: Electric efficiency and TIT at different TIT or SOFC operating temperatures

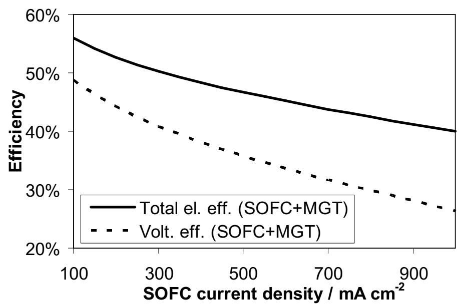

Figure 5: Electrical efficiency and SOFC voltage efficiency as a function of SOFC current density

		Gasifier -MGT	Gasifier -SOFC-MGT
Biomass input	/ kg h^{-1}	154.8	154.8
	/ $kW_{th,LHV}$	499.2	499.2
p_{MGT} or p_{SOFC} / bar		3.75	2.5
$P_{MGT,net}$ / kW_{el}		140.1	59.2
$P_{SOFC,net}$ / kW_{el}		-	191.8
$P_{total,net}$ / kW_{el}		140.1	251.0
DH production / kJ s^{-1}		239.7	146.7
η_{el} / % (LHV)		28.1	50.3
η_{CHP} / % (LHV)		76.1	79.7

Table 5: Key data for the studied systems

CONCLUSION

A study on the system performance of an up scaled Viking gasifier (~500 kW_{th}) with either a downstream MGT or SOFC-MGT has been conducted by zero dimensional process modelling. A SOFC submodel has been developed including an electrochemical model predicting the SOFC performance at different operating conditions. This submodel has been calibrated against published TOFC stack performance data. The reference conditions for the SOFC has been an operating temperature of 800°C, a fuel utilization of 85% and a current density of 300 mA cm^{-2}. The optimal operating MGT and SOFC-MGT pressure has been found for the two system configurations to 3.75 and 2.5 bar, respectively. The SOFC converted the syngas more efficient than the MGT reflected in the efficiency of the gasifier and MGT system configuration in opposition to the gasifier and SOFC-MGT configuration - η_{el}=28.1% versus η_{el}=50.3%. These efficiencies were very sensitive to the SOFC operating temperature (or TIT in the Gasifier-MGT arrangement), while only a moderate sensitivity to the SOFC current density was observed.

REFERENCES

[1] Karellas S, Karl J, Kakaras E. *An innovative biomass gasification process and its coupling with microturbine and fuel cell systems*. Energy 2008;33:284–291.

[2] Fryda L, Panopoulos KD, Kakaras E. *Integrated CHP with autothermal biomass gasification and SOFC–MGT*. Energy Conversion and Management 2008;49:281–290.

[3] Ahrenfeldt J, Henriksen U, Jensen TK, Gøbel B, Wiese L, Kather L, Egsgaard H. *Validation of a Continuous Combined Heat and Power (CHP) Operation of a Two-Stage Biomass Gasifier*. Energy & Fuels 2006;20:2672-2680.

[4] Hofmann Ph, Schweiger A, Fryda L, Panopoulos KD, Hohenwarter U, Bentzen JD, Ouweltjes JP, Ahrenfeldt J, Henriksen U, Kakaras E. *High temperature electrolyte supported Ni-GDC/YSZ/LSM SOFC operation on two-stage Viking gasifier product gas*. J. Power Sources 2007;173:357–366.

[5] Elmegaard B, Houbak N. *DNA – A General Energy System Simulation Tool*, In: Proceedings of the 46th Conf. on Simulation and Modeling, Trondheim, 2005. (cf. http://www.scansims.org/sims2005)

[6] Smith JM, Van Ness HC, Abbott MM. *Introduction to Chemical Engineering Thermodynamics*. 7th ed. Boston: McGraw-Hill, 2005.

[7] Larminie J, Dicks A. *Fuel Cell Systems Explained*. 2nd ed. West Sussex: John Wiley & Sons Ltd., 2003.

[8] Aloui T, Halouani K. *Analytical modeling of polarizations in a solid oxide fuel cell using biomass syngas product as fuel*. Appl. Therm. Eng. 2007;27:731-737.

[9] Calise F, Dentice d'Accadia M, Palombo A, Vanoli L. *Simulation and exergy analysis of a hybrid Solid Oxide Fuel Cell (SOFC)–Gas Turbine System*. Energy 2006;31:3278-3299.

[10] Chan SH, Khor KA, Xia ZT. *A complete polarization model of a solid oxide fuel cell and its sensitivity to the change of cell component thickness*. J. Power Sources 2001;93:130-140.

[11] Chan SH, Low CF, Ding OL. *Energy and exergy analysis of simple solid-oxide fuel-cell power systems*. J. Power Sources 2002;103:188-200.

[12] Bessette NF II, Wepfer WJ, Winnick J. *A Mathematical Model of a Solid Oxide Fuel Cell*. J. Electrochem. Soc. 1995;142:3792-3800.

[13] Christiansen N, Hansen JB, Holm-Larsen H, Linderoth S, Larsen PH, Hendriksen PV, Mogensen M. *Solid oxide fuel cell development at Topsoe Fuel Cell and Risø*. Fuel Cells Bulletin 2006;2006(8):12-15.

[14] Linderoth S, Larsen PH, Mogensen M, Hendriksen PV, Christiansen N, Holm-Larsen H. *Solid Oxide Fuel Cell (SOFC) Development in Denmark*. Materials Science Forum 2007;539-543:1309-1314.

Appendix I PAPER III

Proceedings Paper - Peer Reviewed Abstract

Bang-Møller C., Rokni M. Modelling of a Biomass Gasification Plant Feeding a Hybrid Solid Oxide Fuel Cell and Micro Gas Turbine System. In: Sønderberg P.L., Larsen H.H. (eds.), *Proceedings of Risø International Energy Conference 2009: Energy solutions for* CO_2 *emission peak and subsequent decline*. ISBN 978-87-550-3783-0. Risø National Laboratory for Sustainable Energy. Roskilde, Denmark. 2009, pp. 289-299.

Presented at the Risø International Energy Conference in September 2009 in Roskilde, Denmark.

Modelling of a Biomass Gasification Plant Feeding a Hybrid Solid Oxide Fuel Cell and Micro Gas Turbine System

Christian Bang-Møller* and Masoud Rokni

Technical University of Denmark

Department of Mechanical Engineering

2800 Kgs. Lyngby, Denmark

Abstract

A system level modelling study on two combined heat and power (CHP) systems both based on biomass gasification. One system converts the product gas in a solid oxide fuel cell (SOFC) and the other in a combined SOFC and micro gas turbine (MGT) arrangement. An electrochemical model of the SOFC has been developed and calibrated against published data from Topsoe Fuel Cells A/S (TOFC) and Risø National Laboratory. The modelled gasifier is based on an up scaled version of the demonstrated low tar gasifier, Viking, situated at the Technical University of Denmark. The MGT utilizes the unconverted syngas from the SOFC to produce more power as well as pressurizing the SOFC bettering the electrical efficiency compared to operation with the SOFC alone - from η_{el}=36.4% to η_{el}=50.3%.

Keywords: System modelling, biomass gasification, micro gas turbine, SOFC

Nomenclature

a_{ohm}, b_{ohm}	coefficients for Eq. (24)
ASR	area specific resistance
E	reversible open circuit voltage
F	Faradays constant
g_f	Gibbs free energy of formation
i	current density
LHV	lower heating value
$\dot{n}$	molar flow
n_e	transferred electrons per molecule of fuel
p	pressure/partial pressure
P	power production
R	universal gas constant
T	temperature
UF	fuel utilization factor for SOFC
V	potential/overpotential
y	molar fraction
δ	SOFC layer thickness
η	efficiency

Subscripts:

a	anode
c	cathode
con	consumption
e	electrolyte
i	interconnect

* Corresponding author: Email: chrbm@win.dtu.dk Phone: +45 45254123

1 Introduction

Development of sustainable and efficient production plants of combined heat and power (CHP) tends to gain more attention as climate changes, security of supply and depletion of fossil fuels have become well known issues. The share of biomass in CHP production are expected to increase in the future and decentralized CHP plants are also of interest to avoid costs of biomass transportation. Efficient power producing technologies for small scale productions are typically gas engines, micro gas turbines (MGT) and fuel cells – all requiring gaseous fuel. Gasification can deliver biomass based gaseous fuel so the combination of biomass gasification and efficient syngas conversion are potentially a sustainable and efficient CHP plant.

Solid oxide fuel cells (SOFCs) can electrochemically convert H_2 and CO as well as internally reform CH_4 into more H_2 and CO due to their high operating temperature. This makes SOFCs very fuel flexible and ideal for converting syngas compared to other fuel cell types.

The performance and system design of integrated biomass gasifier and SOFC systems in the 100-1000kW_e class have been investigated by several. An innovative design including heat pipes between a SOFC stack and an allothermal gasifier is described in [1]. Fryda et al. [2] studies the performance of a CHP system of less than 1MW_e and consisting of an autothermal gasifier combined with a MGT and/or SOFC.

This study focus on the performance of a system combining an up scaled version (~500kW_{th}) of the two-stage gasifier named Viking and a SOFC or a SOFC-MGT system. Viking is a 75kW_{th} autothermal (air blown) fixed bed biomass gasifier demonstrated at the Technical University of Denmark and it is described in detail in [3]. The Viking gasifier produces almost no tars, which is favourable for downstream SOFC operation. Hofmann et al. [4] has operated a SOFC on cleaned syngas from the Viking gasifier for 150 hours without degradation.

The present study is based on zero dimensional and steady-state modelling in the simulation tool DNA [5]. DNA has incorporated thermodynamic property data, is component based and is developed at The Technical University of Denmark.

2 System description

Two different combined heat and power systems are investigated in this study, both based on syngas production from an up scaled Viking gasifier. A flow sheet of the two systems is depicted in Figure 1. The modelled gasifier system is slightly simplified, but aims at the same resulting gas composition and cold gas efficiency as for the Viking gasifier. In the gasifier model the dryer is heated by hot syngas. The steam production from the dryer is added to the preheated air and dry wood together with mixed air and steam are fed to the gasifier. The raw product gas is cooled to 90°C in three steps; air preheating, wood drying and syngas cooling producing hot water for district heating. The cooled syngas is then cleaned from impurities as particles and sulphur compounds before some of the water in the gas is condensed through cooling to 50°C. The cleaned and partly dried syngas is then converted into electricity and heat in a bottoming cycle consisting of a SOFC or both a SOFC and a MGT. These two system configurations will from now on be referred as the Gasifier-SOFC and the Gasifier-SOFC-MGT configuration, respectively. In the Gasifier-SOFC-MGT configuration all the components in the flow sheet are in use. With respect to Figure 1 the recuperator and gas turbine are bypassed in the Gasifier-SOFC arrangement, thus the syngas and air compressors work as blowers due to no pressurization. In addition the syngas compressor works as a roots blower for the gasifier system and not illustrated is a generator. In the Gasifier-SOFC configuration the syngas and air blowers are driven by an electric motor.

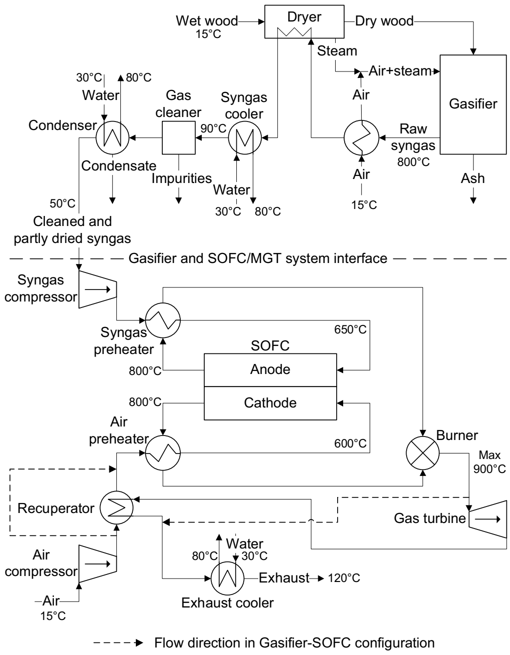

Figure 1: Flow sheet of the hybrid systems

3 Gasifier model

The gasifier component calculates the produced syngas composition as well as the produced ashes based on the inlet media composition and the operating conditions. The input parameters defining the operating conditions for the gasifier submodel are given in Table 1. The gasifier pressure loss is defined as the difference between the inlet air and steam mixture and the outlet syngas.

Operating pressure	$p_{gasifier}$	0.998 bar
Operating temperature	$T_{gasifier}$	800°C
Pressure loss	$\Delta p_{gasifier}$	5 mbar
Non-equilibrium methane	*METH*	0.01

Table 1: Inputs to the gasifier submodel

In the gasifier the incoming flows are converted into a syngas and ashes. The ashes come from a defined ash content in the biomass. The syngas can consist of the following species: H_2, O_2, N_2, CO, NO, CO_2, H_2O, NH_3, H_2S, SO_2, CH_4, NO_2, HCN, COS and Ar. It is assumed that equilibrium is reached at the operating temperature and pressure, where the total Gibbs energy has its minimum value. With this assumption the syngas outlet composition can be found by the Gibbs minimization method [6]. A possibility for bypassing an amount of methane from the equilibrium calculations is added in order to reach syngas compositions, which contain more methane than the corresponding one at equilibrium. Thus the syngas composition can be adjusted to match real syngas compositions, e.g. from the Viking gasifier. The input parameter *METH* is used for this bypassing and is defined as the fraction of methane that is not included in the equilibrium calculations and instead flows through the gasifier and appears in the outlet syngas.

3.1 Gasifier model validation

The model validation for the gasifier is done for all of the gasification plant from the biomass input to the cleaned and dried syngas. Thus data from the Viking gasifier plant can be used for validation.

Wood chips from beech with small amounts of oak are used in the model as for the Viking gasifier reported in Ahrenfeldt et al. [3].

As seen in Table 2 the produced syngas composition and the lower heating value (LHV) from the gasifier model is close to the Viking data. The overall performance of the modelled gasifier is also similar to the Viking gasifier as expressed in the cold gas efficiencies.

	Viking [3]	Gasifier model
H_2 (vol-%)	30.5	29.9
CO (vol-%)	19.6	20.8
CO_2 (vol-%)	15.4	13.5
CH_4 (vol-%)	1.16	1.19
N_2 (vol-%)	33.3	34.2
LHV (MJ/kg)	6.2	6.3
Cold gas eff.	93%	94%

Table 2: Dry syngas composition, lower heating value as well as cold gas efficiency for the Viking gasifier and the modelled gasifier, respectively

4 Solid Oxide Fuel Cell model

The SOFC stack component calculates the air and fuel outlet compositions as well as the power production. The calculations are based on the inlet air and fuel compositions and flow rates as well as the other operating conditions of the SOFC. The SOFC submodel includes an electrochemical model for predicting the performance of the SOFC. The operating conditions are partly described by input parameters given to the SOFC submodel and these are presented in Table 3.

Fuel utilization factor	UF	0.85
Operating temperature	T_{SOFC}	800°C
Anode pressure loss	Δp_a	5 mbar
Cathode pressure loss	Δp_c	10 mbar
Current density	i	300 mA cm^{-2}

Table 3: Inputs to the SOFC submodel

In the submodel only H_2 is electrochemically converted in the SOFC anode, but the model takes into account that CO produces an extra H_2 through the water-gas-shift (WGS) reaction, while four additional H_2 molecules are produced from CH_4 through internal steam reforming and WGS of produced CO (full conversion is assumed). The total mole flow of H_2 on the anode after internal steam reforming and WGS is expressed in Eq. (1).

$$\dot{n}_{\mathrm{H_2,tot}} = \dot{n}_{\mathrm{H_2,in}} + \dot{n}_{\mathrm{CO,in}} + 4\dot{n}_{\mathrm{CH_4,in}} \qquad (1)$$

$$\mathrm{H_2} + \mathrm{O^{2-}} \rightarrow \mathrm{H_2O} + 2\mathrm{e^-} \qquad (2)$$

$$\tfrac{1}{2}\mathrm{O_2} + 2\mathrm{e^-} \rightarrow \mathrm{O^{2-}} \qquad (3)$$

$$\mathrm{H_2} + \tfrac{1}{2}\mathrm{O_2} \rightarrow \mathrm{H_2O} \qquad (4)$$

The amount of hydrogen that is converted depends on the fuel utilization factor (*UF*) and this amount is electrochemically converted in the anode. The electrode reactions and the overall fuel cell reaction are as shown in Eq. (2) to (4).

From the overall fuel cell reaction it is seen that the amount of consumed oxygen is half the amount of consumed hydrogen. The cathode outlet composition can then be found by the following equations if the only species taking into account are O_2, N_2, CO_2, H_2O and Ar.

$$\dot{n}_{O_2,\text{con}} = \frac{UF\dot{n}_{H_2,\text{in}}}{2} \tag{5}$$

$$\dot{n}_{\text{c,out}} = \dot{n}_{\text{c,in}} - \dot{n}_{O_2,\text{con}} \tag{6}$$

$$y_{O_2,\text{out}} = \frac{\dot{n}_{\text{c,in}} y_{O_2,\text{in}} - \dot{n}_{O_2,\text{con}}}{\dot{n}_{\text{c,out}}} \tag{7}$$

$$y_{j,\text{out}} = \frac{\dot{n}_{\text{c,in}} y_{j,\text{in}}}{\dot{n}_{\text{c,out}}},\ j = \{N_2, CO_2, H_2O\} \tag{8}$$

$$y_{\text{Ar,out}} = 1 - y_{O_2,\text{out}} - y_{N_2,\text{out}} - y_{CO_2,\text{out}} - y_{H_2O,\text{out}} \tag{9}$$

The fuel composition leaving the anode is calculated by the Gibbs minimization method [6] as described for the gasifier submodel. Equilibrium at the anode outlet temperature and pressure is assumed for the following species: H_2, CO, CO_2, H_2O, CH_4 and N_2. The equilibrium assumption is fair since the methane content in this study is low enough for such kind of assumption to be made. The heat consumed by the endothermic internal reforming reactions is taken into account by the Gibbs minimization method. More internal reforming means more cooling of the SOFC.

The power production from the SOFC depends on the amount of chemical energy fed to the anode, the reversible efficiency (η_{rev}), the voltage efficiency (η_{v}) and the fuel utilization factor (*UF*). It is defined in mathematical form in Eq. (10).

$$P_{\text{SOFC}} = \left[LHV_{H_2}\dot{n}_{H_2,\text{in}} + LHV_{CO}\dot{n}_{\text{CO,in}} + LHV_{CH_4}\dot{n}_{CH_4,\text{in}}\right]\eta_{\text{rev}}\eta_{\text{v}}UF \tag{10}$$

The reversible efficiency is the maximum possible efficiency defined as the relationship between the maximum electrical energy available (change in Gibbs free energy) and the fuels LHV. This is shown in Eq. (11) and the definition of the change in Gibbs free energy is shown in Eq. (12). The voltage efficiency express the electrochemical performance of the SOFC and the calculation of the voltage efficiency is described in the following subsection.

$$\eta_{\text{rev}} = \frac{(\Delta\bar{g}_{\text{f}})_{\text{fuel}}}{LHV_{\text{fuel}}} \tag{11}$$

$$\begin{aligned}(\Delta\bar{g}_{\text{f}})_{\text{fuel}} = &\left[(\bar{g}_{\text{f}})_{H_2O} - (\bar{g}_{\text{f}})_{H_2} - \tfrac{1}{2}(\bar{g}_{\text{f}})_{O_2}\right]y_{H_2,\text{in}} \\ &+\left[(\bar{g}_{\text{f}})_{CO_2} - (\bar{g}_{\text{f}})_{CO} - \tfrac{1}{2}(\bar{g}_{\text{f}})_{O_2}\right]y_{\text{CO,in}} \\ &+\left[(\bar{g}_{\text{f}})_{CO_2} + 2(\bar{g}_{\text{f}})_{H_2O} - (\bar{g}_{\text{f}})_{CH_4} - 2(\bar{g}_{\text{f}})_{O_2}\right]y_{CH_4,\text{in}}\end{aligned} \tag{12}$$

4.1 Electrochemical model

The electrochemical model is used to calculate the cell potential and the voltage efficiency of the SOFC. Both depend on the operating conditions such as temperature, pressure, gas compositions, fuel utilization and load (current density). The cell potential and voltage efficiency is defined in Eq. (13) and (14), respectively.

$$V_{\text{cell}} = E - V_{\text{act}} - V_{\text{ohm}} \tag{13}$$

$$\eta_{\text{v}} = \frac{V_{\text{cell}}}{E} \tag{14}$$

In the following the reversible open circuit voltage (E), the activation overpotential (V_{act}) and the ohmic overpotential (V_{ohm}) are calculated. Traditionally a concentration overpotential term is included in Eq. (13). The concentration overpotential is a result of the limitations of transporting the reactants to the active cell area. In Larminie et al. [7] it is described as a voltage drop caused by the pressure change associated with the consumption of reactants. As a result of the current being drawn from the cell, the average partial pressure of reactants is lower than at the inlet. Thus, in this study the concentration overvoltage is taken into account by using average partial pressures when calculating E and V_{act}.

E can be calculated from the Nernst equation:

$$E = \frac{-\Delta \overline{g}_{\mathrm{f}}^{\,0}}{n_{\mathrm{e}}F} + \frac{RT}{n_{\mathrm{e}}F}\ln\left(\frac{\overline{p}_{\mathrm{H_2,tot}}\sqrt{\overline{p}_{\mathrm{O_2}}}}{\overline{p}_{\mathrm{H_2O}}}\right) \tag{15}$$

Since it is assumed that all CO and CH_4 are converted to H_2 before the electrochemical reactions take place, the change in standard Gibbs free energy ($\Delta \overline{g}_{\mathrm{f}}^{\,0}$) is and the number of electrons transferred for each molecule of fuel (n_e) are determined for the reaction of H_2 only. Thus, $n_e = 2$ and $\Delta \overline{g}_{\mathrm{f}}^{\,0} = \left(\overline{g}_{\mathrm{f}}^{\,0}\right)_{\mathrm{H_2O}} - \left(\overline{g}_{\mathrm{f}}^{\,0}\right)_{\mathrm{H_2}} - \frac{1}{2}\left(\overline{g}_{\mathrm{f}}^{\,0}\right)_{\mathrm{O_2}}$. The partial pressure of species j is an average across the respective electrode and is here defined as an arithmetic mean between inlet and outlet as shown in Eq. (16) and (17). The average partial pressure of available hydrogen after internal steam reforming and WGS of CH_4 and CO can be determined from the overall steam reforming and WGS reaction including all species. It is defined in Eq. (18).

$$\overline{p}_j = \left(\frac{y_{j,\mathrm{out}} - y_{j,\mathrm{in}}}{2}\right)p_{\mathrm{a}}, \quad j = \left\{\mathrm{H_2, CO, CH_4, CO_2, H_2O, N_2}\right\} \tag{16}$$

$$\overline{p}_{\mathrm{O_2}} = \left(\frac{y_{\mathrm{O_2,out}} - y_{\mathrm{O_2,in}}}{2}\right)p_{\mathrm{c}} \tag{17}$$

$$\overline{p}_{\mathrm{H_2,tot}} = \left(\frac{\overline{p}_{\mathrm{H_2}} + \overline{p}_{\mathrm{CO}} + 4\overline{p}_{\mathrm{CH_4}}}{\overline{p}_{\mathrm{H_2}} + \overline{p}_{\mathrm{CO}} + 3\overline{p}_{\mathrm{CH_4}} + \overline{p}_{\mathrm{CO_2}} + \overline{p}_{\mathrm{H_2O}} + \overline{p}_{\mathrm{N_2}}}\right)p_{\mathrm{a}} \tag{18}$$

The activation overpotential is due to an energy barrier (activation energy) that the reactants must overcome in order to drive the electrochemical reactions. The activation overpotential is non-linear and is dominant at low current densities (i). The activation overpotential is defined as (cf. [8]):

$$V_{\mathrm{act}} = V_{\mathrm{act,a}} + V_{\mathrm{act,c}} = \frac{2RT}{n_{\mathrm{e}}F}\left[\sinh^{-1}\left(\frac{i+i_{\mathrm{n}}}{2i_{0,\mathrm{a}}}\right) + \sinh^{-1}\left(\frac{i+i_{\mathrm{n}}}{2i_{0,\mathrm{c}}}\right)\right] \tag{19}$$

The internal current density (i_n) is added to the actual fuel cell current density in order to account for the mixed potential caused by fuel crossover. The importance of the internal current density in the case of SOFCs is much less than for low temperature fuel cells and the value of i_n is usually very small [7]. The exchange current density (i_0) is a measure of the level of activity on the electrode at i=0 mA cm^{-2} and is defined as (cf. [9]):

$$i_{0,\mathrm{a}} = 2.13\times10^{7}\left(\frac{\overline{p}_{\mathrm{H_2,tot}}\overline{p}_{\mathrm{H_2O}}}{p_{\mathrm{a}}^{\,2}}\right)\exp\left(\frac{-110000}{RT}\right) \tag{20}$$

$$i_{0,\mathrm{c}} = 1.49\times10^{7}\left(\frac{\overline{p}_{\mathrm{O_2}}}{p_{\mathrm{c}}}\right)^{0.25}\exp\left(\frac{-110000}{RT}\right) \tag{21}$$

The ohmic overpotential is caused by the electrical resistance for the ions passing through the electrolyte as well as for the electrons passing through the electrodes and interconnects. The ohmic overpotential is defined below (cf. [9] and [12]).

$$V_{\text{ohm}} = i\,ASR \tag{22}$$

$$ASR = ASR_{\text{a}} + ASR_{\text{c}} + ASR_{\text{e}} + ASR_{\text{i}} \tag{23}$$

$$ASR_j = \delta_j a_{\text{ohm},j} \exp\left(\frac{b_{\text{ohm},j}}{T}\right),\; j = \{\text{a},\text{c},\text{e},\text{i}\} \tag{24}$$

The thicknesses of the different layers (δ) and the constants a_{ohm} and b_{ohm} used are listed in Table 4.

R	8.314 J K^{-1} mol^{-1}	
F	96485 C mol^{-1}	
n_e	2	
i_n	2 mA cm^{-2}	[9]
δ_a	750×10^{-4} cm	[10]
δ_c	50×10^{-4} cm	[10]
δ_e	40×10^{-4} cm	[10]
δ_i	100×10^{-4} cm	[11]
$a_{\text{ohm,a}}$	0.00298×10^{-3} kΩcm	[12]
$b_{\text{ohm,a}}$	-1392 K	[12]
$a_{\text{ohm,c}}$	0.00811×10^{-3} kΩcm	[12]
$b_{\text{ohm,c}}$	600 K	[12]
$a_{\text{ohm,e}}$	0.00294×10^{-3} kΩcm	[12]
$b_{\text{ohm,e}}$	10350 K	[12]
$a_{\text{ohm,i}}$	0.1256×10^{-3} kΩcm	[12]
$b_{\text{ohm,i}}$	4690 K	[12]

Table 4: Inputs for the electrochemical model

4.2 Electrochemical model calibration

The described electrochemical model has been calibrated against experimental data, see Figure 2.

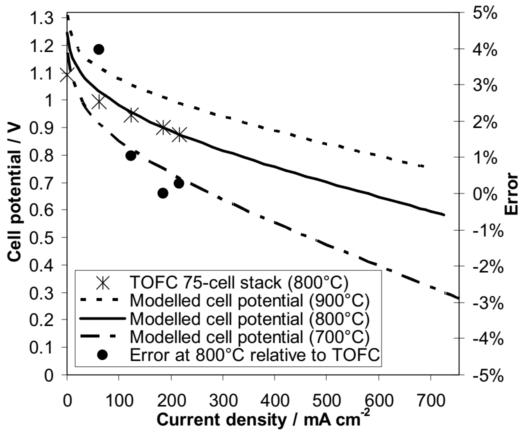

Figure 2: Single cell polarization curves based on a 75-cell stack and the SOFC model, respectively

Since the model aims at the performance of 2nd generation SOFCs from Topsoe Fuel Cell A/S (TOFC) and Risø National Laboratory, published data for this SOFC type has been used. The *ASR* has been calibrated against a value of 0.15 Ω cm^2 at 850°C as published by [13] and the resulting cell potential has been calibrated against a polarization curve

(75-cell stack, 12 x 12 cm^2, 800°C and fuelled with H_2 and N_2) published by [14]. An active cell area of 81 cm^2 has been assumed. Both modelled and experimental data as well as the error relative to the experimental data are presented in Figure 2.

The model shows excellent agreement with the experimental data above a current density of 100 mA cm^{-2}. The current density of 300 mA cm^{-2} is chosen to represent the SOFC load in the following results.

5 Peripheral equipment

Modelling of peripheral components like compressors, turbines and heat exchangers are standard and therefore not described in detail.

The throughput of wet biomass is 154.8 kg h^{-1} (corresponds to 499.2 kW_{th} (LHV)). Thus it is assumed that the Viking gasifier can be scaled up from a nominal ~75 kW_{th} [3]. The biomass dryer reduces the water content in the biomass from 32.2 wt-% to 5 wt-% by heating it to 150°C and the air for the gasifier is preheated to 780°C by the hot product gas.

The inlet temperature to the SOFC anode and cathode are maintained at 150°C and 200°C below the outlet temperature, respectively.

The pressure loss in every component in the SOFC air supply stream and burner exhaust stream is assumed to be 10 mbar, while the pressure loss in each of the rest of the components is assumed to be 5 mbar, except the burner that has a pressure loss of 0.6‰ (equals 1.5 mbar when 2.5 bar at inlet).

The gas cleaner is a baghouse filter removing particulates and it is assumed that the cleaned syngas can be used directly in a SOFC. The condenser removes some of the water content in the syngas resulting in a content of water in the cleaned and dried syngas of 12.7 vol-%. The resulting steam to carbon ratio (S/C) is 0.41, which is somewhat low, but is justified by the very low tar content in the Viking syngas.

The isentropic and mechanical efficiency of the compressors are 75% and 98%, respectively, and the isentropic efficiency of the MGT expander is 84%. The performance of the compressors and the MGT expander are taken from Fryda et al. [2] and corresponds to common performance data for a MGT of this scale. The recuperator effectiveness is assumed to be 85% and the generator efficiency is assumed to be 99%. In the Gasifier-SOFC configuration the SOFC operating pressure is ~1 bar and in the Gasifier-SOFC-MGT case the SOFC operating pressure is 2.5 bar (this pressure is varied in the results section).

No heat losses are taken into account. Introducing heat losses from the gas cleaner will only affect the heat production from the condenser since the temperature after the condenser is fixed to 50°C.

The outlet pressure from the MGT depends on the total pressure loss downstream the MGT, since it is the exhaust pressure which is fixed to 1.013 bar. Because of the recuperator and exhaust cooler the outlet pressure from the MGT is 1.033 bar. The district heating (DH) water is assumed to be 30°C at inlet and 80°C at outlet.

6 Results and discussion

In the following results the inputs presented in the previous sections are used unless something else is stated. The system configurations are previously described in detail.

The performance of the different system configurations vary greatly with the operating conditions and namely the operating pressure of the SOFC (in the Gasifier-SOFC-MGT case) are of great importance to the resulting system performance. The Gasifier-SOFC-MGT configuration has an optimum with regard to its operating pressure, while the

Gasifier-SOFC arrangement always operates at atmospheric pressure – illustrated in Figure 3. The Gasifier-SOFC configuration performs an electric efficiency of 36.4%. By combining the SOFC and MGT in the Gasifier-SOFC-MGT configuration the electrical efficiency reaches 50.3% at an optimum operating pressure of 2.5 bar. This is a substantial increase in efficiency caused by the utilization of unconverted fuel from the SOFC (fuel utilization of 85%) in the MGT as well as the pressurized operation of the SOFC. In the Gasifier-SOFC-MGT case the turbine inlet temperature (TIT) is varying with the SOFC operating pressure and has a value of 697°C at 2.5 bar. It is the recuperator that ensures an optimum at a relatively low operating pressure.

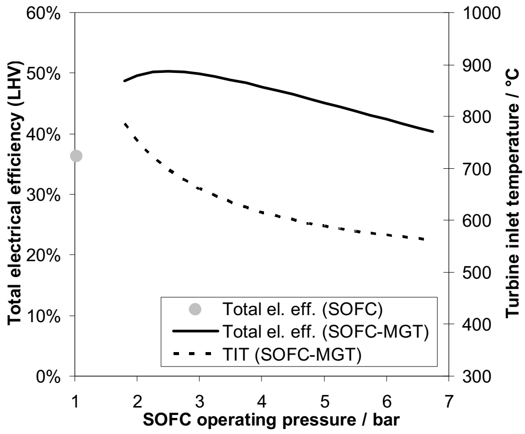

Figure 3: Electric efficiency and TIT at different SOFC operating pressures

The performance of both system arrangements strongly depend on the SOFC operating temperature as depicted in Figure 4. Decreasing the temperature by 100°C to 700°C lowers the electrical efficiency to 28.8% and 44.4% in the Gasifier-SOFC and Gasifier-SOFC-MGT case, respectively. This corresponds to a drop of 7.6 and 5.9 percentage points, respectively. The research and development working on lowering the SOFC operating temperature in order to use cheaper materials will influence the system performance presented here and potentially other bottoming cycles could be beneficial, e.g. a Rankine cycle.

The sensitivity of the model results to the chosen SOFC current density is shown in Figure 5.

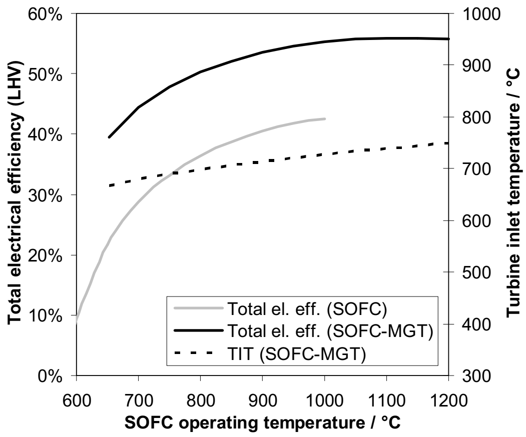

Figure 4: Electric efficiency and TIT at different SOFC operating temperatures

At the reference current density value of 300 mA cm^{-2} the SOFC voltage efficiency is 39.6% in the Gasifier-SOFC arrangement and 40.8% in the Gasifier-SOFC-MGT case. The difference is due to the pressure. Raising the SOFC load to 500 mA cm^{-2} reduces the voltage efficiency (defined in Eq. (14)) to 34.6% and 35.7% in the Gasifier-SOFC and Gasifier-SOFC-MGT cases, respectively, meaning a reduction in the total electrical efficiency to 31.5% and 46.7% - a drop of 4.9 and 3.6 percentage points. This is a relative change in electrical efficiency of 13.5% and 7.2%, respectively, for a 66.7% increase in current density.

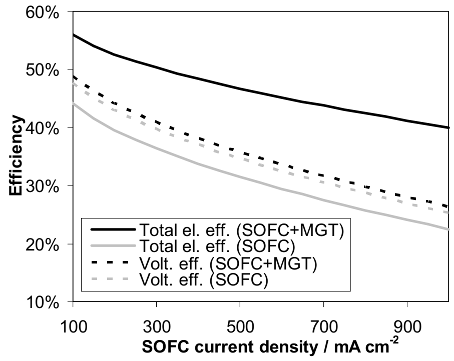

Figure 5: Electrical efficiency and SOFC voltage efficiency as a function of SOFC current density

Key data for the two system configurations studied are presented in Table 5 based on the reference input values presented in the previous sections. The Gasifier-SOFC-MGT configuration clearly has the best electrical efficiency, while the CHP efficiencies do not differ significantly. In the Gasifier-SOFC-MGT case, the power production is mainly from the SOFC producing 76.4% of the power. The exact values of the efficiencies will be slightly lower when incorporating heat losses, a more accurate efficiency of the gasifier system and possible more extensive gas cleaning, but the comparison of the systems performance is still valid.

		Gasifier -SOFC	Gasifier -SOFC-MGT
Biomass input	/ kg h^{-1}	154.8	154.8
	/ $kW_{th,LHV}$	499.2	499.2
p_{SOFC} / bar		1.034	2.5
$P_{MGT,net}$ / kW_{el}		-	59.2
$P_{SOFC,net}$ / kW_{el}		181.5	191.8
$P_{total,net}$ / kW_{el}		181.5	251.0
DH production / kJ s^{-1}		216.6	146.7
η_{el} / % (LHV)		36.4	50.3
η_{CHP} / % (LHV)		79.74	79.68

Table 5: Key data for the studied systems

7 Conclusion

A study on the system performance of an up scaled Viking gasifier (~500 kW_{th}) with either a downstream SOFC or SOFC-MGT arrangement has been conducted by zero dimensional process modelling. A SOFC submodel has been developed including an electrochemical model predicting the SOFC performance at different operating conditions. This submodel has been calibrated against published TOFC stack performance data. The reference conditions for the SOFC has been an operating temperature of 800°C, a fuel utilization of 85% and a current density of 300 mA cm^{-2}. The optimal operating SOFC-MGT pressure has been found to be 2.5 bar, while the SOFC without MGT operated at atmospheric pressure. The MGT utilized the unconverted syngas from the SOFC to produce more power as well as pressurizing the SOFC bettering the electrical efficiency compared to operation with the SOFC alone -

from η_{el}=36.4% to η_{el}=50.3%. These efficiencies were very sensitive to the SOFC operating temperature, while only a moderate sensitivity to the SOFC current density was observed.

8 References

[1] Karellas S, Karl J, Kakaras E. *An innovative biomass gasification process and its coupling with microturbine and fuel cell systems*. Energy 2008;33:284–291.

[2] Fryda L, Panopoulos KD, Kakaras E. *Integrated CHP with autothermal biomass gasification and SOFC–MGT*. Energy Conversion and Management 2008;49:281–290.

[3] Ahrenfeldt J, Henriksen U, Jensen TK, Gøbel B, Wiese L, Kather L, Egsgaard H. *Validation of a Continuous Combined Heat and Power (CHP) Operation of a Two-Stage Biomass Gasifier*. Energy & Fuels 2006;20:2672-2680.

[4] Hofmann Ph, Schweiger A, Fryda L, Panopoulos KD, Hohenwarter U, Bentzen JD, Ouweltjes JP, Ahrenfeldt J, Henriksen U, Kakaras E. *High temperature electrolyte supported Ni-GDC/YSZ/LSM SOFC operation on two-stage Viking gasifier product gas*. J. Power Sources 2007;173:357–366.

[5] Elmegaard B, Houbak N. *DNA – A General Energy System Simulation Tool*, In: Proceedings of the 46th Conf. on Simulation and Modeling, Trondheim, 2005.

[6] Smith JM, Van Ness HC, Abbott MM. *Introduction to Chemical Engineering Thermodynamics*. 7th ed. Boston: McGraw-Hill, 2005.

[7] Larminie J, Dicks A. *Fuel Cell Systems Explained*. 2nd ed. West Sussex: John Wiley & Sons Ltd., 2003.

[8] Aloui T, Halouani K. *Analytical modeling of polarizations in a solid oxide fuel cell using biomass syngas product as fuel*. Appl. Therm. Eng. 2007;27:731-737.

[9] Calise F, Dentice d'Accadia M, Palombo A, Vanoli L. *Simulation and exergy analysis of a hybrid Solid Oxide Fuel Cell (SOFC)–Gas Turbine System*. Energy 2006;31:3278-3299.

[10] Chan SH, Khor KA, Xia ZT. *A complete polarization model of a solid oxide fuel cell and its sensitivity to the change of cell component thickness*. J. Power Sources 2001;93:130-140.

[11] Chan SH, Low CF, Ding OL. *Energy and exergy analysis of simple solid-oxide fuel-cell power systems*. J. Power Sources 2002;103:188-200.

[12] Bessette NF II, Wepfer WJ, Winnick J. *A Mathematical Model of a Solid Oxide Fuel Cell*. J. Electrochem. Soc. 1995;142:3792-3800.

[13] Christiansen N, Hansen JB, Holm-Larsen H, Linderoth S, Larsen PH, Hendriksen PV, Mogensen M. *Solid oxide fuel cell development at Topsoe Fuel Cell and Risø*. Fuel Cells Bulletin 2006;2006(8):12-15.

[14] Linderoth S, Larsen PH, Mogensen M, Hendriksen PV, Christiansen N, Holm-Larsen H. *Solid Oxide Fuel Cell (SOFC) Development in Denmark*. Materials Science Forum 2007;539-543:1309-1314.

Appendix J IMPROVED PREDICTION OF THE SOFC PERFORMANCE

In reality, the electrochemical performance of an SOFC is distributed over the cell area due to varying species concentrations, temperature, and pressure. Thus, making a lumped model reliable can be challenging. Nevertheless, that is a goal of this study, and in this Appendix an improved approach is presented. The improved model is developed after generating the results presented in this thesis.

Eq. (4.23) in the presented SOFC component model assumes that the average partial pressure of hydrogen used to predict the electrochemical performance of the SOFC is the sum of average partial pressure of H_2, CO, and four times CH_4 in the anode compartment due to the steam reforming and water-gas-shift reactions. By using this equivalent hydrogen partial pressure in the presented Nernst equation (eq. (4.24)), the influence of species like CO_2 is neglected. This might be valid in water-rich environments without CO_2, but with substantial amounts of CO_2 present, the balance between reactants and products in the Nernst equation will be off target. Thus, a better way of predicting the average species concentrations and the corresponding electrochemical performance of the SOFC is presented in this Appendix together with estimates on the influence of using the original SOFC model instead of the approach presented here.

Improved Approach

In the improved approach, the partial pressures of all anode species are determined by averaging between the chemical equilibrium composition at the inlet conditions and the chemical equilibrium composition at the outlet conditions, eq. (J.1). Chemical equilibrium at both inlet and outlet are based on the SOFC operating pressure and the temperature of the solid structure of the SOFC (i.e., the SOFC operating temperature). The only difference between the inlet and outlet is the addition of oxygen from the cathode side prior to the outlet. Assuming chemical equilibrium at the anode inlet is fair because the high-temperature and active catalyst containing anode environment ensures fast steam reforming and WGS to reach equilibrium [17]. In the approach presented in Chapter 4, the inlet composition is not at chemical equilibrium, but instead the anode fuel feed composition is directly used. By applying Gibbs free energy minimization at the anode inlet, the gas composition is ensured to be at chemical equilibrium in the improved approach.

$$\overline{p}_j = \left(\frac{y_{j,\text{out,eq}} + y_{j,\text{in,eq}}}{2} \right) \overline{p}_\text{a} \, , \; j = \{\text{H}_2, \text{CO}, \text{CH}_4, \text{CO}_2, \text{H}_2\text{O}, \text{N}_2\} \qquad \text{(J.1)}$$

Furthermore, the Nernst potential is determined at both inlet and outlet. An arithmetic mean between the inlet Nernst potential and the outlet Nernst potential is chosen to represent the average Nernst potential of the cell (eqs. (J.2) to (J.4)). The actual Nernst potential is distributed across the cell area and could be determined more precisely by integrating over the cell length or area, but in a lumped model that is not possible, thus averaging between inlet and outlet is used as an estimate.

$$E_\text{in} = \frac{-\Delta g_\text{f}^{\,0}}{n_\text{e} F} + \frac{RT}{n_\text{e} F} \ln \left(\frac{p_{\text{H}_2,\text{in,eq}} \sqrt{p_{\text{O}_2,\text{in}}}}{p_{\text{H}_2\text{O,in,eq}}} \right) \qquad \text{(J.2)}$$

$$E_\text{out} = \frac{-\Delta g_\text{f}^{\,0}}{n_\text{e} F} + \frac{RT}{n_\text{e} F} \ln \left(\frac{p_{\text{H}_2,\text{out,eq}} \sqrt{p_{\text{O}_2,\text{out}}}}{p_{\text{H}_2\text{O,out,eq}}} \right) \qquad \text{(J.3)}$$

$$\overline{E} = \frac{E_\text{in} + E_\text{out}}{2} \qquad \text{(J.4)}$$

The equations presented above should replace eqs. (4.21), (4.23), and (4.24). By means of this improved alternative, the estimation of the Nernst potential and SOFC performance is valid for a variety of fuel compositions including CO_2-rich mixtures. The improved SOFC model is calibrated in the same way and against the same experimental data as described in Section 4.1.1. By performing the same calibration, the SOFC performance will be similar at the operating conditions of experimental data used for calibration. Since the operating conditions of the SOFC in the studied plant designs are different from the experimental data, the changes in the model will still affect the

SOFC performance in the plant studies and the consequences are estimated and discussed below.

Consequences

The results presented in Chapter 4, Chapter 6, and Chapter 7 will change when applying the suggested improvements above, because the electrical efficiency of the SOFC will be different at the same operating conditions. Instead of recalculating all the results in these Chapters, this Section will deal with how much the operating conditions of the SOFC should be modified to reach similar SOFC performance as in the original results. Several of the operating conditions of the SOFC (e.g., current density and operating temperature) are arbitrary chosen within realistic operational range, thus variation of some of these conditions will not make the results less reliable, and the comparison of conceptual plant designs and the system-level optimization will still be valid.

In Table J.1, the operational data for the SOFC model is presented using the original and improved approaches. It is clear that the SOFC performance is lower in the improved SOFC model at the same operating conditions, and this is mainly due to an increased area specific resitistance (*ASR*). *ASR* includes all overpotentials and is defined as follows:

$$ASR = \frac{E - V_{\text{cell}}}{i} \tag{J.5}$$

Table J.1: Data from original and improved SOFC model using product gas.

	Original SOFC model	Improved SOFC model
p_{SOFC} / bar	2.5	2.5
T_{SOFC} / °C	800	800
i / mA cm^{-2}	300	300
E / V	0.965	0.925
V_{cell} / V	0.820	0.661
ASR / Ω cm^2	0.486	0.880
η_{v} / %	84.9	71.5
η_{rev} / %	70.3	68.8
U_{F} / %	85.0	85.0
η_{SOFC} / %	50.7	41.8

By use of the improved model, the average partial pressure of hydrogen will be lower than in the orginal model (because eq. (4.23) is neglected). The Nernst potential drops 40 mV (cf., Table J.1), but also the *ASR* is affected because of its dependence on the partial pressures. The *ASR* increases mainly because of the expression describing the anodic exchange current density in eq. (4.28), in which CO is considered inert in the modified model and a fuel on equal terms as H_2 in the original model. In reality, CO is neither inert or can be considered on equal terms as H_2 (due to reduced reaction rate), thus the improved model can be seen as a worst case scenario and the original model as a best case scenario. The truth will be somewhere in between.

By changing the operating temperature and current density, the SOFC performance can be adjusted to meet the original SOFC model. This is illustrated in Table J.2, where first the current density, then the operating temperature, and finally both are adjusted.

Table J.2: Data from improved and adjusted SOFC model.

	Improved SOFC model		
	adjusted i	adjusted T_{SOFC}	adjusted i and T_{SOFC}
p_{SOFC} / bar	2.5	2.5	2.5
T_{SOFC} / °C	800	*950*	*875*
i / mA cm^{-2}	*130*	300	*225*
E / V	0.925	0.863	0.894
V_{cell} / V	0.801	0.778	0.788
ASR / Ω cm^2	0.947	0.285	0.472
η_v / %	86.7	90.1	88.1
η_{rev} / %	68.8	63.7	66.2
U_F / %	85.0	85.0	85.0
η_{SOFC} / %	50.7	48.8	49.6

When adjusting either the current density or the SOFC temperature individually to meet similar η_{SOFC} as in the original SOFC model, the resulting *ASR* is still different from the one found in the original model. By adjusting both current density and temperature, similar η_{SOFC} and *ASR* can be obtained. The problem of changing the operating temperature of the SOFC is that it will affect the surrounding system when incoporated into a plant. Therefore it can be concluded that for the original results to be valid for both SOFC component and plant designs, the current density should be lowered to 130 mA cm^{-2} when using the improved SOFC modelling approach. In other words, the original results correspond to an SOFC performance at 130 mA cm^{-2} when using the improved approach. This is a low current density compared to typical operation between 200 and 300 mA cm^{-2}, but when noting that the experimental data used for calibration is based on an SOFC from around year 2005, recent and future development will ensure a similar SOFC performance at a higher and more typical load.

Using the improved and current density-adjusted SOFC component model in the plant simulations, the plant performance results in Table J.3 are obtained. No decisive changes in the overall performances are seen. The lower current density (load) means that the SOFC stack size should increase for the plant to produce the same electric power, though. This will also influence the economic aspects of the plant in a negative manner.

Table J.3: Plant performance data using improved and adjusted SOFC model (values in brackets are the original data from Table 6.1 and Table 7.2).

	Plant configuration		
	SOFC	SOFC-MGT	Optimized SOFC-MGT
i / mA cm^{-2}	130 (300)	130 (300)	130 (300)
T_{SOFC} / °C	800 (800)	800 (800)	800 (800)
Optimal *PR* / -	~1 (~1)	2.5 (2.5)	2.7 (2.7)
V_{cell} / V	0.782 (0.800)	0.801 (0.820)	0.803 (0.822)
$\eta_{el,total\ system}$ / % (LHV)	43.9 (43.1)	55.7 (55.0)	58.8 (58.2)

If the improved SOFC model were to be used without the adjustments, the plant performances would decrease as shown in Table J.4. As discussed above, the original data (in brackets) represents a best case scenario and the new data represents a worst case scenario.

Table J.4: Plant performance data using improved and unadjusted SOFC model (values in brackets are the original data from Table 6.1 and Table 7.2).

	Plant configuration		
	SOFC	SOFC-MGT	Optimized SOFC-MGT
i / mA cm^{-2}	300 (300)	300 (300)	300 (300)
T_{SOFC} / °C	800 (800)	800 (800)	800 (800)
Optimal *PR* / -	~1 (~1)	2.5 (2.5)	2.6 (2.7)
V_{cell} / V	0.641 (0.800)	0.661 (0.820)	0.662 (0.822)
$\eta_{el,total\ system}$ / % (LHV)	35.6 (43.1)	49.5 (55.0)	52.7 (58.2)

Suggestion for Further Improvement

The improved approach presented in this Appendix could be further improved, but that is outside the work of this project. The estimation of the Nernst potential is satisfactory, but the *ASR* is overestimated when CO is considered inert. On the other hand, CO cannot be considered equal to H_2. It is suggested to investigate alternative expressions for the anodic exchange current density, and the following approach is specifically suggested; (1) find separate anodic exchange current density expressions for H_2–H_2O and

CO–CO_2 environments, (2) calculate the anodic exchange current density for H_2–H_2O and CO–CO_2 at both anode inlet and outlet and determine the average between inlet and outlet of H_2–H_2O and CO–CO_2, respectively, and (3) weigh the two average anodic exchange current densities by the concentrations of H_2 and CO in the anode compartment to determine an overall anodic exchange current density. In this manner, the evaluation of the activation overpotential will be more generic, and the SOFC and plant performances will be in between the best and worst case scenarios presented above.

DTU Mechanical Engineering
Section of Thermal Energy Systems
Technical University of Denmark

Nils Koppels Allé, Bld. 403
DK- 2800 Kgs. Lyngby
Denmark
Phone (+45) 45 88 41 31
Fax (+45) 45 88 43 25
www.mek.dtu.dk
ISBN: 978-87-89502-98-4

DCAMM
Danish Center for Applied Mathematics and Mechanics

Nils Koppels Allé, Bld. 404
DK-2800 Kgs. Lyngby
Denmark
Phone (+45) 4525 4250
Fax (+45) 4593 1475
www.dcamm.dk
ISSN: 0903-1685